April 2021

AN EMG OPTIMIZATION MODEL OF THE KINETIC DEMANDS ON THE LOWER BACK DURING ASYMMETRICAL GAIT AND LOAD CARRIAGE

Jacob J. Banks
University of Massachusetts Amherst

AN EMG OPTIMIZATION MODEL OF THE KINETIC DEMANDS ON THE LOWER BACK DURING ASYMMETRICAL GAIT AND LOAD CARRIAGE

A Dissertation Presented

by

JACOB J. BANKS

Submitted to the Graduate School of the
University of Massachusetts Amherst in partial fulfillment
of the requirements for the degree of

DOCTOR OF PHILOSPHY

FEBRUARY 2021

Department of Kinesiology

AN EMG OPTIMIZATION MODEL OF THE KINETIC DEMANDS ON THE LOWER BACK DURING ASYMMETRICAL GAIT AND LOAD CARRIAGE

A Dissertation Presented

by

JACOB J. BANKS

Approved as to style and content by:

_____
Graham E. Caldwell, Committee Chair

_____
Katherine A. Boyer, Member

_____
Brian R. Umberger, Member

_____
Seth W. Donahue, Outside Member

_____
Jane A. Kent, Department Chair
Department of Kinesiology

ACKNOWLEDGEMENTS

The first thing I often find myself perusing in a doctoral dissertation is the Acknowledgements section. I am always interested to see who and how individuals get thanked and then use it to gauge what it must have been like to complete one's dissertation. Now that my own doctorate journey has FINALLY come to an end, I find it difficult, very humbling, and a bit surreal to be writing my own. At any rate…

Thank you, Liberty Mutual Research Institute for Safety (LMRIS) for bringing me out from Ohio to Massachusetts ~13 years ago, providing me with a great job and co-workers for ~10 years, and initiating, encouraging, and financing my first 3 years at UMass. I will forever be grateful of and miss my co-workers who were at 71 Frankland. It was a fantastic work experience (while it lasted!) that will be difficult to ever replicate.

Working on a PhD. is a selfish process, and I am unsure any of my immediate family (Chuck, Mom, Chad and Cricket) realized how it would conflict with going back 'home' to Michigan, but you always understood and supported me. Thank you.

To my beautiful fiancée Jamie. Thank you for putting up with me and the singular focus I required to obtain this degree, your proofreading, believing you came up with the 'boot' idea, and dressing me! It has not always been easy on us, but hopefully it will be worth it.

To my UMass family. What a pleasure it has been to get to know all of you and work with you. You all made even Totman enjoyable, and that is as high a compliment as one can give! Though I wish I could thank everyone, a special acknowledgement needs to be given to a few motor systems grad students who in particular accepted, endured, and pushed me: Dan, Erica, Jan, Jonaz, Russ, Ryan, and Sangsoo. I could not have done it

without you, wish you all the best, and hope to stay in touch. Dr. van Emmerik, thank you for providing funding for me the past few years and insights into your steady and brilliant approach to all things motor systems. Drs. Hamill, Weir, and Boyer, thank you for providing me unfettered access to lab equipment and supplies, and for your frequent yet subtle check-ins.

To my committee members. Dr. Donahue, who would have thought 18 years ago at MTU that you would be on my dissertation committee at UMass? Thank you for your time and insights during committee meetings. Dr. Umberger, thank you for teaching me so much about musculoskeletal modeling, OpenSim, academia, keeping tabs on me while Dr. Caldwell was away, always answering emails in a timely fashion, being a reference, and allowing me to participate in all your journal clubs… I just wish you had not moved to 'that school up North'! Dr. Boyer (again), thank you for what you taught me in all of your courses. For all but 1-2 semesters I had either a course or journal club with you! Your enthusiasm for biomechanics research and study design is inspiring and played a large role in formulating this dissertation. Finally, my advisor Dr. Caldwell… I could not have done any of this without your continued support, patience, teachings, extremely insightful and thorough edits, and friendship. I can never fully thank you for everything, so in lieu of that I will always try my best to limit the number of commas and conjunctive sentences I use in my writing!

ABSTRACT

AN EMG OPTIMIZATION MODEL OF THE KINETIC DEMANDS ON THE LOWER BACK DURING ASYMMETRICAL GAIT AND LOAD CARRIAGE

FEBRUARY 2021

JACOB J. BANKS

B.S., MICHIGAN TECHNOLOGICAL UNIVERSITY

M.S., THE OHIO STATE UNIVERSITY

Ph.D., UNIVERSITY OF MASSACHUSETTS AMHERST

Directed by: Professor Graham E. Caldwell

Gait asymmetries are associated with a high incidence of lower back pain (LBP). Although there are several causes of gait asymmetry (i.e. amputation, injury, or deformities), lower back kinetic demands have not been quantified and suitably compared due to experimental limitations in these clinical populations. Further, the impact of gait asymmetry on lower back demands during carrying tasks has not been established. This dissertation addressed these issues by artificially and safely inducing gait asymmetry in healthy able-bodied participants during walking and carrying tasks. LBP risk was assessed by L5/S1 vertebral joint force levels estimated with an OpenSim musculoskeletal model of the lower back adapted to incorporate participant-specific responses using an EMG optimization approach. The model was evaluated systematically for force estimate efficacy and sensitivity to input parameters prior to gait asymmetry assessments.

Twelve participants performed walking and carrying tasks on a treadmill at individually scaled speeds while kinematics, external kinetics, and muscle activities (EMG) were recorded. Walking conditions consisted of unperturbed symmetrical gait, and asymmetrical gait induced by perturbing the right leg with a 2.54 cm shoe leveler, ~1 kg ankle weight, combined weight and shoe leveler, or a clinical walking boot that restricted ankle joint motion and added mass. Load carrying was performed while holding 7.5% and 15% bodyweight dumbbells in one or two hands during symmetric gait and asymmetric gait induced by the walking boot.

The perturbations were successful in producing different degrees of gait asymmetry. However, L5/S1 joint forces were not significantly different between conditions despite unique spatiotemporal asymmetries. This indicates that LBP in those with gait asymmetry may not be due solely to level planar walking. During carrying tasks, gait asymmetry induced by the walking boot increased some metrics of lower back loading. Further, carrying a load in the hand contralateral to the walking boot produced larger forces than when carried on the same side. These results emphasize the importance of evaluating specific sources of gait asymmetry during daily activities other than walking when assessing LBP risk and would encourage more inclusive ergonomic carrying guidelines.

TABLE OF CONTENTS

Page

LIST OF TABLES

LIST OF FIGURES

CHAPTER 1

INTRODUCTION

The human spine has capabilities that differentiate us from other vertebrates (Gracovetsky, 1985). With its arrangement of vertebrae, intervertebral discs, nerves, muscles, and connective tissues the architecture of our back is engineered to provide structural support, proprioception, and movement control during a myriad of bipedal upright activities. Despite its shrewd design these structures are susceptible to pain, particularly in the lower back or lumbar region (Andersson, 1997; Hoy et al., 2012). Lower back pain (LBP) has been defined as pain between the pelvis and the twelfth ribs that limits activity for at least one day (Hoy et al., 2010b). The annual estimated financial burden associated with LBP is between $100 and $200 billion in the United States alone (Katz, 2006), with 9% of the general population affected at any given time (Hoy et al., 2014). This high socioeconomical burden has resulted in decades of research dedicated to identifying and mitigating the causes of LBP.

The origin of pain is complex and varies by an individual's perception and experience (Marras, 2008; Merskey and Bogduk, 1994), resulting in many LBP cases being diagnosed as idiopathic (Hoy et al., 2010a). However, identifiable sources of nociceptive pain from injury include the vertebral endplates, intervertebral discs, neural arches, ligaments, and muscles (Allegri et al., 2016; Golob and Wipf, 2014; Kuslich et al., 1991). High external loads and repeated awkward and asymmetric trunk postures and movements are well-established mechanical catalysts for these lower back injuries (Bernard, 1997; da Costa and Vieira, 2010; Hoogendoorn et al., 1999; Marras, 2000). Biomechanical models have demonstrated how large external loads are problematic because of the severe

mechanical disadvantage of the stressed internal force producing tissues (Chaffin, 1969; Morris et al., 1961; Troup, 1965). This mechanical disadvantage can worsen during awkward and asymmetric postures, triggering spinal instability and an increase in internal loading and risk of injury (Davis and Marras, 2005; Fathallah et al., 1998; Granata et al., 1999; Marras and Mirka, 1992; Marras and Sommerich, 1991a; Mital and Kromodihardjo, 1986). Prolonged or repeated loading without sufficient recovery time can lower a biological tissue's tolerance to injury in even seemingly benign or non-neutral postures (Marras et al., 2016).

Walking is a fundamental means of locomotion, with activities often generating thousands of steps per day (Tudor-Locke et al., 2011). It is widely recommended for aerobic and musculoskeletal conditioning, and can provide therapeutic relief from LBP (Nutter, 1988). However, a variety of pathological conditions and tasks can result in asymmetric gait, including congenital deformities, injury, disease, amputation, and load carriage (Cappozzo and Gazzani, 1982; Constantinou et al., 2014; Dananberg, 1993; Devan et al., 2014; DeVita et al., 1991; Friberg, 1983; Gulgin et al., 2018; Mündermann et al., 2005; Tanaka et al., 2015; Wolfe et al., 1996). Gait asymmetries are defined as bi-lateral differences in lower limb kinematics or kinetics (Sadeghi et al., 2000). Given the established relationships between LBP, tissue injury, asymmetric postures, and repeated loading, it is not surprising that gait asymmetries are related to LBP. The reported magnitude of the LBP prevalence in those with asymmetric gait is alarming, more than five times that of the general able-bodied population (Ehde et al., 2001; Giles and Taylor, 1981; Smith et al., 1999; Wolfe et al., 1996). Therefore, the cumulative lower back demands associated with asymmetrical gait are of interest to clinicians and researchers looking to

improve the quality of life in these LBP susceptible patients (Dananberg and Guiliano, 1999; Devan et al., 2014; Friel et al., 2005; Morgenroth et al., 2010).

To quantify lower back demands during able-bodied walking, *in vivo* lumbar loading has been directly measured with invasive techniques (Dreischarf et al., 2016; Fowler et al., 2006; Grillner et al., 1978; Nachemson and Elfstrom, 1970; Rohlmann et al., 2014a; Wilke et al., 1999). Spinal loads during gait can be 70% larger than in standing (Rohlmann et al., 2014a), while carrying a 20 kg crate in one hand can double spinal loads compared to standing (Rohlmann et al., 2014c; Wilke et al., 2001). These direct *in vivo* measurements are insightful but susceptible to methodological limitations and ethical concerns (Dreischarf et al., 2016; Wilke et al., 1999) and have not yet been applied to quantify spinal loads during pathological asymmetric gait. To overcome these issues, in the absence of an appropriate animal model, researchers have sought to improve our understanding of lower back demands by developing non-invasive *in silico* biomechanical models (Christophy et al., 2012; de Zee et al., 2007; El-Rich et al., 2004; Marras and Granata, 1997a; McGill and Norman, 1986; Schultz and Andersson, 1981; Stokes and Gardner-Morse, 1995; University of Michigan, 2017). Biomechanical models have been used to quantify peak vertebral loading and potential trunk muscle forces throughout the able-bodied gait cycle (Arshad et al., 2018; Callaghan et al., 1999; Cappozzo, 1984; Cheng et al., 1998a; Cromwell et al., 1989; Khoo et al., 1995), and to calculate lower back kinetic demands during asymmetric gait (Cappozzo and Gazzani, 1982; Hendershot et al., 2018; Hendershot and Wolf, 2014; McGill et al., 2013; Rose et al., 2013; Sagawa et al., 2011; Shojaei et al., 2016; Yoder et al., 2015; Yu et al., 2014). Lower back demands in clinical asymmetric gait have been estimated as 40 to 80% greater for amputees compared to able-

bodied individuals (Cappozzo et al., 1982; Shojaei et al., 2016), while similar increases have been observed for asymmetric versus symmetric load carriage (McGill et al., 2013; Rose et al., 2013). These added demands have been accredited to various "mal-adaptive" changes (Dananberg, 1993; Devan et al., 2014) in lower limb strength, kinematics, and kinetics throughout the gait cycle (DeVita et al., 1991; Hendershot and Wolf, 2014; Sagawa et al., 2011) and are hypothesized to lead to the increased incidence of injury and LBP.

Mal-adaptive gait asymmetries can present themselves in a variety of ways (Dananberg and Guiliano, 1999; Devan et al., 2014; Tazawa, 1997). In amputees, prosthetic devices often lack the necessary ankle range of motion and plantar flexion push-off capabilities observed during able-bodied gait (Sagawa et al., 2011). To overcome these limitations, amputees will increase hip torque, trunk movement, and stance time on their intact leg (Sagawa et al., 2011). Similar compensations have been observed in able-bodied individuals with injuries or deformities to the ankle or foot (Dananberg, 1993; Dananberg and Guiliano, 1999). Another form of gait asymmetry is caused by bi-lateral leg length differences, which exist in able-bodied, injured, and amputee populations (Beal, 1977; Gulgin et al., 2018; Knutson, 2005a; Yu et al., 2014). Discrepancies in leg length greater than 25 mm are associated with LBP and increased trunk demands (Friberg, 1983; Giles and Taylor, 1981; Khamis and Carmeli, 2017; Knutson, 2005b; Murray and Azari, 2015; Yu et al., 2014). Asymmetrically carrying a load can also induce gait asymmetries of increasing trunk lean, stance time, and lower limb abduction moments over the contralateral lower limb (DeVita et al., 1991; Wang and Gillette, 2018, 2017).

Despite a variety of origins, asymmetric gait lower back loading has been studied primarily in lower limb amputees (Devan et al., 2014; Sagawa et al., 2011). Individual

studies on amputees are often compromised by low participant numbers, a lack of a baseline comparison, and a large range of diversity in amputation and prosthetic type (Hafner et al., 2002; Highsmith et al., 2019; Nolan et al., 2003; van der Linden et al., 1999). Furthermore, such studies are not representative of other asymmetric gait populations such as those with leg length discrepancies or joint pain, nor do they fully encompass the daily rigors a clinical population may encounter throughout daily living (Actis et al., 2018b; Devan et al., 2014). Another approach is to study able-bodied participants with artificially-induced asymmetry through modified uni-lateral leg length, leg inertial characteristics, joint restrictions, casting, cadences, or speeds (Brown et al., 2018; Gulgin et al., 2018; Lemaire et al., 2000; Roemmich et al., 2012; Royer and Martin, 2005; Vanicek et al., 2007). Such controlled studies have provided a useful prospective on asymmetric gait in nonamputees and rehab patients, and in the study of underlying motor control processes. A controlled experimental setup that manipulates asymmetries in an otherwise healthy and homogeneous cohort could help us better identify how distinct lower limb bi-lateral differences affect lower back demands during walking and load as calculated with a biomechanical model.

Biomechanical models apply observed kinematics, mathematical equations, established anatomy, and biological assumptions to calculate internal kinetic demands that are impractical to measure *in vivo* (Dreischarf et al., 2016). Each model component contributes to the accuracy of the calculated lower back demand, and their impact on the calculated demands should be established (Hicks et al., 2015). A particularly crucial modeling decision is the implementation of a strategy to predict the internal active and passive tissue forces that are responsible for an observed kinematic response (Marras,

2000). This modeling dilemma arises because there are far more internal force-producing structures (i.e. muscles and ligaments) than there are equations of motion, resulting in an infinite number of possible solutions for individual tissue forces. In lieu of this, researchers often choose to neglect the influence of individual tissues altogether, reduce the number of muscles and ligaments to a deterministic number, or apply a generic optimization technique to quantify muscle recruitment (Bean and Chaffin, 1988; Chaffin, 1969; Kingma et al., 1996; Morris et al., 1961; Schultz and Andersson, 1981; Stokes and Gardner-Morse, 1995; Troup, 1965). These approaches fail to incorporate participant-specific responses to a given task and will often underestimate loading by neglecting antagonistic muscle contributions (Callaghan et al., 1999; Cholewicki et al., 1995; Kingma et al., 2001; Marras, 2008). Therefore, modeling methods incorporating electromyography (EMG) have been developed to represent participant-specific neuromuscular recruitment strategies (Cholewicki and McGill, 1994; Dolan and Adams, 1993; Gagnon et al., 2001; Granata and Marras, 1995a; McGill and Norman, 1986). By directly monitoring muscle activity, EMG-based models are well suited to identify participant-specific lower back demands associated with lower limb asymmetries of varying origins. Such EMG-driven lower back models have been used to estimate muscle forces and the resulting lower back demands during several ergonomic paradigms and able-bodied gait (Callaghan et al., 1999; Gagnon et al., 2018; Jia et al., 2011; Marras and Granata, 1997b; McGill et al., 2013; McGill and Norman, 1986; Rose et al., 2013; van Dieën and Kingma, 1999) but have not yet been used to examine lower back loading during gait asymmetries with or without load carriage.

In summary, the prevalence of LBP in asymmetric gait is very high, but research examining lower back loading during asymmetric gait is limited. To date, studies of

asymmetric gait kinetic demands on the lower back have focused primarily on amputees while using biomechanical models that were evaluated for manual materials handling with generalized muscular recruitment strategies. The proposed research will address these gaps in the literature through three related studies. In Study 1, a lower back musculoskeletal model will be developed from an existing OpenSim (Delp et al., 2007) model (Beaucage-Gauvreau et al., 2019; Christophy et al., 2012), and used to determine lower back kinetic demands with a participant-specific EMG-based optimization solution (Cholewicki and McGill, 1994; Gagnon et al., 2011). The Study 1 model will be used in Study 2 to investigate how various experimentally induced lower limb gait asymmetries affect lower back loading. Study 3 will use the same model to examine how bi-lateral and uni-lateral load carriage can impact lower back loading during lower limb gait asymmetries. By examining lower back loading under different conditions of gait and load carriage asymmetries, clinical strategies to reduce lower back demands could be developed to help improve the quality of life for a broad range of patients with asymmetric gait.

CHAPTER 2

REVIEW OF LITERATURE

This chapter reviews the lower back anatomy and physiology, how it is modeled mathematically and how the lower back can become stressed. Initially the anatomy, pain mechanisms, sites of injury, and pain epidemiology of the lower back are described (Section 2.1). Section 2.2 examines the methodologies and tools employed to mathematically model the lower back musculoskeletal system and determine kinetic demands. The third section (Section 2.3) provides an overview of gait, how the lower limbs are typically employed during a gait cycle and how they can adapt to various circumstances, particularly gait asymmetries. The chapter concludes (Section 2.4) by examining the lower back kinetic demands during normal and asymmetric gaits, with some reference to other tasks for comparison.

2.1. The Lower Back and Pain

This section will provide an anatomical background from which to better appreciate the intricate structure, injury mechanisms, and sources of pain of the lower back. Justification for this dissertation work will be demonstrated by highlighting the scope of lower back pain (LBP) both for the general population and for those with asymmetric gait.

2.1.1. Lower Back Anatomy

The lower back encompasses the area of the trunk between the pelvis and the twelfth ribs (Hoy et al., 2012), including the pelvis, fused sacral vertebrae, five lumbar vertebrae, intervertebral discs, spinal ligaments, surrounding muscles, nerves, vascular and other connective tissues (see Fig. 2.1.1).

The sacrum vertebrae and pelvis are attached at the sacroiliac joint. This largely immobile synovial joint permits the sacrum and pelvis to be modeled as a single rigid structure. The pelvis' size, caudal location, strength, and basin-like shape produce an ideal protective cavity for internal organs, points of attachment for powerful trunk and lower limb muscles, and an essential means of weight transfer between the lower and upper body via the femurs and fifth lumbar vertebrae, respectively.

The five lumbar vertebrae, identified incrementally from cranial to caudal as L1 to L5, are boney structures consisting of a vertebral body and an extending neural arch. These elements of the vertebrae resist loads, protect the spinal cord, restrict movement, and provide attachment points for muscles and ligaments (Adams, 2004). Gelatinous intervertebral discs, comprised of a nucleus pulposus surrounded radially by the fibers of the annulus fibrosus and longitudinally by vertebral end plates, form a symphyseal connection between adjacent lumbar vertebrae. Discs are categorized by the superior and inferior vertebrae sandwiching them (i.e. L5/S1). Largely avascular, most required metabolites are diffused across the disc endplates (Roberts et al., 2006). Acting as the fulcrum of a first-class lever, each disc permits some movement in all three anatomical planes while dampening the load transmission between adjoining vertebrae (Marras, 2008). While the lordotically stacked architecture of the lumbar spine allows the upper body center of mass to be ideally positioned over the supporting lower limbs (Lovejoy, 2005).

The lower back skeletal muscles are categorized as either global or local, depending upon whether they span the lower back (primarily the thoracic erector spinae, latissimus dorsi, rectus abdominals, internal and external obliques) or attach to a lumbar vertebral process (primarily the lumbar erector spinae, multifidus, intertransverse, psoas, and interspinal muscles), respectively (Bergmark, 1989). The larger and more distally positioned global muscles have more potential to

generate torques about the spine and provide most of the frontal plane spinal stiffness and overall strength to perform tasks (Rab et al., 1997). The more mechanically restricted local muscles maintain stability between vertebrae, while detecting and providing some control for vertebral positioning (Bergmark, 1989; Bogduk et al., 1992a; Cholewicki and McGill, 1996; Crisco and Panjabi, 1991). Muscles are essential to maintenance and control of spinal stability. In the absence of trunk muscles, a completely ligamentous lumbar spine would become laterally unstable at compressive loads well below body weight (Crisco and Panjabi, 1991).

Ligaments of the lower back include: the ligamentum flavum, supraspinous, interspinous, posterior and anterior longitudinal ligaments, and sacroiliac ligaments. Passively these ligaments help to maintain stability, aid disc positioning between the vertebrae, provide proprioception, and resist non-neutral movements (Gracovetsky et al., 1981; McGill and Norman, 1986; Panjabi, 1992; Solomonow, 2004). Energy from ligaments is 'free', in that it has no direct metabolic cost. Therefore, it has been suggested that ligaments are often utilized to save energy and aid mechanically disadvantaged muscles. This is most evident during extreme trunk flexion where the large ligamentous contribution to the extensor moment allows the lower back musculature to relax. Floyd and Silver (1955) coined this phenomenon "flexion-relaxation".

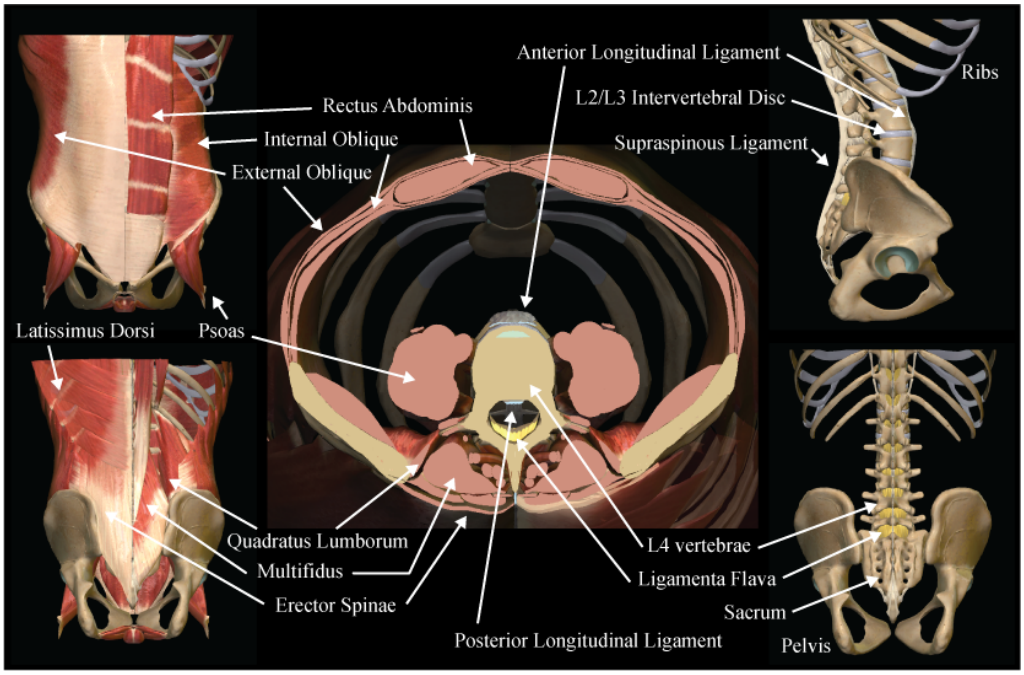

Figure 2.1.1 Anatomy of the lower back. Right panels: sagittal (top) and posterior (bottom) view of the axial and appendicular skeleton elements of the lower back including the intervertebral discs and select ligaments; left panels: anterior (top) and posterior (bottom) view of the trunk musculature (note: to highlight the different muscular layers the latissimus dorsi was made transparent, and the right sides of each panel had the outer most layer of muscles dissected); center panel: cross-sectional view of the trunk at the L4 vertebrae level. (Images courtesy of www.anatomylearning.com)

2.1.2. Sites of Lower Back Pain (LBP) and Injury

Merskey and Bogduk (1994) defined pain as "*an unpleasant sensory and emotional association with actual or potential tissue damage…*", while Robertson (2018) has defined injury as "*damage to the cells and organs from energy exposures…*" Nearly all the structures in the lower back are susceptible to injury or pain and have nociceptors to detect any unwanted stresses or damage (Adams, 2004; Bogduk, 1983). LBP is often diagnosed as idiopathic, in that the exact mechanism of pain is unclear (Braun et al., 2014; Deyo and Weinstein, 2001; Hoy et al., 2010a). However, frequently cited locations of lower back injury linked to nociceptive pain include vertebral body endplates, the posterior longitudinal ligament, the sacroiliac joint, the outer annulus of intervertebral discs, the apophyseal joints of the neural arch, musculotendinous junctions, and impinged spinal nerves (Allegri et al., 2016; Golob and Wipf, 2014; Kuslich et al., 1991). The

most common work-related diagnosis for LBP is the result of a strain to the musculature (Andersson, 1997). Muscular pain can be linked with tissue damage, fibromyalgia, or restricted blood flow due to fatigue (Marras, 2008). Muscles are also indirectly associated with injuries to the vertebrae and discs. The high muscular forces inflicted upon the spine result from the mechanical disadvantage of the muscles relative to the external forces they counter (Fig. 2.1.2a). Collectively the external and internal forces elicit compression and shearing loads upon the vertebral structures and discs. The most vulnerable site of injury from acute or repeated compressive loading are the end plates of the vertebral bodies (Brinckmann, 1986; McGill, 2007). Compressive loads of between 2,000 – 10,000 Newtons (N) in cadaver specimens can elicit microfractures in the end-plates (Jäger and Luttmann, 1989). Shearing, bending, and twisting forces can cause damage at forces as low as 750 N to either the ligaments, discs, end plates or facet joints (Adams, 2004; Gallagher and Marras, 2012). The majority of these compression and shear injuries occur where their magnitudes upon the spine are the greatest, between the most caudal (5^{th}) lumbar and the first sacrum vertebras (Andersson, 1997; Arjmand et al., 2006).

Though the aforementioned thresholds may seem high and difficult to obtain, they can be surpassed during a strenuous lift, awkward posture, or even unpredictably during submaximal tasks (Chaffin, 1969; Cholewicki et al., 1991; McGill and Norman, 1985). Furthermore, tissue tolerances vary and can be affected by age, recovery time, training, body position, and pathologies. Under such circumstances, tissue injury thresholds can diminish to levels that would have otherwise been considered harmless (Fig. 2.1.2b; Adams, 2004; Brinckmann, 1986; Brinckmann et al., 1988; Marras et al., 2016; McGill, 2007).

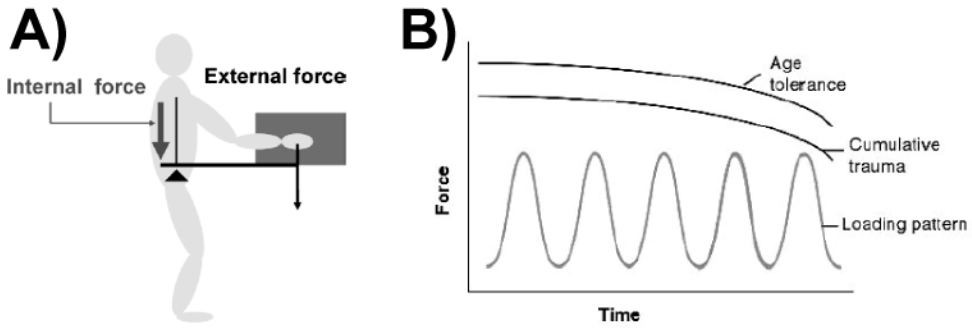

Figure 2.1.2 Figures depicting A) the mechanical disadvantage of the internal lower back and B) theoretical tissue tolerance degradation resulting from age or repetitive loading. (Images adapted from Marras (2008))

2.1.3. Lower Back Pain Epidemiology

LBP has been defined as activity-limiting pain in the lower back lasting for at least one day (Hoy et al., 2010b). It is been recognized as the primary cause of activity limitation and missed days from work (Bigos et al., 1994; Yang et al., 2016). With a lifetime prevalence estimated to be as high as 84% and point prevalence of over 9%, LBP ranks as the largest contributor to years lived with a disability, fifth among motives for visiting a physician, and is the leading cause of disability globally (Buchbinder et al., 2013; Hart et al., 1995; Hoy et al., 2014; Walker, 2000)). In total, the financial burden associated with LBP has been estimated to be between $100 and $200 billion a year and growing (Balague et al., 2012; Freburger et al., 2009; Hoy et al., 2012; Katz, 2006; Liberty Mutual Research Institute for Safety, 2018). Many factors increase the probability of experiencing LBP, including those related to social (work satisfaction, personality type, mindset, and compensation), mechanical (heavy physical work, awkward dynamic postures, shear loads, and lifting) and biological (age, anthropometry, chemical dependence, gender, leg length discrepancy, and lower body injury or amputation) phenomena (Andersson, 1999; da Costa and Vieira, 2010; Ehde et al., 2001; Marras et al., 2016, 1995; Norman et al., 1998).

In some specific populations, individuals with gait asymmetries have reported LBP point prevalence as high as 71% (Devan et al., 2012; Ehde et al., 2001; Ephraim et al., 2005; Parvizi et

al., 2010; Smith et al., 1999; Wolfe et al., 1996). Gait asymmetries are defined as bi-lateral differences in lower limb kinematics or kinetics (Sadeghi et al., 2000). For those with asymmetries as a result of lower limb amputation (LLA), LBP is often cited as being more bothersome and prevalent than other commonly reported secondary pains like phantom limb or residual limb pain (Smith et al., 1999). Those with gait asymmetries resulting from knee, hip or foot pain suffer from LBP on a similar scale (Parvizi et al., 2010; Wolfe et al., 1996). The high association of LBP with asymmetric gait is not fully understood, but has been linked to residual-limb problems, decreased back muscle extensor strength, leg length discrepancies, a higher body mass index, and greater lower back tissue loading (Dananberg and Guiliano, 1999; Devan et al., 2017; Friberg, 1984; Friel et al., 2005; Giles and Taylor, 1981; Knutson, 2005b; Murray and Azari, 2015).

Individuals with gait asymmetries may only represent a small subset of the total population, however the prevalence of such asymmetries is on the rise (Zhang and Jordan, 2010; Ziegler-Graham et al., 2008). Better identification of kinematic and kinetic factors that influence lower back loading could potentially help reduce the impact of LBP on those who exhibit asymmetric gait.

2.2. Lower Back Biomechanical Models

Biomechanics is defined as, "… the study of forces acting on and generated within a body and of the effects of these forces on the tissues, fluids or materials used for diagnosis, treatment or research purposes" (National Research Council, 2001). Due to ethical concerns, the magnitude and distribution of forces internal to the body cannot be measured directly. Therefore, in silico biomechanical models of the lower back have been developed to estimate these illusive internal forces (Bogduk et al., 1992a). Biological models provide researchers a platform to quantitatively describe and expand their interpretation of the lower back system. This section will detail how

biomechanical models of the lower back have evolved, where they are today, and how they can best be applied and evaluated to examine the injury risk of the lower back during asymmetric gait.

2.2.1 The Evolution of Lower Back Modeling

Through rigid-body assumptions and the application of Newton-Euler equations, inverse dynamic modeling techniques can determine the reaction forces and moment demands of a system during a defined task. Beginning over 100 years ago, early biomechanists Braun, Fischer, and Eltman were amongst the first to represent the body as a series of linked rigid-bodies and apply inverse dynamics techniques to study human motion (Selbie et al., 2014). Similar biomechanical models specific to the lower back were later constructed (Fig. 2.2.1; Davis and Jorgensen, 2005; Fisher, 1967). Building upon these pioneering works, lower back models would soon feature a deterministic number of internal force generating mechanisms, i.e. muscles and ligaments, to better estimate spinal demands (Chaffin, 1969; Morris et al., 1961; Troup, 1965). Determinacy in this instance refers to there being enough system equations to solve for the unknown variables. Despite such simplifications to the anatomy, the results from these landmark works were well correlated with measured levels of muscle activation, joint torque potential, and intra-abdominal pressure. Furthermore, they provided invaluable insights into the demands of the lower back during sagittal plane lifting tasks and eventually helped establish workplace standards for manual materials handling tasks (NIOSH, 1981; Waters et al., 1993).

As processing speed and memory evolved with increases in computing power, so did lower back biomechanical models. Optimization software algorithms and measured muscular activation have allowed researchers to expand beyond a deterministic number of muscles and take into consideration each participant's recruitment strategy (Brown and Potvin, 2005; Cheng et al., 1998b; Cholewicki and McGill, 1994; El-Rich et al., 2004; Gagnon et al., 2001; Gracovetsky et

al., 1977; Granata and Marras, 1995a; Jäger and Luttmann, 1989; Marras and Sommerich, 1991b; McGill and Norman, 1986; Nussbaum et al., 1995a; Schultz and Andersson, 1981; Stokes and Gardner-Morse, 2001; van Dieën, 1997). Computer advancements and data acquisition techniques have continued to permit more comprehensive representations of internal forces, quantification of dynamic movements, and the examination of three-dimensional movement tasks (Ayoub and El-Bassoussi, 1976; de Looze et al., 1992; Fisher, 1967; Freivalds et al., 1984; Kingma et al., 1996; McGill and Norman, 1985; Plamondon et al., 1995). As a result, in the past 20 years, biomechanists have developed more biologically complete and individual-specific lower back models that more precisely include biological features such as inter-abdominal pressure (IAP) (Arjmand and Shirazi-Adl, 2006a; Daggfeldt and Thorstensson, 1997; Stokes et al., 2011), Hill-type muscle model properties (Christophy et al., 2012), non-linear muscle paths (Hwang et al., 2017), vertebral compression loading responses (Shirazi-Adl, 2006), partitioning of muscles into multiple muscle slips (de Zee et al., 2007; van Dieën and Kingma, 1999), translating points of rotation (Ghezelbash et al., 2015), and balancing moments at multiple lumbar levels (Arjmand and Shirazi-Adl, 2006a; Stokes and Gardner-Morse, 1995). The additional computational cost of some of these features is not always warranted. All features have trade-offs to consider. Therefore, a key to effective modeling is to decide which biological and modeling design features are necessary to answer a research objective (Marras, 2008).

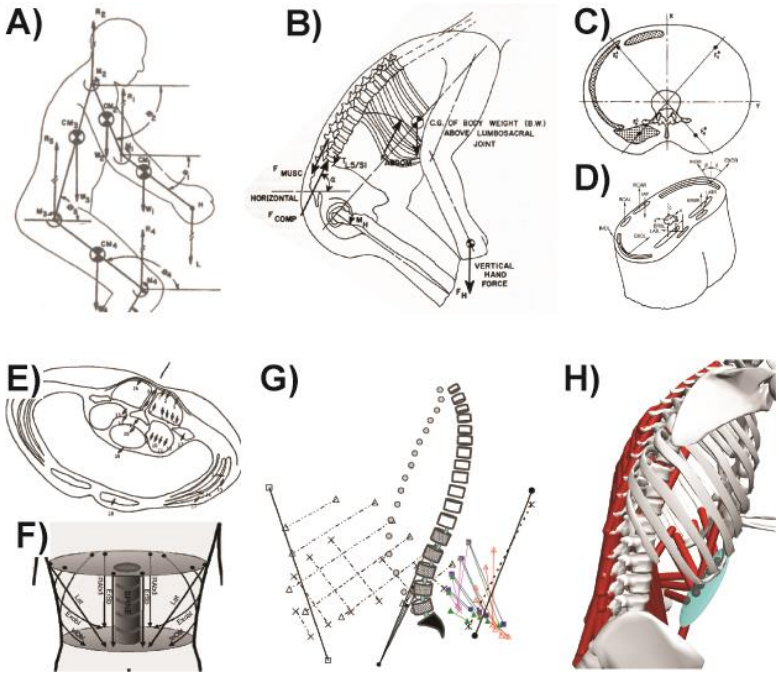

Figure 2.1.3 Select biomechanical models of the lower back. Panel A) Chaffin (2006), B) Chaffin (1969), C) Cappozzo and Gazzani (1982), D) Schultz and Andersson (1981), E) McGill and Norman (1986), F) Marras and Granata (1995), G) El-Rich et al. (2004), and H) Beaucage-Gauvreau (2019). See specified references for complete details of each model.

2.2.2. Approaches to Solving Indeterminacy

Each model component can contribute to the accuracy of the calculated lower back demand. A critical modeling decision is how to distribute the internal active and passive tissue forces that are responsible for an observed kinematic response (Marras, 2000). When the model incorporates more unknown internal force-producing structures (i.e. muscles and ligaments) than independent equations of motion, there are an infinite number of possible solutions that can satisfy the kinetic demands of the task (Schultz, 1990). As previously stated, researchers often choose to either neglect individual tissues altogether, reduce the number of muscles to a deterministic number, apply a generic optimization technique, or use physiological information to quantify muscle recruitment (Callaghan et al., 1999; Chaffin, 1969; Dolan and Adams, 1993; Dreischarf et al., 2016; Granata and Marras, 1995a; Hansen et al., 2006; Kingma et al., 2001, 1996; Marras,

2008; McGill and Norman, 1986; Morris et al., 1961; Schultz and Andersson, 1981; Stokes and Gardner-Morse, 1995; Troup, 1965). There are tradeoffs associated with each approach. Neglecting or reducing the number of muscles to a deterministic number of results in a straightforward solution, but these methods fail to properly represent the complexities of the lower back anatomy and the control strategies of the central nervous system. Therefore, such simplified models do not accurately quantify joint loading, especially during asymmetrical tasks (Marras, 2000; Schultz, 1990). Optimization techniques such as minimizing the sum of the squared muscle activation (Crownshield and Brand, 1981) can accommodate a large number of unknown forces and balance joint moment demands, but do not take into consideration individual subject recruitment strategies between participants or antagonistic muscle coactivations (Gagnon et al., 2001). The opposite is true for directly applying measured physiological responses (electromyography or EMG) to help solve the redundancy issue, as EMG-driven models reflect individual recruitment strategies but have difficulty in satisfying all the joint moment demands (Cholewicki et al., 1995; Lloyd and Besier, 2003; van Dieën, 2005).

In light of the aforementioned limitations, an EMG optimization method (EMGopt) was developed by Cholewicki and McGill (1994). By minimally adjusting the measured EMG activations to match the calculated joint demands, EMGopt is capable of mediating the flaws of both the optimization and EMG approaches while simultaneously incorporating their advantages (Choi and Vanderby, 1999; Cholewicki et al., 1995; Gagnon et al., 2001; Li and Chow, 2019). EMGopt delivers balanced joint moments that are inspired by individual recruitment strategies.

2.2.3. Defining Trunk Musculoskeletal Model Strength Potential

The torque generating potential of the trunk musculature can be affected by age, health status, trunk position, direction, and gender (Burkhart et al., 2018; Graves et al., 1990). During

neutral postures, sagittal plane strength is roughly 100 and 300 Nm for flexion and extension, respectively (Graves et al., 1990; Kienbacher et al., 2014; Smidt et al., 1983; Troup and Chapman, 1969). Individually adjusting the strength potential of a musculoskeletal model to better match an individual's capabilities can improve model fidelity (Davis and Jorgensen, 2005). Overall model strength can be modified by adjusting the number of muscles contributing to a given moment, contributions from antagonistic co-contraction, the associated muscle moment arms about a given joint, muscle pennation angle, muscle dynamics, and the prescribed physiological cross-sectional area (PCSA) and maximal muscular stress (MMS) of each muscle (Umberger and Caldwell, 2014).

PCSA (cm^2) and MMS (N/cm^2) interact to provide a maximal isometric force (N) for each muscle. PCSA is the cross-sectional area of a muscle taken perpendicular to the muscle fibers, or the muscle volume divided by the fiber length. PCSA can be measured from either cadaver dissections or medical images (Caldwell, 2014; Narici, 1999). MMS, or specific tension, is a measure of the force per cross-sectional area of a muscle. MMS can vary between muscles and is difficult to directly define from *in vivo* experimentation (Buchanan, 1995). Therefore it is often assumed to be constant across muscle groups and is calculated indirectly from the ratio of a recorded maximum joint moment and the sum of the products of muscle moment arms and PCSA (Buchanan, 1995). In musculoskeletal models, MMS can be conceptualized as an adjustable gain to fine-tune or evaluate a model's force producing potential (Granata and Marras, 1995a; van Dieën, 2005). For the trunk muscles, reported values range between 25-130 N/cm^2 (Bogduk et al., 1992b; Daggfeldt and Thorstensson, 2003; Hwang et al., 2016; McGill and Norman, 1987; van Dieën, 2005).

2.2.4. The Hill-Type Muscle Model

To compute the force potential of individual muscles and fascicles in their musculoskeletal models, many use some variation of a model developed by Nobel laureate A.V. Hill (Caldwell, 2014; Hill, 1938; Millard et al., 2013; Zajac, 1989). The "Hill-type model" estimates force based on the state of the musculotendon unit relative to some predefined physiological characteristics. Each Hill-type muscle traditionally has three separate components that contribute to force and represent aggregate structural behaviors of the muscle (Millard et al., 2013; Thelen, 2003; Zajac, 1989), including the contractile (CC), series elastic (SEC), and parallel elastic (PEC) components (Fig. 2.2.2a).

The intent of muscle is to produce force (Chapman, 1985). The CC represents active force production controlled by excitation signals from the central nervous system to produce force. The CC force depends on the optimal force (see Section 2.2.2), length, velocity, and activation level of the muscle fibers. There is an optimal length from which a muscle can produce the most force. Any deviation from this length reduces the muscles force potential. In Thelen's (2003) mathematical representation of the Hill-type model, the force-length property of the CC for each muscle is represented by a Gaussian function peaking at a muscle specific optimal fiber length and a common shape factor (Fig. 2.2.2b). Similarly, muscle force potential also depends on the rate of the shortening or lengthening. The force-velocity properties for eccentric and concentric contractions are modeled with rectangular hyperbolas on opposing sides of a muscle specific isometric force potential (Fig. 2.2.2c). The CC force is further dictated by its activation level, with a nonlinear relationship reflecting the neural excitation to activation process associated with the intent of the central nervous system and the initiation of force within the muscle fiber. The resulting CC force is applied to the passive SEC prior to transmission to a body segment. The

SEC responds to this CC force via a nonlinear elastic force-extension relationship according to tendon strain properties and a resting slack length (Zajac, 1989). The SEC length changes influence the CC kinematics. Therefore, the passive SEC indirectly influences the active force capabilities through the CC force-length and force-velocity characteristics that are linked to the tendon dynamics. The PEC behaves independently from both the CC and the SEC. It encompasses the passive nonlinear elastic behavior of muscle in the absence of CC activation and is defined with a standard shape factor and passive strain linked to the isometric potential of the muscle (Zajac, 1989). When the CC is activated, the force from the PEC combines with the CC force to produce the total force exerted by a muscle at both its insertion and origin.

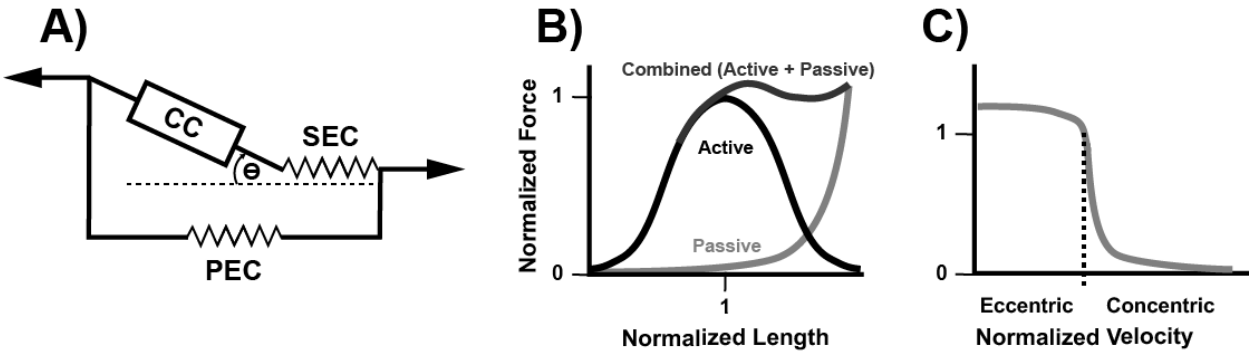

Figure 2.2.1 A Hill-type muscle model. Panel A) the three-components of the Hill-type muscle model including the contractile (CC) at a prescribed pennation angle (Θ), series elastic (SEC), and parallel elastic (PEC) components, B) the normalized force-length relationship of the active CC, the passive PEC, and their combined total force, C) the normalized force-velocity relationship of the CC. (Images adapted from Thelen (2003))

2.2.5. Lower Back Models Applied to Gait

In the early 1980s, Aurelio Cappozzo was the first to apply biomechanical modeling techniques to study loading in the lower back during both normal and asymmetric gait. His models were three-dimensional but only assigned a determinant number of back muscles (bi-lateral flexors and extensors) to be responsible for the calculated joint kinetics. He computed L3/L4 vertebral compression by assuming the minimal amount of muscle activation necessary to simultaneously

balance the sagittal and frontal plane L3/L4 disc level moments from a top-down link-segment model (Cappozzo, 1984, 1983, 1981; Cappozzo et al., 1982). Although this was a relatively simple model, the results compared favorably to in vivo measurements of intradiscal pressure (Nachemson and Elfstrom, 1970) and to measured EMG recordings (Cappozzo, 1981; Cappozzo and Gazzani, 1982).

Over the next thirty-years, there were a limited number of investigations and modeling changes applied to the examination of lower back gait loading (Callaghan et al., 1999; Cromwell et al., 1989; Khoo et al., 1995). Cromwell et al. (1989) repurposed a detailed 22-muscle lower back model (Schultz and Andersson, 1981) to calculate muscle and L3/L4 compressive forces in normal gait based upon the EMG from calibrated tasks. Khoo et al. (1995, 1994) developed a two-dimensional model that incorporated IAP and calculated shear loads during normal gait. In one of the more thorough studies of lower back loading during gait, Callaghan et al. (1999) compared a variety of cadences applying both a three-dimensional bottom-up link-segment model and an anatomically detailed, EMG-driven spine model which included passive ligamentous structures (McGill and Norman, 1986). Their results demonstrated, among other things, that the upright and near neutral postures maintained throughout gait permit only small passive contributions to joint moments. In contrast, consideration for muscular forces can more than triple compressive loading estimates (Callaghan et al., 1999).

More recent studies of lower back loading during gait have utilized highly detailed models based in AnyBody (AnyBody Technology A/S, Aalborg, Denmark) and OpenSim (SimTK, Stanford, CA; Actis et al., 2018b; Angelini et al., 2018; Arshad et al., 2018; Raabe and Chaudhari, 2016; Yoder et al., 2015), finite element modeling techniques (Hendershot et al., 2018; Shojaei et al., 2016), established lifting models (McGill et al., 2013; Rose et al., 2013), or reverted back to

more straightforward link-segment models (Hendershot and Wolf, 2014; Seay et al., 2008; Yu et al., 2014). These approaches have been applied across a variety of gait conditions and tasks and have demonstrated that bottom-up approaches are more sensitive to transient foot-ground contact factors (Callaghan et al., 1999; Hendershot and Wolf, 2014), loading varies by lumbar level (Arshad et al., 2018; Rose et al., 2013; Shojaei et al., 2016), and IAP forces can reduce joint demands (Arshad et al., 2018). For more details on the lower back loads these models have calculated across a variety of tasks, see Sections 2.4.4. – 2.4.6.

2.2.6. OpenSim

OpenSim is an open-source software platform that allows users to readily construct and share musculoskeletal models (Delp et al., 2007). It was developed to improve the transparency of biomechanical models and accelerate our understanding of the human system by combating the difficulty of distributing musculoskeletal models outside of their laboratory of origin. Since its inception, hundreds of musculoskeletal models have been developed and refined by research teams from around the world. Most of these models are freely available to the public on the SimTK website (https://simtk.org/projects).

Within OpenSim there are several modeling tools that can be applied to analyze measured motion capture data. The *scaling* tool scales a given model to match a participant's size, based on the relative distances between pairs of markers during a calibration pose (Delp et al., 2007). The *inverse kinematics* tool calculates the generalized coordinates of each body segment during a recorded motion, using a least-squares method to minimize the difference between the recorded kinematics and the model while accounting for the joint constraints of the model. If external kinetics are available, the kinematics can be further refined with a *reduce residuals* tool which minimizes the differences between the subject and model by subtly adjusting the segmental mass

properties. This step allows the model to become more dynamically consistent, better representing Newton's law of acceleration (Delp et al., 2007), but requires an accurate representation of all external reaction forces. The *inverse dynamics* tool can be applied to determine the net joint reactions and moments during recorded motion following kinematic analysis. Further analyses with either the *static optimization* or *computed muscle control* tool can be used to determine muscle forces that can produce the calculated joint moment demands (Delp et al., 2007; Thelen and Anderson, 2006). *Joint reaction analysis* can be performed to determine the combined effect of reaction and muscular loading on a 'tissue' of interest. These OpenSim tools can be accessed with a Graphical User Interface, an application programming interface (API), or other third-party scripting languages (Lee and Umberger, 2016; Mansouri and Reinbolt, 2012; Seth et al., 2011).

2.2.7. OpenSim Lower Back Model(s)

Christophy et al. (2012) developed the first detailed OpenSim model of the lower back, closely resembling an earlier commercial model (de Zee et al., 2007). The Christophy et al. (2012) model features a rigid sacrum welded to a rigid pelvis, a rigid torso, and five lumbar vertebrae. Lumbar segment motions are controlled by 238 Hill-type muscle fascicles representing the eight primary muscle groups of the lower back (Hill, 1938; Thelen et al., 2003; Zajac, 1989). The eight bi-laterally symmetric muscle groups featured in the model are the erector spinae, rectus abdominis, internal obliques, external obliques, psoas major, quadratus lumborum, multifidus, and latissimus dorsi. Properties of individual muscles (i.e. attachment sites, moment arms, maximal isometric force, pennation angle, fiber length, and stiffness) and segments (i.e. axis of rotation, inertia, mass, and size) were based upon referenced literature (Christophy et al., 2012). Each of the five lumbar vertebrae are connected to adjacent vertebrae by six degree-of-freedom joints, though the lumbar region as a whole has only three degrees-of-freedom. Kinematic constraints

are imposed that negate translational movement between joints and the individual rotations of each lumbar vertebrae are expressed relative to the rotation between the thorax and pelvis (Fujii et al., 2007; Rozumalski et al., 2008; Wong et al., 2006). Other simplifications for added usability of the model include neglecting the passive contribution of ligaments, facet joints, and intra-abdominal pressure. The model was evaluated by comparing computed model muscle moment arms at various flexion and extension angles with those reported in the literature.

Several research teams have further developed the original Christophy et al. (2012) model to satisfy their own research objectives (Actis et al., 2018a; Beaucage-Gauvreau et al., 2019; Bruno et al., 2015; Meng et al., 2015; Raabe and Chaudhari, 2016; Senteler et al., 2016; Zhu et al., 2017). Both Meng et al. (2015) and Senteler et al. (2016) implemented stiffness matrices to better define the movement between vertebrae in place of kinematic restraints that reduced muscular demand and vertebral loading (Meng et al., 2015). Bruno et al. (2015) further developed the thoracic segment of the model to include articulating thoracic vertebrae and ribs and homogenized muscle properties. Three groups (Actis et al., 2018a; Raabe and Chaudhari, 2016; Zhu et al., 2017) each independently increased the functionality of the model by integrating it with other OpenSim musculoskeletal models of the neck, lower, and upper bodies (Anderson and Pandy, 1999; Arnold et al., 2010; Delp et al., 1990; Hamner et al., 2010; Holzbaur et al., 2005; Vasavada et al., 1998). These full-body models have up to 324 muscle fascicles, 23 body segments, and 49 degrees of freedom and have been used to examine lower back loading during fatigued running (Raabe and Chaudhari, 2018), lifting (Beaucage-Gauvreau et al., 2019; Kim and Zhang, 2017), and amputees during sit-to-stand (Actis et al., 2018b) tasks. Prior to implementation, each model was indirectly evaluated against the existing literature or more directly with measured demands from their own

participants (Nachemson, 1965; Raabe and Chaudhari, 2016; Sato et al., 1999; Takahashi et al., 2006; Wilke et al., 2001).

2.2.8. Evaluation of a Biomechanical Model

Variability and errors for lower back model predictions can result both from inconsistency in participant task performance and assumptions within the model (Granata et al., 1999; Marras et al., 1999b; Mirka, 1991; Nussbaum et al., 1995b; Sparto et al., 1998). In order to have confidence in predicted output measures and avoid faulty inferences, a model should first be validated. Validation is a process in which model outputs are compared to real-world results (Thacker, 2001). Unfortunately, our inability to ethically and accurately quantify internal forces in the body makes validation nearly impossible (Oreskes et al., 1994). In lieu of a 'gold standard' with which to validate a given model, there are a number of established best practices that can help us evaluate our results and instill confidence in the predictions from a model (Anderson et al., 2007; Hicks et al., 2015; Lewandowski, 1982).

Musculoskeletal models of the lower back should be built on the basis of well-established natural laws, discriminate between cause and effect, and be deterministic (Cholewicki and McGill, 1996). Lewandowski (Lewandowski, 1982) and Hicks et al. (2015) have both proposed processes of component evaluation, internal validity checks, sensitivity analysis, peer evaluation, implications of assumptions, minimizing complexity, and judgmental evaluation. These recommendations suggest that larger models should be based upon component sub-models that preserve physical laws and that have been directly validated whenever possible, or evaluated when only indirect methods are available (van den Bogert and Nigg, 2006). The effect that each input variable has on the model output should be determined within a realistic range, be both logical and explainable, and compared with available data and other applicable models. Each of these steps

present challenges, but such demands are not insurmountable and are necessary to better ensure that predictions from models can advance their field of application (Hicks et al., 2015).

2.3. Gait

This section on gait will focus on lower limb kinematics and kinetics, specifically in normal able-bodied gait and some forms of abnormal or perturbed gait related to asymmetries. The aim of this section is to provide information about how the lower limbs adapt to different gait demands. The effect of these adaptations on the lower back will be addressed in the subsequent section (Section 2.4.). Neurologically modified gait (i.e. from a stroke or diabetes, see reviews by Lauziere et al. (2014) and Alam et al. (2017)) will not be discussed further, nor will prosthetic designs and their effect on gait (see Godfrey et al. (1977), Selles et al. (1999), and Hafner et al. (2002)).

2.3.1. Gait Lower Limb Kinematics and Kinetics

Walking is a fundamental method of bipedal locomotion which allows movement of the body from point-to-point (Saunders et al., 1953). Healthy individuals walk at an average speed of 1.32 m/s (Boyer et al., 2017) and are recommended to take upwards of 10,000 steps each day to promote good health and to maintain aerobic and musculoskeletal conditioning (Nutter, 1988; Tudor-Locke et al., 2011).

A step results each time a foot strikes the ground in the direction of progression, regardless of limb side. A gait cycle consists of two consecutive steps, or a single stride, and is subdivided into a limb's stance and swing phase. The stance, or support, phase incorporates the portion of the gait cycle where the foot is contact with the ground. Stance phase can be further subcategorized sequentially by the initial heel strike, mid-stance, and terminal toe-off instances (Vaughan et al.,

1999; Winter, 1987). Double support periods occur at the beginning and end of each stance and differentiate walking from running (Gage, 1990; Novacheck, 1998). The swing phase consists of initial, mid, and terminal swing phases (Vaughan et al., 1999; Winter, 1987). Steps and strides are often quantified both temporally and spatially. Step lengths are calculated as the distance between contralateral feet at heel strike (Finley et al., 2015; Zatsiorky et al., 1994) and average 0.70 meters over a 0.52 second duration for healthy young adult gait (Boyer et al., 2017).

The center of mass travels in a sinusoidal path throughout the gait cycle in both the sagittal and transverse planes, reaching its vertical and lateral zeniths near midstance in single support and vertical nadirs in mid-double support (Saunders et al., 1953). The lower limbs aid in propelling the center of mass along this path of progression. At heel contact the hip is flexed and knee is extended while the ankle joint is relatively neutral. The initial braking resistance of the ground is cushioned with a resistive internal dorsiflexor moment at the ankle and subtle internal flexion moment at the knee. During single support, the ankle plantarflexes as the hip and knee extend. Both the hip and ankle internal joint moments facilitate in progressing the body and keeping it upright against gravity. The ankle maintains a plantarflexion moment throughout the rest of stance, however prior to toe-off the hip begins to slow down it's extension in preparation of the swing phase. Meanwhile, the knee is controlled by a flexion moment due to the active ankle plantar flexor gastrocnemius which also crosses the knee joint and leads to a slightly flexed knee posture to help dampen impact stresses. In the frontal plane, strong hip abductors minimize pelvic and trunk drop throughout stance. The propulsion power produced by the ankle and hip during terminal stance minimizes the amount needed to actively swing the leg in the direction of progression. During swing, some ankle dorsiflexion and knee flexion is necessary for toe clearance and to facilitate transfer of angular momentum. At terminal swing, hip extensor and

knee flexor joint moments slow down the leg's momentum and prepare for contact with the ground as the cycle begins again (Gage, 1990; Winter, 2009). Leg dominance can lead to some bi-lateral kinematic, kinetic, and functional differences in normal able-bodied individuals, but these magnitudes are typically minimal and insignificant (Dingwell et al., 1996; Gage, 1990; Gundersen et al., 1989; Hannah et al., 1984; Herzog et al., 1989; Sadeghi et al., 2000; Zatsiorky et al., 1994).

2.3.2. Clinical Gait Asymmetries

Clinical abnormalities such as uni-lateral lower limb amputation (LLA), presence of osteoporosis in the leg joints, and casting most often result in slower and mal-adaptive gaits (Constantinou et al., 2014; Dananberg and Guiliano, 1999; Froud et al., 2014; Gulgin et al., 2018). During stance, for both transtibial and transfemoral LLA gait, the hip joint will increase power production in lieu of the ankle plantar flexion to propel the center of mass and initiate leg swing (Sagawa et al., 2011). Stance times and knee flexion angles of the prosthetic limb are often reduced relative to the contralateral side, an adaptation that is accredited to user uncertainty in the stability of the prosthetic and knee joint (Sagawa et al., 2011; Sanderson and Martin, 1997). Many amputees increase frontal plane pelvic obliquity to void tripping because they can no longer voluntarily dorsiflex the ankle during mid swing (Su et al., 2007). Furthermore, the pelvis has been shown to increase its transverse plane range of motion to help maintain a preferred step length (Rabuffetti et al., 2005; Rueda et al., 2013). Similar compensations can occur in non-amputees with uni-lateral osteoporosis, injuries, or deformities to the leg (Constantinou et al., 2014; Dananberg, 1993; Dananberg and Guiliano, 1999; Ornetti et al., 2010).

Nearly 90% of the general population display leg-length asymmetry that averages around 5 mm (Knutson, 2005a). However, clinically significant levels of leg-length asymmetry of 20 mm are only prevalent in only 2.6% of the population (Gross, 1978; Knutson, 2005a). Adolescents are

often the population of interest for leg-length inequality studies (Kaufman et al., 1996; Perttunen et al., 2004), with the objective of diagnosing the condition in time for corrective measures. Studies in leg-length inequality have presented stance times, ground reaction forces, hip flexion, knee flexion, hip abduction, pelvic obliquities, and knee extensor moments that are typically greater for the longer limb (Gofton, 1971; Kaufman et al., 1996; Khamis and Carmeli, 2017; Liu et al., 1998; Perttunen et al., 2004; Walsh et al., 2000). These compensations are hypothesized to occur in attempt to lengthen the shorter limb, and to shorten the longer limb (Assogba et al., 2018; Kaufman et al., 1996; Khamis and Carmeli, 2017; Walsh et al., 2000).

Casting and walking boots are used to restrict the ankle joint following orthopedic injuries. These interventions not only limit the ankle joint's mobility and increase the mass of the lower limb, but also result in an inequality of leg-lengths due to the boot/cast's sole thickness. Therefore, the lower limb gait kinematics and kinetics of the knee, hip, and pelvis generally resemble those reported for individuals with leg-length inequalities and LLA (Gulgin et al., 2018; Pollo et al., 1999; Powell et al., 2012; White et al., 1999; Zhang et al., 2006).

2.3.3. Artificial Gait Asymmetries

There are several scenarios where gait can be acutely asymmetrical or unnatural. Load carriage is a common everyday task that involves transporting an object from one location to another. Historically, load carriage research has focused on the energetics demands in combat soldiers (Goldman, 1962; Knapik et al., 1996; Legg, 1985; Lind and McNicol, 1968), however there are numerous studies examining biomechanical adaptions (e.g. Badawy et al., 2018; Seay, 2015). Self-selected walking speed during load carriage is typically lower than during normal gait (Nottrodt and Manley, 1989; Zatsiorky et al., 1994). Loads can be carried in a pack (i.e. backpack,

sidepack, or rucksack) or in the arms either bimanually or one-handed (Datta and Ramanathan, 1971; Legg, 1985).

Martin and Nelson (1986) revealed that during rucksack load carriage of up to 36 kg, stride length and swing time decrease while stride rate, trunk forward inclination angle, and double-support time all increase. In addition, increased hip flexion angles, greater knee flexion, increased ankle dorsiflexion, ankle and knee work, and increased pelvic anterior tilt have been identified as biomechanical adaptations to symmetrical rucksack and backpack load carriage (Huang and Kuo, 2014; Knapik et al., 1996; Majumdar et al., 2010; Seay, 2015; Wang et al., 2013). Asymmetrical carriage of a sidepack, loaded up to 20% of a participant's body weight can produce large differences in the contralateral frontal plane demands of the lower limb (DeVita et al., 1991). These kinematic adaptations to load carriage have been accredited to a modified center of mass location, and an attempt to reduce the lower limb kinetic demands brought on by the added load (Chow et al., 2005; Seay, 2015; Tilbury-Davis and Hooper, 1999; Wang et al., 2013).

Single arm load carriage increases the support time and hip demands of the contralateral leg, ipsilateral leg toe-out during stance, and overall step width (An et al., 2010; Bergmann et al., 1997; Crowe and Samson, 1997; Neumann, 1996; Wang and Gillette, 2018; Webb and Bratsch, 2017). Bi-lateral load carriage with arms at the side result in less demands on lower limb joints than does one-handed asymmetric load carriage (Neumann et al., 1992; Neumann and Cook, 1985) or bi-laterally holding the load in front of the trunk (Nottrodt and Manley, 1989).

To date, a biomechanical assessment of load carriage with an existing asymmetric gait has not been conducted. However, Ganguli and Datta (1977) compared the energy expenditure of below knee amputees and able-bodied controls for one-handed verses bi-lateral load carriage. One-handed load carriage of 7.5 kg had the same level of energy expenditure regardless of

amputation side and a lower level of expenditure than did bi-lateral side carrying of 15.0 kg. LLA also were more sensitive to load carriage than were able-bodied controls (Ganguli and Datta, 1977).

Gait alterations to lower limb inertial changes in the able-bodied are of interest to prosthetists and scientists studying motor control adaptions and energetics (Noble and Prentice, 2006; Reid and Prentice, 2001; Royer and Martin, 2005). Adding as little as 2 kg to the lower limbs can lead to hip, knee, and ankle adaptions during swing to insure both toe clearance and control of the added inertia, but results in minimal changes to stance kinematics and kinetics (Noble and Prentice, 2006; Reid and Prentice, 2001). Asymmetrically adding weight decreases the stance and increases the swing durations of the weighted limb relative to the unweighted limb (Skinner and Barrack, 1990). Modifying the moment of inertia or mass properties of the leg both similarly affect energetic costs (Royer and Martin, 2005). When adjusting to an asymmetric load, able-bodied participants require between 1 and 5 minutes of walking to settle upon a consistent gait (Noble and Prentice, 2006; Smith and Martin, 2007).

A treadmill is often utilized to study gait because of the convenience and control it provides (Alton et al., 1998; Riley et al., 2007; Taylor et al., 1996). Unfortunately, treadmill gait has demonstrated some subtle biomechanical differences compared to over ground walking (Alton et al., 1998; Matsas et al., 2000; Mazaheri et al., 2016; Owings and Grabiner, 2004, 2003; Riley et al., 2007; Taylor et al., 1996; Zatsiorky et al., 1994). The differences between treadmill and over ground gait appears to be primarily associated with familiarization and can be minimized by allowing time for inexperienced treadmill walkers to acclimate, reportedly between 4 and 6 minutes of steady walking or roughly 400 steps (Matsas et al., 2000; Owings and Grabiner, 2003; Taylor et al., 1996).

Split-belt treadmills are utilized in both the clinic and for research purposes (Ada et al., 2003; Dietz et al., 1994). During split-belt gait, each leg can be exposed to a different belt speed to encourage gait asymmetry. When healthy able-bodied individuals are perturbed by a split-belt treadmill, they initially take asymmetric steps (Finley et al., 2015; Malone et al., 2012). After roughly 200 strides, participants adjust both their temporal and spatial step parameters to a steady-state gait pattern with a step length symmetry (Choi and Bastian, 2007; Finley et al., 2013; Reisman et al., 2005). However, the gait patterns developed by each limb during split-belt walking are different both kinematically and kinetically than those at a similar speed on a conventional treadmill (Roemmich et al., 2012; Roper et al., 2017).

To better understand prosthetic gait, researchers and engineers have designed lower limb prosthetic simulators for able-bodied individuals (Brown et al., 2018; Lemaire et al., 2000; Ramakrishnan, 2014; Vanicek et al., 2007). Prosthetic simulators typically either restrict movement at one or more joints or artificially 'replace' a fully flexed shank. Though they are not physiologically capable of mimicking prosthetic gait, these simulators have demonstrated reductions in un-restricted limb step length and overall gait speed (Brown et al., 2018; Lemaire et al., 2000; Vanicek et al., 2007) reminiscent of the adaptations observed while new amputees first learn to walk (Seroussi et al., 1996).

2.4. Lower Back Demands During Gait

Numerous studies have quantified lower back kinematics and kinetics both directly and indirectly during a myriad of tasks, including normal and asymmetric gait. Here, the magnitude, timing, causality, and measurement technique for assessing lower back demands from these studies will be emphasized. For reference, most demands will be compared relative to either body weight, a static standing loading/posture, other tasks, or a control scenario. An aim of this section is to

support *in silico* biomechanical modeling and identify a potential research gap as it pertains to induced asymmetric gait.

2.4.1. Kinematics of Lower Back During Gait

Lower back kinematics are generally represented as three Cartesian angles of the trunk/thorax relative to the pelvis (Pearcy, 1986; Wu et al., 2002). Motion capture markers or goniometers positioned above the first lumbar vertebrae and on the sacrum or iliac spines define the trunk and pelvis segments, respectively. The rotational sequence computing the angles is most often initiated in the sagittal plane (Baker, 2001) with the final two rotation sequence orders varying by task. Reported angles are traditionally zeroed about a comfortable standing posture.

Walking speed, cadence, and or level of amputation can increase kinematic measures of the trunk (Callaghan et al., 1999; Feipel et al., 2001; Hendershot et al., 2018; Hendershot and Wolf, 2014; Kubo et al., 2006; van der Hulst et al., 2010) and therefore affect direct comparisons between individuals and studies (Rowe and White, 1996). Other sources of measurement variance are attributed to walking environment (Alton et al., 1998; Lee and Hidler, 2008; Yang and King, 2016), presence of lower back pain (LBP) (Selles et al., 2001), and limitations of motion capture (Della Croce et al., 2005).

To assist in forward progression, a small trunk flexion bias is present throughout the gait cycle (Ceccato et al., 2009; Whittle and Levine, 1995). Peak trunk flexion and extension coincides with center of mass speed fluctuations occurring around heel-strikes and toe-offs (Callaghan et al., 1999; Crosbie et al., 1997; Rice et al., 2004). The total trunk range of motion in the sagittal plane is generally low and less than 10-degrees. Transverse and frontal plane lower back kinematics both oscillate about neutral during symmetric gait. Lateral flexion peaks reach roughly 5-degrees during contralateral toe-off while a second local peak can occur during swing as the trunk and

whole-body center of mass prepares for the next heel-strike. Axial rotation in the transverse plane exhibits a cyclic pattern throughout the gait cycle, with mirroring rotational peaks of roughly 10-degrees near ipsilateral heel-strikes to counter the pelvic twisting associated with stride lengthening (Callaghan et al., 1999; Hendershot and Wolf, 2014; Rice et al., 2004; Thorstensson et al., 1984; Yoder et al., 2015). Even at high walking velocities, the range of motion in any of the three planes does not exceed 40% of maximum (Feipel et al., 2001).

Asymmetric gait lower back kinematics are generally similar to healthy controls, with the marked exceptions that all ranges of motion are larger globally, with more sagittal plane flexion bias, more in sync thoracic and pelvic axial rotation, and greater lateral flexion during the residual/healthy stance (Dananberg and Guiliano, 1999; Goujon-Pillet et al., 2008; Hendershot and Wolf, 2014; Kakushima et al., 2003; Morgenroth et al., 2010; Resende et al., 2016; Seay, 2015; Selles et al., 2001; Yoder et al., 2015). These adaptations are attributed to a decreased strength in the residual/healthy limb, prosthetic limitations, load counter balancing, and guarding against falls (Azizan et al., 2018; Devan et al., 2014; Sagawa et al., 2011; Seay, 2015).

2.4.2. Muscle Activity During Gait

Electromyography (EMG) measures the motor unit action potentials of the surrounding muscular tissue. Activation levels are generally associated with participant-specific muscular contraction intensity and therefore muscular force. Noninvasive surface EMG normalized to a value obtained during maximal effort is a well-established means of reporting muscular activity during most tasks (Kamen and Caldwell, 1996). Surface EMG measurements from superficial trunk muscles has been shown to correlate well with the task demands and with the activity of deeper adjacent muscles measured with intramuscular EMG (Dolan and Adams, 1993; McGill et

al., 1996; Zetterberg et al., 1987). For the trunk muscles, the level of muscle activation can greatly influence vertebral loading (Granata and Marras, 1995b).

EMG estimates during gait reflect the kinematic and kinetic demands of the task (Callaghan et al., 1999; Cappozzo, 1984; Ceccato et al., 2009; Thorstensson et al., 1984; Waters and Morris, 1972). Back extensor and agonistic trunk rotator muscle activity both reach peaks of ~10% of maximum in response to the peak flexion and axial twist occurring at contralateral heel strike (Carlson et al., 1988; Waters and Morris, 1972). To limit extension and enhance stability of the trunk, abdominal flexors constantly maintain a low level of activity throughout the gait cycle, while local lumbar muscles co-contract simultaneously to restrict movement in the frontal plane (Thorstensson et al., 1982; Waters and Morris, 1972). Activation patterns remain similar with increases in walking speed, but mean amplitudes increase across all trunk muscles along with trunk stiffness (Anders et al., 2007; Callaghan et al., 1999; Kubo et al., 2006).

Mal-adaptive gaits can affect the muscular activity of the trunk. Erector spinae activity has more sustained activity during double support transitions in lower limb amputee (LLA) gait (Butowicz et al., 2018; Jaegers et al., 1996). Muscular activity during carrying tasks is influenced by load, load location, and gender (Bobet and Norman, 1984; Cook and Neumann, 1987; Knapik et al., 1996; McGill et al., 2013; Rose et al., 2013). One-handed and anterior load carrying has been shown to significantly increase activity during both 10 and 20% body weight loading conditions (Cook and Neumann, 1987). These findings have been corroborated with increased frontal plane moment demands during asymmetric rucksack carriage (DeVita et al., 1991), uni-lateral carrying while negotiating stairs (Wang and Gillette, 2017), high weight backpack carrying experiments (Li and Chow, 2018), competitive strongman events (McGill et al., 2009), and investigations into the link between arm kinematics and trunk muscle activity (Angelini et al.,

2018; Callaghan et al., 1999). In contrast, light backpack loads can reduce back extensor muscle activity (Knapik et al., 1996).

Muscular activation levels during gait are generally considered to be low when compared to more demanding tasks such as lifting or extreme load carries (Callaghan et al., 1999; McGill et al., 2009). Furthermore, some caution should be taken when interpreting surface EMG of the lower back muscles during dynamic tasks, as isolating activity in these numerously tightly packed muscles is difficult due to the inherent limitations of electrode placement (Stokes et al., 2003).

2.4.3. *In Vivo* Low Back Loading During Gait

Despite the inherent risks and limitations involved, efforts have been made to directly quantify *in vivo* loads in the lower back during walking. Lower lumbar intradiscal pressure has been measured with piezoresistive pressure transducers inserted via a guided needle (Nachemson and Elfstrom, 1970; Wilke et al., 1999). This technique is based upon the principle that the nucleus of the disc behaves hydrostatically and assumes that the transducer is uncompromised during placement and the prescribed activity (Wilke et al., 1999). Compared to standing, slow walking increases the average intradiscal pressure by ~15% from 7.1 to 8.2 kp/cm^2 (Nachemson and Elfstrom, 1970) or from 0.50 MPa during standing to between 0.53-0.65 MPa for self-paced barefoot and shod walking (Wilke et al., 1999). Alternatively, anterior vertebral body stabilizers instrumented with strain gauges have been surgically placed to observe lumbar loading in older compression fracture patients (Rohlmann et al., 1997). Consistent with intradiscal pressure, walking increases the average resultant force across a vertebral body stabilizer. However, this more sensitive technique detected a larger instantaneous load increase from ~140N in quiet standing to a peak near toe-off of ~240N during walking, a rise of ~70% that increases with speed (Rohlmann et al., 2014a, 2013).

Lower back loading during gait has also been describe qualitatively with less invasive but more indirect methods, such as spinal shrinkage and intra-abdominal pressure (IAP) (Fowler et al., 2006; Grillner et al., 1978; Shaw et al., 2014). IAP is monitored via a pressure transducer in the abdomen, and reflects the abdominal pressure resulting from the constriction of the trunk musculature on a limited volume cavity (Bartelink, 1957; Davis, 1981). IAP is believed to help stabilize the trunk and assist the extensor muscles while relieving lumbar loading (Gracovetsky et al., 1981; Morris et al., 1961; Nachemson et al., 1986; Stokes et al., 2010). Coinciding with instances of high trunk EMG activity, phasic increases in IAP during walking can nearly double those measured during standing, and are also speed dependent (Grillner et al., 1978; Shaw et al., 2014). Spinal shrinkage measures are based on the phenomena that temporary fluid loss from compression forces produce a measurable and predictable decrease in back/spine stature (Eklund and Corlett, 1984). Walking has been shown to decrease spine length up to 6 mm during a two-hour 8.5 km walk (Fowler et al., 2006). However, this rate of spinal shrinkage merely parallels that observed during the first few hours upon rising, irrespective of walking activity (Reilly et al., 1984).

While all these measures of lower back loading are insightful, they have numerous limitations including assumptions concerning disc fluid properties, equipment and mounting errors, limited number of participants of varying ages and health statuses, unaccounted for tissue loading, task restrictions, and in some cases the highly invasive nature of the procedure (Dreischarf et al., 2016; Wilke et al., 1999). Although the magnitudes of each may be questioned, more important is the relative change in the observed loads between conditions (Nachemson, 1976). To date, there are no studies reporting *in vivo* loading during unloaded asymmetrical walking.

2.4.4. *In Silico* Low Back Loading During Gait

To combat the inherent limitations of *in vivo* approaches and support our understanding of the mechanisms involved, *in silico* estimates of the lower back loading have been developed and applied during gait. These studies apply techniques ranging from simple link-segment models to more complex EMG-driven models (see Section 2.2). Early biomechanical models estimate that walking can elicit speed-dependent peak compressive loads of 1.0 – 2.5 times body weight during the initiation and termination of double support, while minimums of ~0.2 body weight occur during single limb support (Cappozzo, 1983, 1981; Cappozzo and Gazzani, 1982). Subsequent *in silico* models of the lower back during normal walking have supported Cappozzo's conclusions (Callaghan et al., 1999; Cheng et al., 1998a; Cromwell et al., 1989; Khoo et al., 1995; Shojaei et al., 2016). In addition, vertebral shear loads of up to 0.6 times body weight have been calculated in both the anterior-posterior and medial-lateral directions (Arshad et al., 2018; Callaghan et al., 1999; Cappozzo, 1981; Cheng et al., 1998a; Goh et al., 1998; Khoo et al., 1995; Rose et al., 2013; Shojaei et al., 2016).

Estimates of lower back loads during asymmetric gait have been reported using *in silico* biomechanical models in studies focused on LLA, (Hendershot et al., 2018; Hendershot and Wolf, 2014; Shojaei et al., 2016; Yoder et al., 2015; Yu et al., 2014) other lower limb injuries (Cappozzo and Gazzani, 1982), and ergonomic load carriage applications (see Section 2.4.6.). As with normal symmetrical gait, Professor Cappozzo pioneered examinations into asymmetrical gait lower back loading (Cappozzo and Gazzani, 1982). These early estimates demonstrated that asymmetric gait lower back loading approached ~3.0 times body weight at residual limb toe-off, with compressive loading at 'normal' asymmetric speeds greater than that of healthy individuals walking at their maximum speed (Cappozzo and Gazzani, 1982). Other groups (Hendershot et al., 2018;

Hendershot and Wolf, 2014; Shojaei et al., 2016; Yoder et al., 2015; Yu et al., 2014) have since applied more detailed three-dimensional rigid-link, optimization-based, and kinematically driven finite element models to further examine LLA lower back loading. Mediolateral lower back moments in LLA are estimated to be 41% larger than in able-bodied gait (Hendershot and Wolf, 2014). Lower back loading depends on both amputation level and prosthetic length (Hendershot and Wolf, 2014; Yoder et al., 2015; Yu et al., 2014). Asymmetric peak loads are associated with greater lateral trunk flexion during prosthetic support and the greater trunk forward lean of LLA patients (see Section 2.4.1.). Kinematically driven finite element modeling of the Hendershot et al. (2014) dataset predicted 80% larger trunk muscle forces and 40% larger spinal loading for LLA versus healthy controls (Shojaei et al., 2016). Similar to healthy gait (Callaghan et al., 1999), back loading during asymmetric gait depends on speed and modeling approach (e.g. top-down vs. bottom-up) (Hendershot et al., 2018; Hendershot and Wolf, 2014).

2.4.5. Lower Back Demands During Carrying

The mal-adaptive lower limb changes observed during carrying tasks (see Section 2.3.3) do not occur in isolation, as kinematic and kinetic adjustments are also present in the trunk and lower back. Using instrumented their vertebral body implants in the upper lumbar region, Rohlmann et al. (2014c) directly measured *in vivo* loading during various carrying activities. Walking with a weighted backpack resulted in forces analogous to those of unloaded normal walking. Carrying 10 kg in each hand bi-laterally or 5 kg uni-laterally resulted in increased implant forces that were proportional only to the gravitational force of the added load carried. Interestingly, uni-laterally carrying 10 kg resulted in larger loads than carrying 20 kg split evenly between each hand (Rohlmann et al., 2014c). Measuring lower back intradiscal pressure, Wilke

et al. (Wilke et al., 2001) observed a similar reduction in loading while carrying a larger total load bi-laterally than a lesser load uni-laterally.

As with other tasks, detailed lower back biomechanical models have been used to compare load carriage scenarios (McGill et al., 2013, 2009; McGill and Marshall, 2012; Rose et al., 2013). Rose et al. (2013) examined a variety of lifting styles and suggested that frontal carries of 11.3 kg could potentially produce deleterious anterior-posterior shear forces at the L2/L3 vertebral level. They advised positioning the load close to the spine to minimize shear loads. McGill et al. (2013) demonstrated that lower back (L4/L5) compression loads during one hand carries were higher than when double the total load was evenly split bi-laterally between two hands, which supports measurements made *in vivo* (Rohlmann et al., 2014c; Wilke et al., 2001). The increased loading from uni-lateral versus bi-lateral load carriage is magnified as the total load carried increases. McGill et al. (2009) studied back loading in strength athletes partaking in 'strongman' events, with results emphasizing that carriage can place higher demands on the back than lifting much greater loads. They also estimated that during some extreme events of carrying 91 kg, compression and shear loading on the lower back can exceed 10,000 and 3,000 N, respectively.

2.4.6. Lower Back Demands During 'other' Tasks

The "spinal engine" has been hypothesized as the primary engine of locomotion and most other everyday tasks (Gracovetsky, 1990). Not surprising, loading of the back, particularly in the lumbar region (Andersson, 1997), has been estimated across a myriad of activities.

The highest *in vivo* loading observed from an instrumented vertebral body stabilizer during any task was from lifting a 10 kg load from the ground, with a resultant force of ~1649 and ~100 N of resultant and shear force, respectively (Rohlmann et al., 2014b). Other activities (e.g. forward elevation of hands while holding 9 kg, standing up, and tying one's shoes) also produced resultant

forces of over 1000 N (Rohlmann et al., 2014b). Wilke et al. (2001) reported intradiscal pressures ranging from up to 1.6-2.1 MPa during similar lifting and bending tasks. However, as previously noted, these measurements are beset with limitations (Dreischarf et al., 2016; Wilke et al., 1999).

Perhaps the most frequently reported and modeled lower back loading studies involve manual materials handling tasks (Davis and Jorgensen, 2005). Davis et al. (1998) compared lifting and lowering tasks at various speeds with a detailed lower back model, finding larger compressive loads during lowering than any lifts. However, the inverse was true for shear loading. In tasks involving external loads of 18.2 kg, compressive forces for lowering and lifting averaged 3269 and 2665 N, respectively, but shear forces were 680 and 815 N. Not all lifts are symmetrical within the sagittal plane, as asymmetric lifts are common in the workplace because of their speed and convenience (Hsiang et al., 1997; Marras et al., 1995, 1993; Punnett et al., 1991). Rotating the lift origin of a 13.6 kg box 60-degrees from front center increased compressive and anterior/posterior shear loading by nearly 10% and 60%, respectively (Marras and Davis, 1998). Equivalent results have been reported using an OpenSim musculoskeletal model (Kim and Zhang, 2017). Interestingly, if asymmetric lifts are performed with only the ipsilateral hand, lower back loading is similar to symmetric lifting; as lifting 13.6 kg in either fashion results in a peak compressive, lateral shear, and anterior-posterior shear of 3,600, 200, 900, respectively (Marras and Davis, 1998) . Lifting a 10 kg load asymmetrically with one hand has been shown to increase loads on the L5/S1 by nearly 20% compared to 10 kg in each hand irrespective of lifting technique, despite being a smaller total load (Faber et al., 2009). Pushing and pulling tasks have also been modeled to reveal that anterior/posterior shear loads at upper lumbar levels can exceed 1000 N, nearly matching compressive loading, when the handle height is low and the external load exceeds 40% of body weight (Knapik and Marras, 2009).

Work-related tasks such as sitting also have lower back health implications (Chaffin et al., 2006). Callaghan and McGill (2001) found lower back compressive loads from a musculoskeletal model in unsupported sitting of ~1700 N, over 50% greater than in standing, and directionally different for anterior-posterior shear forces, 135 N sitting vs. -13 N standing. Transitioning from sit-to-stand has also been shown to load the L4/L5 compressively by up to 3 times body weight, using either an OpenSim musculoskeletal or non-linear finite element model of the lumbar spine (Actis et al., 2018b; Shojaei et al., 2019). Similar loading relationships for unsupported sitting and sit-to-stands has been measured *in vivo* (Rohlmann et al., 2014b; Wilke et al., 2001)

Patient handlers have an extremely high prevalence of LBP (Jensen, 1987; Samaei et al., 2017). Simulated one-person patient transfers predict compression and anterior-posterior shear forces to exceed 6,000 and 1,000 N, respectively (Jordan et al., 2011; Marras et al., 1999a; Skotte et al., 2002).

The loads placed on the spine during various fitness exercises and completive events has been examined by the Spine Biomechanics Laboratory at the University of Waterloo. Commonly prescribed exercises for the abdominals can reach L4/L5 disc compression levels between 2,000 - 3,000 N (Axler and McGill, 1997). While at the start of a 16 kg kettlebell swing and snatch the load on the L4/L5 can exceed 3,000 N in compression and 400 N in shear (McGill and Marshall, 2012). Interestingly, during dead lifts, competitive powerlifters have been estimated to load their spine in excess of 20,000 N (Cholewicki et al., 1991; Granhed et al., 1987).

2.5. Concluding Remarks

Without question, LBP is a major societal issue. Daily lower back demands during gait are relatively low in magnitude but are highly repetitive and numerous (Tudor-Locke et al., 2011), and can be adversely affected by physical and task limitations (Callaghan et al., 1999; Hendershot

and Wolf, 2014; McGill et al., 2013; Rose et al., 2013; Yoder et al., 2015). Until more definitive studies concerning the lower back demands and their link to LBP have been conducted, the prescription of walking as a remedy for LBP (Nutter, 1988) should be brought into question for those with atypical gait patterns or task demands. Applying an electromyography-based lower back model during induced and regulated levels of asymmetries in healthy controls should provide important information concerning how gait asymmetries affect lower back loading.

CHAPTER 3

METHODS

The primary objective of this dissertation is to investigate how experimentally induced lower limb gait asymmetries and asymmetrical load carriage in able-bodied individuals can impact lower back loading. Study 1 will develop and evaluate a modeling approach implementing EMG-optimization algorithm (Cholewicki and McGill, 1994; Gagnon et al., 2011) to quantify muscle recruitment within an updated OpenSim lower back model (Appendix C; Beaucage-Gauvreau et al., 2019; Christophy et al., 2012). The lower back demands determined from the model will be compared with previously reported *in vivo* and *in silico* measures of lower back loading during equivalent walking and carrying tasks (Callaghan et al., 1999; McGill et al., 2013; Rohlmann et al., 2014c, 2014a, 2008; Wilke et al., 1999; https://orthoload.com). Study 2 will use the Study 1 model to investigate how various lower limb gait asymmetries induced in able-bodied participants affect lower back demands. Study 3 will apply the same model to examine how lower back demands during gait asymmetries are affected by different load carriage techniques. The goal of this research is to provide insights that can be applied in a clinical setting to understand and help reduce lower back demands and improve the quality of life for a broad range of patients who must endure both acute and chronic asymmetric gait.

3.1. Study 1: An EMG Optimization OpenSim Musculoskeletal Model of the Lower Back Kinetic Demands in Gait

3.1.1. Introduction

Biomechanical musculoskeletal models of the lower back apply observed kinematics, mathematical equations, established anatomy, and biological assumptions to calculate internal

kinetic demands that are impractical to measure *in vivo* (Dreischarf et al., 2016). These internal demands can be compared to established tissue tolerances and injury reports to develop safety guidelines and rehabilitation programs. As part of their development, such models must first be evaluated against either known measures, previous model calculations, or established principles to establish confidence in their calculated outcome measures (Cholewicki and McGill, 1996).

There are several open-source lower back models available in OpenSim (Delp et al., 2007), each based upon the original model of Christophy et al. (2012) and then refined and evaluated for specific applications (Actis et al., 2018a; Beaucage-Gauvreau et al., 2019; Bruno et al., 2015; Meng et al., 2015; Raabe and Chaudhari, 2016; Senteler et al., 2016; Zhu et al., 2017). All these models have used static optimization (SOpt) to estimate the individual muscular forces responsible for the observed kinematics (Crownshield and Brand, 1981), and have not been evaluated for the analysis of lower back demands during walking gait. SOpt is based on the premise that muscles will be recruited to minimize a criterion objective function such as fatigue, and as such it is incapable of predicting antagonistic muscle activation (Marras, 1988). The accurate distribution of individual muscle forces is crucial in estimating the amount of stress on anatomical tissues (Marras, 2000). In contrast, models that incorporate electromyography (EMG) to estimate muscular contributions can reflect participant-specific recruitment strategies, antagonistic activity, and strength potentials (Davis and Jorgensen, 2005; Le et al., 2017). EMG-based models may therefore provide improved accuracy and insight into how tasks and recruitment strategies effect lower back loading.

EMG assisted models come in two forms. Models driven strictly by EMG apply measured and calibrated muscle activity to directly predict muscular forces (Davis and Jorgensen, 2005). Unfortunately, due to physiological complexities and the inherent limitations of EMG (Davis and

Jorgensen, 2005; van Dieën and Visser, 1999), the forces predicted from an EMG-driven model will not necessarily satisfy the joint demands calculated from inverse dynamics (Choi and Vanderby, 1999; Cholewicki et al., 1995; Gagnon et al., 2001). To overcome this limitation, an EMG optimization method (EMGopt) was developed by Cholewicki and McGill (1994). By minimally adjusting the measured EMG activations to match the calculated joint demands, EMGopt is capable of alleviating the flaws of both the optimization and EMG driven approaches while simultaneously incorporating the advantages of each (Choi and Vanderby, 1999; Cholewicki et al., 1995; Gagnon et al., 2001; Li and Chow, 2019).

The primary objective of this study is to develop an EMGopt (Cholewicki and McGill, 1994) framework for defining muscular contributions in a participant-specific OpenSim musculoskeletal model. To evaluate this model, the lower back demands from EMGopt will be compared directly to results from a standard SOpt algorithm, and indirectly to demands reported in the literature (Callaghan et al., 1999; McGill et al., 2013; Rohlmann et al., 2014c, 2014a, 2008; Wilke et al., 1999; https://orthoload.com). The model developed in this study will be applied in subsequent studies to help improve our understanding of how different gait and load carriage asymmetries can adversely affect lower back demands.

3.1.2. Aims and Hypotheses

Aim 1.1: To develop and evaluate an EMG-optimization (EMGopt) framework for defining muscular contributions in an OpenSim musculoskeletal model assessing lower back demands across various gaits.

Hypothesis 1.1: EMGopt will predict antagonist trunk muscle contributions that will result in larger lower back demands than a generic static optimization (SOpt) approach.

Hypothesis 1.2: EMGopt predicted lower back demands will better correlate with *in vivo* measurements than a SOpt approach.

Aim 1.2: To evaluate the sensitivity of the EMGopt algorithm to variation in the EMG amplitude and force potential of the trunk musculature.

Hypothesis 1.2: Lumbar joint loading will be most sensitive to trunk flexor (e.g. rectus abdominis, external obliques, internal obliques, and psoas) muscular activity and force potential.

Aim 1.3: To determine the effect of participant-specific muscular strengths on lower back loading and the amount of adjustments to the EMG signal.

Hypothesis 1.3: The adjustments needed for the EMG measures to balance the joint demands will be reduced when muscular strengths are tailored to individual strength potentials.

3.1.3. Methods

Participants

Six (n=6; male=3) participants will be recruited from a university population (see Appendix A for rationale). Participants with a high body mass index (BMI > 30), age (years > 40), history of lower back pain (LBP), low self-reported level of physical activity, large leg length discrepancy (LLD > 20mm), and any neurological issues will be excluded. All subjects will be required to read and sign an Informed Consent document approved by the University of Massachusetts Amherst Institutional Review Board.

Equipment and Setup

Full-body three-dimensional kinematics will be sampled at 100 Hz with an eight-camera motion analysis system (Qualisys AB, Gothenburg, Sweden). The motion of body segments and select anatomical landmarks from each participant will be captured with a combination of

individual and clustered 12.5 mm reflective markers (Fig. 3.1.1). Specifically for the trunk and pelvis, kinematics will be tracked with markers placed on both anterior superior iliac spines (ASIS), both posterior superior iliac spines, both iliac crests, both acromion, the xiphoid process, sternal notch, C7, and with a rigid-cluster of four markers placed caudally at the mid-thorax level.

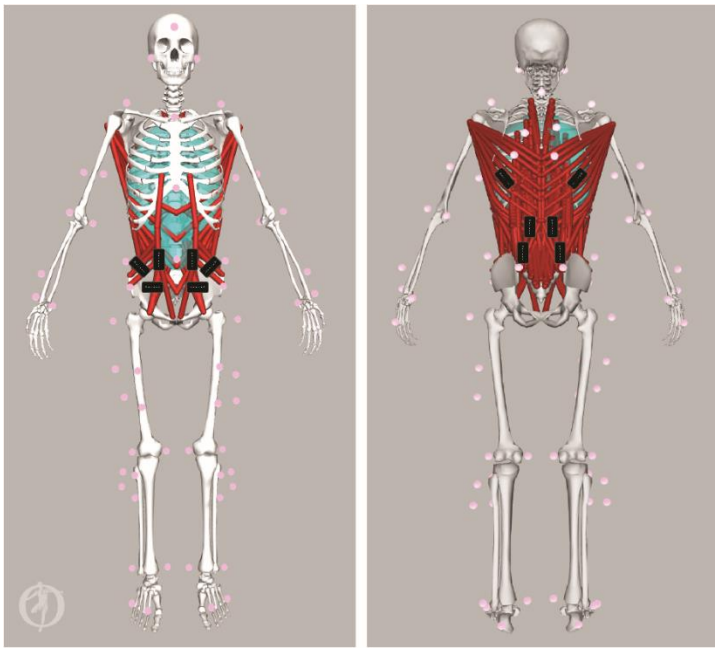

Figure 3.1.1. Full-body OpenSim musculoskeletal model. Spheres represent the location of the 67 reflective markers used for motion tracking. Black rectangles represent the placement for the 12 electromyography (EMG) sensors used to monitor the muscular activity of the trunk.

Electromyography (EMG) from twelve wireless surface electrodes (Delsys Inc., Natick, MA) will be sampled at 2000 Hz. Electrodes will be positioned (Fig. 3.1.1) as described in previous studies (Gagnon et al., 2011; McGill et al., 2013) from bi-lateral trunk muscles the rectus abdominis (3 cm lateral to umbilicus), external obliques (3 cm lateral to the linea semilunaris), internal obliques (at the level of the ASIS but superior to the inguinal ligament and medial to linea semilunaris), latissimus dorsi (inferior to scapula over muscle belly when arms are abducted),

longissimus thoracis pars thoracis (3 cm lateral to L1), and iliocostalis lumborum pars thoracis (6 cm lateral to L3).

Isometric maximal voluntary contractions (MVCs) will be measured with a Biodex dynamometer (Biodex Medical Systems Inc., Shirley, NY) to establish maximal EMG amplitudes and trunk flexion, extension, lateral bending, and axial rotation torques for each participant. Walking and carrying tasks will take place on an instrumented treadmill (Treadmetrix, Park City, UT) to provide gait pacing and measure ground reaction forces (GRF). The dynamometer torque and the gait GRF information will both be sampled at 2000 Hz with a 16-bit A/D convertor (USB-2533, Measurement Computing Corporation, Norton, MA). The motion capture, EMG, and analog GRF and torque signals will be synchronously collected within Qualisys's Track Manager software.

Hand-held adjustable weight dumbbells will be carried both bi- and uni-laterally in symmetrical and asymmetrical conditions. Dumbbell weight(s) will be prescribed based on each participant's body weight.

Procedure

Participants will don form-fitting clothing and comfortable walking or running shoes prior to measurements of anthropometry, self-selected treadmill walking speed (SSS), MVCs, and the experimental "evaluation" conditions. Anthropometry measures of height, body segment circumferences, and body weight will be taken with a tape measure and balance scale. SSS on the treadmill will be determined by prompting participants to correct the treadmill belt-speed from an initial randomly chosen high or low speed to a "comfortable walking speed which they can maintain for 3-5 minutes with minimal effort and discomfort". Incremental speed adjustments blinded from the participant will be made in response to their verbal cues. The SSS process will

be repeated until the participant consistently settles upon the same SSS. A 90% SSS (90S) value will be calculated from each participant's SSS, representing the reported adjustment in walking speed chosen by participants during carrying tasks (Crosbie et al., 1994). After SSS determination, EMG electrodes will be placed on the participant. To improve EMG quality, excess body hair at each electrode site will be shaved and unwanted dead skin and oils removed with fine sandpaper and alcohol wipes. All EMG signals will be continuously monitored for signal quality.

The participants will then perform a series of MVC efforts on the dynamometer against a custom bar designed to resist trunk flexion, extension, bending, and rotation (Fig. 3.1.2). For the MVCs the dynamometer seat back will be in flattened, with the bar positioned dorsally at the midthoracic level during extension, ventrally just below the sternal notch during flexion and axial rotation exertions, and lateral on the arm at the level of the sternal notch during lateral bending exertions. The bar angle and distance to the dynamometer center of rotation will be recorded and used to convert the measured torque into an equivalent force vector applied to the trunk. Six different trunk exertions (McGill, 1991; McGill et al., 2013) will be performed. Five MVC exertions will take place from a sit-up position with the torso, knees, and hips flexed at approximately 45, 90, and 90-degrees, respectively (as estimated by a handheld goniometer): trunk flexion, bi-lateral twisting, and bi-lateral lateral bending. The sixth maximal effort will be back extension performed with the participant prone and safely suspended from the dynamometer seat in a Biering-Sorensen position with a slightly flexed torso (Biering-Sorensen, 1984). During each MVC, the participant will be verbally encouraged and cued to perform maximally against the static bar for 3-5 seconds while EMG activity and dynamometer torque are recorded. Three repetitions of each MVC effort will be performed, separated by 2-minutes of rest. Following the MVCs, the motion capture markers will be placed on the participant.

To help evaluate the model, participants will perform a variety of tasks in which the lumbar loading *in vivo* has been directly quantified (Rohlmann et al., 2014c, 2014a, 2008; Wilke et al., 1999; https://orthoload.com), a similar model has calculated *in silico* loads (Callaghan et al., 1999; McGill et al., 2013), or that can differentiate between various modeling approaches (Table 3.1.1). These tasks will include quiet relaxed standing, standing while breathing heavily, standing with arms abducted to 90 degrees, standing while holding dumbbells of 7.5% or 15.0% body weight (7.5BW and 15BW, respectively) split evenly between both hands, walking at SSS, 90S, and 0.83 m/s, walking at 90S while carrying dumbbells of 7.5BW or 15BW in one hand, and walking at 90S while carrying dumbbells of 7.5BW or 15BW split between both hands. During static standing tasks, participants will be asked to stand in a neutral and upright posture (e.g. minimizing flexion or extension moments) while data is collected for 10 seconds. During each unloaded walking task, participants will walk for 90 seconds to acclimate prior to recording the task for 30 seconds (Matsas et al., 2000; Taylor et al., 1996). For each carrying task, participants will walk and carry the prescribed load for 20 seconds to acclimate prior to recording the task for 30 seconds (Dick et al., 2017). Data from standing calibration poses will be recorded prior to and after all tasks have been performed in a random order. Two minutes of rest will be imposed between each task to minimize fatigue.

Participants will be monitored for fatigue at the conclusion of each walking and carrying task with an 11-point rating-of-fatigue scale developed by Micklewright et al. (2017). In addition, modified Biering-Sorensen tests (Biering-Sorensen, 1984) will be administered before and after the experimental task set. During these isometric tests, the participant will lie prone on the edge of the exam table with their lower limbs secured while maintaining their upper body in a horizontal position for 30 seconds (Fig. 3.1.2b). The intent of these modified tests is to objectively analyze

if any fatigue accumulated from the demands of the entire protocol without inducing further fatigue (Müller et al., 2010; van Dieën et al., 1998a). Fatigue will be assessed post-hoc by comparing iliocostalis lumborum pars thoracis EMG activity from the two tests (Roy et al., 1989).

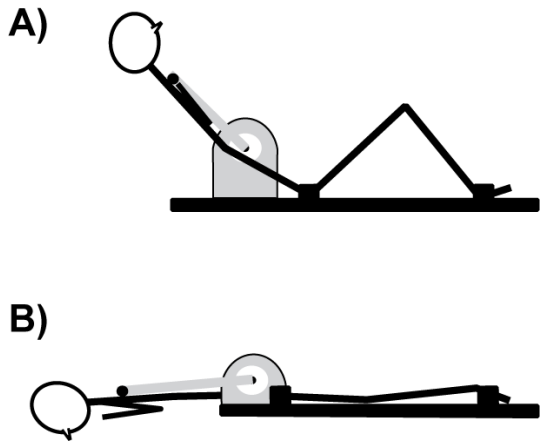

Figure 3.1.2. Positions used for the 5-second static Maximal Voluntary Contractions against the dynameter. Panel A) Sit-up position utilized for maximal trunk flexion, twisting, and lateral bending efforts (note: for lateral bending, the dynamometer resistance will be rotated 90-degrees and positioned laterally against the upper arm(s)) and B) Biering-Sorensen (1984) position used for maximal trunk extension efforts against the bar (pictured) and fatigue testing.

Data Processing

All data will be post-processed in MATLAB (MathWorks, Natick, MA). Marker positions, GRFs, and dynamometer torques will be filtered with a fourth-order zero-lag low pass Butterworth filter with cutoff frequencies determined by residual analysis (Winter, 2009). EMG activity from each muscle will be detrended, band-pass filtered (30 – 500 Hz), full wave rectified, and then low-pass filtered with a fourth-order 3 Hz zero-lag Butterworth filter (Brereton and McGill, 1998) before being time-shifted 10 ms to correct for physiological electromagnetic delay (Corcos et al., 1992). Task EMGs will be scaled to muscle-specific maximum levels recorded during participant-specific MVCs. Filtered external forces and EMG linear envelopes will be synchronously down sampled from 2000 Hz to 100 Hz to match the motion capture sample frequency.

To compare most standing trials, a 5-second average for each dependent variable of interest will be calculated. For the standing deep inhale/exhale trial, the maximum and minimum values from the entire 10-second trial will be computed. All walking and carrying trials will be time normalized by strides, with initiation and termination established from consecutive right heel strikes as identified by heel marker anterior-posterior velocities (Zeni et al., 2008), due to the absence of segregated GRFs. The maximums, minimums, and averages from each dependent variable of interest will be determined from five individual strides randomly extracted from the 30-second data collection.

Table 3.1.1. Experimental tasks and the comparisons used to test the model and approach. Abbreviations: electromyography (EMG), EMG optimization (EMGopt), maximum musculotendon stress (MMS), maximal voluntary contraction (MVC), self-selected speed (SSS), static optimization (SOpt), 15% body weight (15BW), 7.5% body weight (7.5BW), and 90% of SSS. (*) All carrying tasks will be performed at 90S.

Position	Task	Direct Comparison	Indirect Comparison
Standing	Relaxed	EMGopt vs. SOpt	
	Deep inhale/exhale	EMGopt vs. SOpt	Wilke et al., 1999; https://orthoload.com
	Arms abducted to 90°	EMGopt vs. SOpt	https://orthoload.com
	7.5BW split across hands	EMGopt vs. SOpt	
	15BW split across hands	EMGopt vs. SOpt	
Walking	SSS 90S	EMG, MMS, & MVC Sensitivity	Callaghan et al., 1999; Rohlmann et al., 2014a; Wilke et al., 1999;
	0.83 m/s		Rohlmann et al., 2014a
*Carrying**	7.5BW in one hand		Rohlmann et al., 2014c
	15BW in one hand	EMG, MMS, & MVC Sensitivity	McGill et al., 2013; Rohlmann et al., 2014c
	7.5BW split across hands		McGill et al., 2013
	15BW split across hands	EMG, MMS, & MVC Sensitivity	McGill et al., 2013; Rohlmann et al., 2014c

Musculoskeletal Model

Two separate full-body lumbar spine models with 27 segments, six lumbar joints, and 238 Hill-type (Hill, 1938; Thelen, 2003; Zajac, 1989) trunk musculotendon actuators (MTAs) will be

developed within the OpenSim 4.0 modeling system (Delp et al., 2007). Model *m29DoF* with 29 degrees-of-freedom is based on the full-body lifting model of Beaucage-Gauvreau et al. (2019) and will be used to determine the kinematics of each trial from recorded marker positions (Fig. 3.1.3). Several modifications to the original model will be made for simplicity, anatomical consistency and to improve model sensitivity (see Appendix C). Model *m47DoF* will be identical to m29DoF except for the absence of coordinate coupler constraints (CCC) on the lower back and abdominal joints. The kinematic motion from *m29DoF* will be assigned to model *m47DoF* with 47 degrees-of-freedom to determine accurate MTA moment arms (Banks et al., 2019) across all six lumbar joints, and to compute joint loads (Fig. 3.1.3).

Both models will be scaled using the OpenSim *scaling* tool to match the calibration pose and anthropometry of individual participants. The muscular strength potentials of the *m47DoF* MTAs will be adjusted from a nominal 100 N/cm^2 maximal stress to individual maximal muscular stress (MMS) values that can match the maximal torque outputs from the MVC tasks for each participant. For this adjustment, the *inverse dynamics* tool in OpenSim will use the external forces and generic model states during each of the six MVC positions to calculate lumbar joint moments. To incorporate antagonistic muscle forces in the model solution, all MTAs will be assigned a lower activity bound based on their EMG activity observed during the MVC task. The highest calculated MMS from the six maximal MVC positions for each MTA will be used to determine the maximal isometric force potential of that MTA.

Participant-specific models will be used to analyze the standing, walking, and carrying tasks. The OpenSim *inverse kinematics* tool will be used to best fit the *m29DoF* model with the recorded marker position data to determine the generalized segmental coordinates. During carrying tasks, the dumbbell inertial characteristics will be described as cylinders of appropriate

mass and size affixed to the hands by a weld joint. The segmental coordinates along with the recorded GRF will then be assigned to the *m49DoF* model and used to calculate joint moments and model states using the *inverse dynamics* and *analysis* tools, respectively. Static optimization (SOpt; Crownshield and Brand, 1981) and EMG optimization (EMGopt; Cholewicki and McGill, 1994; Gagnon et al., 2011) will be applied to partition the lower back joint moments across the 238 MTAs (see next section for details). Forces associated with passive lower back tissue forces (e.g. ligaments) will not be considered because of insufficient data describing their mechanical properties (Christophy et al., 2012) and their limited contribution during upright standing and walking postures (Callaghan et al., 1999). Model MTA, inertial, and external forces will be input to the OpenSim *joint reaction analysis* tool to calculate the resultant lumbar joint forces from each MTA force optimization method. Lumbar joint forces will be expressed in the most caudal lumbar joint coordinate system. All OpenSim tools and libraries will be integrated with custom MATLAB scripting to minimize error and improved workflow efficiency (Lee and Umberger, 2016).

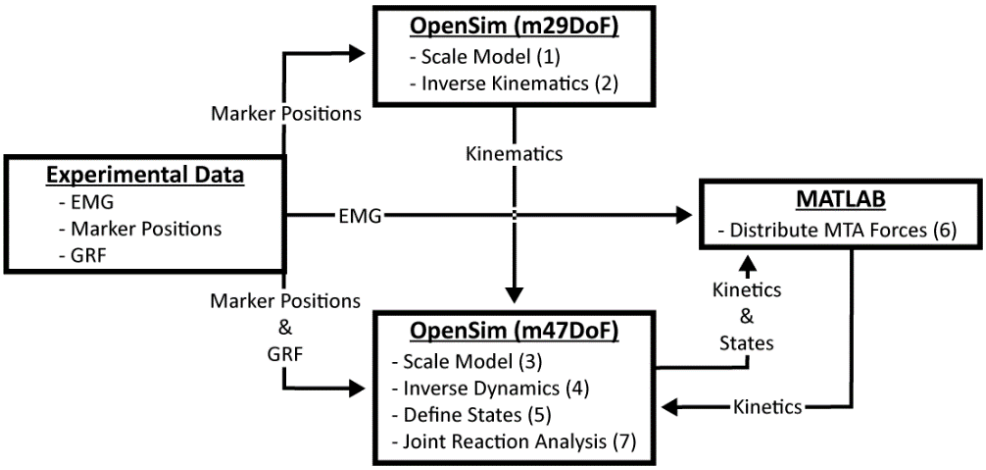

Figure 3.1.3. Flow chart of model input/output processes. Braced numbers depict implementation sequence. Abbreviations: electromyography (EMG), ground reaction forces (GRF), and musculotendon actuator (MTA).

Approaches to Solving Muscle Indeterminacy

The contribution of each individual MTA force towards the calculated joint moments will be solved with two different optimization approaches, both run in MATLAB with the *fmincon* sequential quadratic programming algorithm. The first approach (SOpt) will be based upon the hypothesis that MTAs are recruited in such a way as to minimize muscular fatigue (Crownshield and Brand, 1981), represented by an objective function (J_{SO}) minimizing the sum of the squared activations (a_i) across all the MTAs (i = 1 to 238):

$$J_{SO} = min \sum_{i=1}^{238} (a_i)^2 \qquad \text{(Eq. 3.1.1)}$$

subject to the following inequality constraints for each lumbar joint (j = 1 to 6):

$$\left|M_{MTA_{x_j}} - M_{ID_{x_j}}\right| \leq \left|0.005 * M_{ID_{x_j}}\right| \qquad \text{(Eq. 3.1.2)}$$

$$\left|M_{MTA_{y_j}} - M_{ID_{y_j}}\right| \leq \left|0.005 * M_{ID_{y_j}}\right| \qquad \text{(Eq. 3.1.3)}$$

$$\left|M_{MTA_{z_j}} - M_{ID_{z_j}}\right| \leq \left|0.005 * M_{ID_{z_j}}\right| \qquad \text{(Eq. 3.1.4)}$$

$$0.01 \leq a_i \leq 1.00 \qquad \text{(Eq. 3.1.5)}$$

where x, y, z are the orthogonal moments (M_{MTA}) resulting from the MTA forces predicted by the SOpt constrained to match the moments calculated from inverse dynamics (M_{ID}) to within $\pm$0.5%, with MTA activations positive and below their maximal level of 1.00. All MTA maximal force potentials will be further constrained by their kinematic state and maximal isometric potential (Thelen, 2003; Zajac, 1989).

The second optimization approach (EMGopt) will balance joint moments with minimal adjustments to measured EMG activity (Cholewicki and McGill, 1994). The objective function for EMGopt (J_{EMG}) will follow the multi-joint convention established by Gagnon et al. (2011):

$$J_{EMG} = \min \sum_{i=1}^{238} M_{norm_i} (1 - g_i)^2 \quad \text{(Eq. 3.1.6)}$$

with:

$$M_{norm_i} = \sqrt{\sum_i {M_{MTA_{i,j}}}^2} \quad \text{(Eq. 3.1.7)}$$

which will minimize the adjustments (g_i) made to the predicted muscular forces based on the Euclidean norm (M_{norm}) of the computed moment (M_{MTA}) from each MTA (i = 1 to 238) about each joint (j = 1 to 6) subject to the following constraints:

$$\left| g_i M_{MTA_{x_j}} - M_{ID_{x_j}} \right| \leq \left| 0.005 * M_{ID_{x_j}} \right| \quad \text{(Eq. 3.1.8)}$$

$$\left| g_i M_{MTA_{y_j}} - M_{ID_{y_j}} \right| \leq \left| 0.005 * M_{ID_{y_j}} \right| \quad \text{(Eq. 3.1.9)}$$

$$\left| g_i M_{MTA_{z_j}} - M_{ID_{z_j}} \right| \leq \left| 0.005 * M_{ID_{z_j}} \right| \quad \text{(Eq. 3.1.10)}$$

$$Thres \leq g_i \leq 1/emg_{a_i} \quad \text{(Eq. 3.1.11)}$$

where x, y, z are the orthogonal moments (M_{MTA}) resulting from the MTA forces (i = 1 to 238) and their moment arms. The MTA forces are a product of the current MTA potential, the EMG activations (emg_{a_i}), and the adjustment factors (g_i). The constraints will ensure that the optimized MTA forces produce moments that match the corresponding moments calculated from inverse dynamics to within $\pm$0.5%. Adjustment factors will be confined to be greater than an MTA-specific threshold level ($Thres$) of 0.50 or 0.01. Those MTAs with $Thres$ = 0.50 include the rectus abdominis, external obliques, internal obliques, latissimus dorsi, longissimus thoracis pars thoracis, and iliocostalis lumborum pars thoracis. MTAs without measured EMG data will be assigned a $Thres$ = 0.01, including psoas, multifidus, quadratus lumborum, longissimus thoracis pars lumborum, and iliocostalis lumborum pars lumborum. These muscles

will be assigned emg_{a_i} activations based on a nearby MTA synergist (Gagnon et al., 2011; McGill et al., 1996). Upper constraints on g_i adjustments will ensure that MTA forces remain below their maximal values.

Model Evaluation and Sensitivity Tests

Five different evaluation tests will be performed, including two that will qualitatively examine the validity of the model and EMGopt approach. The first evaluation test will compare muscular demands from EMGopt and SOpt across the five standing trials which require similar resultant lower back joint moments but challenge the stability of the trunk differently. The optimization approach that can better distinguish between the relaxed standing and the other four non-relaxed standing trials should predict increased overall muscular demands for the latter (Cholewicki et al., 1995; Granata and Orishimo, 2001). The second evaluation test will indirectly compare the joint and muscle loading relationships from EMGopt with previously reported *in vivo* and *in silico* loads during equivalent tasks (Callaghan et al., 1999; https://orthoload.com; McGill et al., 2013; Rohlmann et al., 2014c, 2014a, 2008; Wilke et al., 1999).

The sensitivity of the EMGopt approach to the measured EMG activity and trunk force potential, will be evaluated by examining how variations in these measurements can alter the calculated lower back demands. First, the inherent variability associated with EMG activity will be tested by artificially adjusting the measured EMG maximal activity from each of the six bi-lateral trunk muscles by $\pm$10% (Ahern et al., 1986; Lehman, 2002; Yang and Winter, 1983). Similarly, the MVC strength potential will also be adjusted by $\pm$10% for each of the six measured toques (Stokes et al., 1988; van Dieën and Heijblom, 1996). For each sensitivity test, the lower back demands from the SSS normal walking, carrying 15BW in one hand, and carrying 15BW

split between each hand will be quantitively compared to the original unadjusted demands of these tasks.

Finally, the effect of participant-specific MTA strength potential adjustments will be evaluated by comparing the total EMG gain adjustments needed to reach a solution to the nominal 100N/cm^2 MMS solution. Here it is assumed that a lower total gain adjustment (e.g. $\sum_{i=1}^{238}(1-g_i)$) would reflect a better match between the model and the calculated kinetic demands of the task.

Model Limitations

As with any modeling study, the results will be subject to limitations. The model will neglect passive force contributions from non-muscular tissues and intra-abdominal pressure as their contributions during the upright postures and low exertion levels of gait are minimal (Arshad et al., 2018; Callaghan et al., 1999). Similar reasoning justifies disregarding intervertebral and axis of rotation translations (Ghezelbash et al., 2015). The vertebral coupling used in model *m29DoF* to assign the vertebral positions is generic and assigns the total thoracic rotational contributions to the T12/L1. For the present study the complexities in measuring each individually is not justified, while better dispersing the thoracic contributions to trunk movement will be left to future work (Bruno et al., 2017; Ignasiak et al., 2016). Due to a lack of muscle-specific data, the musculotendon dynamics will be assumed uniform and the EMG-force relationship linear for all 238 MTAs, consistent with other musculoskeletal models of the lower back (Granata and Marras, 1995a; McGill, 1992). The model currently relies on a top-down inverse dynamics approach to calculate the kinetic demands at each joint. However, it has been demonstrated that incorporating the GRFs is more sensitive to the impulsive forces which occur at heel strike (Callaghan et al., 1999; Hendershot and Wolf, 2014). Therefore, though a top-down approach will be initially

applied because of potential inaccuracies in the GRFs resulting from the moving treadmill belt, a bottom-up solution will also be investigated.

3.2. Study 2: Lower Back Demands During Induced Lower Limb Gait Asymmetries

3.2.1. Introduction

Walking is a fundamental means of locomotion, with activities often generating thousands of steps per day (Tudor-Locke et al., 2011). It is widely recommended for aerobic and musculoskeletal conditioning, and can provide therapeutic relief from lower back pain (LBP; Nutter, 1988). However, a variety of lower limb conditions can result in asymmetric gait kinematics and kinetics, including congenital deformities, injury, rehabilitative joint restriction, disease, and amputation (Cappozzo and Gazzani, 1982; Constantinou et al., 2014; Dananberg, 1993; Devan et al., 2014; DeVita et al., 1991; Dingwell et al., 1996; Friberg, 1983; Gulgin et al., 2018; Mündermann et al., 2005; Tanaka et al., 2015; Wolfe et al., 1996). Gait asymmetries are often classified with a symmetry index to quantify the degree of bi-lateral differences in limb kinematic or kinetic parameters (Robinson et al., 1987). Given the established relationship between LBP, asymmetric postures, and repeated loading (Bernard, 1997; da Costa and Vieira, 2010; Hoogendoorn et al., 1999; Marras, 2000), it is not surprising that gait asymmetries are related to LBP. In fact, the reported magnitude of LBP prevalence in those with asymmetric gait is alarming, more than quintupled that of the general able-bodied population (Ehde et al., 2001; Giles and Taylor, 1981; Ready et al., 2018; Smith et al., 1999; Wolfe et al., 1996). Therefore, the cumulative lower back demands associated with asymmetrical gait are of interest to clinicians and researchers looking to improve the quality of life in these LBP susceptible patients (Dananberg and Guiliano, 1999; Devan et al., 2014; Friel et al., 2005; Morgenroth et al., 2010).

Despite a wide range of asymmetry origins, lower back loading during asymmetric gait has been studied primarily in lower limb amputees (Devan et al., 2014; Sagawa et al., 2011).

Biomechanical models have predicted lower back demands to be ~40 to 80% greater for amputees compared to able-bodied individuals (Cappozzo and Gazzani, 1982; Hendershot et al., 2018; Hendershot and Wolf, 2014; Sagawa et al., 2011; Shojaei et al., 2016; Yoder et al., 2015; Yu et al., 2014). Unfortunately, individual studies on amputees are often compromised by low participant numbers, between-subject differences in amputation and prosthetic type (e.g. kinetic abilities, inertial properties, and prosthetic fit), and a lack of a baseline comparison (Chow et al., 2006; Hafner et al., 2002; Highsmith et al., 2019; Nolan et al., 2003; Selles et al., 1999; van der Linden et al., 1999; Windrich et al., 2016; Yu et al., 2014).

An alternative approach to understanding the link between gait asymmetries and lower back demands is to study able-bodied participants with asymmetry artificially-induced through uni-lateral modifications in leg length, leg inertial characteristics, joint motion restrictions, casting, or step cadences (Brown et al., 2018; Gulgin et al., 2018; Lemaire et al., 2000; Roemmich et al., 2012; Royer and Martin, 2005; Vanicek et al., 2007). This approach would be representative of other clinical asymmetric gait populations such as those with isolated pain, leg length discrepancies, or lower limb casting. Perturbing able-bodied participants with uni-lateral leg lengthening via thickened shoe sole or a clinical "walking boot" (Fig. 3.2.1) has been shown to increase trunk range of motion and trunk muscular activity (Gulgin et al., 2018; Kakushima et al., 2003; Vink and Huson, 1988), but their effects on trunk tissue demands have not yet been investigated. A controlled experimental setup that can induce asymmetries in a healthy and homogeneous cohort may help us better identify how different types of asymmetries can affect lower back demands during locomotion.

Therefore, the objective of this study is to investigate how experimentally induced asymmetric gait causalities can impact the lower back. Gait asymmetries will be induced by uni-

laterally altering the leg length, leg mass, and joint motion (via a walking boot). The effects of each condition on lower back demands will be examined with the EMG-optimization musculoskeletal model described in Study 1. Results from this study will provide insights into sources of gait asymmetry that can most adversely affect lower back demands.

3.2.2. Aims and Hypotheses

Aim 2.1: To investigate how different experimentally induced asymmetric gait causalities can impact the lower back kinetic demands. The effects of altered uni-lateral leg length, leg mass, and a clinical walking boot on lower back demands will be examined with an EMG-optimization musculoskeletal model.

Hypothesis 2.1: The combination of joint restriction, added mass and leg lengthening inherent in a walking boot will more greatly affect lower back demands than equivalent uni-lateral leg lengthening or added lower limb mass applied independently.

Exploratory Aim 2.2: To examine the relationship between level of gait asymmetry and lower back demands.

Exploratory Hypothesis 2.2: Lower back demands will in general increase with the level of asymmetry, but their linear relationship will not be significant.

3.2.3. Methods

Participants

Eight (n=12; male=6) participants will be recruited from the general university population (see Appendix B for the rationale). Inclusion / exclusion criteria will be the same as in Study 1. All subjects will be required to read and sign an Informed Consent document approved by the University of Massachusetts Amherst Institutional Review Board.

Equipment and Setup

The experimental setup described in Study 1 will be used to collect motion capture, electromyography (EMG), treadmill, dynamometer data, and test for fatigue for a variety of symmetric and asymmetric gait conditions (Table 3.2.1). Perturbations to symmetric gait will be administered with an EvenUp^{TM} adjustable Shoe Leveler (2.54 cm) affixed to the sole of one shoe to simulate a leg length discrepancy, with a 1.2 kg sand ankle-weight placed superior to the medial malleolus on one leg to simulate leg mass discrepancy, and with a uni-lateral medical-grade walking boot (AirCast FP Walker Foam Pneumatic) (Fig. 3.2.1). The selected leg length and ankle-mass perturbation magnitudes will be based on the characteristics of the walking boot. All perturbations will be applied to the right limb of each participant. For the walking boot conditions, all motion capture markers below the right knee will be removed and placed in equivalent locations on the surface of the walking boot.

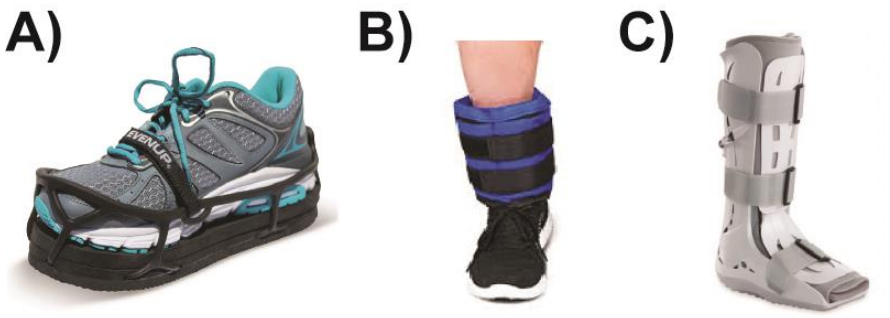

Figure 3.2.1. Individual perturbations mechanisms applied to induce asymmetric gait. Panel A) adjustable shoe leveler, B) ankle-weight, C) walking boot. (Photos courtesy of A) www.rehabmart.com, B) JBM International via www.amazon.com, and C) www.SourceOrtho.net)

Table 3.2.1. The five experimental trials and the corresponding perturbations. After the initial symmetrical control task (1), all other trials will be block randomized by conditions involving the walking boot (5) or not (2-4). *All trials will be performed at 90% of a participant's self-selected treadmill walking speed (90S) and with perturbations applied to the right limb.

Symmetry Perturbation(s)*	Ankle Weight 1.2 kg	Shoe Leveler 2.54 cm	Walking Boot
Control / Symmetrical (1)			
Single	2		
		3	
Combination	4	4	
Walking Boot			5

Procedure

Participants will don form-fitting clothing and comfortable footwear prior to measurements of anthropometry, self-selected treadmill walking speed (SSS), maximal voluntary contractions (MVC), shoe sole depth, and experimental conditions. Leg length discrepancy, leg dominance, and shoe sole depth will be measured for each participant. Bi-lateral leg lengths will be measured from the anterior superior iliac spine (ASIS) to the medial malleolus while the participant is lying supine on an exam table (Murray and Azari, 2015). Leg dominance will be assigned by asking the participant, "with which leg would you prefer to kick a ball?" (van Melick et al., 2017). Shoe sole depth will be measured by comparing standing lateral malleolus height barefoot versus shod for each participant.

Five different walking trials will be performed at 90% of each participant's SSS (90S). The 90S condition represents the reported adjustment in walking speed chosen by participants wearing a similar walking boot (Gulgin et al., 2018). The five walking trials will include a symmetrical unperturbed control (1), with a 1.2 kg ankle weight (2), with a 2.54 cm shoe leveler (3), with a 2.54 cm shoe leveler and a 1.2 kg ankle weight (4), and with a walking boot (5). The unperturbed 90S walking trial will consist of 90 seconds of acclimation and 30 seconds of data

collection. The four perturbed walking trials will each consist of 270 seconds of acclimation and 30 seconds of data collection.

To reduce the number of necessary motion capture marker adjustments and corresponding model calibration poses, a randomized block design will introduce the walking boot trial following the other four trials. Two minutes of rest will be provided between each trial to minimize fatigue. Data from standing calibration poses will be recorded prior to and after all tasks have been performed in a random order.

Data Processing and Calculation of Lower Back Demands

All experimental data will be post-processed in MATLAB (MathWorks, Natick, MA) as described in Study 1. The OpenSim (Delp et al., 2007) musculoskeletal model and EMG-optimization (EMGopt) approach described in Study 1 will be used to determine lower back loading across all five task conditions. For the ankle weight and walking boot trials, the inertial characteristics of the appropriate lower limb segments in the model will be modified. A point mass of appropriate inertial characteristics will be added to the model 3 cm above the ankle joint center to represent the ankle weight, while the mass of the walking boot will be proportionally distributed between the right shank and foot for walking boot trials.

All gait trials will be time-normalized by individual strides, with initiation and termination established from consecutive right (perturbed) heel strikes. Heel and toe marker anterior-posterior velocities will be used to distinguish heel strikes and toe offs (Zeni et al., 2008) due to the absence of segregated ground reaction forces. Five individual strides will be randomly extracted from the 30-second data collection. The maximum, minimum, and average lower back demands from each stride and the standing calibration pose will be computed. These demands include vertebral joint compression, anterior-posterior shear, and medial-lateral shear forces, and the resultant moments.

Other lower back demands are the total force exerted by eight different muscle groupings (e.g. rectus abdominis, external obliques, internal obliques, multifidus, quadratus lumborum, latissimus dorsi, erector spinae, and psoas major). Levels of asymmetry for bi-lateral differences in stance time, stride length, peak ground reaction force, and muscular group forces will be determined by calculating the symmetry index (SI) (Robinson et al., 1987):

$$SI = \frac{2(X_R - X_L)}{(X_R + X_L)} \times 100\% \qquad \text{(Eq. 3.2.1)}$$

where X_R and X_L represent the variable of interest associated with either the perturbed (right) or unperturbed (left) side, respectively.

Preliminary Statistical Analysis

The manipulated independent variable for this study is perturbation type (e.g. shoe leveler, ankle weight, ankle weight and shoe leveler, and walking boot) (Table 3.2.1). Lower back demands and levels of asymmetry will be used as the dependent variable(s) in a one-way (5 tasks) repeated-measures analysis of variance (ANOVA; $\alpha = 0.05$) tests, with Tukey post hoc testing. The five tasks include the walking boot, ankle weight, shoe leveler, ankle weight in combination with the shoe leveler, and symmetric control. An exploratory analysis will compare levels of asymmetry and lower back demands with Pearson correlation coefficients. All statistical tests will be performed in SAS (SAS Institute Inc., Cary, NC).

3.3. Study 3: Demands on the Lower Back During Load Carriage in Asymmetrical Gait

3.3.1. Introduction

Gait asymmetries are defined as bi-lateral differences in lower limb kinematics or kinetics (Sadeghi et al., 2000). Individuals who demonstrate asymmetrical gait have a higher incidence of lower back pain (LBP) than those with normal gait (Devan et al., 2014; Kelsey et al., 1984; Knutson, 2005b; Ready et al., 2018; Wolfe et al., 1996). There are several chronic and acute causalities for asymmetrical gait. Chronic pathologies associated with asymmetric gait include lower limb injuries, deformities, bi-lateral leg length differences, and amputations (Constantinou et al., 2014; Dananberg, 1993; Devan et al., 2014; Knutson, 2005b; Mündermann et al., 2005). Acute lower limb gait asymmetries can result from localized pain or a prescribed joint motion restriction (Gulgin et al., 2018). Carrying an uneven load, awkward object, or with only one arm can by themselves temporarily induce asymmetric gait (Bergmann et al., 1997; DeVita et al., 1991; Wang and Gillette, 2018).

Studies using *in vivo* measurements and *in silico* biomechanical musculoskeletal models to determine lower back loading have demonstrated that both upper and lower limb induced asymmetries result in larger lower back demands than that of symmetrical healthy gait (Cappozzo and Gazzani, 1982; Hendershot et al., 2018; Hendershot and Wolf, 2014; McGill et al., 2013; Rohlmann et al., 2014c; Rose et al., 2013; Shojaei et al., 2016; Wilke et al., 2001; Yoder et al., 2015; Yu et al., 2014). In fact, carrying a weight solely in one hand can produce higher compressive loads than when twice the total weight is carried evenly in two hands (McGill et al., 2013; Rohlmann et al., 2014c; Wilke et al., 2001). However, the combined effect of load carriage asymmetries and lower limb asymmetrical gait on lower back demands has not been determined.

Therefore, the objective of this study is to determine how upper extremity load carriage techniques affect lower back demands during both symmetrical and asymmetrical gait. To study this, healthy able-bodied participants will wear a medical-grade walking boot on one leg to induce a lower limb gait asymmetry (see Study 2) and in addition will be asked to carry prescribed weights in either one or two hands. Lower back demands will be determined with an EMG optimization (EMGopt) driven OpenSim musculoskeletal model of the lower back (Study 1). By establishing how an everyday activity such as load carriage can affect lower back demands for those a lower limb asymmetry, clinicians and ergonomists may be able to help reduce lower back pain and injury in individuals with asymmetric gait (Devan et al., 2014).

3.3.2. Aims and Hypotheses

Aim 3.1: To examine how upper extremity load carriage can affect lower back demands during asymmetrical gait.

Hypothesis 3.1.1: Uni-lateral loads carried on the side contralateral to the walking boot will be more demanding on the lower back compared to ipsilateral load carriage.

Hypothesis 3.1.2: Upper extremity load carriage combined with lower limb asymmetry will produce greater lower back demands than either upper extremity load carriage or lower limb asymmetries alone.

3.3.3. Methods

Participants

Eight (n=12; 6 male) participants will be recruited from the general university population (see Appendix B for the rationale). Inclusion / exclusion criteria will be the same as in Studies 1

and 2. All subjects will be required to read and sign an Informed Consent document approved by the University of Massachusetts Amherst Institutional Review Board.

Equipment and Setup

The experimental setup and techniques described in Studies 1 and 2 will be used to collect motion capture, dynamometer and electromyography (EMG) data, implement treadmill walking and load carrying trials, test for fatigue, and effect a walking boot asymmetry perturbation. Walking trials will include normal symmetrical gait, and asymmetrical gait with the walking boot worn on the right limb of each participant. Hand-held adjustable weight dumbbells will be carried both bi- and uni-laterally in symmetrical and asymmetrical conditions (Fig. 3.3.1). Dumbbell weight will be specified based on each participant's body weight.

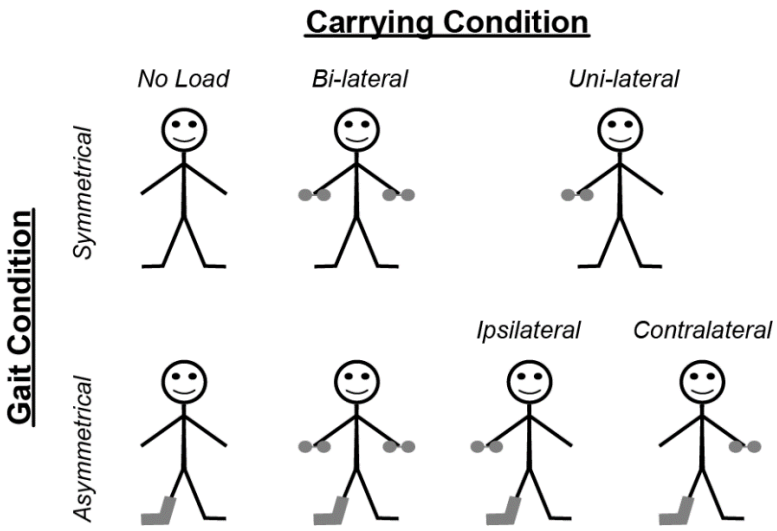

Figure 3.3.1. Schematic of the gait and load carriage experimental conditions. See Table 3.3.1 and in text *Procedure* for complete details on walking trial sets.

Procedure

Participants will wear form-fitting clothing and comfortable footwear during measurements of anthropometry, leg length discrepancy, leg dominance, shoe sole depth, self-selected treadmill walking speed (SSS), MVCs, and experimental walking conditions.

Twelve experimental walking and load carriage tasks will be performed at 90% of each participant's SSS (90S; Table 3.3.1.). The 90S condition represents the speeds reported while participants wore a similar walking boot or were required to carry a load (Crosbie et al., 1994; Gulgin et al., 2018; Nottrodt and Manley, 1989). The twelve trials will consist of five symmetrical walking trials and seven asymmetrical walking trials with the walking boot on the right leg. For the symmetrical tasks, upper extremity load carriage conditions include a no-load control trial and trials of 7.5% (7.5BW) and 15.0% (15BW) body weight loads carried in two hands (bi-lateral) and in the right hand only (uni-lateral). In the asymmetrical walking boot trials, uni-lateral one-hand carries will be conducted with the weight in both the contralateral and ipsilateral hands with respect to the walking boot. Thus, seven asymmetrical trials will include a no-load trial, two bi-lateral two-handed carries of 7.5BW and 15BW, and four uni-lateral carriage trials (7.5BW and 15BW in both right and left hands).

The control 90S walking trial will consist of 90 seconds of acclimation and 30 seconds of data collection (Matsas et al., 2000; Taylor et al., 1996). The unloaded walking boot trial will consist of 270 seconds acclimation and 30 seconds of data collection. Due to manual material handling recommendations (Dick et al., 2017), each carrying task will be restricted to only 20 seconds of acclimation prior to recording the task for 30 second. Data from standing calibration poses will be recorded prior to and after all tasks have been performed.

To reduce the number of necessary motion capture marker adjustments and corresponding model calibration poses, a randomized block design will separate the seven walking boot trials from the five symmetrical gait trials. The symmetrical walking block will always precede the walking boot block to prevent post-adaptations, and both blocks will commence with their respective no-load control trial. After the symmetrical gait conditions, all motion capture markers below the right knee will be removed and placed in equivalent locations on the surface of the walking boot. Two minutes of rest will be provided between each walking and carrying trial to minimize fatigue.

Table 3.3.1. The twelve different walking and load carriage trials. Each trial will be performed at 90% of a participant's self-selected treadmill walking speed (90S). All conditions will be block randomized by trials involving and not involving the walking boot. Loads will be participant-specific and based on a percentage of bodyweight (%BW). Uni-lateral-contralateral and uni-lateral-ipsilateral carrying locations represent the load carriage side relative to the walking boot on the right foot. Superscripts denote the analysis of variance (ANOVA) test group(s) assigned to that trial. *Only the uni-lateral asymmetrical carrying location that results the largest lower back demands will be used in test 'b'. **Bi-lateral loads will be equally distributed between the left and right hands.

	Gait Condition	Carrying Location	Total Load Carried (%BW)	
	*Symmetrical (Shoes)*	*None*		
		*Bi-lateral***	7.5[b]	15[b]
		Uni-lateral (Right Hand)	7.5[b]	15[b]
	*Asymmetrical (Walking Boot)*	*None*		
		*Bi-lateral***	7.5[b]	15[b]
		Uni-lateral (Contralateral)	7.5[a,b*]	15[a,b*]
		Uni-lateral (Ipsilateral)	7.5[a,b*]	15[a,b*]

Data Processing and Calculation of Lower Back Demands

All experimental data will be post-processed in MATLAB (MathWorks, Natick, MA) as described in Study 1. The OpenSim (Delp et al., 2007) musculoskeletal model and EMG-

optimization (EMGopt) approach described in Study 1 will be used to determine lower back loading during all twelve tasks. During walking boot trials, the right lower limb inertial characteristics of the model will be adjusted to account for the mass of the walking boot. The dumbbell inertial characteristics will be described as cylinders of appropriate mass and size affixed to the hands by a weld joint.

Preliminary Statistical Analysis

Dependent variables of interest, including lower back demands and symmetry indices, will be computed as described in Study 2. Two separate analysis of variance (ANOVA; $\alpha = 0.05$) tests will determine a) if there is an effect of uni-lateral hand carriage location relative to the walking boot side and b) if different load carriage techniques can be more deleterious for those with gait asymmetries (Table 3.3.1). For the former test (a) a two-way (2 uni-lateral hand locations × 2 weights carried) repeated-measures ANOVA test will compare the effects of contra- versus ipsilateral to the walking boot uni-lateral load carriage demands. The uni-lateral carrying location (contra- or ipsilateral) resulting in higher lower back demands will be applied in the second test on load carriage and gait asymmetries. For this second test (b) a three-way (2 gait symmetries × 2 carriage types × 2 weights carried) ANOVA will compare lower back demands and levels of asymmetry across different gait types, load carriage types, and load magnitudes. Tukey post hoc testing will analyze significant ANOVA findings, while paired t-tests can potentially compare select conditions to symmetrical or asymmetrical control conditions. All statistical tests will be performed in SAS (SAS Institute Inc., Cary, NC).

3.4. Amendments to the Proposed Methods

Due to unforeseen data and modeling complications, several alterations were made to the details in the original proposal (see Chapter 3.1-3.3). This section briefly describes all pertinent modifications to the proposed methods.

Musculoskeletal Model

After careful qualitative examination of pilot date, the musculoskeletal model (see Appendix C) applied a top-down approach to determine the lumbar joint moments. This approach was chosen because high frequency noise from the treadmill's ground reaction forces contaminated the lower back resultant joint moments from the bottom-up approach (Fig. 3.4.1). Future evaluations of the model should compare bottom-up and top-down approaches with an overground setup using fixed force plates (Kingma et al., 1996).

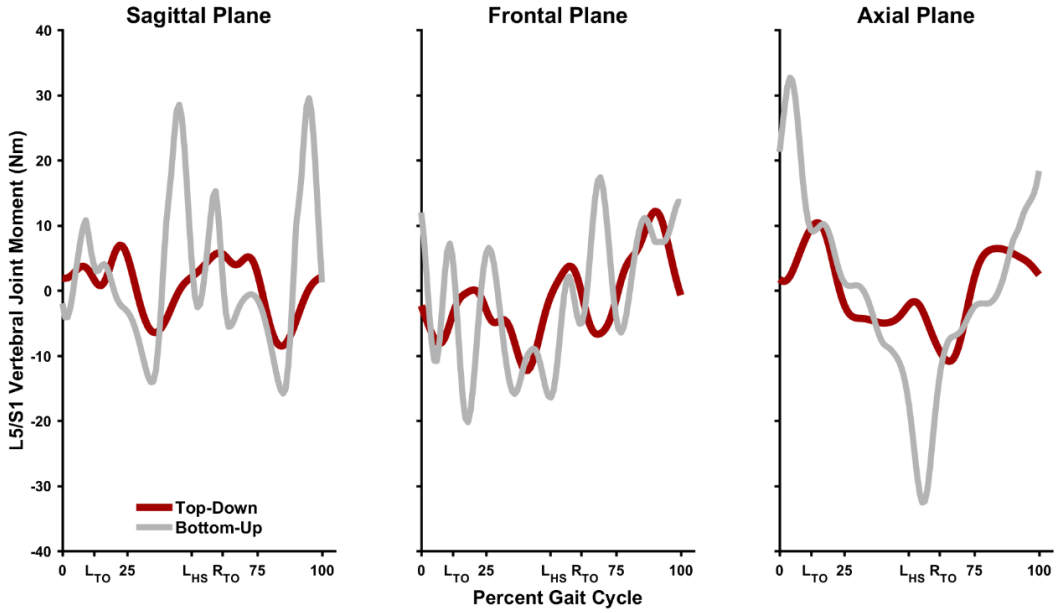

Figure 3.4.1. L5/S1 vertebral joint internal moments from a representative participant during steady state gait calculated with top-down and bottom-up computational approaches. Positive values are representative of extensor, right lateral flexor, and right axial rotation moments (N*m) in the sagittal, frontal, and axial planes, respectively. The gait cycle was defined from consecutive right heel strikes. *Maroon* and *grey lines* represent top-down and bottom-up approaches, respectively. Abbreviations: left heel strike (L_{HS}), left toe-off (L_{TO}), and right toe-off (R_{TO}).

General Experimental Setup

Due to issues with electromyography (EMG) electrodes, the experimental protocol regarding maximal voluntary contractions (MVCs) was changed. Preliminary assessments revealed that EMG data from several initial participants (n=6) was unusable due to electrode movement occurring during MVCs when they were performed before the gait trials. To solve the issue MVCs instead were performed at the end of the protocol and with only two repetitions in each posture. Secondly, it was found that a rigid marker cluster could not be effectively and comfortably attached to the participant's upper back (thorax) as proposed. Instead, a single marker was placed over the T6 vertebra. The thorax kinematics were tracked with the T6 and five other markers placed anterior and posterior above L1 and below C7 vertebrae (see Fig. 4.2.1).

General Analysis

All statistics tests were performed in MATLAB (MathWorks, Natick, MA) and not SAS (SAS Institute Inc., Cary, NC) as originally proposed. The decision to switch programs was based on personal preference, the statistical comparisons being made, and restricted access to on-campus SAS software during the COVID-19 pandemic.

Study 1

The unloaded walking condition at 90% of self-selected speed (90S) was not included in the Study 1 comparisons because it was not applicable to any published comparisons. For sensitivity tests, EMG activity was artificially adjusted $\pm$10% for each of the 6 bilateral electrode groups rather than each of the 12 individual electrodes to reduce the number of comparisons to a more manageable number. Finally, participant-specific maximum muscle strengths were compared to a nominal maximum muscle strength of 100 N/cm^2 used in other models (e.g.

Beaucage-Gauvreau et al., 2019). This was determined to be a more severe and relevant comparison than the proposed ±10% adjustment scheme.

Study 2

Due to a lack of any statistical effects from any of the asymmetry perturbations on L5/S1 vertebral joint forces, Pearson-correlation comparisons between spatiotemporal asymmetries and joint forces were deemed not useful and were therefore omitted.

Study 3

Uni- and bilateral dumbbell hand load location comparisons were made relative to each dumbbell's mass rather than to the total load being carried by the participants. While this was a more conservative comparison, it prevented the two-handed 3.75% bodyweight dumbbell carries from being incorporated into the statistical analysis because one-hand 3.75% carries were not administered.

CHAPTER 4

STUDY 1

AN EMG OPTIMIZATION OPENSIM MUSCULOSKELETAL MODEL OF THE LOWER BACK KINETIC DEMANDS IN GAIT

4.1. Introduction

Lower back pain is a multifactorial musculoskeletal disorder with a reported global point prevalence of 7.5% (Wu et al., 2020). Internal kinetic demands on the lower back from everyday tasks are an important risk factor associated with the occurrence of lower back pain (da Costa and Vieira, 2010; Norman et al., 1998) and are often compared to alternative tasks, established tissue tolerances, and injury reports to develop safety guidelines and rehabilitation programs. However, internal kinetic demands are impractical to measure *in vivo* (Dreischarf et al., 2016), so biomechanical musculoskeletal models of the lower back which apply observed kinematics, mathematical equations, established anatomy, and biological assumptions have been developed. Such models should be evaluated through comparisons with known measures, previous model calculations, established principles, and tested for input parameter sensitivity to generate confidence in their calculated outcome measures (Cholewicki and McGill, 1996; Hicks et al., 2015; Neptune, 2000).

There are several open-source lower back models available in OpenSim (Delp et al., 2007), most based on an original model of Christophy et al. (2012) and then refined and evaluated for specific applications (Actis et al., 2018a; Beaucage-Gauvreau et al., 2019; Bruno et al., 2015; Molinaro et al., 2020; Raabe and Chaudhari, 2016; Senteler et al., 2016; Zhu et al., 2017). The majority of these models have used static optimization (SOpt) to estimate the individual muscular forces responsible for the observed kinematics (Crownshield and Brand, 1981), and none have

been explicitly evaluated for the analysis of lower back demands during walking gait. SOpt is based on the premise that muscles will be recruited to minimize a criterion objective function such as fatigue, and therefore it is inherently biased against the prediction of antagonistic muscle activation (Marras, 1988). In contrast, models that incorporate electromyography (EMG) to estimate muscular contributions can reflect participant-specific recruitment strategies, antagonistic activity, and strength potentials (Davis and Jorgensen, 2005; Le et al., 2017). The accurate distribution of individual muscle forces is crucial in estimating the amount of stress on anatomical tissues (Marras, 2000). EMG-based models may therefore provide improved accuracy and insight into how tasks and recruitment strategies effect lower back loading.

EMG-assisted models come in two forms. Models driven strictly by EMG apply measured and calibrated muscle activity to directly predict muscular forces (Davis and Jorgensen, 2005). Unfortunately, due to physiological complexities and the inherent limitations of EMG (Davis and Jorgensen, 2005; van Dieën and Visser, 1999), the forces predicted from an EMG-driven model will not necessarily satisfy the joint demands calculated from inverse dynamics (Choi and Vanderby, 1999; Cholewicki et al., 1995; Gagnon et al., 2001). To overcome this limitation, an EMG optimization method (EMGopt) was developed by Cholewicki and McGill (1994). By minimally adjusting the measured EMG activations to match the calculated joint demands, EMGopt is capable of alleviating the flaws of both the optimization and EMG-driven approaches while simultaneously incorporating some of the advantages of each (Choi and Vanderby, 1999; Cholewicki et al., 1995; Gagnon et al., 2001; Li and Chow, 2019). An EMGopt framework has not yet been developed for use in OpenSim.

Therefore, the primary objective of this study was to develop and evaluate an EMGopt framework for defining muscular contributions in a participant specific OpenSim musculoskeletal

model. For evaluation, the lower back demands predicted by EMGopt were compared directly to results from a standard SOpt algorithm, and indirectly to demands reported in the literature during similar gait tasks (Callaghan et al., 1999; McGill et al., 2013; Rohlmann et al., 2014a, 2014c, 2008; Rose et al., 2013; Wilke et al., 1999). The sensitivity of the model's estimated joint demands to reported variability in muscular activity and participant-specific strength potentials was also investigated. The motivation of this study was to develop an EMGopt model that could be applied in subsequent studies to help improve our understanding of how different gait and load carriage asymmetries can adversely impact lower back demands.

4.2. Methods

Participants

Six (n=6; male=3) participants were recruited from a university population. The participants were on average 25 (SD±3) years old, 65.2 (±9.6) kgs, and 171 (±9.1) cm tall. Participants over 40 years old, or with a high body mass index (BMI > 30), history of lower back pain, low self-reported level of physical activity, or any neurological issues were excluded. All subjects read and signed an Informed Consent document approved by the University of Massachusetts Amherst Institutional Review Board.

Equipment and Setup

Full-body three-dimensional kinematics were collected at 100 Hz with an eight-camera motion analysis system (Qualisys AB, Gothenburg, Sweden). The motion of body segments and select anatomical landmarks from each participant were captured with a combination of individual and clustered 12.5 mm reflective markers (Fig. 4.2.1). Specifically, for the trunk and pelvis, kinematics were tracked with markers placed on both anterior superior iliac spines (ASIS), both

posterior superior iliac spines, both iliac crests, both acromion, the xiphoid process, sternal notch, and over the C7 and T6 vertebrae.

Electromyograms (EMG) from twelve wireless surface electrodes (Delsys Inc., Natick, MA) were sampled at 2000 Hz. Electrodes were positioned (Fig. 4.2.1) based on previous studies (Gagnon et al., 2011; McGill et al., 2013) over six bilateral trunk muscles: rectus abdominis (3 cm lateral to umbilicus), external oblique (3 cm lateral to the linea semilunaris), internal oblique (at the level of the ASIS but superior to the inguinal ligament and medial to linea semilunaris), latissimus dorsi (inferior to scapula over muscle belly when arms are abducted), longissimus thoracis pars thoracis (3 cm lateral to L1), and iliocostalis lumborum pars thoracis (6 cm lateral to L3).

Isometric maximal voluntary contractions (MVCs) were measured with a Biodex dynamometer (Biodex Medical Systems Inc., Shirley, NY) to establish maximal EMG amplitudes and trunk flexion, extension, lateral bending, and axial rotation torques for each participant. A series of static stance, walking and carrying tasks took place on an instrumented treadmill (Treadmetrix, Park City, UT) which provided gait pacing and measured ground reaction forces (GRF). The dynamometer torque and the gait GRF information were both sampled at 2000 Hz with a 16-bit A/D convertor (USB-2533, Measurement Computing Corporation, Norton, MA). The motion capture, EMG, and GRF signals were all synchronously collected within Qualisys's Track Manager software.

Hand-held adjustable weight dumbbells were held statically and carried both bi- and uni-laterally (right hand only) in symmetrical and asymmetrical gait carriage conditions. Dumbbell weight magnitudes were based on each participant's body weight.

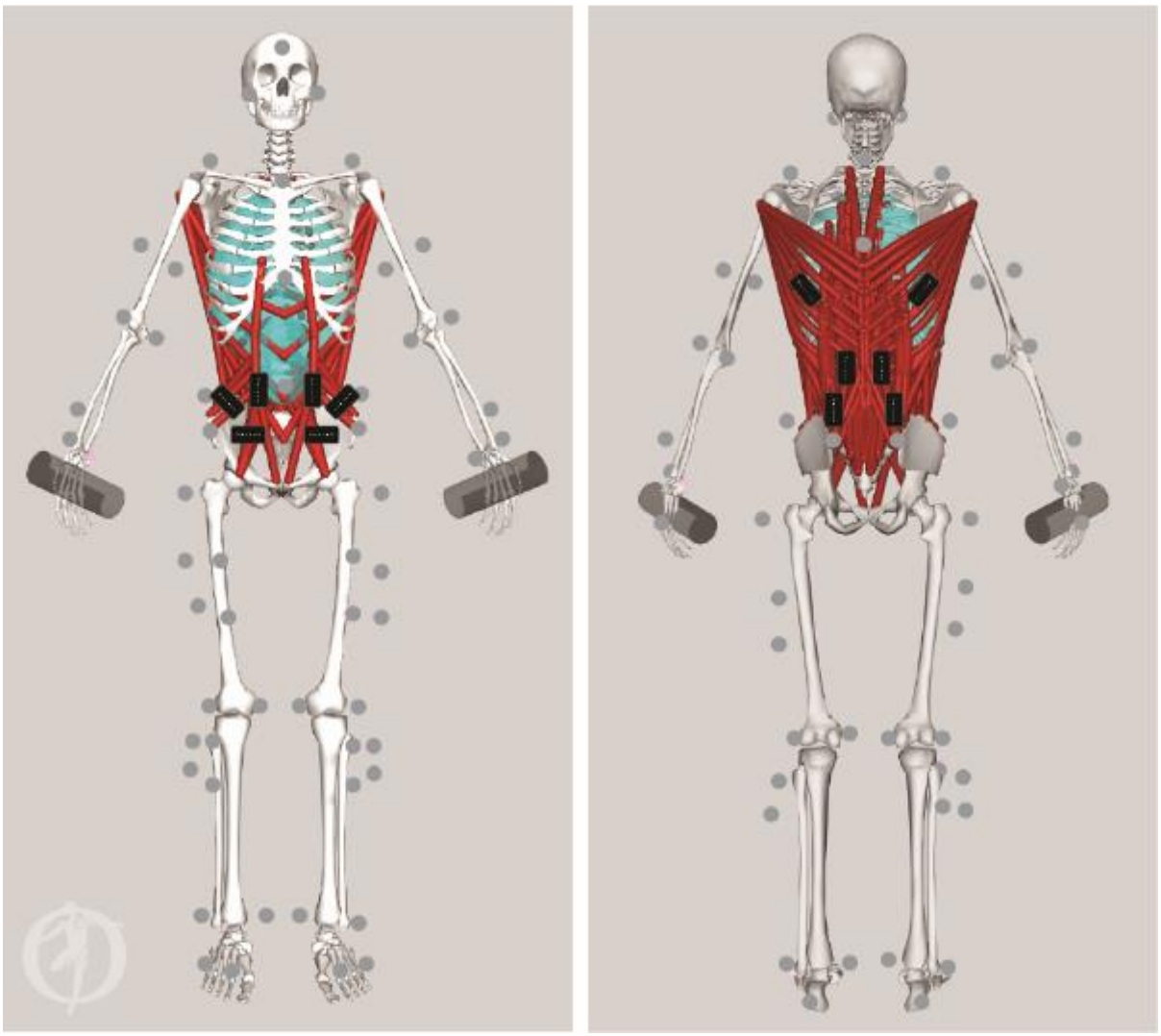

Figure 4.2.1. Full-body OpenSim musculoskeletal model. Dark grey spheres represent the location of the 64 reflective markers used for motion tracking, black rectangles the placement for the 12 electromyography (EMG) sensors used to monitor the muscular activity of the trunk, and the cylindrical rods simulate the added inertia of dumbbell's during carrying tasks.

Procedure

Participants donned form-fitting clothing and comfortable walking or running shoes prior to measurements of anthropometry, self-selected treadmill walking speed (SSS), the experimental evaluation tasks, and MVCs. Anthropometry measures of height and body weight were taken with a tape measure and balance scale. SSS on the treadmill was determined by prompting participants to correct the treadmill belt-speed from an initial randomly chosen high or low speed to a

"*comfortable walking speed which they can maintain for 3-5 minutes with minimal effort and discomfort*". Incremental speed adjustments blinded from the participant were made by the investigator in response to verbal cues from the participant. The SSS process was repeated until the participant consistently identified the same SSS. A 90% SSS (90S) value was calculated for each participant, representing the reported walking speed adaptation of participants during carrying tasks (Crosbie et al., 1994). After SSS determination, EMG electrodes were placed on the participant. To improve EMG quality, excess body hair at each electrode site was shaved and unwanted dead skin and oils removed with fine sandpaper and alcohol wipes. All EMG signals were continuously monitored for signal quality (Tankisi et al., 2020). Following electrode placement, the motion capture markers were attached to the participant.

The model was initially developed and pre-tested while participants stood quietly, and while holding dumbbells of 3.75%, 7.5%, or 15% body weight (3.75BW, 7.5BW, and 15BW, respectively) in each hand (see Supplemental Material). To fully evaluate the model for gait, participants performed a variety of tasks in which 1) the lumbar loading *in vivo* has been directly quantified (Rohlmann et al., 2014c, 2014a; Wilke et al., 1999), 2) a similar EMG-assisted computer model has calculated loads (Callaghan et al., 1999; McGill et al., 2013; Rose et al., 2013), 3) various modeling approaches can be differentiated, and 4) the sensitivity of EMGopt parameters across a variety of gait tasks can be determined (Table 4.2.1). These tasks included walking at SSS and 0.83 m/s, walking at 90S while carrying a dumbbell of 7.5% (r7.5BW) or 15% (r15BW) of bodyweight in only their right hand, and walking at 90S while carrying dumbbells of 7.5% (b7.5BW) or 15% (b15BW) in each hand. During both unloaded walking tasks, participants walked for 90 seconds to acclimate prior to recording the task for 30 seconds (Matsas et al., 2000; Taylor et al., 1996). For each carrying task, participants carried the prescribed load uninterrupted

for 20 seconds to acclimate followed by 30 seconds in which the task was recorded (Dick et al., 2017). Data from standing calibration poses were recorded prior to all tasks being performed in a random order. Two minutes of rest were imposed between each task to minimize fatigue.

After completion of all the tasks, each participant performed a series of MVC efforts on the dynamometer against a custom bar designed to resist trunk flexion, extension, lateral bending, and axial rotation (Fig. 4.2.2). MVCs were performed following the tasks to minimize the risk of compromising the electrodes' connection to the skin prior to the evaluation tasks. For the MVCs the dynamometer seat back was flattened horizontally, with the bar positioned dorsally at the midthoracic level during extension, ventrally just below the sternal notch during flexion and axial rotation exertions, and lateral on the arm at the level of the sternal notch during lateral bending exertions. The bar angle, distance of bar to the dynamometer center of rotation and the participants' pelvic position were recorded and applied to convert the measured torque into an equivalent bar reaction force vector applied to the trunk. Six different trunk exertions were performed (McGill, 1991; McGill et al., 2013). Five of the MVC exertions (trunk flexion, bi-lateral twisting, and bi-lateral lateral bending) took place from a sit-up position with the torso, knees, and hips flexed at approximately 45, 90, and 90-degrees, respectively (as estimated by a handheld goniometer). The sixth maximal effort (back extension) was performed with the participant prone and safely suspended from the dynamometer seat in a horizontal position with a slightly flexed torso (Biering-Sorensen, 1984). During each MVC, the participant was verbally encouraged and cued to perform maximally against the static bar for 3-5 seconds while EMG activity and dynamometer torque were recorded. To lessen participant discomfort and fatigue, only two repetitions of each MVC effort were performed with all exertions separated by 2-minutes of rest.

Table 4.2.1. Experimental tasks and the comparisons used to test the model and approach. The dependent variables (in *parenthesis*) used in each comparison were task and study specific. Abbreviations: anterior-posterior (AP), electromyography (EMG), EMG optimization (EMGopt), maximum musculotendon stress (MMS), self-selected speed (SSS), static optimization (SOpt), 15% body weight (15BW), and 7.5% body weight (7.5BW). *All carrying tasks were performed at 90% of SSS.

Position	Task	Direct Comparison(s)	Indirect Comparison(s)
Walking	SSS	EMGopt vs. SOpt (Lumbar Joint Loads); EMG & MMS Sensitivity (L5/S1 Joint Loads & EMG)	Callaghan et al., 1999 (peak L4/L5 compression); Rose et al., 2013 (peak L2/L3 AP shear); Rohlmann et al., 2014a (L1/L2 resultant force); Wilke et al., 1999 (peak L4/L5 compression)
	0.83 m/s	EMGopt vs. SOpt (Lumbar Joint Loads)	Rohlmann et al., 2014a (L1/L2 Resultant Force)
*Carrying**	7.5BW in right hand	EMGopt vs. SOpt (Lumbar Joint Loads)	Rohlmann et al., 2014c (peak L1/L2 resultant force); Rose et al., 2013 (peak L2/L3 AP shear)
	15BW in right hand	EMGopt vs. SOpt (Lumbar Joint Loads); EMG & MMS Sensitivity (L5/S1 Joint Loads & EMG)	McGill et al., 2013 (average L4/L5 joint loads); Rohlmann et al., 2014c (peak L1/L2 resultant force); Rose et al., 2013 (peak L2/L3 AP shear)
	7.5BW in each hand	EMGopt vs. SOpt (Lumbar Joint Loads); EMG & MMS Sensitivity (L5/S1 Joint Loads & EMG)	McGill et al., 2013 (average L4/L5 joint loads);
	15BW in each hand	EMGopt vs. SOpt (Lumbar Joint Loads)	McGill et al., 2013 (average L4/L5 joint loads); Rohlmann et al., 2014c (peak L1/L2 resultant force);

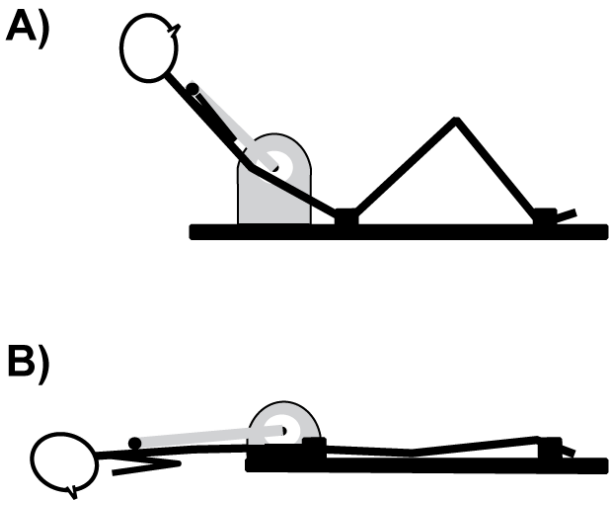

Figure 4.2.2. Positions used for the 5-second static Maximal Voluntary Contractions against the dynameter. Panel A) Sit-up position utilized for maximal trunk flexion, twisting, and lateral bending efforts (note: for lateral bending, the dynamometer resistance were rotated 90-degrees and positioned laterally against the upper arm) and B) Biering-Sorensen (1984) horizontal position used for maximal trunk extension efforts against the bar.

Data Processing

All data were post-processed in MATLAB (MathWorks, Natick, MA). Marker positions, GRFs, and dynamometer torques were filtered using a fourth-order zero-lag low pass Butterworth filter with a 6-Hz cutoff frequency selected from a residual analysis (Winter, 2009). EMG activity from each muscle was detrended, band-pass filtered (30 – 500 Hz), full wave rectified, and then low-pass filtered with a fourth-order 3 Hz zero-lag Butterworth filter (Brereton and McGill, 1998) before time-shifting by 10 ms to account for physiological electromagnetic delay (Corcos et al., 1992). Participant-specific EMGs were first scaled to their muscle-specific MVC maximum levels and then non-linearly scaled to better match the reported EMG-to-force relationship (Cholewicki et al., 1995). Filtered external forces and EMG linear envelopes were synchronously down sampled from 2000 Hz to 100 Hz to match the motion capture sample frequency.

All walking and carrying trials were time normalized by strides, with initiation and termination established from consecutive right heel strikes as identified by heel marker anterior-posterior velocities (Zeni et al., 2008), due to the absence of leg-independent GRFs. Maximum, minimum, and average values from each dependent variable of interest were derived from an ensemble average of three consecutive strides extracted from the latter portion of the 30-second data collection. Joint forces were normalized relative to each participant's bodyweight.

Musculoskeletal Model

Two separate full-body lumbar spine models with 27 segments, six lumbar joints, and 238 Hill-type trunk musculotendon actuators (MTAs; Hill, 1938; Thelen, 2003; Zajac, 1989) were developed within the OpenSim 4.0 modeling system (Delp et al., 2007). Model *m29DoF* with 29 degrees-of-freedom was based on the full-body lifting model of Beaucage-Gauvreau et al. (2019) and was used to determine the kinematics of each trial from recorded marker positions (Fig. 4.2.3).

Several modifications to the original model were made for simplicity, anatomical consistency and to improve model sensitivity (see section C of Appendices). Model *m47DoF* was identical to *m29DoF* except for the absence of coordinate coupler constraints on the lower back and abdominal joints. The kinematic motion from *m29DoF* was assigned to model *m47DoF* with 47 degrees-of-freedom to determine accurate MTA moment arms (Banks et al., 2019) across all six lumbar joints, and to compute joint loads (Fig. 4.2.3).

Both models were sized using the OpenSim scaling tool to match the calibration pose and anthropometry of the individual participants. The muscular strength potentials of the *m47DoF* MTAs were adjusted from a default nonspecific 100 N/cm^2 maximal stress to individual maximal muscular stress (MMS) values matching the maximal torque outputs from the MVC tasks for each participant. For this adjustment, the inverse dynamics tool in OpenSim was used along with the external forces and generic model states during each of the six MVC positions to calculate lumbar joint moments. To incorporate a level of antagonistic muscle forces in the model solution, all MTAs were assigned a minimal lower activity level of 0.05, based on the average antagonistic EMG activity observed during the MVC task. The highest calculated MMS from the six (five sit-up and an extension) positions was used to determine the maximal isometric force potential of the trunk flexors and extensors, respectively.

Participant-specific models were used to analyze the walking and carrying tasks. During carrying tasks, the dumbbell inertial characteristics were described as cylinders of appropriate mass and size affixed to the hands by a weld joint. The OpenSim inverse kinematics tool was used to best fit the *m29DoF* model with the recorded marker position data to determine generalized segmental coordinates. These segmental coordinates were then used to calculate the *m47DoF* model states and the "top-down" lower back joint moments from OpenSim's analysis and inverse

dynamics tools, respectively. Both SOpt and EMGopt approaches were separately applied to partition the lower back joint moments across the 238 MTAs (see next section for details). Model MTA, inertial, and external forces were input into the OpenSim joint reaction analysis tool to calculate the resultant lumbar joint forces from both optimization approaches. Lumbar joint forces were expressed in the most caudal lumbar joint coordinate system. All OpenSim tools and libraries were integrated with a custom MATLAB application programming interface in order to minimize error, implement the optimization algorithms, and improve workflow efficiency (Lee and Umberger, 2016).

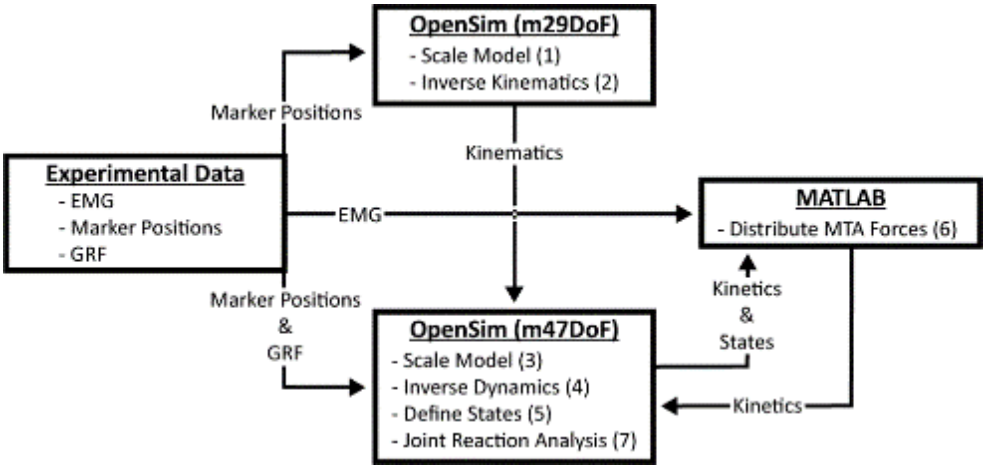

Figure 4.2.3. Flow chart of EMGopt model input/output processes. Braced numbers depict implementation sequence. Abbreviations: electromyography (EMG), ground reaction forces (GRF), and musculotendon actuator (MTA). Notes: 1) in addition to the above processes, MTA strength potential was also scaled to participant-specific maximal muscular stresses (see text for further details), and 2) the static optimization (SOpt) processes were similar, but did not make use of EMG information in Step 6.

Approaches to Solving Muscle Indeterminacy

The contribution of each individual MTA force towards the calculated joint moments was solved with two different optimization approaches, both run in MATLAB with the *fmincon* sequential quadratic programming algorithm. The first approach (SOpt) was based upon the hypothesis that MTAs are recruited in such a way as to minimize muscular fatigue (Crownshield

and Brand, 1981), represented by an objective (J_{SO}) minimizing the sum of the squared activations (a_i) across all the MTAs (i = 1 to 238):

$$J_{SO} = min \sum_{i=1}^{238} (a_i)^2 \quad \text{(Eq. 4.2.1)}$$

subject to the following inequality constraints for each lumbar joint (j = 1 to 6):

$$\left|M_{MTA_{x_j}} - M_{ID_{x_j}}\right| \leq \left|0.005 * M_{ID_{x_j}}\right| \quad \text{(Eq. 4.2.2)}$$

$$\left|M_{MTA_{y_j}} - M_{ID_{y_j}}\right| \leq \left|0.005 * M_{ID_{y_j}}\right| \quad \text{(Eq. 4.2.3)}$$

$$\left|M_{MTA_{z_j}} - M_{ID_{z_j}}\right| \leq \left|0.005 * M_{ID_{z_j}}\right| \quad \text{(Eq. 4.2.4)}$$

$$0.01 \leq a_i \leq 1.00 \quad \text{(Eq. 4.2.5)}$$

where x, y, z are the orthogonal moments (M_{MTA}) resulting from the MTA forces predicted by the SOpt constrained to match the moments calculated from inverse dynamics (M_{ID}) to within ±0.5%, with MTA activations positive and between 0.01 and 1.00. All MTA maximal force potentials were further constrained by their kinematic state and maximal isometric potential (Thelen, 2003; Zajac, 1989).

The second optimization approach (EMGopt) balanced joint moments with minimal adjustments to measured EMG activity (Cholewicki and McGill, 1994). The objective function for EMGopt (J_{EMG}) followed the multi-joint convention established by Gagnon et al. (2011):

$$J_{EMG} = \min \sum_{i=1}^{238} M_{norm_i} (1 - g_i)^2 \quad \text{(Eq. 4.2.6)}$$

with:

$$M_{norm_i} = \sqrt{\sum_i (M_{MTA_{x(i,j)}}{}^2 + M_{MTA_{y(i,j)}}{}^2 + M_{MTA_{z(i,j)}}{}^2)} \quad \text{(Eq. 4.2.7)}$$

which will minimize the adjustments (g_i) made to the predicted muscular forces based on the Euclidean moments norm (M_{norm}) from each MTA (i = 1 to 238) about each joint (j = 1 to 6) subject to the following constraints:

$$\left|g_i M_{MTA_{x_j}} - M_{ID_{x_j}}\right| \leq \left|0.005 * M_{ID_{x_j}}\right| \quad \text{(Eq. 4.2.8)}$$

$$\left|g_i M_{MTA_{y_j}} - M_{ID_{y_j}}\right| \leq \left|0.005 * M_{ID_{y_j}}\right| \quad \text{(Eq. 4.2.9)}$$

$$\left|g_i M_{MTA_{z_j}} - M_{ID_{z_j}}\right| \leq \left|0.005 * M_{ID_{z_j}}\right| \quad \text{(Eq. 4.2.10)}$$

$$Thres \leq g_i \leq 1/emg_{a_i} \quad \text{(Eq. 4.2.11)}$$

where x, y, z are the orthogonal moments (M_{MTA}) resulting from the MTA forces (i = 1 to 238) and their moment arms. The MTA forces are a product of the current MTA potential, the EMG activations (emg_{a_i}), and the adjustment factors (g_i). The constraints ensure that the optimized MTA forces produce moments that match the corresponding moments calculated from inverse dynamics to within $\pm$0.5%. Adjustment factor ranges were MTA-specific and designed to keep all MTA forces below their maximal force potential and above a specified fraction of their measured activation (Gagnon et al., 2016). MTAs with surface EMG electrodes (rectus abdominis, external obliques, internal obliques, latissimus dorsi, longissimus thoracis pars thoracis, and iliocostalis lumborum pars thoracis) were assigned a stringent $Thres$ = 0.50 for g_i which kept activations at or above 50% of their recorded magnitude. MTAs without an assigned electrode (psoas, multifidus, quadratus lumborum, longissimus thoracis pars lumborum, and iliocostalis lumborum pars lumborum) were provided a more lenient $Thres$ = 0.01 for g_i and had their activations based on electrode activity (emg_{a_i}) from nearby MTA synergists (see Appendix C, Table C.1; Gagnon et al., 2011; McGill et al., 1996).

Model Evaluation

Five different evaluation tests were performed, including three designed to examine the validity of the model and EMGopt approach. The first evaluation test compared predicted EMGopt and SOpt lumbar joint forces across all the walking and carrying tasks. The second test was designed to indirectly compare equivalent joint loads and tasks from the current EMGopt and SOpt approaches with previously reported *in vivo* and EMG-assisted *in silico* loads (Callaghan et al., 1999; McGill et al., 2013; Rohlmann et al., 2014a, 2014c, 2008; Rose et al., 2013; Wilke et al., 1999). Loads from all studies were normalized to bodyweights. The pressure measurements from Wilke et al. (1999) were converted to an estimation of force by the methods described by Nachemson (Dreischarf et al., 2016; Nachemson, 1966, 1960). Thirdly, the ability of the both EMGopt and SOpt activations to reflect the recorded EMG activity were quantified with cross-correlations and root mean squared errors (RMSE) across tasks of SSS, carrying 15BW in only their right hand, and carrying 7.5BW in each hand.

The sensitivity of the EMGopt approach to the measured EMG activity and trunk force potential was evaluated by assessing how absences or variations in these measurements can alter the calculated lower back demands at the L5/S1 joint. First, the inherent variability associated with EMG activity was tested by artificially adjusting the measured EMG maximal activity from each of the six bi-lateral trunk muscles by $\pm$10% (Ahern et al., 1986; Lehman, 2002; Yang and Winter, 1983). Next the impact of participant-specific MTA strength potential adjustments was evaluated by comparing the total EMG gain adjustments from the standard model with a model using an arbitrary generic 100 N/cm^2 MMS solution. Here it was assumed that a lower total gain adjustment applied in Eq. 4.2.6 ($\sum_{i=1}^{238}(1-g_i)$) would reflect a more representative and efficient match between the model and the calculated kinetic demands of the task. For each sensitivity test

scenario, the peak L5/S1 joint loads from SSS normal walking, carrying 15BW in only their right hand, and carrying 7.5BW in each hand were compared to either their unadjusted EMG (baseline) or nominal MMS task demands.

Statistical Analysis

Three-way repeated-measures analysis of variances (ANOVAs) with appropriate Tukey post-hoc testing were performed to test ($\alpha < .05$) the main effects of the two optimization approaches (EMGopt and SOpt), six walking and carrying conditions, and six lumbar vertebral joint levels (L5/S1 thru T12/L1) on the absolute peak compressive and shear forces (dependent variables). To evaluate our results from both optimization approaches with previously reported model joint forces (*in vivo*), independent ANOVAs compared lumbar loads (dependent variable) across equivalent lumbar joint levels and task(s) (Table 4.2.1). In addition, when there were multiple tasks to contrast, independent one-way ANOVAs tested if task differences from each model and approach were significant. For the third evaluation test, paired t-tests compared ($\alpha < .05$) the cross-correlation and RMSE values of EMGopt and SOpt for each bilateral muscle group across the experimental tasks. Similarly, paired t-tests compared the L5/S1 loading sensitivity from each of the twelve different altered muscle group activation scenarios to the baseline results. Finally, paired t-tests again compared the L5/S1 compression, anterior-posterior shear, medial-lateral shear maximums, and total gain adjustments between the participant specific baseline MMS models and an unadjusted nonspecific model. All statistical tests were performed using MATLAB's Statistical Toolbox.

4.3. Results and Discussion

Evaluation 1: Predicted Joint Forces for EMGopt and SOpt

Across all walking and carrying tasks, lumbar vertebral joint force estimates from EMGopt and SOpt followed similar patterns throughout the gait cycle (see Fig. 4.3.1 for SSS walking; 1.19 ± 0.19 m/s) and resembled previous reports (Callaghan et al., 1999). All joint forces generally peaked following heel strikes and were at their lowest around contralateral toe-off.

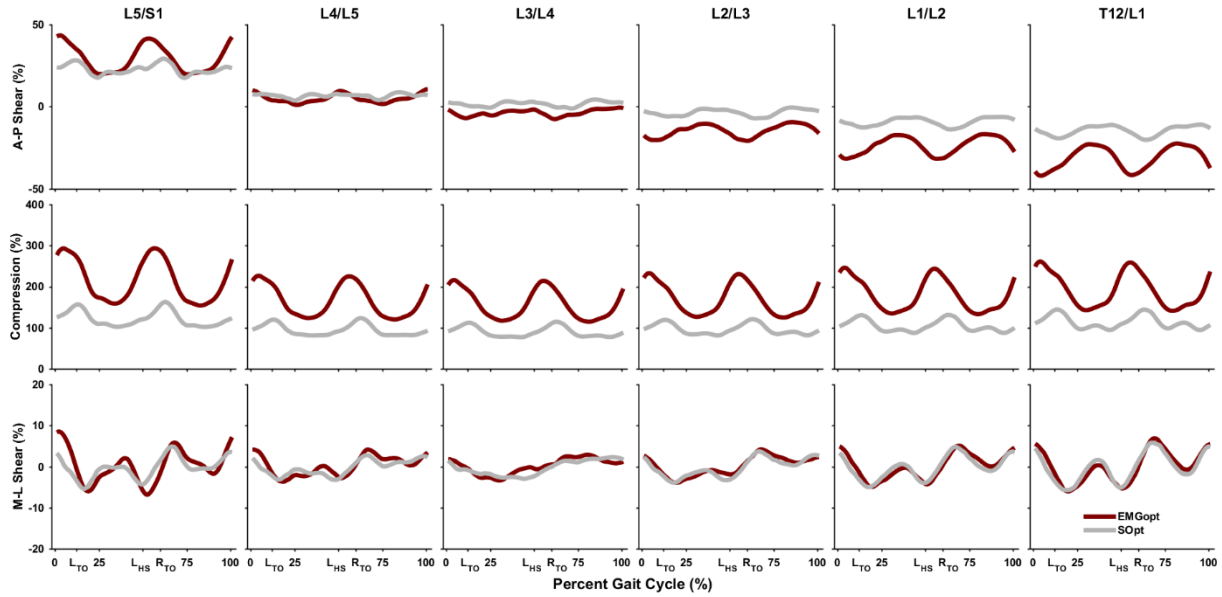

Figure 4.3.1. Average participant vertebral joint forces estimated from EMGopt and SOpt models across all lumbar levels throughout the gait cycle during self-selected speed treadmill walking. The gait cycle was defined from right to right leg heel strike and forces are expressed as a percentage of bodyweight. *Maroon* and *grey lines* represent estimates from the EMGopt and SOpt approaches, respectively. Positive anterior-posterior (A-P) and medial-lateral (M-L) values represent shear forces in the posterior and left directions, respectively. Additional conditions (not shown) were similar in pattern; error bars were excluded for clarity. Abbreviations: left toe-off (L_{TO}) or right toe-offs (R_{TO}) and left heel-strike (L_{HS}).

The average absolute peak compressive and shear force estimates from both EMGopt and SOpt during all tested conditions are depicted in Fig. 4.3.2 and Table 4.3.1. Joint forces were dependent on vertebral level ($p < .01$), with lower joint force magnitudes generally located at the mid lumbar level where the spine's lordotic curve positioned them closer to the trunk's center of mass (Bruno et al., 2017; Raabe and Chaudhari, 2018). This differs from vertebral joint level force

distribution patterns during lifting tasks, when the more superior (e.g. T12/L1) lumbar joints are flexed closer to the external load, often resulting in lower joint forces compared to inferior joints such as the L5/S1 (Arjmand and Shirazi-Adl, 2006b; Bruno et al., 2017).

As expected, given the range of walking tasks and speeds tested, joint forces differed across gait conditions ($p < .01$). In general, the four carrying tasks usually resulted in larger forces than either of the two walking tasks (Table 4.3.1). A more detailed comparison of between-task effects within each model and with previous reports will follow in Evaluation 2, and Studies 2 and 3.

EMGopt predicted significantly larger joint forces than SOpt (Table 4.3.1; $p < .01$). SOpt aims to resolve kinetic equilibrium in a metabolically economical manner, while EMGopt considers participant-specific MTA activity patterns that may include supplementary antagonistic co-contraction in response to perceived stability demands (Cholewicki et al., 1995; Cholewicki and McGill, 1996; Granata and Orishimo, 2001). Because joint loads are dictated by muscular forces in addition to gravitational and internal forces, modeling approaches that solve for kinetic equilibrium with added internal forces will inherently calculate greater joint loads (Li and Chow, 2019). This observed effect would imply that the EMGopt approach optimization was implemented correctly. However, it should be noted that larger joint forces do not necessarily reflect more accurate estimates and the results from this test alone are not enough to justify the implementation of one optimization technique over another.

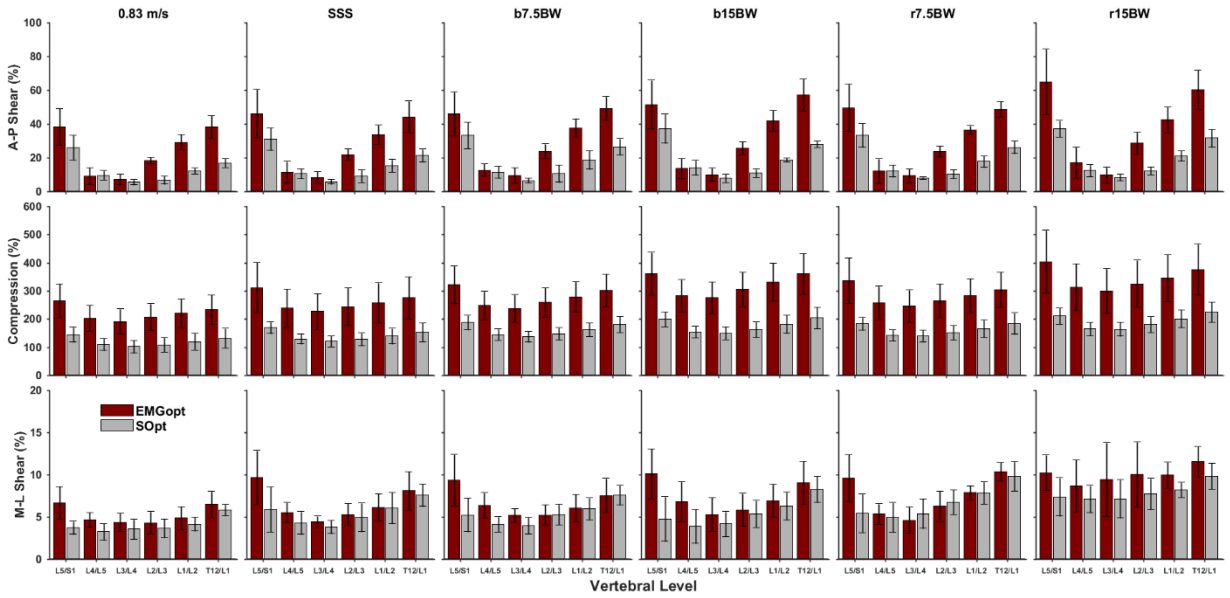

Figure 4.3.2. Average absolute peak vertebral lumbar joint forces for EMGopt and SOpt model estimates across each condition and lumbar level. Error bars show the standard deviation for each estimated peak force. All force values are normalized to a percentage of bodyweight. Data whiskers indicate ±1 standard deviation and maroon and grey bars indicate estimates from EMGopt and SOpt models, respectively. Abbreviations: anterior-posterior (A-P), carrying dumbbells in each hand of 15% (b15BW) or 7.5% bodyweight (b7.5BW), carrying a dumbbell in the right hand of 15% (r15BW) or 7.5% (r7.5BW) bodyweight, self-selected walking speed (SSS), and medial-lateral (M-L).

Table 4.3.1. Average absolute peak vertebral lumbar joint forces and level of significances for each main effect. All force values are normalized to a percentage of bodyweight. Letters denote post hoc pairings from significant (in *bold*; $p < .05$) differences between main effects of gait and carrying condition, optimization approach, and vertebrae level. Interaction effects were excluded for brevity. Abbreviations: anterior-posterior (A-P), carrying dumbbells in each hand of 15% (b15BW) or 7.5% bodyweight (b7.5BW), carrying a dumbbell in the right hand of 15% (r15BW) or 7.5% (r7.5BW) bodyweight, self-selected walking speed (SSS), and medial-lateral (M-L).

Source	Descriptive Statistic	Independent Variable						*p*-value
		0.83 m/s	**SSS**	**b7.5BW**	**b15BW**	**r7.5BW**	**r15BW**	
Condition (C)	**A-P Shear**	18.1 (12.5)a	21.5 (14.8)a,d	23.8 (15.3)c,d	26.3 (17.4)b,c,e	23.9 (15.5)b,d	28.8 (20.0)e	**<.01**
	Compression	169.4 (66.1)a	199.2 (81.4)c	217.1 (74.1)c	246.9 (90.9)b,d	221.3 (80.0)b,c	267.0 (102.9)d	**<.01**
	M-L Shear	4.6 (1.5)a	6.0 (2.3)a,b,d	6.0 (2.1)a,b,c	6.4 (2.7)b,d	7.0 (2.5)c,d	8.9 (2.7)e	**<.01**
		EMGopt	**SOpt**					
Optimization (O)	**A-P Shear**	30.2 (18.6)b	17.3 (10.3)a					**<.01**
	Compression	282.8 (79.8)b	157.5 (38.7)a					**<.01**
	M-L Shear	7.2 (2.9)b	5.8 (2.3)a					**<.01**
		L5/S1	**L4/L5**	**L3/L4**	**L2/L3**	**L1/L2**	**T12/L1**	
Vertebral Level (V)	**A-P Shear**	41.2 (8.)d	12.2 (16.8)a,b	8.0 (27.0)a	16.8 (37.3)b	27.0 (14.8)c	37.3 (5.2)d	**<.01**
	Compression	257.6 (190.6)e	198.8 (206.6)a,b	190.6 (223.5)a	206.6 (243.9)b	223.5 (100.2)c	243.9 (77.5)d	**<.01**
	M-L Shear	7.3 (5.1)c,d	5.4 (5.9)a	5.1 (6.7)a	5.9 (8.5)a,b	6.7 (3.2)b,c	8.5 (2.2)d	**<.01**

Evaluation 2: Indirect Comparisons with Literature

When evaluating a new model, it is important to demonstrate some level of consistency with previous models and *in vivo* measurements at equivalent tasks if they exist (Hicks et al., 2015). Given differences between models (e.g. included MTAs, MTA moment arms, joint representation etc.), some level of discrepancy between computer models is to be expected. Similarly, *in vivo* measurements can be flawed by numerous factors including their invasive nature, low participant numbers varying by age and health status, and unaccounted tissue loading (Dreischarf et al., 2016; Wilke et al., 1999). Therefore, we tested for differences between models and compared how each model ranked the various gait task conditions.

in silico Models

The normalized joint forces from EMGopt and SOpt are compared with computer-based EMG-assisted models (Callaghan et al., 1999; McGill et al., 2013; Rose et al., 2013) across different gait tasks in Fig. 4.3.3. During SSS walking, there were model differences between the Callaghan model, EMGopt, and SOpt for L4/L5 lumbar joint compression (p = .04; post-hoc differences between SOpt and both the Callaghan and EMGopt models) but not shear force estimates (p = .83). During carrying tasks, there were model differences for L4/L5 force estimates in both compression (p < .01; post-hoc difference between EMGopt and both SOpt and McGill models) and shear force estimates (p < .01; post-hoc difference between McGill and both EMGopt and SOpt models). Each model qualitatively ranked the L4/L5 force magnitudes from the three carrying tasks in the same order. All three models found no significant differences between carrying tasks (p-values all > .55). Finally, anterior-posterior shear forces at the L2/L3 level (Rose et al., 2013) were different across models (p < .01; post-hoc difference between Rose and both EMGopt and SOpt models). Each model ranked the tasks in the same order according to average

normalized force values; however, only the Rose model identified a significantly ($p < .01$) larger r15BW force compared to SSS and r7.5BW.

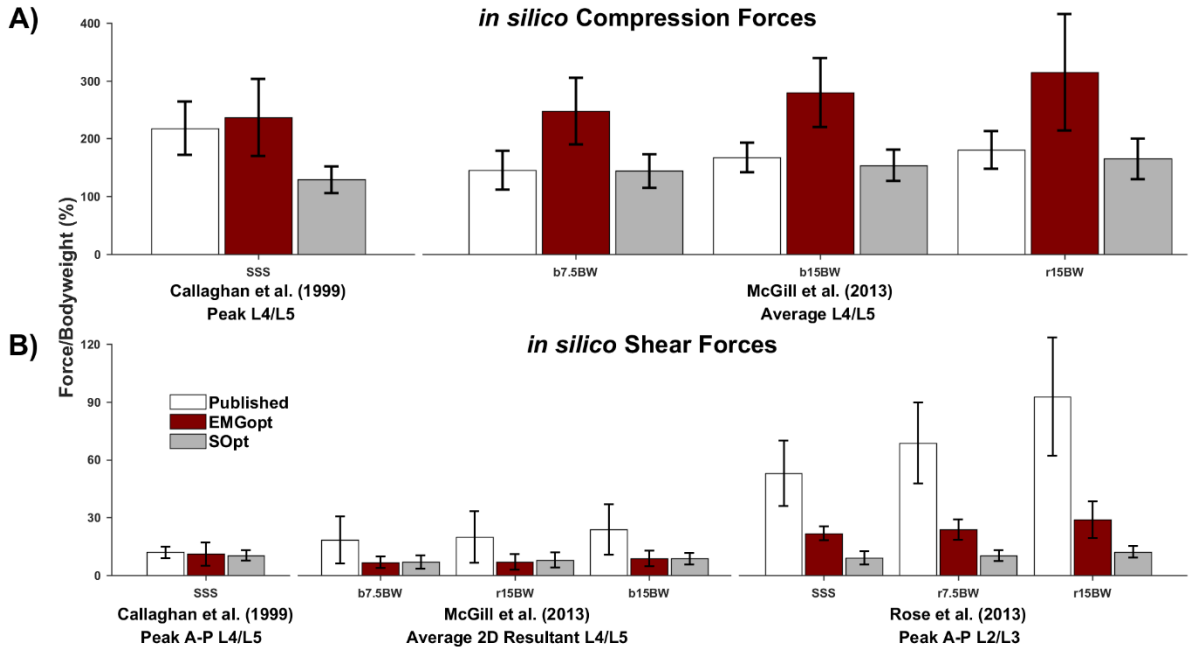

Figure 4.3.3. Indirect model comparisons of maximum or average *in silico* lumbar joint forces between EMGopt and SOpt and published models across equivalent tasks. *Row A*) Compression force values; *row B*) shear force values. All force values are normalized to a percentage of bodyweight and reflect the vertebral level and measure from the original published model (as depicted under each comparison and also in Table 4.2.1). *White, maroon*, and *grey bars* represent force estimates from the EMGopt, SOpt, and published measurements, respectively. Abbreviations: self-selected walking speed (SSS), carrying dumbbells in each hand of 15% (b15BW) or 7.5% body weight (b7.5BW), carrying a dumbbell in the right hand of 15% (r15BW) or 7.5% (r7.5BW) bodyweight. Note: tasks are displayed in ascending order of force magnitudes from left to right within each comparison.

in vivo Measurements

The normalized joint forces from EMGopt, SOpt and the *in vivo* measurements across different gait tasks and lumbar vertebral levels are depicted in Fig. 4.3.4. Very low sample sizes ($n \leq 2$) from the *in vivo* reports (Rohlmann et al., 2014a, 2014c; Wilke et al., 1999) limit the usefulness of quantitative statistical comparisons. Qualitatively, both EMGopt and SOpt models predicted larger joint demands than were measured *in vivo*. Rankings of force magnitudes across conditions were similar for the EMGopt and SOpt models and the *in vivo* measurements.

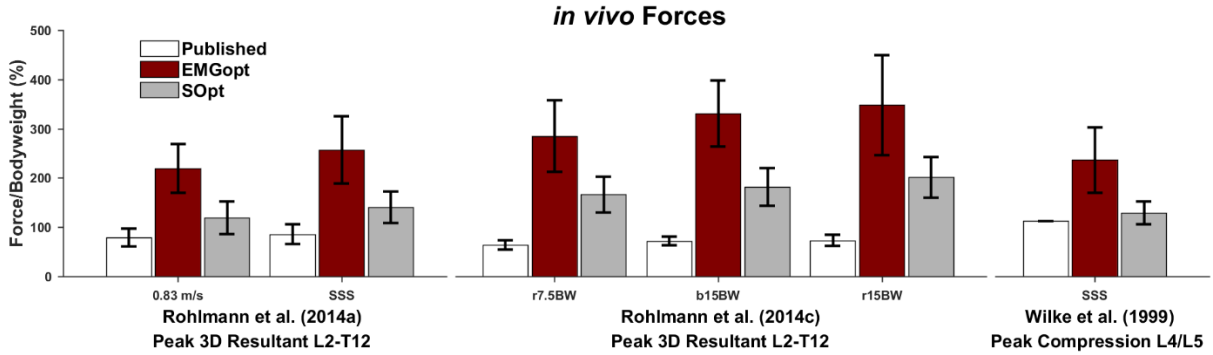

Figure 4.3.4. Indirect model comparisons of lumbar joint forces between EMGopt and SOpt models and published *in vivo* measurements across equivalent tasks. All force values are normalized to a percentage of bodyweight and reflect the vertebral level and measure from the original published measurement (as depicted under each comparison and also in Table 4.2.1). *White, maroon,* and *grey bars* represent force estimates from the EMGopt, SOpt, and published measurements, respectively. Abbreviations: self-selected walking speed (SSS), carrying dumbbells in each hand of 15% (b15BW) or 7.5% bodyweight (b7.5BW), and carrying a dumbbell in the right hand of 15% (r15BW) or 7.5% (r7.5BW) bodyweight. Note: tasks are displayed in ascending order of force magnitudes from left to right within each comparison.

In general, both EMGopt and the SOpt models are comparable to published *in silico* and *in vivo* reports across the various walking tasks and different lumbar levels. There were instances where models differed within a single task, but only a single case (L2/L3 A/P shear force) in which the models disagreed across tasks. This lone discrepancy with the Rose et al. (2013) model is not overly troubling, as force estimates from the models were ranked similarly and shear loads are typically more sensitive than compression forces to model and task kinematic differences (Kingma et al., 2016). Our overall level of observed agreement with published reports is comparable to other lower back models (Actis et al., 2018a; Arjmand and Shirazi-Adl, 2006c; Beaucage-Gauvreau et al., 2019; Bruno et al., 2015; Malakoutian et al., 2018; Raabe and Chaudhari, 2016; Schultz et al., 1982; Senteler et al., 2016). These findings support the application of the proposed model and optimization algorithms to compare walking and carrying tasks.

Evaluation 3: Predicted vs. Recorded EMG Activity

In the absence of participant-specific *in vivo* joint load information, the comparison of predicted muscular activity with recorded EMG is a recognized method of direct model evaluation (Hicks et al., 2015). For this evaluation test we quantitatively determined how well optimization model muscle activities correlated with recorded EMG in timing and amplitude for SSS walking and carrying weights in one (r15BW) or both (b7.5BW) hands. Temporal correlations were defined with zero-lag cross-correlation coefficients (*r*-values); *r*-values approaching 1.0 signify good temporal correspondence (Hinkle et al., 2003). To quantify how predicted muscle activities matched the amplitude of the recorded EMG, RMSEs were calculated with respect to the EMG of each bilateral muscle group for both optimization models. Here, lower RMSE values represent model muscle activity magnitudes that better match recorded EMG magnitudes.

Average predicted muscle group activity from EMGopt and SOpt optimization models and from recorded EMG for the three tasks are shown in Figure 4.3.5. Both optimization models predicted muscular activities which temporally correlated well with the recorded EMG, with *r*-values ranging from .69 to .99 (Table 4.3.2). However, EMGopt consistently outperformed SOpt across temporal comparisons (average r-values SSS: .93 vs. .77; b7.5BW: .95 vs. .81; r15BW: .96 vs. .92; *p*-values all $< .05$). The only exception was while carrying 15% bodyweight in the right hand, in which the right rectus abdominis *r*-value was higher for SOpt (.97 vs. .86; $p < .01$). Table 4.3.2 illustrates that EMGopt more closely matched the activity magnitudes of the recorded EMG, with lower RMSE values than SOpt across most muscle groups and all tasks (average RMSE SSS: .03 vs. .06; b7.5BW .03 vs. .07; r15BW: .05 vs. .11; *p*-values all $< .05$).

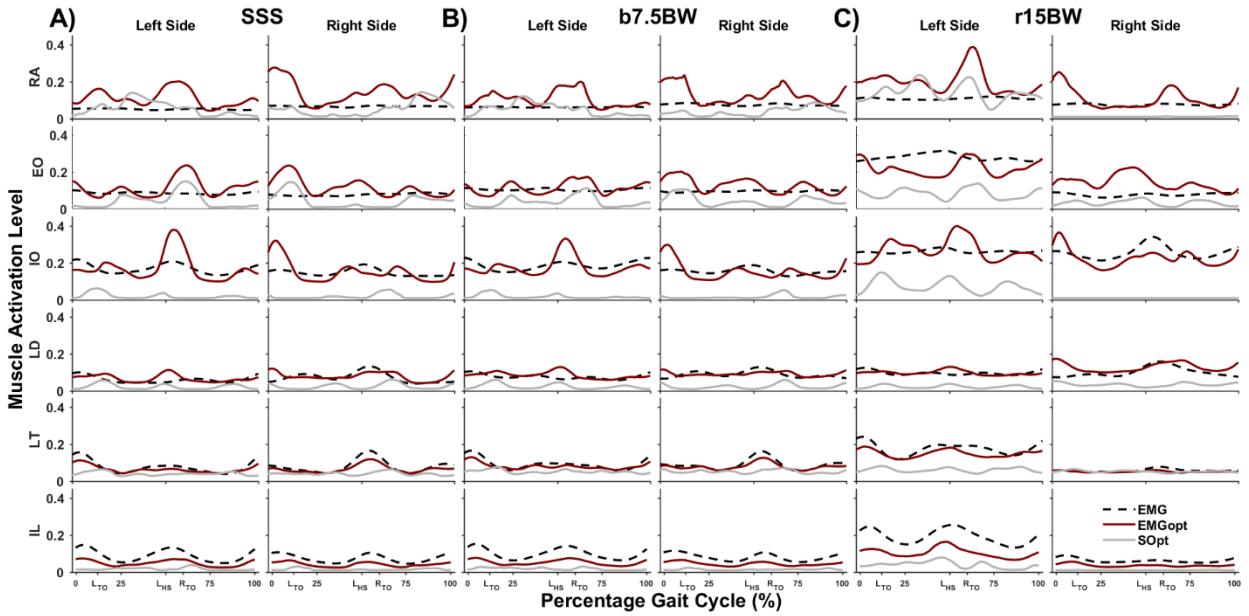

Figure 4.3.5. Average participant muscle group activity predicted from recorded EMG and predictions from EMGopt and SOpt optimization approach models. Columns depict left and right trunk muscles during A) self-selected walking speed (SSS), B) carrying 7.5% bodyweight in each hand (b7.5BW), and C) carrying 15% bodyweight in the right hand only (r15BW). *Maroon, grey, and dashed black lines* represent activations from the EMGopt, SOpt, and EMG, respectively. Standard deviations have been excluded for clarity. Abbreviations: external oblique (EO), iliocostalis lumborum (IL), internal oblique (IO), latissimus dorsi (LD), longissimus thoracis (LT), rectus abdominis (RA), left toe-off (L_{TO}) or right toe-offs (R_{TO}), and left heel-strike (L_{HS}).

Table 4.3.2. Average temporal cross-correlation *(r)* and root mean squared error comparisons between muscle group activity predicted from either optimization approach and recorded EMG across three tasks. Significant ($p < .05$) differences between EMGopt and SOpt approaches are in bold. Abbreviations: lower case letter in front of muscle group represents side (L=left; R=right), carrying dumbbells of 7.5% body weight in each hand (b7.5BW), self-selected walking speed (SSS), or carrying a dumbbell of 15% bodyweight in the right hand only (r15BW), root mean squared error (RMSE), and external oblique (EO), iliocostalis lumborum (IL), internal oblique (IO), latissimus dorsi (LD), longissimus thoracis (LT), and rectus abdominis (RA) muscles.

		Cross-Correlation (r)						RMSE					
		SSS		b7.5BW		r15BW		SSS		b7.5BW		r15BW	
		EMGopt	SOpt	EMGopt	SOpt	EMGopt	SOpt	EMGopt	SOpt	EMGopt	SOpt	EMGopt	SOpt
Muscle Group	lRA	**.88 (.03)**	**.69 (.05)**	**.87 (.07)**	**.69 (.07)**	.93 (.03)	.87 (.04)	0.06 (0.04)	0.02 (0.02)	0.06 (0.03)	0.04 (0.04)	0.09 (0.05)	0.07 (0.04)
	rRA	**.89 (.04)**	**.70 (.09)**	**.89 (.05)**	**.76 (.06)**	**.86 (.06)**	**.97 (.04)**	0.08 (0.06)	0.03 (0.02)	0.06 (0.05)	0.04 (0.05)	0.04 (0.03)	0.06 (0.03)
	rEO	**.89 (.07)**	**.72 (.09)**	**.92 (.04)**	**.72 (.10)**	.95 (.04)	.89 (.06)	0.03 (0.02)	0.04 (0.05)	0.03 (0.02)	0.07 (0.07)	**0.10 (0.06)**	**0.20 (0.13)**
	lEO	**.88 (.06)**	**.72 (.09)**	**.92 (.03)**	**.75 (.07)**	**.92 (.03)**	**.86 (.03)**	0.04 (0.02)	0.04 (0.03)	0.03 (0.02)	0.05 (0.04)	0.07 (0.04)	0.04 (0.05)
	rIO	.92 (.04)	.86 (.09)	**.94 (.04)**	**.85 (.05)**	**.96 (.01)**	**.85 (.06)**	**0.01 (0.01)**	**0.15 (0.06)**	**0.01 (0.02)**	**0.17 (0.07)**	**0.02 (0.02)**	**0.22 (0.14)**
	lIO	**.92 (.06)**	**.80 (.08)**	**.93 (.04)**	**.76 (.11)**	.96 (.04)	.98 (.02)	**0.02 (0.01)**	**0.13 (0.06)**	**0.01 (0.01)**	**0.14 (0.05)**	**0.03 (0.04)**	**0.25 (0.16)**
	lLD	**.94 (.03)**	**.79 (.08)**	**.96 (.03)**	**.81 (.08)**	**.98 (.02)**	**.90 (.06)**	**0.01 (0.01)**	**0.04 (0.02)**	**0.01 (0.01)**	**0.05 (0.02)**	**0.02 (0.01)**	**0.07 (0.02)**
	rLD	**.94 (.03)**	**.75 (.08)**	**.97 (.02)**	**.78 (.10)**	**.96 (.03)**	**.87 (.08)**	**0.01 (0.00)**	**0.05 (0.02)**	**0.00 (0.00)**	**0.07 (0.02)**	0.03 (0.02)	0.07 (0.03)
	lLT	**.99 (.01)**	**.86 (.02)**	**.99 (.00)**	**.92 (.02)**	**.99 (.01)**	**.94 (.02)**	**0.01 (0.01)**	**0.04 (0.02)**	0.01 (0.01)	0.04 (0.04)	**0.03 (0.02)**	**0.11 (0.03)**
	rLT	**.99 (.01)**	**.87 (.02)**	**.99 (.01)**	**.93 (.02)**	**.99 (.01)**	**.97 (.02)**	**0.01 (0.01)**	**0.04 (0.02)**	**0.01 (0.01)**	**0.04 (0.03)**	0.01 (0.01)	0.01 (0.01)
	lIL	**.99 (.00)**	**.81 (.09)**	**.99 (.00)**	**.87 (.07)**	**.99 (.01)**	**.87 (.05)**	**0.04 (0.01)**	**0.07 (0.02)**	**0.05 (0.02)**	**0.08 (0.03)**	**0.09 (0.02)**	**0.15 (0.04)**
	rIL	**.99 (.01)**	**.86 (.07)**	**.99 (.00)**	**.91 (.03)**	.99 (.01)	.97 (.02)	**0.03 (0.01)**	**0.06 (0.03)**	**0.04 (0.02)**	**0.07 (0.03)**	**0.03 (0.02)**	**0.05 (0.04)**
Average		**.93 (.06)**	**.77 (.09)**	**.95 (.05)**	**.81 (.10)**	**.96 (.04)**	**.92 (.06)**	**0.03 (0.03)**	**0.06 (0.05)**	**0.03 (0.03)**	**0.07 (0.06)**	**0.05 (0.04)**	**0.11 (0.10)**

The degree of temporal correlation and magnitude correspondence with recorded EMG for both optimization approaches was comparable to published lower back model evaluation studies (Actis et al., 2018a; Beaucage-Gauvreau et al., 2019; Cappozzo and Gazzani, 1982; El-Rich et al., 2004; Molinaro et al., 2020; Raabe and Chaudhari, 2016). However, EMGopt more closely matched participant-specific muscular activity in both magnitude and temporal correspondence than did SOpt. These results would suggest that the EMGopt algorithm was successfully implemented and is preferable whenever sufficient EMG data are available.

Evaluation 4: Sensitivity of EMGopt model to EMG magnitudes

A critical component to the EMGopt approach is the inclusion of recorded EMG that is absent from SOpt. However, the EMG data introduces further sources of potential error and variation. To test the sensitivity of the L5/S1 joint load predictions to the potential day-to-day variability of EMG, we artificially adjusted the recorded EMG activity of each bilateral muscle group electrode pairing by ±10% (Ahern et al., 1986; Lehman, 2002; Yang and Winter, 1983).

The level of sensitivity in EMGopt L5/S1 joint loading was muscle group dependent (Table 4.3.3). L5/S1 joint loads appeared to be more sensitive to variation in internal obliques (IO), longissimus thoracic activity (LT), and iliocostalis lumborum (IL) activity and less sensitive to variation in rectus abdominis (RA), external obliques (EO), and latissimus dorsi (LD) activity. Muscle groups less sensitive to variation tended to be those that had previously exhibited poorer similarity between predicted and recorded activity (EO and RA; see Fig. 4.3.3 and Table 4.3.2) or those with fewer MTAs crossing the L5/S1 joint (LD). The reverse was true for more sensitive muscle groups (i.e. IO, LT, and IL), in which EMG better matched predicted activity or had more L5/S1 MTAs. When differences between baseline were present, artificially reducing the EMG magnitude by 10% usually reduced joint loading and increasing the EMG activity usually led to

increased joint loads. No one gait task appeared to be particularly sensitive to EMG variation than others, but this was not tested statistically.

Table 4.3.3. Peak L5/S1 forces for EMGopt model with participant-specific maximal muscle stress. *Baseline* represents model with recorded EMG levels; *Muscle Group* rows represent models in which EMG activity levels were modified by ±10% of their *Baseline* activity. *Nonspecific MMS* row represents *Baseline* model with arbitrary MMS of 100 N/cm^2 for all MTAs. Significant ($p < .05$) differences from *Baseline* model are in bold. Forces are reported as a percentage of bodyweight. Abbreviations: carrying dumbbells of 7.5% body weight in each hand (b7.5BW), self-selected walking speed (SSS), or carrying a dumbbell of 15% bodyweight in the right hand only (15BW), maximal muscle stress (MMS), and external oblique (EO), iliocostalis lumborum (IL), internal oblique (IO), latissimus dorsi (LD), longissimus thoracis (LT), and rectus abdominis (RA) muscles.

Adjustment		Anterior-Posterior			Compression			Medial-Lateral		
		SSS	b7.5BW	r15BW	SSS	b7.5BW	r15BW	SSS	b7.5BW	r15BW
Baseline		46.1 (14.3)	46.0 (12.9)	64.9 (19.5)	311.3 (89.4)	321.5 (66.6)	403.1 (111.8)	9.7 (3.2)	9.3 (3.1)	10.2 (2.1)
Muscle Group	RA +10%	45.9 (14.2)	45.9 (13.0)	64.9 (19.3)	311.0 (88.9)	321.4 (66.8)	402.9 (111.0)	9.6 (3.2)	**9.3 (3.1)**	10.2 (2.1)
	RA -10%	46.2 (14.4)	46.0 (12.9)	64.8 (19.7)	311.7 (89.9)	321.7 (66.4)	403.2 (112.6)	9.7 (3.2)	**9.4 (3.1)**	10.2 (2.1)
	EO +10%	**46.3 (14.4)**	46.1 (13.0)	65.5 (19.3)	312.0 (89.4)	**322.3 (66.6)**	**404.5 (112.1)**	9.7 (3.3)	9.4 (3.1)	10.3 (2.1)
	EO -10%	**45.7 (14.3)**	**45.5 (12.9)**	**64.2 (19.6)**	310.7 (89.4)	**320.8 (66.6)**	**401.6 (111.4)**	9.6 (3.1)	9.3 (3.0)	10.1 (2.1)
	IO +10%	**45.7 (14.4)**	**45.6 (13.0)**	**64.4 (19.5)**	**312.8 (89.8)**	**322.9 (66.7)**	**404.8 (112.4)**	**9.9 (3.3)**	**9.6 (3.2)**	**10.6 (2.1)**
	IO -10%	**46.4 (14.3)**	**46.3 (12.9)**	**65.3 (19.4)**	**309.8 (89.1)**	**320.2 (66.5)**	**401.2 (111.1)**	**9.4 (3.1)**	**9.1 (2.9)**	**9.8 (2.1)**
	LD +10%	**46.2 (14.4)**	46.3 (12.9)	65.1 (19.6)	311.6 (89.7)	**321.8 (66.8)**	403.6 (112.4)	9.7 (3.2)	9.4 (3.0)	10.3 (2.1)
	LD -10%	**45.9 (14.2)**	45.7 (12.9)	64.7 (19.3)	311.1 (89.1)	321.3 (66.4)	402.5 (111.1)	9.7 (3.2)	9.3 (3.1)	10.2 (2.1)
	LT +10%	**47.8 (15.1)**	**47.3 (13.4)**	**67.3 (20.9)**	**316.7 (92.3)**	**326.6 (68.5)**	**411.5 (118.6)**	9.7 (3.3)	**9.4 (3.1)**	10.2 (2.2)
	LT -10%	**44.3 (13.6)**	**44.2 (12.5)**	**62.4 (17.9)**	**305.7 (86.5)**	**316.5 (64.6)**	**394.1 (104.9)**	9.6 (3.2)	**9.3 (3.0)**	**10.1 (2.2)**
	IL +10%	**47.0 (14.9)**	46.6 (13.2)	**66.5 (20.2)**	**317.1 (92.0)**	**327.0 (68.6)**	**412.0 (117.8)**	9.6 (3.2)	9.3 (3.0)	10.1 (2.2)
	IL -10%	**45.1 (13.8)**	**45.0 (12.7)**	**63.2 (18.6)**	**305.4 (86.7)**	**315.9 (64.7)**	**393.7 (105.1)**	9.7 (3.3)	9.4 (3.1)	10.3 (2.2)
Nonspecific MMS		41.1 (13.5)	43.5 (16.8)	61.6 (15.3)	309.6 (69.1)	325.1 (61.0)	380.6 (52.3)	11.6 (3.0)	11.6 (2.7)	15.5 (8.8)

While previous studies (Brand et al., 1986; Marras et al., 1999b; Nussbaum et al., 1995b; Sparto et al., 1998) have reported sensitivity of lower back models to various model components (e.g. MTA orientation and cross-sectional area, the EMG-force relationship, the daily variation of variation of static/dynamic exertions), this is the first known report of EMGopt model sensitivity to potential EMG variation during level walking and carrying tasks. There were significant differences from baseline in 57 of 108 variability tests, but the largest variation in L5/S1 joint loads was only ±4% from the baseline values. These results suggest that this EMGopt model is appropriate to compare different gait tasks in a repeated-measures study design with normal day-to-day variability in recorded EMG.

Evaluation 5: Sensitivity of EMGopt model to Maximal Muscle Stress

In the present model, maximal muscle stress (MMS) values were based on participant-specific strengths measured from MVCs, an approach that should improve model fidelity compared to models using a single generic MMS value for all muscle MTAs (Davis and Jorgensen, 2005; Lloyd and Besier, 2003). To test this concept for the EMGopt model, L5/S1 joint loads and the total gain adjustments (g_i) required in Eq. 4.3.6 were compared for our participant-specific MMS (baseline) and an identical version containing a single nominal MMS value based on literature estimates of 100 N/cm^2 inherent to the unaltered lower back model (Beaucage-Gauvreau et al., 2019).

The overall average of the 6 participant-specific values were 123±51 N/cm^2 for the trunk extensors and 64±24 N/cm^2 for the flexors (Fig. 4.3.6). As expected based on size, the male participant extensor (168±14 N/cm^2) and flexor (83±12 N/cm^2) MTAs were stronger ($p < .01$ and $p = .02$, respectively) than the females (78±10 N/cm^2 for extensors and 45±15 N/cm^2 for flexors). The average total unitless gain adjustments (g_i) necessary across all three tasks were reduced by >30% (from 1121±509 to 753±199) for the baseline model with participant-specific MMS, although this reduction did not reach significance for the SSS ($p = .08$) or b7.5BW tasks ($p = .07$; Table 4.3.4). Finally, L5/S1 joint loads were not significantly different (p values from .07 to .97) with or without the application of participant-specific MMS (Table 4.3.3).

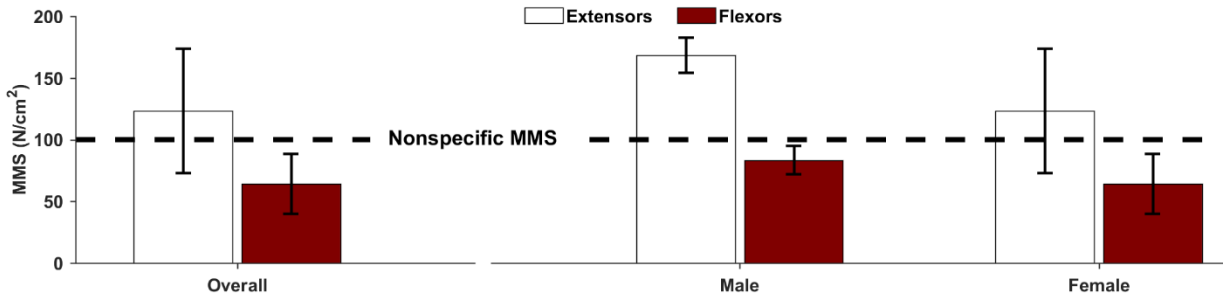

Figure 4.3.6. Overall and gender stratified average participant-specific maximal muscle stress for trunk extensor and flexor musculotendon actuators applied to the baseline model. The *white* and *maroon bars* represent trunk extensor and flexor maximal muscle stresses (MMS), respectively. The *dashed line* represents the 100 N/cm^2 value used in the single-value generic MMS model (Nonspecific MMS).

Table 4.3.4. Average total gain adjustment required to reach a satisfactory EMG optimization solution when applying the participant-specific baseline and a *Nonspecific* maximal muscle stress. The gain adjustments are a unitless number. A 100 N/cm^2 maximal muscle stress (MMS) was used for nonspecific conditions. Significant ($p < .05$) differences from Baseline model are in bold. Abbreviations: carrying dumbbells of 7.5% body weight in each hand (b7.5BW), self-selected walking speed (SSS), or carrying a dumbbell of 15% bodyweight in the right hand only (15BW), and musculotendon actuator (MTA).

MTA Properties	Gain Adjustment (g_i)		
	SSS	b7.5BW	r15BW
Baseline	733.7 (164.4)	662.2 (143.7)	862.9 (250.5)
Nonspecific MMS	992.1 (356.8)	1004.7 (479.2)	1366.6 (643.9)
***p*-values**	.08	.07	**.05**

Some of our participant-specific MMS are above those found from single muscle fibers and used in other lower back models in the literature (6-110 N/cm^2; Buchanan, 1995; McGill and Norman, 1987; van Dieën, 2005). However, these higher values are within the range of what other researchers have deemed necessary with a similar OpenSim model (Beaucage-Gauvreau et al., 2019; Bruno et al., 2015; Burkhart et al., 2018). Because trunk strength is a function of both muscle strength and mechanical advantage, our MMS values could suggest that some of the model's MTAs have inaccurate moment arm lengths. We chose only to adjust the former however, because of the implications of attempting to individualize 238 MTA moment arms (Nussbaum et al., 1995b). Further, MTA strengths are determined by both MMS and muscle physiological cross-sectional areas (PCSA). Model PCSA values were not participant-specific and were

extracted from several literature sources (Christophy et al., 2012). Such generalizations along with several experimental and physiological variables (Buchanan, 1995) could further contribute to the discrepancies we observed from previously reported MMS values, and between both the model's extensor and flexor group MMS values. Future work should examine the impact of adjusting the moment arms, possibly by moving the location of the lumbar joint rotational axes more anteriorly. Along with the use of participant-specific PCSAs, this might better align the model's MMS values with the literature values.

The application of participant-specific versus nonspecific MMS did not significantly impact the predicted joint loads. The lack of an effect on joint loads despite some apparent quantitative differences in average peak forces (up to 25 and 52% for medial-lateral shear forces in the b7.5BW and r15BW conditions, respectively) were due primarily to inconsistent between-participant effects. Beaucage-Gauvreau et al. (2019) and Bruno et al. (2015) also found that MMS values did not significantly impact joint loading, using a similar SOpt model applied to different movement tasks. Therefore, while participant-specific MMS may allow for more efficient optimizations and physiological relevance, they may not be necessary to compare lower back loads between tasks.

Limitations of Model and Evaluation

Our results are subject to limitations associated with the musculoskeletal model and the EMGopt computational approach. The current model neglects passive force contributions from non-muscular tissues and intra-abdominal pressure. However, these neglected contributions are minimal during the upright postures and low exertion levels of gait (Arshad et al., 2018; Callaghan et al., 1999). Similar reasoning justifies our omission of intervertebral and axis of rotation translations (Ghezelbash et al., 2015). The vertebral coupling used in model m29DoF to assign

the vertebral positions is generic and assigns the total thoracic rotational contributions to the T12/L1. For the present study and proposed applications, the complex measurement of each joint individually is not justified, and while more accurately dispersing the thoracic contributions to trunk movement can impact thoracic loading, its impact on lumbar loads is often insignificant (Ignasiak et al., 2016). The EMGopt approach optimizes a generic gain adjustment factor which is not directly related to any physiological characteristic(s) of the MTAs. Other musculoskeletal modeling approaches aim to optimize physiological properties of the MTAs to closely match the kinetics of calibration tasks (Granata and Marras, 1993; Lloyd and Besier, 2003; van Dieën and Visser, 1999) but they are not without their own limitations (Cholewicki et al., 1995; Davis and Jorgensen, 2005). Ultimately, EMGopt's frame-by-frame gain adjustment can be viewed as an aggregate of all (un)known physiological factors thereby reducing the number of parameters being optimized and simplifying the process. Our experimental setup could not utilize OpenSim's Residual Reduction Algorithm because separate GRFs from each foot were unavailable from the force treadmill. The model applies a top-down inverse dynamics approach to calculate the kinetic demands at each joint, although a bottom-up model with separate GRFs may be more sensitive to the impulsive forces which occur at heel strike (Callaghan et al., 1999; Hendershot and Wolf, 2014). Future work should examine how well top-down and bottom-up approaches agree within this full-body OpenSim model during a variety of gait and other tasks performed on a stationary force plate. The musculoskeletal model described here only provides an estimate of the net joint contact forces. Developing a multiscale modeling approach which combines the results from this musculoskeletal model with a finite-element model capable of distributing contact forces across soft tissues may be beneficial and worthy of future work (Honegger et al., 2020). Finally, our results were drawn from only fit, young, and healthy individuals during walking and carrying tasks,

with the number of participants similar to other evaluation studies (Actis et al., 2018a; Beaucage-Gauvreau et al., 2019; Cholewicki et al., 1995; Gagnon et al., 2011; Raabe and Chaudhari, 2016).

4.4. Conclusion

The goals of this study were to develop the framework for an EMGopt approach for a modified OpenSim lower back model and to evaluate its efficacy in studying lower back demands during gait and carrying tasks. Across different gait and carrying tasks, the proposed EMGopt approach estimated similar responses to a more traditional SOpt approach, and to models previously reported in the literature. By incorporating EMG, the EMGopt approach estimated larger joint loads and more closely matched individual participant muscular recruitment strategies than SOpt. Joint loads from EMGopt were sensitive to the inherent variability in recorded EMG, but the magnitude of these differences did not impact the between task comparisons. Participant-specific MMS strength scaling reduced the level of gain factor adjustments needed to solve for kinetic equilibrium but did not lead to significantly different joint loads. Overall, the model and EMGopt optimization approach were successfully implemented and well-suited for evaluating the lower back joint demands of walking and carrying tasks.

4.SM. Supplemental Material

The model described in Study 1 was preliminarily developed and tested by comparing the estimated vertebral joint forces from EMGopt and SOpt approaches while participants stood in a neutral and upright posture while relaxed, and while holding dumbbells of 3.75%, 7.5% or 15.0% body weight (b3.75BW, b7.5BW and b15BW, respectively) in each hand. These bilateral static standing conditions were designed to require minimal resultant lower back joint moments but incrementally challenge the stability demands of the trunk as dumbbell masses increased. Such

conditions have previously resulted in distinct internal force estimates from each optimization approaches (Cholewicki et al., 1995).

To test if the EMGopt model was sensitive to this situation, a repeated-measures analysis of variance (ANOVA) with Tukey post-hoc testing compared ($\alpha < .05$) L4/L5 compression force (dependent variable) differences from the two optimization approaches (O), four standing conditions (C), and their interaction (O × C). Further, muscle recruitment and stability demand differences were assessed by comparing the average bilateral EMG activity level from each recorded muscle (dependent variable) across the four standing conditions (independent variable). Results from each statistical test are shown in Tables 4.SM.1 and 4.SM.2. The average normalized L4/L5 joint compression forces from EMGopt and SOpt across the four different standing conditions are shown in Figure 4.SM.1.

Table 4.SM.1. Average L4/L5 vertebral lumbar joint compression force and level of significance for each main effect of standing condition and optimization. Forces are reported as a percentage of bodyweight. Letters denote post hoc pairings from significant (in *bold*; $p < .05$) differences between main effects. Abbreviations: holding dumbbells of 3.75% (b3.75BW), 7.5% (b7.5BW), or 15% (b15BW) of bodyweight in each hand, and relaxed unweighted standing (Relax).

Source	Main & Interaction Effects				*p*-value
Condition (C)	**Relax**	**b3.75BW**	**b7.5BW**	**b15BW**	
	101.6 (27.7)a	106.1 (24.5)a	117.4 (28.1)b	129.1 (28.6)c	**<.01**
Optimization (O)	**EMGopt**	**SOpt**			
	133.9 (24.5)a	93.2 (14.)b			**<.01**
C x O	*SEE FIG. 4.SM.1*				.07

Table 4.SM.2. Average bilateral recorded EMG activity from each recorded muscle and level of significance for the main effect of standing condition. Forces are reported as a percentage of bodyweight. Letters denote post hoc pairings from significant (in *bold*; $p < .05$) differences of the main effect. Abbreviations: holding dumbbells of 3.75% (b3.75BW), 7.5% (b7.5BW), or 15% (b15BW) of bodyweight in each hand, relaxed unweighted standing (Relax), external oblique (EO), iliocostalis lumborum (IL), internal oblique (IO), latissimus dorsi (LD), longissimus thoracis (LT), rectus abdominis (RA).

Bilateral Muscle Tested	Independent Variable				*p*-value
	Relax	b3.75BW	b7.5BW	b15BW	
RA	5.5 (1.7)	5.4 (1.5)	5.6 (2.1)	5.7 (1.8)	.65
EO	6.8 (5.3)	5.8 (4.8)	6.6 (4.2)	6.7 (4.2)	.32
IO	11.5 (4.9)	10.9 (3.1)	13.8 (7.9)	13.5 (6.9)	.17
LD	4.2 (1.2)a	4.8 (1.3)a	5.5 (1.5)a,b	7.0 (2.7)b	**<.01**
LT	5.3 (1.4)	5.0 (1.5)	6.4 (2.5)	6.0 (2.1)	.06
IL	5.2 (1.9)	5.1 (1.9)	5.6 (2.1)	5.5 (1.8)	.34

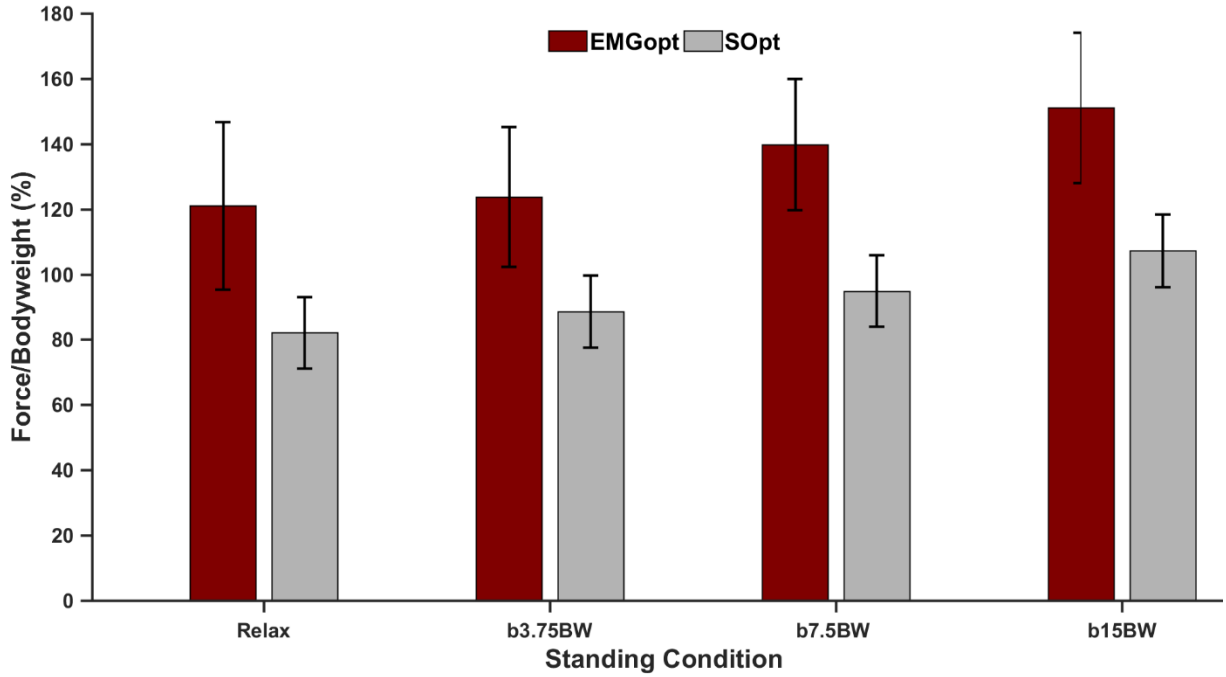

Figure 4.SM.1. Comparison of predicted average normalized L4/L5 compression forces from EMGopt and SOpt optimization approaches across four standing conditions. Data whiskers indicate ±1 standard deviation, maroon and grey bars represent EMGopt and SOpt forces, respectively. Forces are reported as a percentage of bodyweight. Abbreviations: holding dumbbells of 3.75% (b3.75BW), 7.5% (b7.5BW), or 15% (b15BW) of bodyweight in each hand, and relaxed unweighted standing (Relax).

During these static standing conditions, the L4/L5 compression force increased as expected as hand-held weights were increased (Cholewicki et al., 1995). L4/L5 compression estimates increased (Table 4A.1; $p < .01$) with hand weights above 3.75% of body weight. While SOpt aims to resolve kinetic equilibrium in a metabolically economical manner (Crownshield and Brand, 1981), EMGopt considers participant-specific MTA activity patterns and co-contractions that are metabolically less economical but often perceived as necessary to increase spinal stability (Cholewicki et al., 1995; Cholewicki and McGill, 1996; Granata and Orishimo, 2001). Because joint loads are dictated by muscular forces in addition to ligament, gravitational, and inertial forces, modeling approaches that solve for kinetic equilibrium and include more muscle forces will inherently calculate greater joint loads (Li and Chow, 2019). This rationale was supported in our model estimates. EMGopt predicted significantly larger L4/L5 compression forces than SOpt ($p < .01$). Surprisingly, there was no optimization approach × standing condition interaction effect, although there was a trend in that direction ($p = .07$). L4/L5 vertebral joint force estimate differences between optimization approaches were largely reflective of only gravitational force differences. The lack of an interaction effect may be due to the complexities of resolving kinetic equilibrium with a multi-joint model (Arjmand et al., 2009), but it could also result from our selected dumbbell masses (which only went up to 15% of bodyweight) producing low trunk stability demands. The latter notion is supported by similar EMG activity levels (p-values ranging from .06 to .65) for all muscle groups except latissimus dorsi ($p < .01$). Larger dumbbell loads such as those used by Cholewicki et al. (1995) could challenge the trunk stability enough to amplify MTA recruit strategies and result in an optimization approach × standing condition interaction effect. Overall, this initial test demonstrated many expected effects and verified the proper implementation of the musculoskeletal model and EMGopt approach.

CHAPTER 5

STUDY 2

LOWER BACK DEMANDS DURING INDUCED LOWER LIMB GAIT ASYMMETRIES

5.1. Introduction

Walking is a fundamental means of locomotion, with activities often generating thousands of steps per day (Tudor-Locke et al., 2011). It is widely recommended for aerobic and musculoskeletal conditioning and can provide therapeutic relief from lower back pain (LBP; Nutter, 1988). However, a variety of clinical conditions can result in asymmetric gait kinematics and kinetics, including congenital deformities, injury, rehabilitative joint restriction, disease, and amputation (Cappozzo and Gazzani, 1982; Constantinou et al., 2014; Dananberg, 1993; Devan et al., 2014; DeVita et al., 1991; Dingwell et al., 1996; Friberg, 1983; Gulgin et al., 2018; Mündermann et al., 2005; Tanaka et al., 2015; Wolfe et al., 1996). Gait asymmetries are often classified with a level of symmetry index to quantify the degree of bi-lateral differences in lower limb kinematic or kinetic parameters (Robinson et al., 1987). It is not surprising that gait asymmetries are related to LBP, given its established relationship with asymmetric postures and repeated loading (Bernard, 1997; da Costa and Vieira, 2010; Gallagher et al., 2005; Hoogendoorn et al., 1999; Marras, 2000). The reported magnitude of LBP prevalence in those with asymmetric gait is alarming, more than quintupled that of the general able-bodied population (Ehde et al., 2001; Giles and Taylor, 1981; Ready et al., 2018; Smith et al., 1999; Wolfe et al., 1996). Therefore, the cumulative lower back demands associated with asymmetrical gait are of interest to clinicians and researchers looking to improve the quality of life in those susceptible to LBP (Dananberg and Guiliano, 1999; Devan et al., 2014; Friel et al., 2005; Morgenroth et al., 2010).

Despite a wide range of asymmetry origins, lower back loading during asymmetric gait has been studied primarily in lower limb amputees (Devan et al., 2014; Farrokhi et al., 2017; Sagawa et al., 2011). Biomechanical models have predicted walking lower back demands to be greater for amputees compared to able-bodied individuals (Cappozzo and Gazzani, 1982; Hendershot et al., 2018; Hendershot and Wolf, 2014; Sagawa et al., 2011; Shojaei et al., 2016; Yoder et al., 2015; Yu et al., 2014). Unfortunately, individual studies on people with unilateral lower limb amputation (PULLA) are often compromised by low participant numbers, between-subject differences in amputation and prosthetic characteristics (e.g. kinetic abilities, inertial properties, and prosthetic fit), preferred gait speed differences (Hendershot et al., 2018), and a lack of a baseline comparison (Chow et al., 2006; Hafner et al., 2002; Highsmith et al., 2019; Nolan et al., 2003; Selles et al., 1999; van der Linden et al., 1999; Wasser et al., 2019; Windrich et al., 2016; Yu et al., 2014).

An alternative approach to understanding the link between gait asymmetries and lower back demands is to study able-bodied participants with asymmetries artificially induced through uni-lateral modifications in leg length, leg inertial characteristics, or joint motion restrictions (Brown et al., 2018; Gulgin et al., 2018; Lemaire et al., 2000; Roemmich et al., 2012; Royer and Martin, 2005; Vanicek et al., 2007). This approach may better represent clinical asymmetric gait populations such as those with lower limb inertial discrepancies, leg length discrepancies, joint dysfunction, or unilateral lower limb casting. Perturbing able-bodied participants with unilateral leg lengthening via a thickened shoe sole or a clinical “walking boot” (Fig. 5.2.1) has been shown to increase trunk range of motion and associated muscular activity (Gulgin et al., 2018; Kakushima et al., 2003; Vink and Huson, 1988), but the impact on trunk tissue demands has not yet been investigated. A controlled experimental setup that can induce asymmetries in a healthy and

homogeneous cohort could help identify how different types of asymmetry can affect lower back demands during locomotion.

Therefore, the objective of this study was to investigate how various experimentally induced asymmetric gaits can impact lower back tissue demands. Gait asymmetries were induced by unilaterally altering the leg length, leg mass, and ankle joint motion in various combinations. The effects of each condition on lower back demands were examined with an EMG-optimization (EMGopt; Cholewicki et al., 1995) musculoskeletal model of the lower back (see Study 1). We hypothesized that perturbations resulting in greater gait asymmetry would place larger demands on the lower back.

5.2. Methods

Participants

A convenience sample of twelve participants (6 males; 25$\pm$5 years of age, 64.7$\pm$8.3 kgs, and 1.71$\pm$0.07 meters in stature) were recruited and consented to participate in the study. The exclusion criteria for participation in this study were a self-reported age of over 40 years, history of lower back pain, diagnosed neurological disorders, a low level of physical activity (less than 90 minutes a week), or a calculated body mass index greater than 30.

Equipment and Setup

As described in Study 1, data were collected to capture full-body motion (Qualisys AB, Sweden), ground reaction forces (Treadmetrix, USA) and muscle activity (electromyography [EMG]; Delsys Inc., USA) from 12 trunk muscles across a variety of symmetric and asymmetric gait conditions (Table 5.2.1). Motion capture data were recorded at 100 Hz, force and EMG data at 2000 Hz. Perturbations to symmetric gait were administered with an EvenUp^{TM} adjustable Shoe

Leveler (2.54 cm) affixed to the sole of one shoe to simulate leg length discrepancy, a 0.9 or 1.2 kg sand-filled ankle weight placed superior to the medial malleolus on one leg to simulate leg mass discrepancy, and a uni-lateral medical-grade walking boot (AirCast FP Walker Foam Pneumatic) (Fig. 5.2.1). The selected leg length and ankle-mass perturbation magnitudes were based on the characteristics of the walking boot size (small or medium) which best fit the participant. All perturbations were applied to the right lower limb.

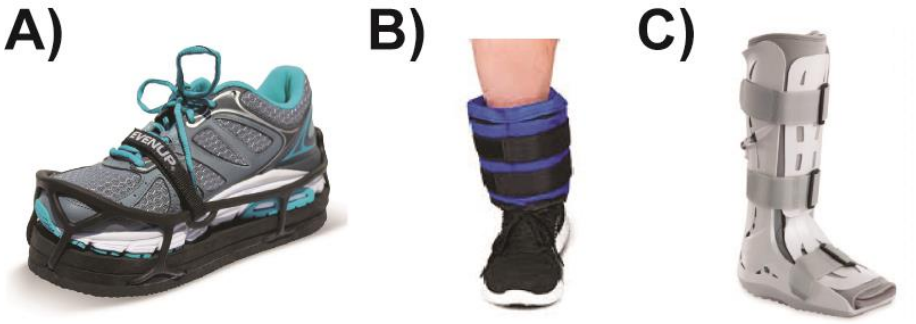

Figure 5.2.1. Individual perturbations mechanisms applied to the right lower limb to induce asymmetric gait. Panel A) adjustable shoe leveler, B) ankle-weight, C) walking boot. [Photos courtesy of A) www.rehabmart.com, B) JBM International via www.amazon.com, and C) www.SourceOrtho.net]

Table 5.2.1. The five experimental gait conditions and the corresponding perturbations. Conditions *2-4* were randomly assigned following the initial symmetrical control (*1*) condition and prior to the concluding walking boot condition (*5*). *All conditions were performed at 90% of a participant's self-selected treadmill walking speed and with perturbations applied to the right lower limb.

Symmetry Perturbation(s)*	Ankle Weight	Shoe Leveler	Walking Boot
Control / Symmetrical (1)			
Single	2	3	5
Combination	4		

Procedure

Participants donned form-fitting clothing and comfortable footwear prior to manual measurements of height and body mass, identification of self-selected treadmill walking speed, experimental gait conditions (Table 5.2.1), and a series of maximal voluntary contractions (MVC).

Five different gait conditions were performed at 90% of each participant's self-selected treadmill walking speed (90S), representing the reported adjustment in walking speed chosen by participants wearing a similar walking boot (Gulgin et al., 2018). The five conditions included a symmetrical unperturbed control (1), with an ankle weight (2), with the shoe leveler (3), with both the ankle weight and shoe leveler (4), and with a walking boot (5). The symmetric 90S walking condition consisted of 90 seconds of acclimation concluding with 30 seconds of data collection. The four perturbed walking conditions consisted of 270 seconds of acclimation concluding with 30 seconds of data collection. Two-minute rest breaks were provided between each condition to minimize fatigue.

To reduce changes in motion capture markers, model calibration poses, and acclimation effects, the experimental gait conditions started with the control conditions and ended with the boot condition, with the three perturbations without the boot randomly assigned between them. Prior to the walking boot condition, all motion capture markers below the right knee were removed and placed in their equivalent locations on the surface of the walking boot, and a new model calibration pose was captured.

As described in Study 1, MVCs were administered to establish maximal reference levels of each EMG signal and the musculoskeletal model strength potential. The MVCs were performed at the end of the experiment protocol to guard against fatigue and mitigate potential electrode displacement while being positioned in the dynamometer (Biodex Medical Systems Inc., Shirley, NY).

Data Processing and Calculation of Dependent Variables

All experimental data were post-processed in MATLAB (MathWorks, Natick, MA) as described in Study 1. Briefly, an OpenSim (Delp et al., 2007) musculoskeletal model and EMGopt

approach were used to determine lower back loading across the five conditions. Prior to kinematic and kinetic analysis, musculoskeletal models were individually scaled relative to participant anthropometry and strength potentials. For the ankle weight and walking boot conditions, a hollow cylinder of corresponding inertial characteristics was added to the model 3 cm above the right ankle joint center.

Each gait condition was time-normalized by individual strides, with initiation and termination established from consecutive right (perturbed) heel strikes. Heel and toe marker anterior-posterior velocities were used to distinguish heel strikes and toe offs (Zeni et al., 2008) due to the absence of individual foot ground reaction forces. Representative examples of three consecutive strides were extracted from the 30 seconds of data collection for each participant across all conditions. Each leg's stance time was calculated from heel strike to ipsilateral toe off. Step lengths were calculated at heel strike from the anterior-posterior distance of the ipsilateral (leading) and contralateral (trailing) ankle markers. Stance time and stride length were calculated from each stride and then averaged across condition. All other dependent variables were calculated from participants' ensemble kinematic or kinetic patterns averaged across their three time-normalized strides.

A priori it was decided to focus the analysis on the impact of each perturbation on normalized peak and mean vertebral L5/S1 joint compressive, anterior-posterior, medial-lateral, and resultant shear forces estimated from our musculoskeletal model. Differences in internal L5/S1 joint moments, muscle group forces, and trunk kinematics were also investigated. Trunk muscles were uniquely categorized and grouped (Christophy et al., 2012) as right (perturbed) and left stabilizers (e.g. latissimus dorsi, multifidus, psoas major, and quadratus lumborum), flexion locomotors (e.g. external obliques, internal oblique, and rectus abdominis), or extension

locomotors (e.g. iliocostalis lumborum pars lumborum, iliocostalis lumborum pars thoracis longissimus thoracis pars lumborum, and longissimus thoracis pars thoracis). Trunk orthogonal kinematics were defined relative to the pelvis, with ranges and directional peaks determined from the sum of all the lower back joints (e.g. L5/S1 – T12/L1).

Levels of asymmetry for bi-lateral spatiotemporal (step length and stance time) and muscle group force differences were determined by calculating their symmetry index (SI; Robinson et al., 1987):

$$SI = \frac{2(V_R - V_L)}{(V_R + V_L)} \times 100\% \qquad \text{(Eq. 5.2.1)}$$

where V_R and V_L represent the variable of interest associated with either the right (perturbed) or left side, respectively.

Statistical Analysis

The only independent variable for this study was the gait condition (1. Control/symmetrical, 2. shoe leveler, 3. ankle weight, 4. ankle weight and shoe leveler, and 5. walking boot; Table 5.2.1). Lower back kinematic and kinetic demands and levels of asymmetry were assigned as dependent variable(s) in one-way repeated-measures analysis of variance (ANOVA; $\alpha = .05$) tests, with Tukey post-hoc testing when appropriate. All statistical tests were performed using MATLAB's statistical toolbox.

5.3. Results

Spatiotemporal Asymmetries

The average 90S treadmill speed across the twelve participants was 1.11 ± 0.12 m/s. The five gait conditions yielded unique spatiotemporal gait asymmetries for both step length ($p < .01$) and stance time ($p < 0.01$; Fig. 5.3.1). Step length asymmetries for the shoe leveler alone (9.42 ±

5.21), combined ankle weight and shoe leveler (7.70 ± 6.89), and walking boot (-5.54 ± 4.40) conditions differed from the more symmetric control condition (0.85 ± 2.97). The ankle weight alone condition (-1.47 ± 5.01) demonstrated step length asymmetries similar to both the control and walking boot conditions. Donning a shoe leveler (with or without an ankle weight) led to the participants taking longer steps on the right (perturbed) versus left leg (positive SI), while the walking boot resulted in the opposite effect, longer steps on the left (negative SI).

Stance time asymmetry patterns were different than the step length patterns across the five conditions. The control (-0.61 ± 0.91) and shoe leveler (-0.40 ± 0.98) conditions displayed similar low asymmetry levels, while the ankle weight (-2.27 ± 0.98), combined ankle weight and shoe leveler (-2.56 ± 1.63), and walking boot (-2.06 ± 1.21) conditions resulted in prolonged left (unperturbed) stances (negative SI).

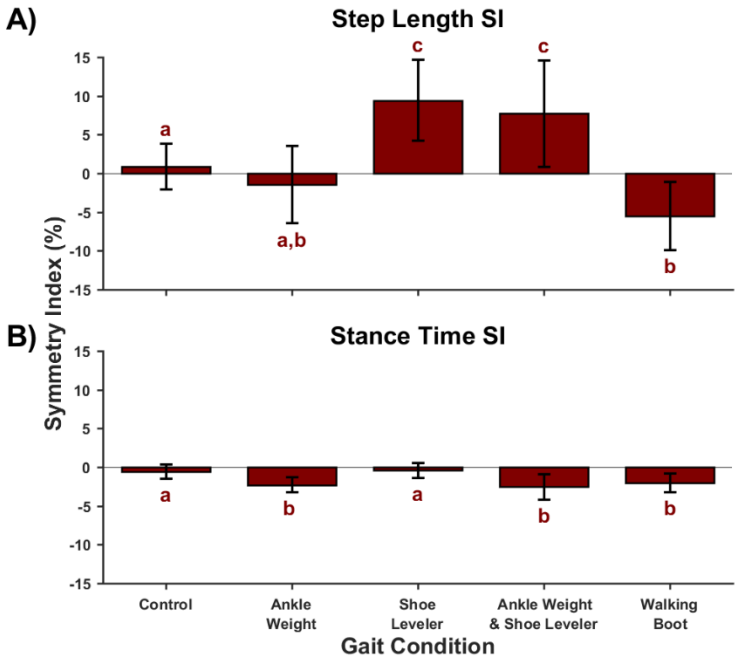

Figure 5.3.1. Spatiotemporal symmetry indexes across the five gait conditions. Positive symmetry index (SI) values denote longer steps (row A) and stances (row B) of the right (perturbed) side. Letters (a-c) are indicative of post-hoc pairings following significant main (gait condition) effect differences ($\alpha < .05$) for each SI.

Trunk Kinematics

Gait cycle trunk kinematic patterns were qualitatively similar across conditions (Fig. 5.3.2), but there were significant peak magnitude and range of motion differences between conditions (Table 5.3.1). Across all conditions the trunk maintained a degree of sagittal plane forward flexion throughout the gait cycle. The walking boot condition displayed increased sagittal plane range of motion ($p < .01$) compared to the other four conditions, stemming from reduced trunk flexion following left (unperturbed) heel strike. Peaks of frontal plane lateral flexion to either side corresponded to right (perturbed) and left toe-offs (at ~12% and ~62% of the gait cycle, respectively). Frontal plane ranges of motion were similar across conditions ($p = .06$), but the distribution of motion differed. The two shoe leveler conditions resulted in right (perturbed) flexion bias, represented in an increased right ($p < .01$) and decreased left peak flexion ($p < .01$). Transverse plane peak rotations oscillated between perturbed heel strikes, with the walking boot leading to more rotation directed towards the right side ($p < .01$). There was more transverse plane range of motion present in the walking boot condition than the control condition ($p = .01$), with the other three conditions similar to both.

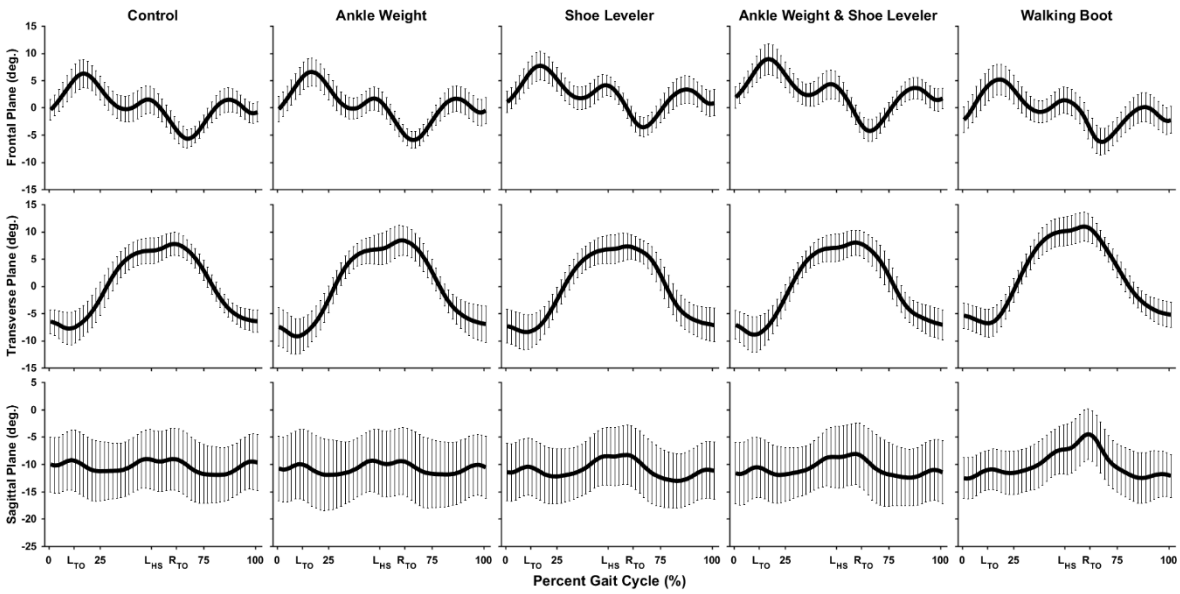

Figure 5.3.2. Trunk kinematics across the five conditions as a percentage of the gait cycle. The gait cycle was defined from right (perturbed) to right heel strike. Positive angles (degrees) are representative of left side lateral flexion, right side axial rotation, and trunk extension in the frontal, axial, and sagittal planes, respectively. Error bars show the standard deviation of particular points on each curve. Abbreviations: left (unperturbed) heel strike (L_{HS}) and toe-off (L_{TO}), and right toe-off (R_{TO}).

Table 5.3.1. Trunk kinematics and L5/S1 kinetics across the five conditions. Peak, minimum, range (RoM), and average joint forces and moments are normalized to a percentage of bodyweight and bodyweight × height, respectively. Kinematics are referenced in degrees. Letters denote within condition differences (α < .05) and their respective condition level post-hoc pairings, whenever applicable.

			Condition					
			Control	Ankle Weight	Shoe Leveler	Ankle Weight & Shoe Leveler	Walking Boot	*p value*
Trunk Kinematics (degrees)	Sagittal Plane	RoM	5.0 (1.4)a	5.3 (1.5)a	6.5 (1.8)a	6.1 (1.9)a	9.4 (3.3)b	***<.01***
		Min Flexion	-7.7 (5.4)a	-8.0 (6.0)a	-7.6 (5.4)a	-7.3 (5.7)a	-4.4 (4.7)b	***<.01***
		Peak Flexion	-12.7 (4.9)	-13.3 (5.7)	-14.1 (4.9)	-13.4 (5.0)	-13.9 (3.8)	.45
	Frontal Plane	RoM	12.3 (3.0)	12.9 (2.6)	11.5 (2.3)	13.4 (3.3)	12.0 (3.3)	.06
		Peak Right	6.4 (2.6)a	6.8 (2.4)a,b	7.8 (2.6)b,c	9.0 (2.8)c	5.4 (2.6)a	***<.01***
		Peak Left	-5.9 (1.6)a	-6.1 (1.6)a	-3.8 (1.8)b	-4.4 (2.0)b	-6.6 (2.5)a	***<.01***
	Transverse Plane	RoM	16.4 (4.2)a	18.3 (3.7)a,b	16.6 (4.0)a,b	17.8 (3.7)a,b	18.7 (2.8)b	**.01**
		Peak Left	8.2 (2.3)a	8.7 (2.8)a	7.8 (2.4)a	8.5 (2.3)a	11.5 (2.7)b	***<.01***
		Peak Right	-8.1 (2.9)a,b	-9.6 (3.3)a	-8.8 (3.2)a	-9.3 (3.2)a	-7.2 (2.5)b	***<.01***
L5/S1 Internal Moments (%)	Sagittal Plane	Extensor	1.0 (0.5)a	1.2 (0.7)a,b	1.4 (0.9)b	1.3 (0.7)b	1.3 (0.5)a,b	***<.01***
		Flexor	-0.6 (0.3)a	-0.7 (0.3)a,b	-0.7 (0.3)a,b	-0.7 (0.3)a,b	-0.9 (0.3)b	**.01**
	Frontal Plane	Peak Right	0.8 (0.3)a	0.9 (0.3)a,b	0.9 (0.3)a,b	1.0 (0.4)b	1.3 (0.4)c	***<.01***
		Peak Left	-1.0 (0.3)	-1.0 (0.3)	-1.0 (0.4)	-1.2 (0.4)	-1.2 (0.4)	.12
	Transverse Plane	Peak Left	0.9 (0.3)	1.0 (0.3)	0.9 (0.3)	0.9 (0.3)	1.0 (0.2)	.58
		Peak Right	-0.9 (0.3)	-1.0 (0.3)	-0.9 (0.3)	-0.9 (0.3)	-1.0 (0.3)	.07
L5/S1 Joint Forces (%)	A-P Shear	Peak	43.0 (12.4)	43.9 (10.8)	44.9 (12.2)	45.0 (11.5)	45.2 (11.2)	.62
		Average	27.2 (6.3)	27.0 (5.8)	26.9 (5.9)	27.3 (6.1)	26.8 (5.3)	.87
	Compression	Peak	307.8 (68.8)	307.8 (62.8)	312.7 (63.1)	319.7 (66.1)	311.3 (64.7)	.34
		Average	212.1 (29.1)	214.3 (28.6)	211.8 (26.2)	217.2 (31.3)	218.0 (29.1)	.09
	M-L Shear	Peak	10.0 (3.2)	10.1 (4.8)	11.2 (4.3)	11.1 (4.3)	10.3 (4.7)	.30
		Average	0.5 (1.6)a,b	0.5 (2.0)a,b	1.1 (2.1)a,b	1.5 (2.1)b	0.1 (1.9)a	**.02**
	Resultant Shear	Peak	43.9 (12.5)	45.1 (10.7)	46.1 (12.1)	46.1 (11.6)	46.4 (11.7)	.53
		Average	27.6 (6.3)	27.5 (5.7)	27.4 (5.8)	27.9 (6.0)	27.3 (5.2)	.84

L5/S1 Joint Kinetics

Similar to trunk kinematics the L5/S1 internal joint moments displayed a qualitatively consistent pattern across all conditions (Fig. 5.3.3), but with significant variation in peak magnitude (Table 5.3.1). Peak extensor and flexor moments in the sagittal plane occurred near toe off and midstance, respectively. The symmetric control condition resulted in lower extensor moments than either of the conditions involving the shoe leveler ($p < .01$) and lower flexor moments than the walking boot condition ($p = .01$). Frontal plane demands generally peaked during midstance, with larger peak right lateral flexor moments during left (unperturbed) stance in the boot condition ($p < .01$) but similar between condition left lateral flexor moments ($p = .12$).

Transverse plane left and right internal moment peak magnitudes were similar (right $p = .07$; left $p = .58$) across all conditions and occurred at toe-offs.

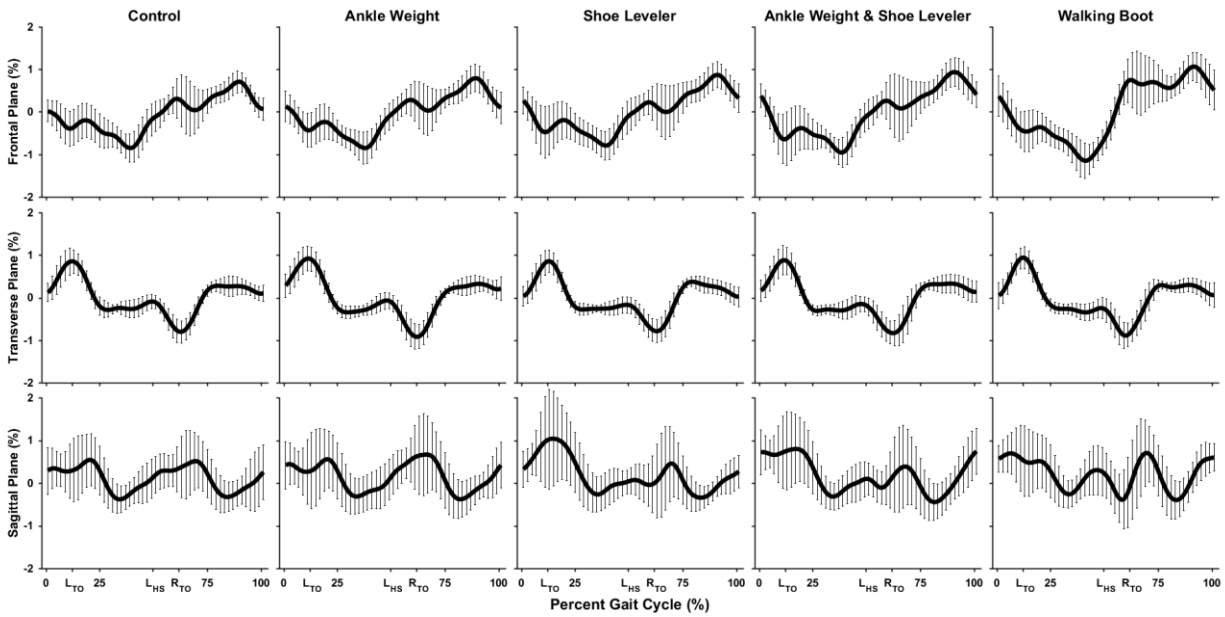

Figure 5.3.3. L5/S1 internal joint moments across the five conditions as a percentage of the gait cycle. The gait cycle was defined from right (perturbed) to right heel strike. Positive values are representative of right lateral flexor, right axial rotation, and trunk extensor moments (as a percentage of bodyweight × height) in the frontal, axial, and sagittal planes, respectively. Error bars show the standard deviation of particular points on each curve. Abbreviations: left (unperturbed) heel strike (L_{HS}) and toe-off (L_{TO}), and right toe-off (R_{TO}).

The L5/S1 joint forces predicted from the musculoskeletal model were mostly similar across all five conditions (Fig. 5.3.4 and Table 5.3.1). Peak compression and shearing forces occurred around heel strike. Only average medial-lateral shear forces were significantly different ($p = .02$) between conditions, with the walking boot condition lower than the combined ankle weight and leg leveler condition, and the other three conditions similar to both.

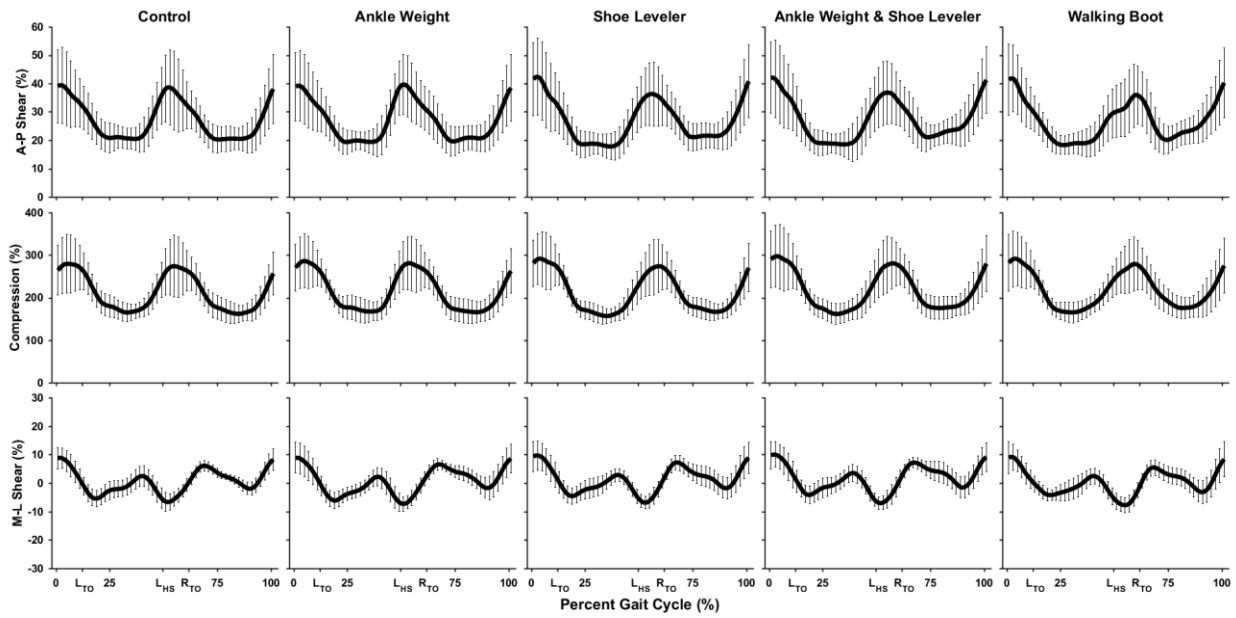

Figure 5.3.4. L5/S1 joint forces across the five conditions as a percentage of the gait cycle. The gait cycle was defined from right (perturbed) to right heel strike and forces are expressed as a percentage of bodyweight. Positive anterior-posterior (A-P) and medial-lateral (M-L) values represent shear forces in the posterior and left directions, respectively. Error bars show the standard deviation of particular points on each curve. Abbreviations: left heel strike (L_{HS}) and toe-off (L_{TO}), and right toe-off (R_{TO}).

Muscle Forces

Model-predicted trunk muscle group forces maintained consistent patterns across conditions (Fig. 5.3.5). Peak muscle forces for the stabilizers and flexion locomotors occurred around heel strikes. Peak forces of the extension locomotors occurred following heel strikes of the contralateral lower limbs. Only four of the eighteen tests on muscle group variables (peak force, average force, or bilateral SI) indicated significant differences between conditions (Table 5.3.2). Gait condition differences were detected in peak force for the right flexion locomotor group ($p < .01$) and the left extension locomotor group ($p = .02$), in average force for the right stabilizer group ($p < .01$), and in the SI for average force in the right stabilizer group ($p < .01$). Post-hoc tests showed both leg lengthener conditions had lower average right-side stabilizer forces than the walking boot condition, resulting in differences in their respective symmetry indexes. For the trunk flexion locomotors, the peak force was lower during control and ankle weight conditions.

For the trunk extension locomotors, the peak force was lower in the control than the combined ankle weight and shoe leveler condition, with the other three conditions similar to both.

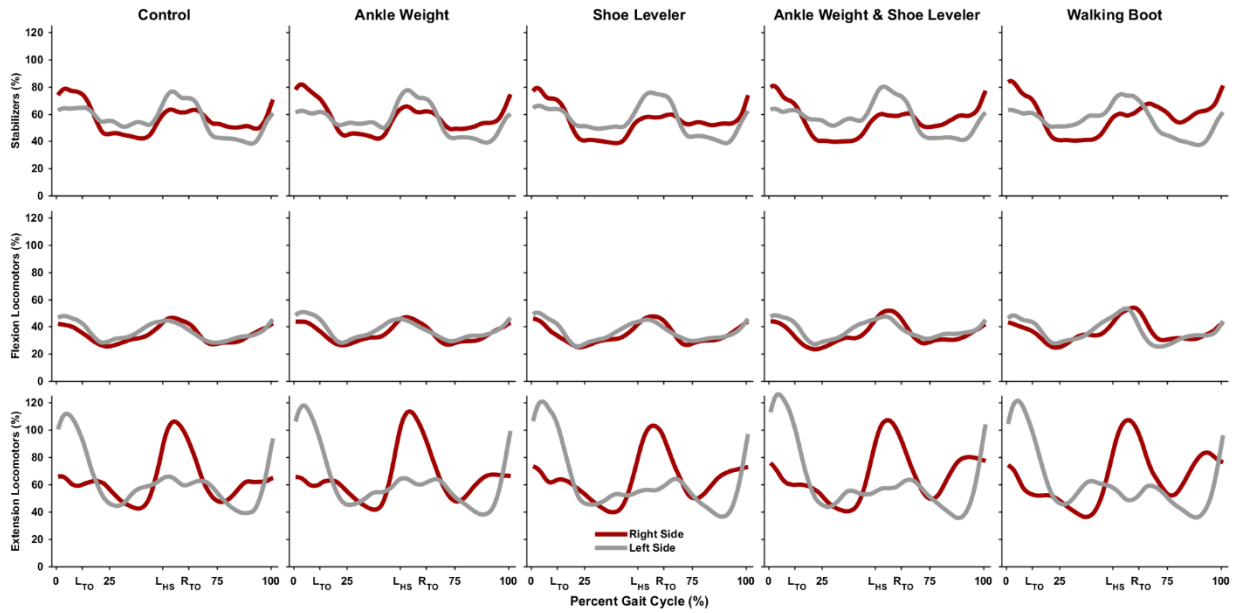

Figure 5.3.5. Muscle group forces across the five conditions as a percentage of the gait cycle. The gait cycle was defined from right (perturbed) to right heel strike and forces are expressed as a percentage of bodyweight. *Maroon lines* represent right and *grey lines* the left (unperturbed) side muscle groups. All lines represent the group averages, standard deviation bars were excluded from the plots for clarity. See text for Methods muscles comprising stabilizer (*top row*), flexion locomotors (*middle row*), and extension locomotor (*bottom row*) groups. Abbreviations: left heel strike (L_{HS}) and toe-off (L_{TO}), and right toe-off (R_{TO}).

Table 5.3.2. Muscle group force descriptive statistics across the five conditions. Peak and average forces are expressed as a percentage of bodyweight. Letters denote within group differences (α < .05) and their respective group level post-hoc pairings, whenever applicable. Right and left correspond to the perturbed and the unperturbed side, respectively. See text in Methods for muscle grouping assignments and equation to calculate symmetry indexes (SI; percentile).

Muscle Group		Condition					
		Control	Ankle Weight	Shoe Leveler	Ankle Weight & Shoe Leveler	Walking Boot	*p* value
				Peak			
Stabilizers	Right	85.3 (25.3)	86.6 (23.4)	83.6 (18.3)	85.7 (22.1)	89.5 (21.1)	.47
	Left	86.8 (27.6)	83.9 (24.0)	85.3 (25.8)	88.5 (23.5)	85.2 (23.7)	.50
	SI	-1.4 (11.7)	3.4 (10.2)	-0.7 (16.6)	-3.4 (13.4)	5.6 (14.8)	.28
Flexion Locomotors	Right	49.9 (10.3)a	50.9 (11.8)a	52.8 (11.3)a,b	54.3 (12.1)a,b	57.1 (11.8)b	***<.01***
	Left	54.4 (12.9)	56.2 (14.0)	54.9 (12.2)	56.4 (11.0)	58.0 (12.1)	.58
	SI	-8.1 (15.8)	-9.3 (12.5)	-3.8 (19.0)	-4.5 (16.0)	-1.4 (13.7)	.13
Extension Locomotors	Right	108.5 (42.7)	116.4 (38.4)	106.6 (31.6)	113.0 (34.9)	110.7 (33.1)	.44
	Left	113.0 (37.2)a	119.2 (30.8)a,b	124.7 (38.8)a,b	128.7 (43.2)b	123.4 (35.0)a,b	***.02***
	SI	-4.8 (24.7)	-3.8 (23.1)	-14.7 (22.0)	-11.1 (24.0)	-11.0 (21.8)	.06
				Average			
Stabilizers	Right	56.4 (11.9)a,b	56.9 (11.5)a,b	54.5 (10.2)a	55.3 (11.7)a	58.2 (11.8)b	***<.01***
	Left	56.0 (15.0)	55.5 (13.7)	55.5 (12.7)	56.9 (13.8)	55.3 (13.1)	.64
	SI	1.6 (14.4)a,b,c	3.3 (8.4)b,c	-1.1 (10.9)a,b	-2.2 (11.3)a	5.6 (10.5)c	***<.01***
Flexion Locomotors	Right	34.4 (6.9)	35.0 (7.5)	34.5 (6.5)	34.8 (7.2)	36.2 (7.1)	.39
	Left	36.5 (8.9)	37.8 (8.5)	36.4 (6.6)	37.7 (7.5)	36.9 (6.4)	.68
	SI	-5.1 (15.7)	-7.3 (14.8)	-5.4 (14.8)	-8.2 (14.1)	-2.2 (16.2)	.26
Extension Locomotors	Right	63.5 (15.8)	65.6 (14.6)	64.5 (12.7)	66.8 (14.4)	65.2 (11.7)	.30
	Left	62.5 (11.3)	62.5 (10.7)	62.2 (10.9)	62.7 (12.3)	61.9 (8.1)	.99
	SI	0.6 (24.1)	3.8 (21.7)	3.4 (20.6)	6.1 (19.9)	4.5 (16.7)	.27

5.4. Discussion

In this study we experimentally induced gait asymmetries by artificially perturbing healthy able-bodied participants who normally walk with symmetry. Our aim was to investigate specific factors associated with spatiotemporal gait asymmetry such as uneven leg length, leg mass, or ankle motion restrictions, and determine their impact on lower back demands estimated with a musculoskeletal computer model. We hypothesized that perturbations resulting in more gait asymmetry would also result in larger L5/S1 vertebral joint forces. However, we found that while

some of the four imposed perturbations resulted in different step length or stance time asymmetries relative to the symmetrical control condition, L5/S1 vertebral joint forces were not different and therefore our hypothesis was not supported.

Adaptations to Imposed Asymmetries

In response to our perturbations, participants generally spent more time in stance on the left limb, opposed to the side on which we added a perturbing element. The increased left stance time generally resulted in longer steps with the perturbed right limb. Artificial leg length discrepancies have not been previously reported to cause spatiotemporal adaptions, but here they resulted in similar step length and stance time changes similar to those observed with artificially increased unilateral leg mass or in PULLA (Hendershot and Wolf, 2014; Sagawa et al., 2011; Skinner and Barrack, 1990; Smith and Martin, 2007). However, the walking boot step asymmetry we observed contradicts a previous report where step length symmetry was similar between walking boot and normal shod walking (Gulgin et al., 2018). This discrepancy between studies could be the result of subtle lower limb kinematic differences between conditions administered on a treadmill as opposed to over ground (Riley et al., 2007) or possibly by boot marker offsets causing SI artifacts. Nonetheless, adaptations to a unilateral lower limb change in inertia, ankle joint motion, and leg length reflect either a preference of the unperturbed limb during stance or perturbed limb swing phase demands that are not present in unperturbed symmetric gait, and yet do not result in significant changes in the L5/S1 vertebral joint forces.

Trunk kinematics and L5/S1 joint moments during the walking boot and shoe leveler conditions were different than in the baseline symmetry condition. When wearing a walking boot our participants featured greater trunk sagittal and transverse plane ranges of motion with larger internal peak sagittal plane flexor moments and left (contralateral to the perturbation) lateral frontal

plane L5/S1 joint moments. These responses, in addition to altered lower limb and pelvic kinematics (see Supplemental Material, Tables 5.SM.1 and 5.SM.2 for more details), hypothetically were needed to generate forward momentum and sufficient toe clearance with a restricted ankle joint. Gulgin et al. (2018) noted similar kinematic changes with walking boot usage but did not report on the impact on lower back kinetic demands. The shoe leveler led to asymmetric frontal plane trunk kinematics offset on the right lateral side and increased L5/S1 extensor moments. This adaptation has been previously described in both artificial and clinical cases of leg length discrepancy (Azizan et al., 2018; Khamis and Carmeli, 2017). Such changes could be employed to balance the whole body center of mass as the participant strives to make the shorter left limb "longer" by reducing hip and knee flexion and the longer perturbed limb "shorter" by increasing them, and by modifying pelvic obliquity to enhance both effects. However, trunk kinematic and L5/S1 kinetic adaptations for the walking boot and shoe leveler conditions did not lead to significant changes in the L5/S1 vertebral joint forces estimates from our model.

Muscle group forces predicted from the model were generally similar across conditions. Shojaei et al. (2016) reported some general muscle group differences in transfemoral PULLA but did not describe them relative to the prosthetic lower limb, making comparisons with our study difficult. Trunk muscle activities and forces resulting from artificial unilateral lower limb perturbations have not been reported previously. The current results show only an increase in peak force for the right contralateral-side flexion locomotors while wearing the walking boot compared to the symmetric control condition. Flexion locomotors can act to flex the trunk anteriorly, laterally, or axially, or to stabilize the trunk by resisting antagonist muscles. Since the added flexor locomotor forces occurred near right toe-off when initiating forward momentum, they were likely involved in supporting and flexing the trunk (and thigh) in the absence of normal ankle

plantarflexion. However, vertebral joint forces are highly influenced by internal muscle forces (Marras, 2000), and differences in muscle force (Table 5.3.2) and activity level (see Supplemental Material, Table 5.SM.3) between conditions were limited. Thus, it is understandable that overall L5/S1 vertebral joint forces were also similar across the five conditions.

L5/S1 Vertebral Joint Forces

This is the first study to quantify lower back vertebral joint forces in able-bodied participants while undergoing external unilateral lower limb perturbations. This novelty led to a hypothesis based on reported lower limb kinematic and kinetics from similar perturbations and previous investigations of lower back vertebral joint forces in lower limb amputees (PULLA). Several studies have reported gait asymmetries and lower back vertebral joint force estimates for PULLA versus able-bodied controls (Cappozzo and Gazzani, 1982; Hendershot et al., 2018; Hendershot and Wolf, 2014; Shojaei et al., 2016; Yoder et al., 2015; Yu et al., 2014). Vertebral joint forces during gait have been shown to be amputation level dependent, with transfemoral above-knee amputations experiencing 40-60% larger compressive and shear force magnitudes than either transtibial below-knee PULLA or able-bodied controls (Hendershot et al., 2018; Shojaei et al., 2016). However, transtibial amputee gait will often demonstrate lower back loads similar to able-bodied controls (Hendershot et al., 2018; Yoder et al., 2015). Our perturbations were all applied below the knee joint and therefore resulting vertebral joint forces may more closely resemble those from transtibial PULLA. This may explain why we saw no L5/S1 vertebral joint force differences across conditions and why our hypothesis was not supported. Future work should attempt to clarify if different perturbation magnitudes or more proximal joint restrictions can impact the L5/S1 joint loading and better reflect the reported demands of transfemoral PULLA.

Peak vertebral compression (1,244 – 2,895 N) and shear (166 - 469 N) force magnitudes from across the five conditions were similar and safely below reported spinal unit failure tolerances (Gallagher and Marras, 2012; Jäger and Luttmann, 1989). However, spinal unit tolerances can be lowered by cumulative loading (Brinkmann et al., 1988; Gallagher et al., 2005) such as seen in walking (Tudor-Locke et al., 2011). Hendershot and Bazrgari (2020) recently examined this concept in PULLA with a fatigue model. Interestingly, they found no significant difference in vertebral disc failure rates (in years) between PULLA and healthy controls. A potential weakness of their comparison was the omission of trunk kinematic differences in their fatigue model. Nonneutral spine postures like those found in PULLA and from our perturbations can lower tolerances to injury (Adams and Dolan, 2005). Future work should consider including the impact of altered trunk kinematics and loading variability on disc time to failure predictions.

An underlying assumption in our study design is that the high reported incidence of LBP observed in those with gait asymmetry is the result of injuries from added or unsafe biomechanical demands (da Costa and Vieira, 2010; Norman et al., 1998). These unsafe demands are not restricted to level gait. Alternatively, lower back demands from other daily activities (Devan et al., 2015) such as sit-to-stand transitions (Actis et al., 2018b; Shojaei et al., 2019), ramp or stair negotiation (Acasio et al., 2019; Bae et al., 2007), fatigue gait, or carrying tasks (see Study 3), could also instigate LBP in those with gait asymmetry. We also did not consider other physiological and psychosocial risk factors which can contribute to LBP in those with gait asymmetries (Butowicz et al., 2020; Devan et al., 2017; Farrokhi et al., 2017; Hendershot and Bazrgari, 2020). Considering our null findings on lower back kinetics, other movement paradigms could be promising avenues for future research in those with gait asymmetries.

Limitations

The interpretation of our results may be impacted by experimental limitations. First, the length of the adaptation period for each perturbation may be inadequate to represent the targeted scenarios. Although we applied guidelines from previous studies (Noble and Prentice, 2006; Smith and Martin, 2007), all participants were inherently more familiar with the baseline condition. Secondly, all conditions were performed on a treadmill to allow for precise control of gait speed, and to facilitate efficient data collection of consecutive gait cycles and conditions. Differences in spine kinematics and ground reaction forces have been reported for treadmill versus over ground walking (Riley et al., 2007). Due to our treadmill's single belt and force platform, we could not calculate individual lower limb kinetic demands. Future work should examine if lower back kinetic demands differ between over ground and treadmill gait and attempt to associate lower limb kinetic changes with vertebral forces. Finally, all perturbations were examined on healthy controls who may have been able to adapt to the perturbations and modify their lower back demands. PULLA and those who locomote asymmetrically due to anatomical or clinical conditions may develop chronic adaptions or secondary conditions such as muscle weakening, postural instability, or scoliosis which amplify lower back demands (Azari et al., 2018; Devan et al., 2014; Kim et al., 2019). Limitations specifically pertaining to our EMGopt approach and musculoskeletal model have been previously discussed in Study 1.

Summary

Our experimental protocol was successful in causing gait asymmetries and demonstrated changes in trunk kinematics with asymmetric gait while walking on a treadmill. However, the unilateral lower limb perturbations did not lead to increases in our musculoskeletal model-estimates of L5/S1 vertebral joint forces relative to baseline symmetrical walking. These results

suggest that the high LBP incidence associated with analogous clinical levels and causes of asymmetric gait may not be the direct consequence of increased L5/S1 vertebral joint forces changes during level walking. In addition to consideration of non-biomechanical pathways, future work aimed at reducing LBP prevalence in those with asymmetric gait should investigate how L5/S1 vertebral joint forces and tissue tolerances are impacted during more severe perturbation levels, muscle fatigue, repeated and augmented joint kinematics, or additional daily tasks (e.g. sit-to-stand, stair negotiation, or carrying).

5.SM. Supplemental Material

Lower limb kinematics, pelvis kinematics, and muscle activation from all gait cycles were examined post-hoc to support conclusions drawn from our primary analyses. Statistical tests on descriptive statistics (peaks, averages, and ranges of motion) were conducted with one-way repeated-measures analysis of variance (ANOVA; $\alpha = .05$) where the independent variable was the perturbation condition (Table 5.2.1) with each descriptive statistic of interest assigned as dependent variables, and Tukey post-hoc testing when appropriate.

Lower Limb Kinematics

Right (perturbed) and left (unperturbed) leg limb sagittal plane kinematic patterns were asynchronously offset by gait events but qualitatively similar across conditions (Fig. 5.SM.1). There were between-condition differences for all right leg (p-values $< .01$) and most left leg kinematic metrics (p-values $\leq .02$). Post-hoc tests showed donning a shoe leveler increased peak hip and knee flexion, hip and knee range of motion, and peak ankle dorsiflexion. These adaptations were most likely employed to "shorten" the artificially induced longer leg. The ankle weight and walking boot conditions were similar to the symmetric control condition in right leg peak flexion

and extension angles and ranges of motion for the hip, knee, and ankle. One exception in right ankle kinematic pattern and metrics was the walking boot condition, where physical joint restrictions decreased ankle dorsiflexion, plantarflexion, and range of motion relative to the four unrestricted conditions (n.b. these magnitudes were not assumed zero for the walking boot). On the left side, the ankle weight condition was consistently similar to the control, while the shoe leveler and walking boot conditions generally decreased hip and knee flexion, hip and knee range of motion, decreased ankle dorsiflexion, and increased ankle plantar flexion in an attempt to either "lengthen" the limb or facilitate right limb toe clearance. See Table 5.SM.1 for specific condition averages, descriptive effects, and post-hoc pairings.

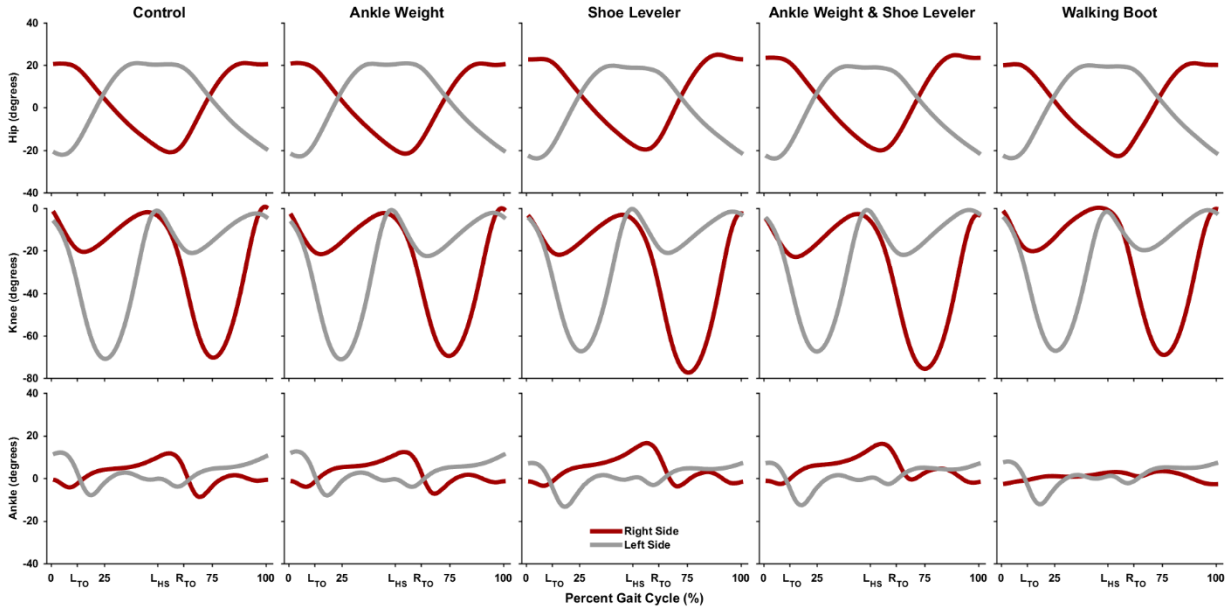

Figure 5.SM.1. Lower limb sagittal plane joint angles across the five conditions as a percentage of the gait cycle. Right (*maroon lines*) and left (*grey lines*) sides coincide with the perturbed and unperturbed lower limbs, respectively. The gait cycle was defined from right (perturbed) to right heel strike. All lines represent the group averages, standard deviation bars were excluded from the plots for clarity. Positive hip, knee, and ankle angle (degrees) values are representative of flexion, extension, and dorsiflexion, respectively. Abbreviations: left heel strike (L_{HS}) and toe-off (L_{TO}), and right toe-off (R_{TO}).

Table 5.SM.1 Lower limb sagittal plane joint ranges, and peak flexion and extension angles across the five conditions. Right and left sides coincide with the perturbed and unperturbed lower limbs, respectively. All angles are expressed in degrees. Bolded *p*-values and letters (a-c) denote within group differences ($\alpha < .05$) and their respective group level post-hoc pairings, whenever applicable. Abbreviation: range of motion (RoM).

			Condition					
			Control	Ankle Weight	Shoe Leveler	Ankle Weight & Shoe Leveler	Walking Boot	*p*- value
Right	Hip	RoM	43.1 (4.1)a	43.5 (3.9)a	45.6 (4.4)b	45.6 (4.7)b	44.9 (5.9)a,b	***<.01***
		Peak Flexion	22.0 (3.5)a	21.7 (3.1)a	25.8 (3.9)b	25.3 (3.6)b	22.0 (3.1)a	***<.01***
		Peak Extension	-21.1 (5.4)a,b,c	-21.8 (4.9)a,b	-19.8 (5.4)c	-20.3 (5.3)b,c	-22.9 (6.5)a	***<.01***
	Knee	RoM	72.1 (3.7)a,c	70.4 (3.1)a	77.3 (4.1)b	75.1 (5.3)b,c	71.7 (4.3)a,c	***<.01***
		Peak Extension	1.5 (2.7)a,b	0.7 (2.2)a,b	-0.2 (3.2)b	-0.7 (2.7)b	2.4 (2.6)a	***<.01***
		Peak Flexion	-70.5 (2.4)a	-69.7 (2.1)a	-77.6 (2.2)b	-75.8 (3.4)b	-69.3 (4.1)a	***<.01***
	Ankle	RoM	21.3 (5.0)a	21.3 (7.3)a	23.0 (6.1)a	20.2 (3.4)a	6.6 (1.4)b	***<.01***
		Peak Dorsiflexion	11.8 (2.9)a	12.5 (3.2)a	16.7 (2.4)b	16.5 (2.4)b	3.7 (0.9)c	***<.01***
		Peak Plantarflexion	-9.5 (5.4)a	-8.8 (7.6)a	-6.3 (6.2)a,b	-3.7 (2.3)b	-2.9 (1.1)b	***<.01***
Left	Hip	RoM	44.1 (4.3)	45.0 (4.2)	44.2 (3.9)	44.3 (4.1)	44.8 (3.6)	.28
		Peak Flexion	21.9 (3.8)a	21.9 (3.9)a	20.2 (4.1)b	20.3 (3.8)b	20.9 (4.1)a,b	***<.01***
		Peak Extension	-22.3 (5.4)a	-23.1 (4.6)a	-24.0 (5.3)a	-24.0 (4.7)a	-24.0 (4.8)a	***.02***
	Knee	RoM	71.0 (4.0)a	71.6 (4.1)a	68.6 (3.8)b	68.3 (4.1)b	67.8 (5.1)b	***<.01***
		Peak Extension	-0.1 (2.8)	0.1 (2.8)	1.1 (2.3)	0.7 (2.7)	0.4 (2.2)	.06
		Peak Flexion	-71.1 (3.4)a	-71.4 (3.5)a	-67.5 (3.0)b	-67.7 (3.0)b	-67.5 (4.8)b	***<.01***
	Ankle	RoM	20.9 (3.7)	21.6 (3.3)	21.6 (4.0)	21.1 (3.8)	21.0 (3.0)	.68
		Dorsiflexion	12.2 (3.5)a	12.7 (3.0)a	7.6 (2.6)b	7.9 (2.7)b	8.3 (3.2)b	***<.01***
		Plantarflexion	-8.8 (4.8)a	-8.9 (4.3)a	-13.9 (4.8)b	-13.2 (4.7)b	-12.7 (3.4)b	***<.01***

Pelvis Kinematics

Pelvis kinematic patterns were qualitatively similar across conditions but exhibited some between condition magnitude and range of motion differences (Fig. 5.SM.2). In response to the added leg length of the right (perturbed) leg, the shoe leveler conditions raised the pelvis on the right side and increased tilting throughout the gait cycle relative to the symmetry condition (*p*-values < .01). The restricted ankle motion and added mass of the walking boot increased pelvic listing, tilting and posterior rotation, but decreased anterior rotation and anterior tilt compared to the control condition (*p*-values $\leq$ .01). These walking boot responses may be compensations for the right ankle joint restriction but could also be reflective of calibration pose differences. Pelvic kinematics for ankle weight and control conditions were similar. See Table 5.SM.2 for specific condition averages, descriptive statistic effects, and post-hoc pairings.

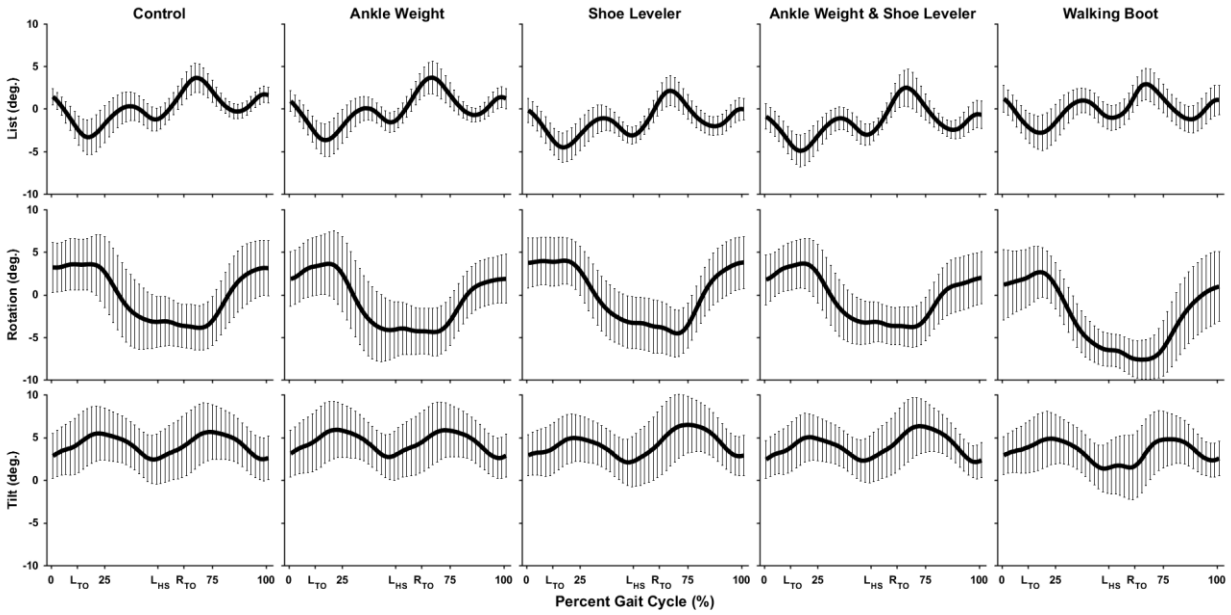

Figure 5.SM.2. Pelvic angles relative to global coordinate system across the five conditions as a percentage of the gait cycle. The gait cycle was defined from perturbed (right) to perturbed heel strike. Positive list, rotation, and tilt represent right fall, right anterior rotation, and posterior tilt, respectively. Lines represent the group averages angles (degrees) with error bars showing the standard deviation of particular points on each curve. Abbreviations: left heel strike (L_{HS}) and toe-off (L_{TO}), and right toe-off (R_{TO}).

Table 5.SM.2. Pelvis ranges and directional maximum angles across the five conditions. The right side coincides with perturbed lower limb. All angles are expressed in degrees. Bolded *p*-values and letters (a and b) denote within group differences ($\alpha < .05$) and their respective group level post-hoc pairings, whenever applicable.

		Condition					
		Control	Ankle Weight	Shoe Leveler	Ankle Weight & Shoe Leveler	Walking Boot	*p* value
List	RoM	7.2 (3.3)a,b	7.5 (3.2)a	7.0 (2.6)a,b	7.6 (3.4)a	6.3 (2.9)b	**.01**
	Right Side-Fall	3.7 (1.7)a	3.7 (1.9)a	2.3 (1.6)b	2.6 (2.1)b	3.2 (1.8)a,b	***<.01***
	Right Side-Rise	-3.4 (2.0)a	-3.8 (2.0)a	-4.7 (1.7)b	-5.0 (1.9)b	-3.1 (1.9)a	***<.01***
Rotation	RoM	10.6 (2.9)	10.5 (2.7)	10.9 (3.5)	9.7 (2.2)	11.9 (2.3)	.07
	Right Side-Anterior	5.3 (2.6)a	4.6 (2.9)a,b	5.3 (2.9)a	4.5 (2.3)a,b	3.2 (3.0)b	**.01**
	Right Side-Posterior	-5.3 (3.2)a	-5.9 (3.4)a	-5.6 (2.9)a	-5.2 (2.4)a	-8.6 (2.3)b	***<.01***
Tilt	RoM	4.2 (1.3)a	4.5 (1.4)a,b	5.3 (1.4)b	5.2 (1.6)b	5.2 (1.4)b	***<.01***
	Posterior	6.1 (3.3)	6.5 (3.2)	6.9 (3.4)	6.7 (3.2)	5.8 (3.2)	.19
	"Anterior"	1.9 (2.7)a	2.0 (2.5)a	1.6 (2.8)a,b	1.5 (2.1)a,b	0.6 (2.5)b	**.01**

EMG Activity

Right (perturbed side) and left side trunk muscle activation patterns were asynchronously offset by gait events but qualitatively similar across conditions (Fig. 5.SM.3). Quantitatively there were only three statistical differences across conditions (Table 5.SM.3). The shoe leveler alone and in combination with the ankle weight condition displayed higher peak activity in left longissimus thoracis (LT; $p < .01$) than the symmetrical control condition. The combined ankle weight and shoe leveler condition had lower average right latissimus dorsi (LD; $p = .03$) activity compared to the control condition. There were also right LD peak activity differences between conditions ($p = .03$) that the more conservative post-hoc Tukey tests could not distinguish. See Table 5.SM.3 for specific condition averages, descriptive statistic effects, and post-hoc pairings.

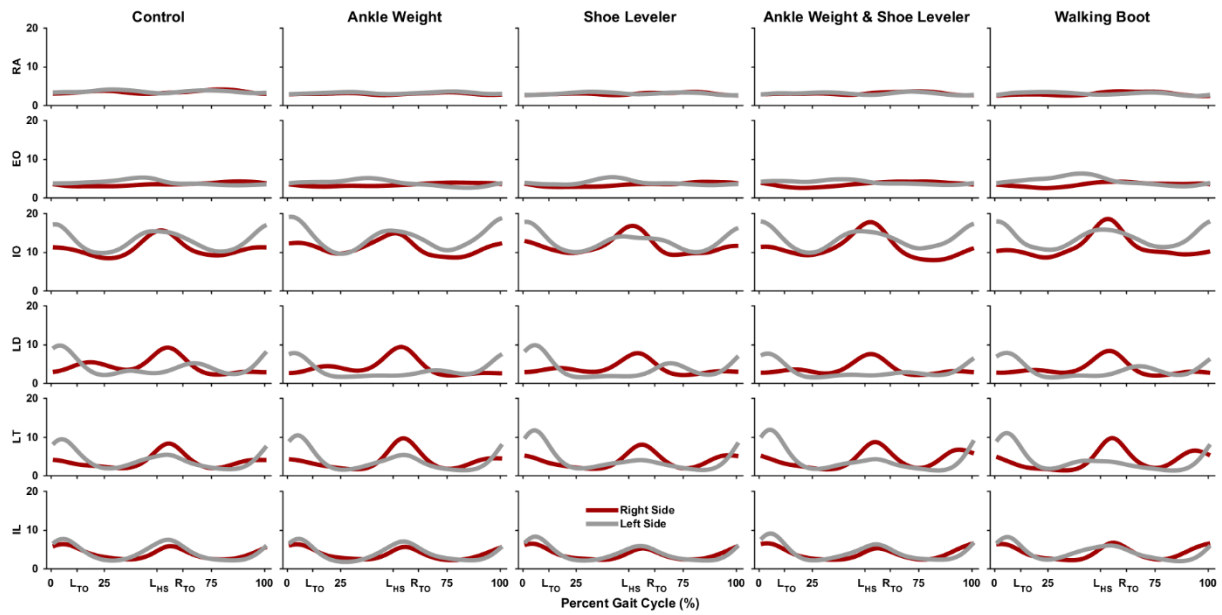

Figure 5.SM.3. EMG activity across the five conditions as a percentage of the gait cycle. The gait cycle was defined from perturbed (right) to perturbed strike. *Maroon lines* represent right (perturbed) and *grey lines* the left (unperturbed) side of each muscle. All lines represent the normalized group averages, standard deviation bars were excluded from the plots for clarity. Abbreviations: left heel strike (L_{HS}) and toe-off (L_{TO}), and right toe-off (R_{TO}), and external oblique (EO), iliocostalis lumborum (IL), internal oblique (IO), latissimus dorsi (LD), longissimus thoracis (LT), rectus abdominis (RA) muscles.

Table 5.SM.3. EMG peak and average activity across the five conditions. Right and left sides coincide with the perturbed and unperturbed lower limbs, respectively. Bolded *p*-values and letters (a and b) denote within group differences ($\alpha < .05$) and their respective group level post-hoc pairings, whenever applicable. Abbreviations: external oblique (EO), iliocostalis lumborum (IL), internal oblique (IO), latissimus dorsi (LD), longissimus thoracis (LT), rectus abdominis (RA) muscles.

		Condition					
		Control	Ankle Weight	Shoe Leveler	Ankle Weight & Shoe Leveler	Walking Boot	*p*- value
				Peak			
Right Side	RA	4.8 (2.2)	4.1 (1.9)	4.1 (2.0)	4.3 (1.8)	4.2 (2.0)	.25
	EO	5.0 (2.7)	4.5 (2.2)	4.9 (2.7)	5.1 (2.5)	5.3 (4.2)	.66
	IO	16.6 (8.2)	17.3 (8.8)	18.8 (8.0)	18.7 (8.7)	19.8 (8.8)	.21
	LD	9.6 (5.5)	9.9 (6.8)	8.4 (4.9)	8.0 (4.3)	8.6 (6.2)	.12
	LT	8.4 (3.4)a	9.8 (3.2)a	8.5 (3.8)a	9.3 (3.8)a	9.9 (4.5)a	**.03**
	IL	8.1 (4.0)	7.8 (3.6)	7.6 (3.8)	7.8 (3.8)	8.2 (3.4)	.75
Left Side	RA	4.6 (3.4)	4.3 (3.1)	4.1 (3.1)	4.1 (2.9)	4.2 (2.6)	.65
	EO	6.2 (4.3)	5.7 (4.3)	5.9 (5.1)	6.3 (5.9)	7.2 (6.5)	.19
	IO	20.6 (11.8)	21.2 (9.6)	19.7 (9.4)	20.2 (9.9)	20.4 (9.0)	.91
	LD	9.9 (11.7)	8.3 (8.2)	10.1 (12.2)	8.2 (6.4)	8.1 (7.7)	.41
	LT	9.5 (5.6)a	10.7 (7.3)a,b	11.9 (7.4)b	12.1 (7.4)b	11.2 (6.2)a,b	***<.01***
	IL	9.8 (4.2)	9.2 (3.8)	8.9 (4.1)	9.5 (3.9)	9.3 (3.8)	.55
				Average			
Right Side	RA	3.4 (1.3)	3.0 (1.4)	2.9 (1.4)	3.0 (1.3)	2.9 (1.2)	.08
	EO	3.4 (2.0)	3.3 (1.9)	3.4 (1.9)	3.5 (2.0)	3.4 (2.3)	.96
	IO	10.8 (5.9)	11.1 (5.6)	11.5 (5.9)	11.1 (5.5)	11.3 (5.8)	.94
	LD	4.4 (2.4)a	4.0 (2.6)a,b	3.7 (2.1)a,b	3.6 (1.9)b	3.6 (2.3)a,b	**.03**
	LT	3.6 (1.5)	3.8 (1.4)	3.8 (1.5)	4.1 (1.8)	4.0 (1.6)	.11
	IL	3.8 (1.8)	3.7 (1.7)	3.7 (1.7)	3.8 (1.7)	4.0 (1.9)	.06
Left Side	RA	3.5 (2.5)	3.2 (2.4)	3.0 (2.4)	3.0 (2.3)	3.0 (2.0)	.16
	EO	3.9 (2.8)	3.7 (3.1)	3.8 (3.5)	4.0 (3.6)	4.3 (3.9)	.29
	IO	12.8 (7.4)	13.5 (6.2)	12.6 (5.9)	13.3 (6.2)	13.6 (6.4)	.84
	LD	4.1 (4.9)	3.2 (2.7)	3.7 (4.0)	3.0 (2.1)	3.3 (3.0)	.25
	LT	3.9 (2.6)	3.8 (2.5)	3.9 (2.4)	3.9 (2.4)	3.8 (2.0)	.83
	IL	4.2 (1.8)	4.0 (1.6)	3.9 (1.6)	4.2 (1.6)	4.1 (1.6)	.20

CHAPTER 6

STUDY 3

DEMANDS ON THE LOWER BACK DURING LOAD CARRIAGE IN ASYMMETRICAL GAIT

6.1. Introduction

Gait asymmetries are defined as bi-lateral differences in lower limb kinematics or kinetics during locomotion (Sadeghi et al., 2000). Individuals who demonstrate asymmetrical gait have a higher incidence of lower back pain (LBP) than those with normal gait (Devan et al., 2014; Kelsey et al., 1984; Knutson, 2005b; Ready et al., 2018; Wolfe et al., 1996). There are several chronic and acute causalities for asymmetrical gait. Chronic pathologies associated with asymmetric gait include lower limb injuries, deformities, bi-lateral leg length differences, and amputations (Constantinou et al., 2014; Dananberg, 1993; Devan et al., 2014; Knutson, 2005b; Mündermann et al., 2005). Acute lower limb gait asymmetries can result from localized pain, an imbalance in footwear, or a prescribed joint motion restriction (Gulgin et al., 2018; also see Study 2). Carrying an uneven load, an awkward object, or with only one arm can by themselves temporarily induce asymmetric gait (Bergmann et al., 1997; DeVita et al., 1991; Wang and Gillette, 2018).

Biomechanical studies using *in vivo* measurements and *in silico* biomechanical musculoskeletal models to determine lower back loading have demonstrated that both upper and lower limb induced asymmetries result in larger lower back demands compared to symmetrical healthy gait (Cappozzo and Gazzani, 1982; Gillette et al., 2009; Hendershot et al., 2018; Hendershot and Wolf, 2014; McGill et al., 2013; Rohlmann et al., 2014c; Rose et al., 2013; Shojaei et al., 2016; Wilke et al., 2001; Yoder et al., 2015; Yu et al., 2014). Carrying a weight solely in one hand can produce higher compressive loads than when twice the total weight is carried evenly

in two hands (McGill et al., 2013; Rohlmann et al., 2014c; Wilke et al., 2001). However, despite being a routine activity and cited as a potential factor contributing to LBP (Devan et al., 2015) the combined effect of load carriage asymmetries and lower limb asymmetrical gait on lower back demands has not been determined.

Therefore, the objective of this study is to determine how upper extremity load carriage techniques affect lower back demands during both symmetrical and asymmetrical gait. To study this, healthy able-bodied participants wore a medical-grade walking boot on one leg to induce a lower limb gait asymmetry (Study 2) and were asked to carry prescribed weights in either one or two hands. Lower back demands were estimated with an EMG optimization (EMGopt) driven OpenSim musculoskeletal model of the lower back (Study 1). We hypothesized that a) upper extremity load carriage combined with lower limb asymmetry would produce greater lower back demands than either upper extremity load carriage or lower limb asymmetries alone (Badawy et al., 2018; Ganguli and Datta, 1977) and b) unilateral loads carried on the side contralateral to the walking boot would be more demanding on the lower back than ipsilateral load carriage (DeVita et al., 1991; McGill et al., 2013; Rose et al., 2013; Study 2). By establishing how an everyday activity such as load carriage can affect lower back demands for those with a lower limb asymmetry, clinicians and ergonomists may be able to help reduce lower back pain and injury in individuals with asymmetric gait.

6.2. Methods

Participants

Twelve (n=12; 6 male) young (26±5), healthy (no history of lower back pain or neurological disorders), and fit (1.71±0.07 meters tall; 64.7±8.3 kgs) participants were recruited

from the general university population. *A priori*, participation, participants consented to this University of Massachusetts Amherst Institutional Review Board approved study.

Equipment and Setup

The experimental protocol was described in Study 2 which examined how different lower limb asymmetries impact lower back demands. In brief, full-body motion capture (Qualisys AB, Sweden), electromyography (EMG; Delsys Inc. USA) on six bilateral trunk muscle groups (rectus abdominis, external and internal obliques, latissimus dorsi, longissimus thoracis pars thoracis, and iliocostalis lumborum pars thoracis; Gagnon et al., 2011; McGill et al., 2013), and directional trunk rotation strength data (Biodex Medical Systems Inc. USA) were collected to estimate the lower back demands during load carrying conditions performed on a powered force treadmill (Treadmetrix, USA). The three-dimensional position of up to 64 reflective markers were collected (100 Hz) along with time-synced digital (EMG) and analog inputs (both at 2000 Hz) within the motion capture software. Hand-held adjustable weight dumbbells were carried either bi- or uni-laterally in symmetrical and asymmetrical conditions (Fig. 6.2.1), with dumbbell weights based on each participant's body weight. During normal symmetrical carries participants wore their own athletic shoes, while in asymmetrical carries a medical-grade walking boot (Aircast® FP Walking Brace) was worn in place of their shoe on the right limb. All participants donned form-fitting clothing and comfortable footwear during measurements of anthropometry, self-selected treadmill walking speed, maximal voluntary contractions (MVC) to establish trunk strength, and experimental carrying conditions.

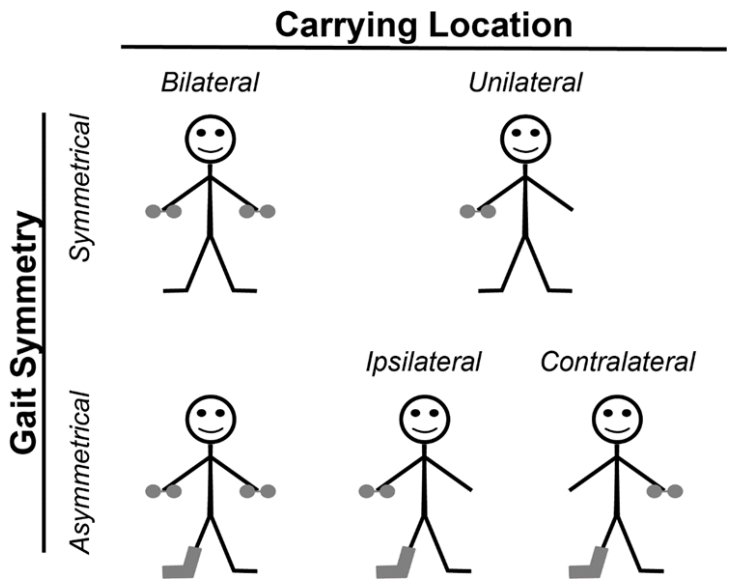

Figure 6.2.1. Schematic of the gait and load carriage experimental conditions. See Table 6.2.1 and in text *Procedure* for complete details on conditions.

Procedure

Ten experimental load carriage conditions were performed at 90% of each participant's self-selected treadmill walking speed (90S; Table 6.2.1.). 90S represents the speeds reported while participants wore a similar walking boot or were required to carry a load (Crosbie et al., 1994; Gulgin et al., 2018; Nottrodt and Manley, 1989). The ten conditions consisted of six asymmetrical conditions with the walking boot on the right leg and four symmetrical conditions without the boot. For the symmetrical tasks, upper extremity load carriage consisted of 7.5% (7.5BW) and 15.0% (15BW) body weight carried in one (unilateral) or two (bilateral) hands. In the asymmetrical walking boot conditions, one-hand carries were conducted with the weight in either the contralateral or ipsilateral hand with respect to the walking boot, resulting in six asymmetrical conditions (bilateral carries of 7.5BW and 15BW, and unilateral carries of 7.5BW and 15BW on both ipsi- and contra-lateral sides).

Table 6.2.1. The ten different load carriage conditions. All conditions were block randomized by conditions involving and not involving the walking boot and performed at 90% of a participant's self-selected treadmill walking speed. Loads were participant-specific based on a percentage of bodyweight (%BW). One handed contralateral and ipsilateral carrying locations represent the load carriage side relative to the walking boot on the right foot. Superscripts denote the analysis of variance (ANOVA) test group(s) assigned to that condition. *the unilateral asymmetrical carrying location that resulted in the largest lower back demands as determined from test 'b' was applied to the principle test 'a'.

	Gait Symmetry	Carrying Location	Total Load Carried (%BW)	
	*Symmetrical (Shoes)*	*Bilateral*	15[a]	30[a]
		*Unilateral (Right Hand)*	7.5[a]	15[a]
	*Asymmetrical (Walking Boot)*	*Bilateral*	15[a]	30[a]
		*Unilateral (Contralateral)* *	7.5[a,b]	15[a,b]
		*Unilateral (Ipsilateral)**	7.5[a,b]	15[a,b]

To prevent post-adaptations and minimize necessary motion capture marker adjustments and corresponding model calibration poses, the six walking boot conditions always followed the four symmetrical gait conditions in a randomized block design. After the symmetrical gait conditions, all motion capture markers below the right knee were removed and placed in equivalent locations on the surface of the walking boot. Data collection from standing calibration poses and unloaded walking acclimation periods of at least 120 seconds for the symmetric and 300 seconds for the less familiar walking boot conditions (Matsas et al., 2000; Taylor et al., 1996) commenced each block. Each carrying condition was then restricted to only 50 total seconds, with the first 20 seconds dedicated to acclimation followed immediately by 30 seconds of data collection, in accordance with manual material handling recommendations (Dick et al., 2017). Two minutes of rest were provided between each condition to minimize fatigue.

At the conclusion of the experimental carrying conditions, MVCs of trunk strength were administered against a dynamometer (Biodex Medical Systems Inc., USA; Study 1). The MVCs

were used to both scale the musculoskeletal model to participant-specific trunk strengths and establish upper activity limits for the normalization of each EMG (McGill et al., 1991).

Musculoskeletal Model and Data Processing

Prior to model implementation, marker positions, ground reaction forces, and dynamometer torque were filtered with a 6 Hz fourth-order zero-lag low pass Butterworth filter (Winter, 2009). Recorded EMG data were sequentially detrended, band-pass filtered (30-500 Hz), full wave rectified, low-pass filtered (3 Hz), time-shifted (10 ms), and scaled to highest MVC values (Study 1). Force, torque, and EMG data were down sampled to 100 Hz to sync with motion capture data. Post processing and statistical tests were performed within MATLAB (MathWorks, USA).

The OpenSim (Delp et al., 2007) lower back musculoskeletal model described and evaluated in Study 1 was used to estimate the lower back kinetic demands from the experimental data. Participant-specific models were built from calibration poses and MVC strength data (Study 1). The model's six lower back joints were controlled by 238 muscle tendon actuators (MTA) representing three trunk muscle groups. MTA forces were computed with an EMG optimization algorithm (EMGopt; Cholewicki and McGill, 1994). EMGopt includes participant-specific muscle activity from recorded EMG to help distribute the calculated joint reaction moments among the MTAs on a frame-by-frame basis (Cholewicki and McGill, 1994; Gagnon et al., 2011; Study 1). The walking boot inertial characteristics were described as appropriately sized tubed cylinders "welded" around the distal shank. Dumbbell weights were modeled as solid cylinders of 7.5% or 15% BW welded to the hands. Three consecutive individual strides from each participant and condition were established from consecutive right (walking boot) heel strikes (Zeni et al., 2008).

For each participant, dependent variables were calculated from ensemble patterns formed by averaging their three time-normalized strides.

Standard OpenSim toolboxes were accessed within custom MATLAB API scripts (Lee and Umberger, 2016) to incorporate EMGopt and to calculate select dependent variables. For each participant, the dependent variables of interest were peak and average L5/S1 compression, resultant shear, and muscle group forces from all ten conditions. Muscles were grouped (Christophy et al., 2012) as either stabilizers (e.g. latissimus dorsi, multifidus, psoas major, and quadratus lumborum), flexion locomotors (e.g. external obliques, internal oblique, and rectus abdominis), or extension locomotors (e.g. iliocostalis lumborum pars lumborum, iliocostalis lumborum pars thoracis, longissimus thoracis pars lumborum, and longissimus thoracis pars thoracis).

Statistical Analysis

Two separate analysis of variance (ANOVA; $\alpha = .05$) tests were used to determine a) if load carriage was more deleterious during asymmetric gait; and b) if there was an effect of unilateral hand carriage location relative to the walking boot side (Table 6.2.1). For the latter test (b) a two-way (2 unilateral hand locations × 2 dumbbell loads) repeated-measures ANOVA test compared the main effect of contra- versus ipsilateral load location on L5/S1 compression and resultant shear force metrics during asymmetric gait. The unilateral carrying side which resulted in the larger lower back compression and shear forces was applied in the principle test (a) on load carriage and gait asymmetries. In the absence of any unilateral carrying side differences, the ipsilateral (right) carrying location would be used in test (a) for consistency with symmetrical gait trials. For test (a) a three-way (2 gait [a]symmetries × 2 carriage locations × 2 dumbbell loads) ANOVA

compared main effect differences for all dependent variables. Tukey post-hoc tests were used to analyze significant ANOVA findings.

6.3. Results

Gait cycle patterns for L5/S1 vertebral joint forces across all load carrying conditions are depicted in Fig. 6.3.1. In general, L5/S1 forces exhibited qualitatively similar bimodal patterns with some differences in magnitude. Peak and minimum force values for both force directions occurred in conjunction with double and single stance phases of the gait cycle, respectively. Carrying dumbbells of 15BW versus 7.5BW generally resulted in larger magnitudes throughout the gait cycle. Compression and shear force curves from one hand carries were less symmetrical but of similar peak magnitudes than two handed carries with equivalent dumbbells in each hand. During one hand carries the curves tended to peak following heel strikes on the dumbbell side, which was more evident with the heavier 15BW dumbbell conditions. In gait asymmetry conditions, patterns were qualitatively similar to symmetric gait but tended to result in slightly higher magnitudes.

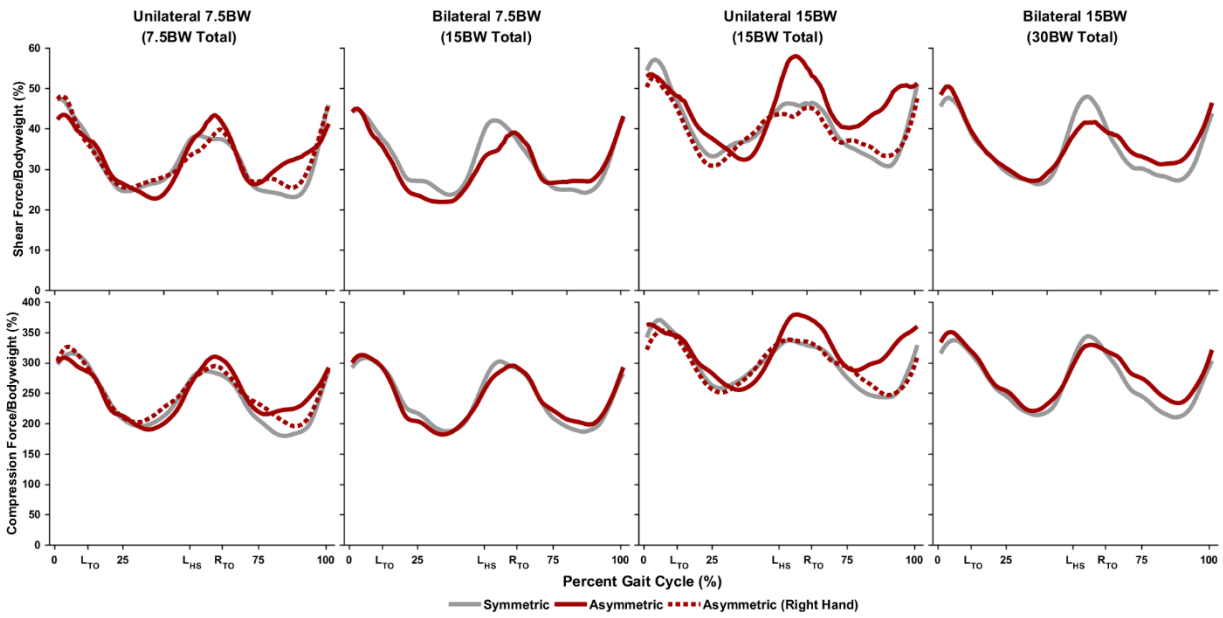

Figure 6.3.1. L5/S1 vertebral joint forces across asymmetric and symmetric walking conditions as a percentage of the gait cycle. Gait cycles started and ended at right (walking boot) heel strikes. Shear (*top row*) and compression (*bottom row*) forces were all normalized to bodyweight (%). Unilateral carries were held in the right hand for symmetric (*grey lines*) gait trials, and either left (contralateral; *solid maroon lines*) hand or right (ipsilateral; *dashed maroon lines*) hand for asymmetric (walking boot) gait conditions. All lines represent the group averages, standard deviation bars were excluded from the plots for clarity. Abbreviations: dumbbells of 7.5% (7.5BW) or 15% (15BW) bodyweight, left heel strike (L_{HS}) and toe-off (L_{TO}), and right toe-off (R_{TO}).

Gait cycle patterns for muscle group forces across all load carrying conditions are shown in Fig. 6.3.2. Muscle group force patterns across conditions were akin to L5/S1 vertebral joint force trends, with larger force magnitudes being generated by the extension locomotor group, followed by the stabilizers and then the flexion locomotors. The unilateral carries demonstrated larger differences in patterns across gait symmetries than the bilateral carries, particularly with 15BW dumbbells.

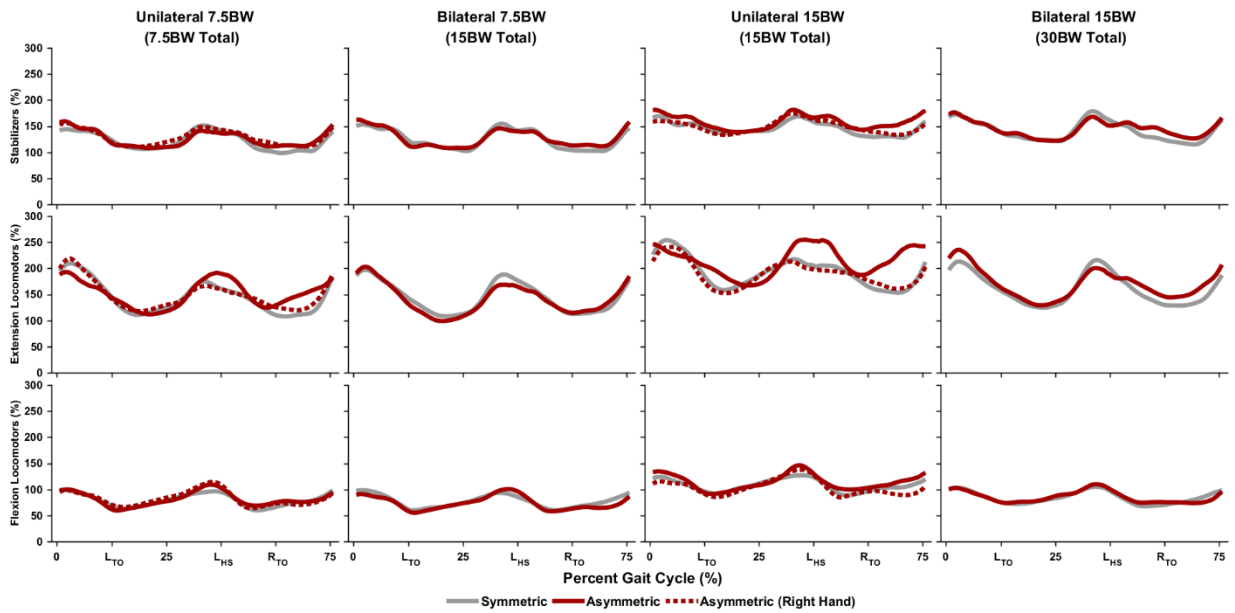

Figure 6.3.2. Muscle group forces across asymmetric and symmetric walking conditions as a percentage of the gait cycle. Unilateral carries were held in the right hand for symmetric (*grey lines*) gait trials, and either left (contralateral; *solid maroon lines*) hand or right (ipsilateral; *dashed maroon lines*) hand for asymmetric (walking boot) gait conditions. All lines represent the group force averages (as a percentage of bodyweight), gait cycles started and ended with right (walking boot) heel strike, while standard deviation bars were excluded from the plots for clarity. See *Methods* for muscles contained in Stabilizers (*top panel*), Extension Locomotors (*middle panel*), and Flexion Locomotors (*bottom panel*). Abbreviations: dumbbells of 7.5% (7.5BW) or 15% (15BW) bodyweight, left heel strike (L_{HS}) and toe-off (L_{TO}), and right toe-off (R_{TO}).

Test b - Impact of unilateral hand carriage location on L5/S1 joint forces during asymmetric gait

Normalized L5/S1 vertebral joint force magnitudes and statistical results for unilateral carrying with asymmetric gait can be found in Table 6.3.1. As expected, carrying 15BW dumbbells resulted in larger L5/S1 average and peak forces than 7.5BW dumbbells, with *p*-values < .01. However, compression and shear forces were not significantly impacted by which hand was holding the weighted dumbbell across 7.5BW and 15BW conditions (*p*-values ranged from .07 to .29). There was a consistent trend for greater L5/S1 forces when the weight was held in the left hand, and the dumbbell load × hand location interaction showed differences across all descriptive metrics (Table 6.3.1); *p*-values <.01 to .02). Post-hoc analysis of the interaction effect showed that carrying a 15BW dumbbell in the left hand contralateral to the walking boot limb resulted in significantly larger shear force (peak: 66.5 ± 16.6 *vs* 56.3 ± 10.7 %BW; average: 45.0 ± 8.5 *vs* 39.6

± 6.2) and compression force (peak: 404.9 ± 79.6 *vs* 373.3 ± 70.8; average: 318.7 ± 51.3 *vs* 296.8 ± 47.0) than when carried in the right hand. Therefore, in the subsequent test (a) only data from the asymmetrical unilateral carries with the weight in the left hand were included.

Table 6.3.1. Peak and average L5/S1 vertebral joint shear and compression force effects during asymmetric gait for unilateral carry locations in the left or right hand. Forces were normalized and expressed as a percentage of bodyweight. Asymmetry was induced with a walking boot worn on the right lower limb. Letters denote post-hoc pairings from significant differences *(in bold*; $p < .05$) between main effects of dumbbell load, location, and dumbbell × location interaction. Abbreviations: dumbbells of 7.5% (7.5BW) or 15% (15BW) bodyweight.

Source	Metrics		Main & Interaction Effects				*p*-value
Dumbbell (D)			7.5BW	15BW			
	Shear	Peak	49.7 (11.7)a	61.4 (14.6)b			**<.01**
		Average	32.4 (5.9)a	42.3 (7.8)b			**<.01**
	Compression	Peak	335.3 (53.7)a	389.1 (75.4)b			**<.01**
		Average	247.5 (27.6)a	307.8 (49.4)b			**<.01**
Location (L)			Left	Right			
	Shear	Peak	57.5 (16.2)	53.6 (12.3)			.29
		Average	38.8 (9.6)	35.9 (7.0)			.07
	Compression	Peak	368.4 (74.8)	355.9 (66.4)			.22
		Average	283.1 (54.3)	272.2 (45.6)			.10
D × L			7.5BW		15BW		
			Left	Right	Left	Right	
	Shear	Peak	48.5 (9.9)a	50.9 (13.6)a,b	66.5 (16.6)c	56.3 (10.7)b	**<.01**
		Average	32.7 (6.1)a	32.1 (5.8)a	45.0 (8.5)c	39.6 (6.2)b	**.02**
	Compression	Peak	331.9 (49.4)a	338.6 (59.6)a	404.9 (79.6)c	373.3 (70.8)b	**<.01**
		Average	247.5 (27.9)a	247.6 (28.6)a	318.7 (51.3)c	296.8 (47.0)b	**.02**

Test a – Impact of asymmetric gait on lower back demands during carrying tasks

Normalized L5/S1 vertebral joint force magnitudes and statistical results for each carrying condition can be found in Table 6.3.2. As expected, both peak and average normalized L5/S1 vertebral joint compression and shear forces were larger when carrying 15BW *versus* 7.5BW dumbbells (all *p-values* < .01). For three of the four metrics, carrying a load in one hand resulted in significantly larger vertebral joint forces than when the same dumbbell weight was carried in

each of the hands and thus doubling the total weight carried (p-values ranged from <.01 to .02). The lone exception was for the peak compression force, which was larger but not statistically different in the unilateral carry (p = .10). The presence of lower limb gait asymmetry induced by the walking boot led to larger average compression forces (Fig. 6.3.4; p = .03). No asymmetry-related statistical differences were found for the L5/S1 shear force measures (p-values ranged from .10 to .42) or for peak compression force (p = .10). The interaction effect of dumbbell load and gait symmetry was significant for average L5/S1 shear force, with post-hoc comparisons showing symmetric and asymmetric gait to have similar average shear forces while carrying 7.5BW but not 15BW dumbbells (p < .01). All other interactions involving gait symmetry were insignificant (p-values from >.05 to .94).

Table 6.3.2. L5/S1 vertebral joint shear and compression force peak and average effects during carries. Dumbbells were carried either in one or two hands, in the latter task the total hand load was therefore doubled. During asymmetric gait, the lower limb perturbation was located on the right side and one hand carries were held in the left contralateral hand, while during symmetric gait one hand carries were held in the right hand. Letters next to group averages denote post-hoc groupings following statistical *(in bold*; $p < .05$) differences. Abbreviations: dumbbells of 7.5% (7.5BW) or 15% (15BW) bodyweight.

Source	Metrics		Main & Interaction Effects								*p*-value
Dumbbell (D)			7.5BW	15BW							
	Shear	Peak	48.2 (9.3)a	57.8 (14.8)b							**<.01**
		Average	31.7 (5.5)a	39.0 (7.8)b							**<.01**
	Compression	Peak	329.0 (49.2)a	378.0 (69.5)b							**<.01**
		Average	241.7 (24.6)a	290.8 (43.2)b							**<.01**
Hands (H)			One	Two							
	Shear	Peak	56.1 (15.1)b	49.9 (10.2)a							**.02**
		Average	37.5 (8.5)b	33.2 (6.1)a							**<.01**
	Compression	Peak	361.7 (75.9)	345.2 (50.8)							.10
		Average	275.7 (50.9)b	256.7 (30.4)a							**<.01**
Gait Symmetry (G)			Symmetric	Asymmetric							
	Shear	Peak	52.2 (12.6)	53.8 (13.8)							.42
		Average	34.7 (6.8)	36.0 (8.4)							.10
	Compression	Peak	348.1 (67.0)	358.8 (62.7)							.10
		Average	261.2 (39.5)a	271.2 (45.7)b							**.03**
D × H			7.5BW				15BW				
			One		Two		One		Two		
	Shear	Peak	49.0 (9.8)a,b		47.5 (9.0)a		63.3 (16.2)c		52.3 (11.0)b		**<.01**
		Average	32.2 (5.6)a		31.3 (5.4)a		42.8 (7.6)c		35.2 (6.2)b		**<.01**
	Compression	Peak	329.0 (54.7)a		328.9 (44.2)a		394.5 (80.8)c		361.4 (52.6)b		**<.01**
		Average	243.3 (26.9)a		240.1 (22.4)a		308.2 (48.7)c		273.4 (28.4)b		**<.01**
D × G			7.5BW				15BW				
			Symmetric		Asymmetric		Symmetric		Asymmetric		
	Shear	Peak	48.3 (9.9)		48.2 (8.9)		56.2 (14.0)		59.4 (15.7)		.16
		Average	31.7 (5.5)a		31.7 (5.6)a		37.7 (6.8)b		40.3 (8.7)c		**.01**
	Compression	Peak	325.9 (55.4)		332.1 (43.1)		370.3 (71.2)		385.6 (68.4)		.28
		Average	239.7 (24.1)		243.6 (25.4)		282.8 (40.5)		298.9 (45.2)		.05
H × G			One				Two				
			Symmetric		Asymmetric		Symmetric		Asymmetric		
	Shear	Peak	54.8 (14.0)		57.5 (14.0)		49.7 (9.9)		50.1 (9.9)		.55
		Average	36.1 (7.2)		38.8 (7.2)		33.3 (6.1)		33.2 (6.1)		.10
	Compression	Peak	355.1 (78.0)		368.4 (78.0)		341.1 (47.5)		349.2 (47.5)		.70
		Average	268.4 (47.3)		283.1 (47.3)		254.1 (32.1)		259.4 (32.1)		.18
D × H × G			7.5BW						15BW					
			One				Two				One		Two		
			Symmetric		Asymmetric		Symmetric		Asymmetric		Symmetric	Asymmetric	Symmetric	Asymmetric	
	Shear	Peak	49.5 (10.0)		48.5 (9.9)		47.2 (10.1)		47.9 (8.2)		60.1 (15.8)	66.5 (16.6)	52.3 (11.2)	52.3 (11.2)	.09
		Average	31.6 (5.3)		32.7 (6.1)		31.8 (5.9)		30.7 (4.9)		40.6 (6.1)	45.0 (8.5)	34.7 (6.4)	35.7 (6.3)	.61
	Compression	Peak	326.1 (61.7)		331.9 (49.4)		325.6 (51.1)		332.2 (38.1)		384.0 (84.2)	404.9 (79.6)	356.6 (55.7)	366.3 (51.3)	.46
		Average	239.0 (26.5)		247.5 (27.9)		240.3 (22.6)		239.8 (23.3)		297.7 (45.8)	318.7 (51.3)	267.9 (29.1)	279.0 (27.7)	.94

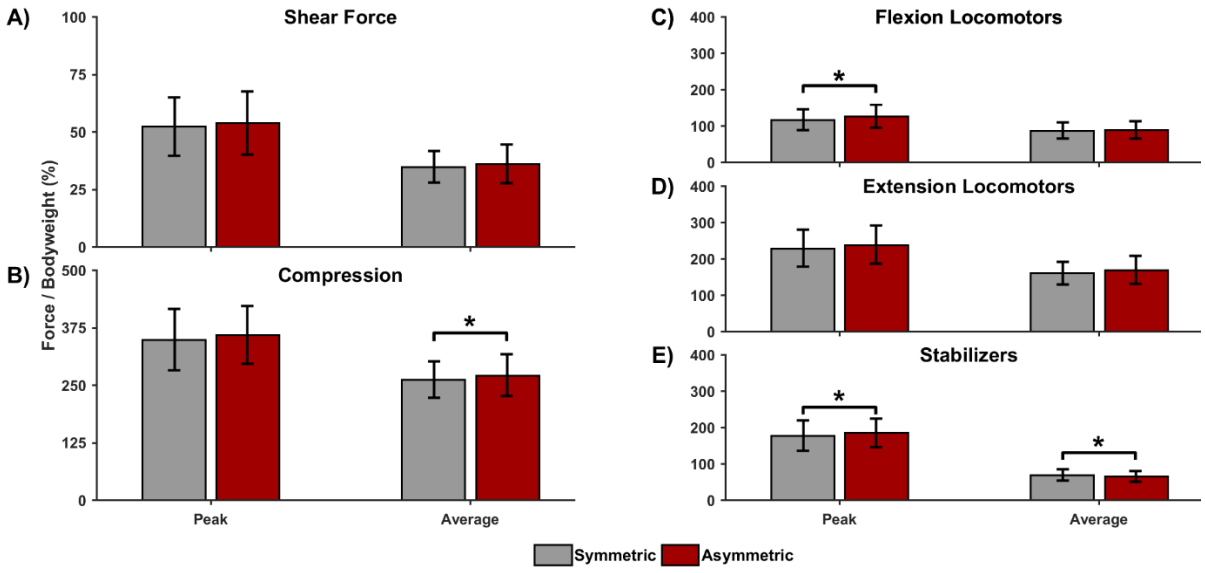

Figure 6.3.4. L5/S1 vertebral joint and muscle group force metrics for carrying loads with symmetric and asymmetric gait. *Panel A*) L5/S1 vertebral joint shear force; *panel B*) L5/S1 vertebral joint compression force; *panel C*) flexion locomotors; *panel D*) extension locomotors; *panel E*) stabilizers. Forces are normalized as a percentage of bodyweight and are averaged across 7.5BW and 15BW loads to emphasize the effect of gait symmetry. During asymmetric gait (*maroon bars*), the walking boot perturbation was located on the right lower limb, while during symmetric (*grey bars*) gait conditions participants donned their own athletic shoes. See Tables 6.3.2 (L5/S1 joint force) and 6.3.3 (muscle group force) for data from individual load carrying conditions. Whiskers represent ±1 standard deviation and asterisks (*) denote statistical differences ($\alpha < .05$) between gait types. See *Methods* for muscles contained in each of the three groups.

Muscle group force magnitudes and statistical results for each load carrying condition can be found in Table 6.3.3. Muscle group force statistical trends resembled L5/S1 vertebral joint force effects. For all three muscle groups, normalized peak and average forces increased when carrying 15BW *versus* 7.5BW dumbbells (all *p*-values < .01). One hand load carries resulted in significantly greater peak and average forces compared to two-handed carries for flexion locomotors (*p*-values < .01) and extension locomotors (*p*-values < .05), but not peak ($p = .84$) or average ($p = .17$) stabilizer forces. Compared to symmetric gait, asymmetric gait increased peak forces for flexion locomotor ($p = .02$) and stabilizer ($p = .03$) muscle groups and increased average force for the stabilizer group ($p < .01$). The interaction effect of dumbbell load and gait type was significant ($p = .03$) for average force in the extension locomotor group, with post-hoc comparisons indicating similar gait type results while carrying 7.5BW but larger muscle forces when carrying

15BW dumbbells with asymmetric gait. All other interactions involving gait type were insignificant (with *p*-values ranging from .07 to .96).

Table 6.3.3. Muscle group effects during load carriage. Dumbbells were carried either in one or two hands, in the latter the total carried load was therefore doubled. During asymmetric gait, the walking boot was located on the right lower limb. In unilateral carries the dumbbell was held in the left hand during asymmetric gait (see Test b) and the right hand during symmetric gait. Letters next to group averages denote post-hoc groupings following statistical differences *(in bold*; $p < .05$). See *Methods* for muscles contained in each group. Statistical tests were only performed on the peak and average of summed muscle group forces and not individual muscles or sides. Abbreviations: dumbbells of 7.5% (7.5BW) or 15% (15BW) bodyweight.

Source	Metrics		Main & Interaction Effects								*p*-value
Dumbbell (D)			7.5BW	15BW							
	Flexion Locomotors	Peak	109.7 (21.3)a	133.7 (33.9)b							**<.01**
		Average	77.8 (12.9)a	97.8 (25.7)b							**<.01**
	Extension Locomotors	Peak	210.7 (33.2)a	255.7 (56.4)b							**<.01**
		Average	145.3 (18.3)a	184.1 (36.8)b							**<.01**
	Stabilizers	Peak	170.3 (35.8)a	191.3 (41.7)b							**<.01**
		Average	124.9 (21.8)a	147.3 (28.9)b							**<.01**
Hands (H)			One	Two							
	Flexion Locomotors	Peak	130.9 (35.5)b	112.5 (21.6)a							**<.01**
		Average	95.5 (27.0)b	80.0 (13.4)a							**<.01**
	Extension Locomotors	Peak	244.0 (60.0)b	222.5 (38.4)a							**.05**
		Average	175.6 (41.3)b	153.8 (22.6)a							**<.01**
	Stabilizers	Peak	180.3 (41.5)	181.3 (39.0)							.84
		Average	137.9 (30.0)	134.3 (25.7)							.16
Gait Symmetry(G)			Symmetric	Asymmetric							
	Flexion Locomotors	Peak	116.9 (28.5)a	126.5 (32.2)b							**.02**
		Average	87.0 (22.4)	88.6 (23.0)							.50
	Extension Locomotors	Peak	228.5 (50.3)	237.9 (52.3)							.26
		Average	160.4 (31.0)	169.0 (38.3)							.08
	Stabilizers	Peak	176.9 (41.2)a	184.7 (39.0)b							**.03**
		Average	133.5 (26.4)a	138.7 (29.2)b							**<.01**
D x H			7.5BW				15BW				
			One		Two		One		Two		
	Flexion Locomotors	Peak	112.7 (22.0)a		106.7 (20.6)a		149.0 (37.5)b		118.4 (21.4)a		**<.01**
		Average	80.4 (13.1)a		75.3 (12.4)a		110.7 (29.0)b		84.8 (12.8)a		**<.01**
	Extension Locomotors	Peak	212.4 (35.6)a		209.1 (31.3)a		275.5 (63.4)c		235.8 (40.9)b		**<.01**
		Average	148.0 (19.3)a		142.5 (17.2)a		203.2 (39.1)c		165.0 (21.9)b		**<.01**
	Stabilizers	Peak	167.3 (34.0)		173.2 (38.0)		193.3 (44.9)		189.4 (39.0)		.07
		Average	123.9 (21.4)a		126.0 (22.6)a		152.0 (31.1)c		142.6 (26.3)b		**<.01**
D x G			7.5BW				15BW				
			Symmetric		Asymmetric		Symmetric		Asymmetric		
	Flexion Locomotors	Peak	106.9 (21.5)		112.6 (21.1)		127.0 (31.4)		140.3 (35.7)		.07
		Average	78.0 (12.7)		77.6 (13.3)		96.0 (26.3)		99.5 (25.6)		.26
	Extension Locomotors	Peak	210.0 (39.0)		211.5 (27.0)		247.1 (54.2)		264.3 (58.4)		.16
		Average	144.4 (18.2)a		146.2 (18.7)a		176.5 (33.1)b		191.8 (39.4)c		**.03**
	Stabilizers	Peak	165.2 (38.2)		175.3 (33.2)		188.6 (41.4)		194.0 (42.6)		.39
		Average	123.5 (22.7)		126.3 (21.3)		143.5 (26.4)		151.1 (31.2)		.14
H x G			One				Two				
			Symmetric		Asymmetric		Symmetric		Asymmetric		
	Flexion Locomotors	Peak	123.5 (31.8)		138.2 (31.8)		110.4 (19.6)		114.7 (19.6)		.20
		Average	93.6 (27.1)		97.5 (27.1)		80.5 (12.8)		79.6 (12.8)		.36
	Extension Locomotors	Peak	240.2 (58.4)		247.8 (58.4)		216.9 (38.4)		228.0 (38.4)		.79
		Average	168.6 (36.7)		182.7 (36.7)		152.3 (23.8)		155.3 (23.8)		.10
	Stabilizers	Peak	173.6 (41.0)		187.0 (41.0)		180.2 (36.5)		182.3 (36.5)		.15
		Average	134.1 (27.4)		141.8 (27.4)		132.9 (25.9)		135.7 (25.9)		.21
D x H x G			7.5BW						15BW					
			One				Two				One				Two			
			Symmetric		Asymmetric		Symmetric		Asymmetric		Symmetric		Asymmetric		Symmetric		Asymmetric	
	Flexion Locomotors	Peak	108.5 (20.6)		116.9 (23.4)		105.2 (23.2)		108.2 (18.5)		138.5 (34.6)		159.5 (38.8)		115.5 (24.0)		121.2 (19.2)	.20
		Average	79.4 (12.3)		81.3 (14.4)		76.6 (13.6)		73.9 (11.5)		107.7 (30.8)		113.7 (28.0)		84.3 (14.2)		85.3 (11.8)	.96
	Extension Locomotors	Peak	215.8 (42.1)		208.9 (29.1)		204.2 (36.4)		214.0 (25.7)		264.5 (63.8)		286.6 (63.7)		229.7 (37.6)		242.0 (44.7)	.17
		Average	144.6 (18.1)		151.5 (20.6)		144.2 (19.2)		140.8 (15.7)		192.6 (35.2)		213.9 (41.3)		160.3 (21.9)		169.8 (21.9)	.89
	Stabilizers	Peak	160.0 (34.1)		174.7 (33.7)		170.5 (42.8)		175.9 (34.1)		187.3 (44.0)		199.3 (47.0)		189.9 (40.6)		188.8 (39.2)	.68
		Average	122.1 (23.1)		125.6 (20.5)		125.0 (23.2)		127.0 (23.0)		146.1 (26.8)		157.9 (35.0)		140.9 (27.0)		144.3 (26.6)	.35

6.4. Discussion

In this study we sought to answer two questions concerning lower limb gait asymmetry induced with a walking boot: a) Are lower back forces during load carriage different than in symmetric gait? and b) In one-handed carries, does the hand side with respect to the walking boot affect L5/S1 joint forces? The original hypotheses were that a) gait asymmetry would have greater back forces during carrying tasks than with symmetrical gait, and b) unilaterally carrying a load on the side contralateral to the walking boot would result in higher L5/S1 joint forces. Both hypotheses were partially supported. Compared to symmetric gait, load carriage demands were larger in several key lower back variables during asymmetrical gait in bi- and uni-lateral carries. For one-handed carries, carrying a weight on the side contralateral to the walking boot resulted in larger average L5/S1 vertebral joint compression forces than when carried on the boot side.

Biomechanical studies on unilateral load carrying have demonstrated that one hand load carriage moves the carrier's center of mass (CoM) in the direction of the load. Compared to unloaded normal walking, this CoM shift results in larger L5/S1 frontal plane internal joint moments due to increased muscle forces on the unloaded side, and increased anterior/posterior shearing (DeVita et al., 1991; McGill et al., 2013; Rose et al., 2013). In Study 2, peak frontal plane L5/S1 joint moments were larger during unloaded asymmetrical walking boot conditions compared to symmetrical gait. Together these findings led to the hypothesis that L5/S1 joint forces would be larger during one-handed load carriage when loads were carried in the left hand when the walking boot was on the right side. While all L5/S1 joint force metrics were generally larger with the load in the left rather than right hand, there was no significant main effect of dumbbell hand location. However, the hand by dumbbell weight interaction analysis showed that there were significant differences between hands for larger 15BW dumbbell loads but not for the 7.5BW

loads. For the larger 15BW dumbbells, all L5/S1 force metrics were significantly larger when the weight was held in the left hand, supporting the second hypothesis.

A potential factor during asymmetric gait could be that individuals generally seek to minimize ground contact time on a perturbed limb (e.g. walking boot). A reduction in ground contact time causes the body's CoM medial-lateral acceleration to increase while quickly transitioning from perturbed to unperturbed limb stance (Tesio and Rota, 2019). In the present case, carrying an added mass (dumbbell) on the left side opposite to the walking boot could compound this asymmetric gait lateral acceleration. To control the trunk CoM's enhanced lateral motion, trunk muscles on the right walking boot side (opposite the load) would be called upon to exert larger forces, leading to increased vertebral joint loads (Marras, 2000). Post hoc analyses showed that participants spent less time in stance on the right walking boot side than on the left side (see Supplemental Material, Table 6.SM.1) and had larger lateral accelerations when a dumbbell was carried in the left, as opposed to the right, hand (see Supplemental Material, Table 6.SM.2). Further, there is evidence of increased contralateral (i.e. right) side trunk muscle group forces during unilateral carries with the left hand as compared to contralateral muscle group forces in the right hand carries (see Supplemental Material, Tables 6.SM.2) which would contribute to larger L5/S1 vertebral joint forces.

In contrast to unilateral carries, bilateral carries evenly distribute the load between both hands in the frontal plane and therefore do not substantially move the carrier's CoM, although they still affect the spine by adding gravitational force from the load, extra work requirements, and possible perceived stability demands to the spine (McGill et al., 2009). Several *in vivo* and computer model evaluations of lower back joint demands across different load carriage techniques support this rationale (see review by Badawy et al., 2018). Our data and these studies suggest that

carrying weight in one hand results in back forces often greater than carrying the same weight in each hand, a situation which might be expected to have larger demands because of the doubled total load. However, the impact of carrying loads in either one or two hands with gait asymmetry has largely gone unresearched. Ganguli and Datta (1977) compared load carriage energy expenditures for individuals with and without unilateral lower limb amputations, finding the higher energy expenditure levels often associated with lower limb amputation were amplified during carrying tasks. Our data indicate that load carrying with a lower limb asymmetry led to larger average L5/S1 vertebral joint compression force, and larger force metrics in the flexion locomotor and stabilizer muscle groups, supporting our first hypothesis. Gait symmetry effects tended to be influenced by one-handed carries and higher dumbbell loads and again may be a consequence of the CoM movement when transitioning from the walking boot stance to unperturbed side stance (see Supplemental Material, Table 6.SM.3). Symmetric or asymmetric gait carries with two hands would not have the combined influence of these effects and thus would not be as demanding on the lower back.

The magnitude of the L5/S1 vertebral joint peak forces during these carrying tasks ranged from 1291 to 3551 Newtons in compression and 181 to 604 Newtons in shear. Greater peak values were associated with unilateral 15BW dumbbell conditions during asymmetric gait, while lower values were found in the bilateral 7.5BW dumbbell conditions. Such force levels are larger than the 1,244 to 2,895 Newtons in compression and 166 to 469 Newtons in shear estimated from the same cohort during unloaded walking (Study 2) but generally are considered safe for the L5/S1 spinal unit tissues when given sufficient recovery time between repetitions and with relatively neutral trunk postures (Gallagher and Marras, 2012; Jäger and Luttmann, 1989). However, forces of this magnitude may lead to tissue injury during the sustained and awkward postures of

asymmetric gait (Adams and Dolan, 2005; Brinckmann et al., 1988; Gallagher et al., 2005; Marras, 2008; Study 2). This chronic injury mechanism could potentially account for the high LBP prevalence seen clinically in asymmetric gait populations (Devan et al., 2014; Kelsey et al., 1984; Knutson, 2005b; Ready et al., 2018; Wolfe et al., 1996), and warrants additional epidemiological and biomechanical research.

While our data provide support for our hypotheses, a larger and more diverse range of carrying situations and lower limb asymmetries potentially could produce more pronounced effects. Lower back demands are dependent on load, speed, duration, fatigue, and gait (a)symmetry (Hendershot et al., 2018; Marras et al., 2006; McGill et al., 2013; van Dieën et al., 1998b). The combination of these factors applied in the present study were chosen to be relevant to activities of daily living, allowed for a repeated-measures design, and were based on ergonomic guidelines and common clinical treatments (Dick et al., 2017; Zhang et al., 2006). Lower back demands from carrying with different perturbations, across a variety of gait speeds, clinical populations, with muscle fatigue, and greater loads or durations could uncover different effects and thus merit further investigation. Finally, although our model was evaluated for the comparison of gait and carrying tasks in Study 1, improved musculoskeletal modeling approaches may lead to further insights.

In summary, this was the first study to assess lower back demands during load carriage with a gait asymmetry induced by a walking boot. We found that carry tasks resulted in a) larger lower back forces in the presence of a gait asymmetry than without, and b) larger L5/S1 forces when unilateral loads were held in the hand contralateral to the walking boot. Thus, clinicians and ergonomists aiming to reduce lower back demands for those with gait asymmetries should perhaps

endorse carrying loads in two hands or in the hand on the same side as the walking boot whenever possible.

6.SM. Supplemental Material

Stance Time (A)symmetry

To evaluate the impact of load carriage and gait symmetry on lower limb stance time asymmetry, a symmetry index (SI) calculated as a percentile of right *versus* left leg stance time was determined for all carrying conditions (see Study 2 for calculation procedure). Positive SI percentile values represent longer right (walking boot) stance times, while negative SI denotes longer left stance times. SIs were compared ($\alpha = .05$) with a three-way ANOVA and Tukey post-hoc testing when appropriate.

Average SIs and statistical results are shown in Table 6.SM.1. As intended the walking boot induced more asymmetric gait (i.e. further from 0) relative to normal shod conditions, with longer left side stance times as indicated by the negative stance time SI ($p < .01$). However, carrying different dumbbell loads ($p = .09$), one versus two hand carries ($p = .83$), and all interaction effects (p-values ranging from .20 to .85) surprisingly did not significantly impact lower limb stance time SIs, unlike previous results (Wang and Gillette, 2018).

Table 6.SM.1. Stance time symmetry index effects during carrying conditions. Negative symmetry index (SI; percentile) values denote longer left stance times, while SIs closer to zero would represent more symmetry between lower limb stance times. Dumbbells were carried either in one or two hands, in the latter task the total hand load was therefore doubled. During asymmetric gait, the walking boot was located on the right lower limb; in one hand carries, the dumbbell was held in the left hand (see Test b for rationale). During symmetric gait unilateral dumbbell carries were held in the right hand. Letters denote post-hoc pairings from significant differences *(in bold*; $p < .05$) between effects of dumbbell load (D), hand location (H), gait symmetry (G), and their interactions. Abbreviations: dumbbells of 7.5% (7.5BW) or 15% (15BW) bodyweight.

Source	Stance SI Main & Interaction Effects								*p*-value
Dumbbell (D)	7.5BW	15BW							
	-1.1 (1.7)	-1.6 (1.9)							.09
Hand (H)	One	Two							
	-1.3 (1.9)	-1.4 (1.8)							.83
Gait Symmetry (G)	Symmetric	Asymmetric							
	-0.2 (1.2)b	-2.5 (1.6)a							**<.01**
D × H	7.5BW				15BW				
	One	Two			One	Two			
	-0.9 (1.7)	-1.3 (1.8)			-1.8 (2.1)	-1.5 (1.7)			.20
D × G	7.5BW				15BW				
	Symmetric	Asymmetric			Symmetric	Asymmetric			
	0.0 (1.1)	-2.2 (1.5)			-0.4 (1.2)	-2.9 (1.7)			.74
H × G	One				Two				
	Symmetric	Asymmetric			Symmetric	Asymmetric			
	-0.2 (1.4)	-2.5 (1.4)			-0.2 (1.6)	-2.6 (1.6)			.85
D × H × G	7.5BW						15BW				
	One		Two				One		Two		
	Symmetric	Asymmetric	Symmetric	Asymmetric			Symmetric	Asymmetric	Symmetric	Asymmetric	
	0.2 (1.2)	-1.9 (1.5)	-0.1 (1.1)	-2.5 (1.6)			-0.5 (1.6)	-3.1 (1.8)	-0.3 (.7)	-2.7 (1.7)	.53

Center of Mass Lateral Acceleration

To support our Test (a) and (b) conclusions, the corresponding impact of a) load carriage during asymmetric gait; and b) unilateral hand carriage location relative to the walking boot side on peak CoM lateral acceleration was evaluated. Whole body CoM lateral acceleration in the frontal plane was calculated for each trial using OpenSim's *Analysis Tool* and referenced relative to global coordinates. A positive value indicates an acceleration directed towards the participant's right side, while a negative value indicates an acceleration to the left side. Three- and two-way repeated-measures analysis of variance (ANOVA) tests were used for Test (a) and (b),

respectively, along with Tukey post-hoc tests to further analyze significant ANOVA findings (α= .05).

Peak CoM lateral accelerations and statistical results comparing one hand asymmetry carries (Test b) are shown in Table 6.SM.2. There were no significant effects of dumbbell load on peak acceleration towards either the right (p = .83) or left side (p = .66). Larger peak acceleration towards the right side (p = .03) occurred when the dumbbell was held in the left versus the right hand, but hand location did not have a significant effect on acceleration towards the left side (p = .18). No significant dumbbell load × hand location effect was present for either right (p = .50) or left (p = .86) side accelerations.

Table 6.SM.2. Center of mass peak lateral acceleration effects during asymmetric gait for unilateral carry locations in the left or right hand. Asymmetry was induced with a walking boot worn on the right lower limb. Letters denote post-hoc pairings from significant differences (*in bold; p* < .05) in acceleration (in m/s^2) between main effects of dumbbell load, location, and dumbbell × location interaction. Abbreviations: dumbbells of 7.5% (7.5BW) or 15% (15BW) bodyweight.

Source	Metrics	Main & Interaction Effects				*p*-value
Dumbbell (D)		7.5BW	15BW			
	Towards Right	0.87 (0.16)	0.87 (0.16)			.83
	Towards Left	-0.84 (0.16)	-0.85 (0.15)			.66
Location (L)		Left	Right			
	Towards Right	0.90 (0.17)b	0.84 (0.14)a			**.03**
	Towards Left	-0.87 (0.17)	-0.82 (0.14)			.18
D × L		7.5BW		15BW		
		Left	Right	Left	Right	
	Towards Right	0.88 (0.15)	0.85 (0.16)	0.91 (0.19)	0.83 (0.11)	.50
	Towards Left	-0.86 (0.17)	-0.81 (0.16)	-0.87 (0.18)	-0.83 (0.12)	.86

Peak CoM lateral accelerations and statistical results comparing carries during different gait symmetries (Test a) are shown in Table 6.SM.3. As with Test b, there were no significant effects of dumbbell load on peak acceleration towards either the right (p = .17) or left side (p = .64). One hand dumbbell carries led to significantly larger peak acceleration directed towards both the right (p < .01) and left (p < .01) sides than two hand carries. Load carriage while donning a walking boot (asymmetric gait) also led to significantly larger peak acceleration towards both the right (p < .01) and left (p < .01) sides than during symmetrical gait. No significant interaction effects (p-values ranging from .18 to .64) were found for peak accelerations in either direction.

Table 6.SM.3. Center of mass peak lateral acceleration effects during carrying conditions. Dumbbells were carried either in one or two hands, in the latter task the total hand load was therefore doubled. During asymmetric gait, the walking boot was located on the right lower limb; in one hand carries, the dumbbell was held in the left hand (see Test b for rationale). During symmetric gait unilateral dumbbell carries were held in the right hand. Letters denote post-hoc pairings from significant differences *(in bold*; p < .05) in acceleration (in m/s^2) between effects of dumbbell load (D), hand location (H), gait symmetry (G), and their interactions. Abbreviations: dumbbells of 7.5% (7.5BW) or 15% (15BW) bodyweight.

Source		Main & Interaction Effects								p-value
Dumbbell (D)		7.5BW	15BW							
	Towards Right	0.80 (0.15)	0.76 (0.18)							.17
	Towards Left	-0.77 (0.16)	-0.76 (0.18)							.64
Hands (H)		One	Two							
	Towards Right	0.82 (0.18)b	0.74 (0.15)a							**<.01**
	Towards Left	-0.80 (0.17)b	-0.73 (0.16)a							**<.01**
Gait Symmetry (G)		Symmetric	Asymmetric							
	Towards Right	0.71 (0.15)b	0.84 (0.16)a							**<.01**
	Towards Left	-0.70 (0.16)b	-0.83 (0.15)a							**<.01**
D × H		7.5BW		15BW						
		One	Two	One	Two					
	Towards Right	0.83 (0.16)	0.77 (0.14)	0.81 (0.20)	0.71 (0.15)					.27
	Towards Left	-0.80 (0.16)	-0.74 (0.15)	-0.80 (0.17)	-0.73 (0.17)					.64
D × G		7.5BW		15BW						
		Symmetric	Asymmetric	Symmetric	Asymmetric					
	Towards Right	0.74 (0.14)	0.85 (0.15)	0.69 (0.16)	0.83 (0.18)					.20
	Towards Left	-0.72 (0.15)	-0.82 (0.15)	-0.68 (0.16)	-0.84 (0.16)					.19
H × G		One		Two						
		Symmetric	Asymmetric	Symmetric	Asymmetric					
	Towards Right	0.74 (0.15)	0.90 (0.15)	0.69 (0.13)	0.79 (0.13)					.18
	Towards Left	-0.73 (0.14)	-0.87 (0.14)	-0.68 (0.13)	-0.79 (0.13)					.53
D × H × G		7.5BW				15BW				
		One		Two		One		Two		
		Symmetric	Asymmetric	Symmetric	Asymmetric	Symmetric	Asymmetric	Symmetric	Asymmetric	
	Towards Right	0.78 (0.14)	0.88 (0.15)	0.71 (0.14)	0.82 (0.13)	0.70 (0.16)	0.91 (0.19)	0.67 (0.16)	0.76 (0.13)	.30
	Towards Left	-0.74 (0.14)	-0.86 (0.17)	-0.71 (0.17)	-0.78 (0.13)	-0.72 (0.14)	-0.87 (0.18)	-0.65 (0.18)	-0.80 (0.14)	.61

Bilateral Muscle Group Forces During One Hand Asymmetric Carries

To avoid conflicting and confounding factors when referencing one hand carries, muscle group forces (normalized to body weight) were combined bilaterally for qualitative (Fig. 6.3.2) and Test (a) comparisons (Table 6.3.3). However, to better support our Test (b) conclusions additional analyses of peak and average trunk muscle group forces partitioned ipsi- and contralateral to the one hand carry load location were performed post-hoc for asymmetric gait induced by the walking boot on the right leg. Each bilateral muscle group metric was compared ($\alpha = .05$) with a two-way ANOVA and Tukey post-hoc testing when appropriate.

Peak and average bilateral muscle group forces and statistical results are shown in Table 6.SM.4. As expected, the larger 15BW dumbbell load resulted in larger muscle group forces (p-values all $\leq .03$), with the lone exception of peak force in the ipsilateral extension locomotor muscle group ($p = .96$). Muscle group forces were the same whether the dumbbell was in the left or right hand, with the exception of the stabilizer muscle group which displayed significantly larger contralateral (i.e. right) side peak ($p = .05$) and average ($p < .01$) forces when the load was carried in the left hand. Dumbbell load × hand location interaction effects were present for the extension locomotor and flexion locomotor muscle groups. For both muscle groups, peak and average contralateral (but not ipsilateral) forces were larger in the 15BW carries than in the 7.5BW carries (p-values all $\leq .02$). In the 15BW condition, average contralateral (right side) force magnitudes were larger during left hand carries for the extension locomotor group (average force) and flexion locomotor group (peak force), compared to contralateral forces in right hand carries.

Table 6.SM.4. Peak and average bilateral muscle group force effects during asymmetric gait for unilateral carry locations in the left or right hand. Forces were normalized and expressed as a percentage of bodyweight partitioned relative to the hand holding (ipsilateral) and not holding (contralateral) the dumbbell. Asymmetry was induced with a walking boot worn on the right lower limb. Letters denote post-hoc pairings from significant differences (*in bold; p* < .05) for main effects of dumbbell load and location, and for the dumbbell load × location interaction. Abbreviations: dumbbells of 7.5% (7.5BW) or 15% (15BW) bodyweight.

Source		Metrics		Main & Interaction Effects				*p*-value
Dumbbell (D)				7.5BW	15BW			
	Stabilizers	Ipsilateral	Peak	89.0 (20.6)a	102.1 (23.7)b			**<.01**
			Average	59.2 (11.6)a	71.5 (15.8)b			**<.01**
		Contralateral	Peak	96.2 (17.9)a	108.6 (24.6)b			**<.01**
			Average	67.7 (11.5)a	82.0 (17.3)b			**<.01**
	Extension Locomotors	Ipsilateral	Peak	86.2 (21.7)	86.6 (18.0)			.96
			Average	52.8 (7.4)a	57.4 (10.2)b			**.03**
		Contralateral	Peak	157.8 (33.7)a	202.4 (52.1)b			**<.01**
			Average	97.2 (17.3)a	144.2 (36.1)b			**<.01**
	Flexion Locomotors	Ipsilateral	Peak	59.3 (14.8)a	68.9 (22.5)b			**.01**
			Average	37.3 (8.7)a	44.9 (15.0)b			**<.01**
		Contralateral	Peak	66.1 (14.2)a	90.8 (24.5)b			**<.01**
			Average	44.6 (9.3)a	63.9 (16.0)b			**<.01**
Location (L)				Left	Right			
	Stabilizers	Ipsilateral	Peak	94.6 (26.3)	96.5 (19.5)			.61
			Average	64.4 (16.9)	66.3 (13.2)			.42
		Contralateral	Peak	106.8 (23.7)b	97.9 (20.1)a			**.05**
			Average	77.3 (17.4)b	72.3 (14.9)a			**<.01**
	Extension Locomotors	Ipsilateral	Peak	87.6 (19.7)	85.2 (20.1)			.72
			Average	54.6 (8.8)	55.6 (9.5)			.75
		Contralateral	Peak	182.2 (54.6)	178.0 (43.6)			.63
			Average	128.1 (42.0)	113.3 (29.5)			.07
	Flexion Locomotors	Ipsilateral	Peak	65.7 (20.7)	62.5 (18.5)			.49
			Average	42.3 (13.6)	39.9 (12.0)			.48
		Contralateral	Peak	82.4 (26.4)	74.5 (19.7)			.16
			Average	55.2 (17.4)	53.3 (15.3)			.52
D × L				7.5BW		15BW		
				Left	Right	Left	Right	
	Stabilizers	Ipsilateral	Peak	85.1 (21.2)	92.8 (20.1)	104.1 (28.4)	100.1 (18.9)	.09
			Average	56.7 (10.8)	61.8 (12.2)	72.1 (18.8)	70.9 (13.1)	.12
		Contralateral	Peak	99.9 (19.9)	92.4 (15.5)	113.7 (26.0)	103.5 (23.2)	.51
			Average	68.9 (10.6)	66.5 (12.7)	85.8 (19.1)	78.2 (15.1)	.09
	Extension Locomotors	Ipsilateral	Peak	84.4 (20.2)	88.0 (23.9)	90.9 (19.6)	82.3 (16.0)	.12
			Average	50.7 (5.3)	54.8 (8.8)	58.5 (10.1)	56.4 (10.6)	.08
		Contralateral	Peak	152.3 (29.6)a	163.3 (37.9)a	212.1 (58.3)b	192.7 (45.6)b	**<.01**
			Average	100.8 (20.2)a	93.6 (13.7)a	155.4 (40.8)c	132.9 (28.0)b	**.02**
	Flexion Locomotors	Ipsilateral	Peak	59.7 (16.7)	58.8 (13.4)	71.6 (23.2)	66.1 (22.5)	.29
			Average	37.4 (9.6)	37.2 (8.0)	47.1 (15.6)	42.7 (14.8)	.12
		Contralateral	Peak	66.3 (15.8)a	65.8 (13.0)a	98.5 (25.4)c	83.2 (21.9)b	**<.01**
			Average	43.9 (8.3)a	45.4 (10.5)a	66.6 (16.8)b	61.2 (15.5)b	**.02**

CHAPTER 7

CONCLUSION

Our bodies are built for and thrive on locomotion. For centuries doctors have touted the benefits of walking with some claiming it as a near perfect exercise, a potential remedy of minor discomforts, and a means of maintaining our psychological well-being (Nutter, 1988). Unfortunately, not everyone may be able to capitalize on the benefits of walking. Individuals exhibiting gait asymmetry, such as differences between left and right step lengths and stance times, have a greater prevalence of lower back pain (LBP) than reported in the general population (Ehde et al., 2001; Giles and Taylor, 1981; Ready et al., 2018; Smith et al., 1999; Wolfe et al., 1996). Gait asymmetries are common in people with lower limb amputation, leg length discrepancy, leg mass differences, or lower limb joint disfunction (Cappozzo and Gazzani, 1982; Constantinou et al., 2014; Dananberg, 1993; Devan et al., 2014; DeVita et al., 1991; Dingwell et al., 1996; Friberg, 1983; Gulgin et al., 2018; Mündermann et al., 2005; Tanaka et al., 2015; Wolfe et al., 1996). Due to several compounding characteristics associated with gait asymmetry, it is difficult to control for and isolate specific LBP risk-factors experimentally (Chow et al., 2006; Hafner et al., 2002; Hendershot et al., 2018; Highsmith et al., 2019; Nolan et al., 2003; Selles et al., 1999; van der Linden et al., 1999; Wasser et al., 2019; Windrich et al., 2016; Yu et al., 2014). Identifying modifiable risk-factors and hazardous tasks is of importance to clinicians treating LBP in those with gait asymmetries. Therefore, this dissertation aimed to examine how specific artificially induced lower limb imbalances common to gait asymmetry can impact lower back demands during normal gait (Study 2) and how the presence of a lower limb gait asymmetry can impact lower back demands while carrying a load (Study 3). To accomplish this, an experimental paradigm was developed which safely induced lower limb gait asymmetries in healthy able-bodied participants.

LBP risk was quantified by comparing kinematic and kinetic task demands from a musculoskeletal computer model of the lower back specifically evaluated (Study 1) for use in walking and carrying tasks.

Study 1 evaluated the efficacy of an *in silico* model of the lower back to estimate demands during gait tasks, as *in viv*o measurements of these kinetics are highly invasive (Dreischarf et al., 2016). A recent OpenSim (Delp et al., 2007) musculoskeletal model by Beaucage-Gauvreau et al. (2019) used recorded kinematic and kinetic information to estimate lower back forces. This model was modified for the current study to include participant-specific trunk muscular strength and activity (i.e. recorded EMG). Muscular strength scaling was estimated for each participant from maximal voluntary contractions against a dynamometer, while recorded muscular activity levels were incorporated into an EMG optimization (EMGopt) approach used to resolve redundant muscle forces (Cholewicki et al., 1995). Kinematic, external kinetic, and EMG data were recorded from six participants (n=6) as they performed a variety of walking and carrying tasks on a motorized treadmill. To evaluate the lower back demands estimated from the musculoskeletal model, lumbar vertebral joint force comparisons were made with estimates from a generic static optimization approach (SOpt; Crownshield and Brand, 1981), previous *in vivo* and *in silico* reports (Callaghan et al., 1999; McGill et al., 2013; Rohlmann et al., 2014a, 2014c, 2008; Rose et al., 2013; Wilke et al., 1999), and predicted versus recorded muscular activities. Further, the sensitivity of the model to day-to-day EMG variability and the use of participant-specific muscular strength were evaluated. Results showed that when applying either the EMGopt or SOpt approach, the model predicted vertebral joint force patterns qualitatively similar to those previously reported. Compared to SOpt, the EMGopt approach estimated larger joint loads ($p < .01$) and model muscle activations more closely matched individual participant EMG patterns (quantified by lower

RMSEs and larger cross-correlation *r*-values). L5/S1 vertebral joint forces from EMGopt were sensitive to the inherent variability in recorded EMG for 57 out of 108 statistical tests, but the magnitude of these differences (±4%) did not impact between-condition comparisons. Participant-specific muscular strength scaling arrived at an optimal solution with fewer gain adjustments (lower total g_i) to the recorded EMG activity but did not lead to significantly different joint loads (*p*-values > .07). Therefore, the musculoskeletal model and EMGopt approach was well-suited for evaluating the lower back joint demands of walking and carrying tasks.

Study 2 sought to assess how a variety of experimentally induced asymmetric gait causalities can impact lower back demands relative to unperturbed symmetric gait. In this repeated-measures study design, gait asymmetries were induced temporarily in healthy able-bodied participants (n=12) by unilaterally increasing the right leg length with a 2.54 cm shoe leveler, increasing leg mass with a ~1 kg ankle weight, increasing leg length and mass in combination, and restricting ankle joint motion and increasing leg mass with a clinical walking boot. Results from this study confirmed the hypothesis that the four perturbations caused participants to walk more asymmetrically, with generally longer stance times on the unperturbed limb, longer step lengths with the perturbed limb (*p*-values < .01), and with altered trunk kinematics (*p*-values $\leq$ .01 for several kinematic variables). Similar spatiotemporal asymmetries are often characteristic of patients with clinical gait asymmetries or participants exposed to equivalent perturbations (Gulgin et al., 2018; Hendershot and Wolf, 2014; Sagawa et al., 2011; Skinner and Barrack, 1990; Smith and Martin, 2007). However, unlike previous biomechanical studies in transfemoral amputees (Hendershot et al., 2018; Shojaei et al., 2016), these changes did not result in L5/S1 vertebral joint compressive or shear forces that were statistically different (*p*-values > .09) from a symmetrical (unperturbed) control condition. These null findings indicate

that the high incidence of LBP often associated with equivalent clinical gait asymmetry (Ehde et al., 2001; Giles and Taylor, 1981; Ready et al., 2018; Smith et al., 1999; Wolfe et al., 1996) may not be a direct effect of increased level gait lower back demands. Alternatively, LBP in this population could either be the result of chronic or secondary conditions which compound lower back forces, subtle insignificant increases in lower back forces during straight and level walking, other daily activities (Devan et al., 2015) such as load carriage tasks (Study 3), sit-to-stand transitions (Actis et al., 2018b; Shojaei et al., 2019), gait on uneven terrain or non-linear paths, ascending or descending stairs (Acasio et al., 2019; Bae et al., 2007), or a complex interaction of multiple contributing factors (Farrokhi et al., 2017).

Carrying tasks are a part of everyday life for both able-bodied individuals and those with clinical gait asymmetries (Devan et al., 2015). While carrying tasks and gait asymmetries have each independently been associated with LBP (Ehde et al., 2001; Kelsey et al., 1984), surprisingly the combination of these two factors on lower back demands has not been investigated. Study 3 addressed this research gap by employing the Study 1 musculoskeletal model and the Study 2 experimental protocol to induce gait asymmetries with a clinical walking boot in healthy able-bodied participants (n=12) while carrying dumbbells weighing 7.5% and 15% of bodyweight in one or two hands. The lower back forces from asymmetric and symmetric gait load carriage were compared. Study 3 also investigated if one-handed carry locations (relative to the walking boot) resulted in different L5/S1 vertebral joint forces. The latter test indicated that 15% bodyweight dumbbell loads carried in the hand contralateral to the walking boot resulted in larger L5/S1 vertebral joint shear and compression forces than when carried on the same side as the walking boot ($p < .05$ for peak and average forces). Similar increases in lower back force variables were seen when carrying with the walking boot, such as higher average L5/S1 joint compression

compared to symmetrical gait (p = .03). Overall, peak compression (1291 – 3551 N) and shear (181 – 604 N) forces during all carrying tasks were safely below spinal unit tissue injury tolerances (Gallagher and Marras, 2012; Jäger and Luttmann, 1989). However, the compounding effect of carrying across numerous gait cycles in nonneutral postures may contribute to tissue injury and LBP for those with gait asymmetries. These findings support the development of specific carrying task guidelines for clinical and acute cases of gait asymmetry.

These results are the first to reveal how isolated sources of gait asymmetry may not be as detrimental to lower back demands as previous findings based on amputees may suggest. Furthermore, this work highlights the importance of examining and developing recommendations for those with clinical gait asymmetries for activities of daily living (e.g. carrying tasks) outside of level straight-line walking. Future research should emulate Study 1 and follow the recommendations of others to properly evaluate biomechanical models prior to applying them to specific tasks (Hicks et al., 2015). Where possible, models should incorporate participant-specific information. In terms of studying gait asymmetries and lower back demands, it would be useful to compare additional lower limb artificial perturbations (e.g. restricting the knee or numbing a limb), daily activities, the potential effects of fatigue, internal force distributions, additional biomechanical parameters, and perturbation magnitudes to better understand how asymmetry may be detrimental to the lower back. A more robust comparison of different loads, alternative carrying locations and lower limb perturbations, and the effect of fatigue on carrying tasks could help establish guidelines and inform clinical practices. Continuing to build upon this line of biomechanical research can help address the alarmingly high incidence of LBP in those with gait asymmetry and provide guidance to improve their quality of life.

APPENDICES

A. Study 1: Participant Number Rationale

The proposed model will be used to estimate lower back demands across various gaits. It will be applied to both genders and will need to adapt to between-between subject variance in trunk muscle strength and anthropometry. Because the qualitative and exploratory methodology of evaluating a musculoskeletal model and optimization approach do not lend themselves to more traditional a priori estimates of sample size (e.g. see Appendix B), the number of participants will be based upon experimenter judgment and the enrollment of previous equivalent studies (Table A.1.).

I propose using six (n=6; male=3) participants to evaluate the model. This number is based on the average number used (6.88 participants) in previous musculoskeletal model evaluations while encompassing a more heterogenous population and an equal number from both genders.

Table A.1. Comparison of previous lumbar model evaluation studies. Evaluation type reflects whether the model was compared to their own (direct) or previous (indirect) experimental results. Abbreviations: EMG optimization (EMGopt), female (F), male (M), manual materials handling (MMH), Optimization (Opt), transtibial amputee (TTA).

Study	Base Model	Optimization	Model Application	Evaluation Type	Number of Participants
Actis et al. (2018a)	Christophy et al. (2012)	Opt	Sit-to-Stand	Direct & Indirect	15 (M;F;TTA=5)
Beaucage-Gauvreau et al. (2019)	Christophy et al. (2012)	Opt	MMH	Direct & Indirect	3 (M = 3)
Bruno et al. (2015)	Christophy et al. (2012)	Opt	General	Direct & Indirect	simulation
Cholewicki et al. (1995)	McGill & Norman (1986)	EMG-driven, EMGopt, & Opt	General	Direct	4 (M = 4)
de Zee et al. (2007)		Opt	General	Indirect	simulation
Gagnon et al. (2001)		EMG-driven, EMGopt, & Opt	MMH	Direct	11 (M = 11)
Granata and Marras (1995a)		EMG-driven	MMH	Direct	10 (M = 10)
Han et al. (2012)	de Zee et al. (2007)	Opt	General	Indirect	simulation
Raabe & Chaudhari (2016)	Christophy et al. (2012)	Opt	Jogging	Direct & Indirect	1 (M = 1)
Senteler et al. (2016)	Christophy et al. (2012)	Opt	General	Indirect	simulation
Zetterberg et al., (1987)	Schultz & Andersson (1981)	Opt	MMH	Direct	10 (M = 10)
Gagnon et al. (2011)	Gagnon et al. (2001)	EMGopt	MMH	Direct	1 (M=1)

B. Studies 2 and 3: Participant Number Rationale

Sample size estimates for Studies 2 and 3 were estimated in MATLAB from equivalent studies examining within-subjects' differences in trunk demands while walking at different cadences, with a walking boot, and while uni-laterally carrying a load (Table B.1.). Cohen-d effect sizes for paired t-tests were calculated as the ratio of the mean and standard deviation of differences. Sample size estimations were calculated with the *samplesizepwr* function using a power of 0.8 and significance (α) of 0.05. The average sample sized based on these estimates was 8.25 participants. However, to better ensure statistical significance and publication, it was decided to exceed that estimated number. 12 participants will be used for Studies 2 & 3.

Table B.1. Effect and sample size estimations from previous gait and load carriage studies.

Study	Dependent Variable	Condition	Effect Size	Sample Size Estimation
Callaghan et al. (1999)	Max L4/L5 Compression	Fast vs. Slow Cadence	0.926	12
Gulgin et al. (2018)	Peak Trunk Lateral Flexion	Shod vs. Boot with unshod	1.942	5
McGill et al. (2013)	Average L4/L5 Compression	5 kg bi-lateral vs. 10 kg uni-lateral carry	1.045	10
Rose et al. (2013)	Max L2/L3 A/P Shear	Normal walking vs. 11.3 kg uni-lateral briefcase	1.607	6

C. Musculoskeletal Model

The proposed OpenSim (Delp et al., 2007) musculoskeletal models *m29DoF* and *m47DoF* are based on a recently developed full-body lifting model (Beaucage-Gauvreau et al., 2019) but modified for improved usability, simplicity, and anatomical consistency. First, the model was updated to be compatible with OpenSim 4.0, allowing for improved usability. The model wrist joints were welded in a neutral posture, and the patellae segments and associated joints removed (Fig. C.1). These modeling details minimally contribute to lower back demands and were altered to simplify the model and the required marker set. Cylindrical "dumbbells' and a "lower limb mass" of adjustable inertial properties were welded to the hands and right lower shank for simulations of carrying tasks and certain gait asymmetries tasks (i.e. ankle weight and walking boot), respectively. Generic Hill-type (Hill, 1938; Thelen, 2003; Zajac, 1989) model parameters (e.g. shape factors for the active and passive force-lengths and force-velocity) and external oblique and rectus abdominis musculotendon actuator (MTA) attachment points were corrected to better represent those in the literature (Table C.1; Stokes and Gardner-Morse, 1999; Thelen, 2003). All MTA physiological cross section areas (PCSA) were adjusted to match a more homogeneous data set (Bruno et al., 2015). To determine initial MTA maximal isometric forces, maximal muscular stresses (MMS) were set to 100 N/cm^2 prior to adjusting to participant-specific strengths. MTA optimal fiber and tendon slack lengths were calculated based on a simulated neutral standing posture (Table C.1; Bruno et al., 2015). In *m29DoF* the eighteen coordinate coupler constraints (CCC) of the lower back and abdominals were adjusted to represent the *in vivo* contributions of the thoracic vertebrae to trunk kinematics and abdomen movement relative to the L5/S1 (Table C.2; Bruno et al., 2015). Finally, to more accurately determine MTA moment arms, model *m47DoF* was constructed without any of the eighteen CCC (Fig. C.2; Banks et al., 2019).

The proposed m47DoF model used electromyography optimization (EMGopt; Cholewicki and McGill, 1994) to balance the MTA forces responsible for the observed movement. In brief, EMGopt uses measured electromyography (EMG) activity to estimate muscle activation. This muscle activation is input to a Hill-type MTA model (see section 2.2.4 of the Literature Review) to estimate the force and, in conjunction with their respective moment arms, contribution to joint moments for each MTA. Unfortunately, the computed moments from the sum of the EMG-derived MTA force estimates rarely match those calculated from inverse dynamics (Cholewicki et al., 1995; van Dieën and Visser, 1999). Therefore, in EMGopt the MTA forces are then optimized to match the more reliable net joint moments from inverse dynamics (Chapter 3; Cholewicki and McGill, 1994; Gagnon et al., 2011).

For this dissertation, 12 (6 bi-lateral) EMG electrodes will be used to monitor and assign the activations of the 238 (119 bi-lateral) MTA encompassing 8 muscle groups. The allocation and placement of the EMG electrodes is based on previous literature investigations and is outlined in Table C.1 (Gagnon et al., 2011; McGill et al., 1996; Stokes et al, 1999).

The model's reference and most proximal segment is the pelvis. Therefore, when calculating the lower back kinetic demands with the *inverse dynamics* tool in OpenSim, a top-down approach is utilized. With this approach, the segmental analysis starts at the head/hands and works from distal to proximal down the kinetic chain towards the pelvis. A more traditional bottom-up approach (Hendershot and Wolf, 2014; Kingma et al., 1996) starting from the feet and working up can only be employed if the body set referenced to the ground were switched to the thorax. The top-down solution will be initially applied in the current model due to the potential for inaccuracies in the ground reaction force (GRF) resulting from the moving treadmill belt. It is hypothesized that these inaccuracies would negate any potential errors in the assumption of trunk

rigidity, however the impact of using either the top-down or bottom-up approach will be explored while evaluating the model in Study 1. Ideally, the *reduced residual analysis* (RRA) tool within OpenSim would be applied to minimize the differences between the top-down and bottom-up (Chapter 2.2.6; Delp et al., 2007), but this feature is unavailable due to an inability to segregate the GRF between the lower limbs.

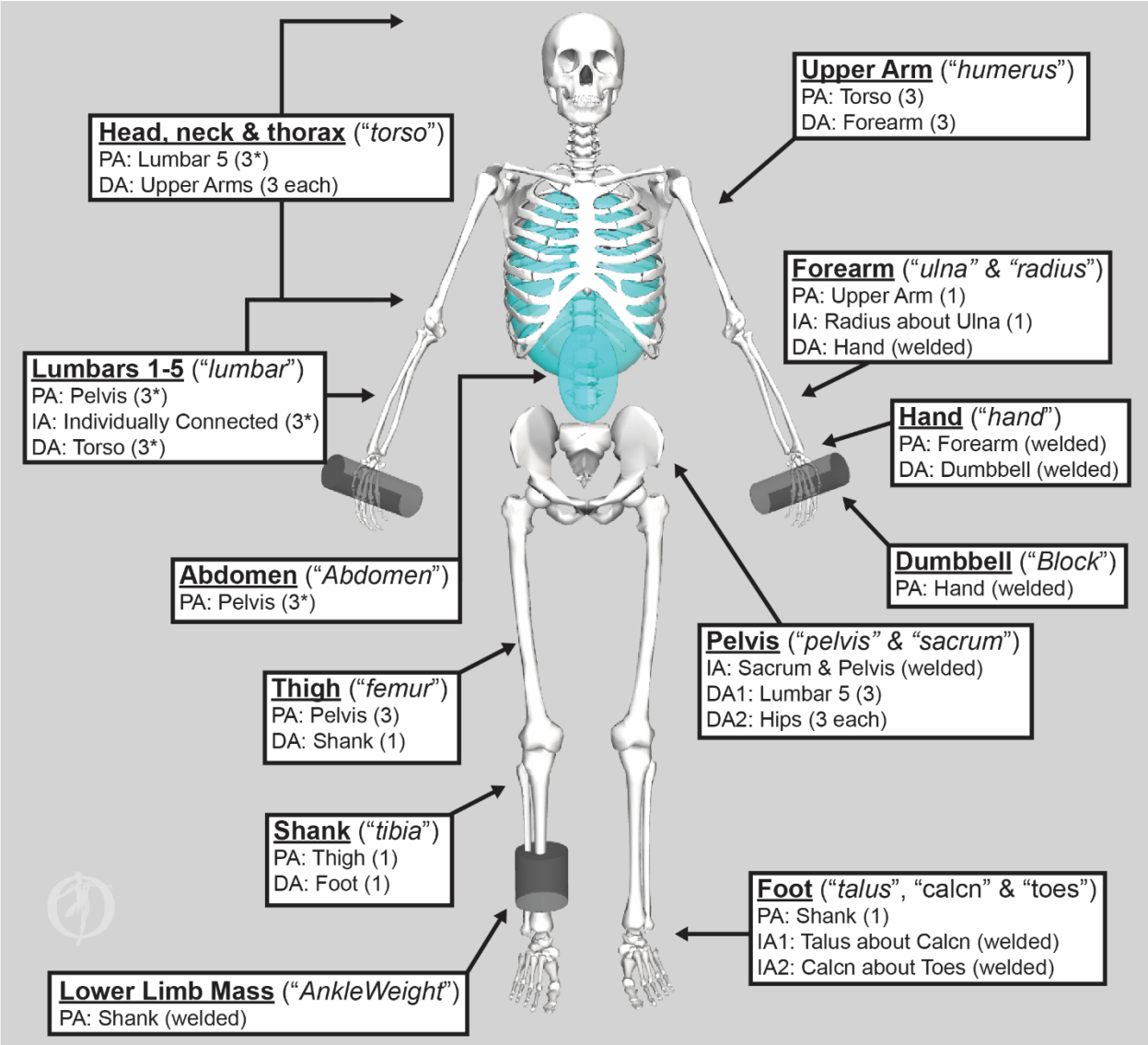

Figure C.1. Full-body musculoskeletal model. The model's twenty-seven segments (not including dumbbells and the added lower limb mass) were characterized by their .osim body set identification (in quotes), degrees of freedom (DoF; in parenthesis), proximal (PA), distal (DA), and internal (IA) attachments for the full-body OpenSim musculoskeletal model. To improve visualization, the model is depicted without musculotendon actuators (MTA). *denotes DoF apply only if the coordinate coupler constraint (CCC) is present.

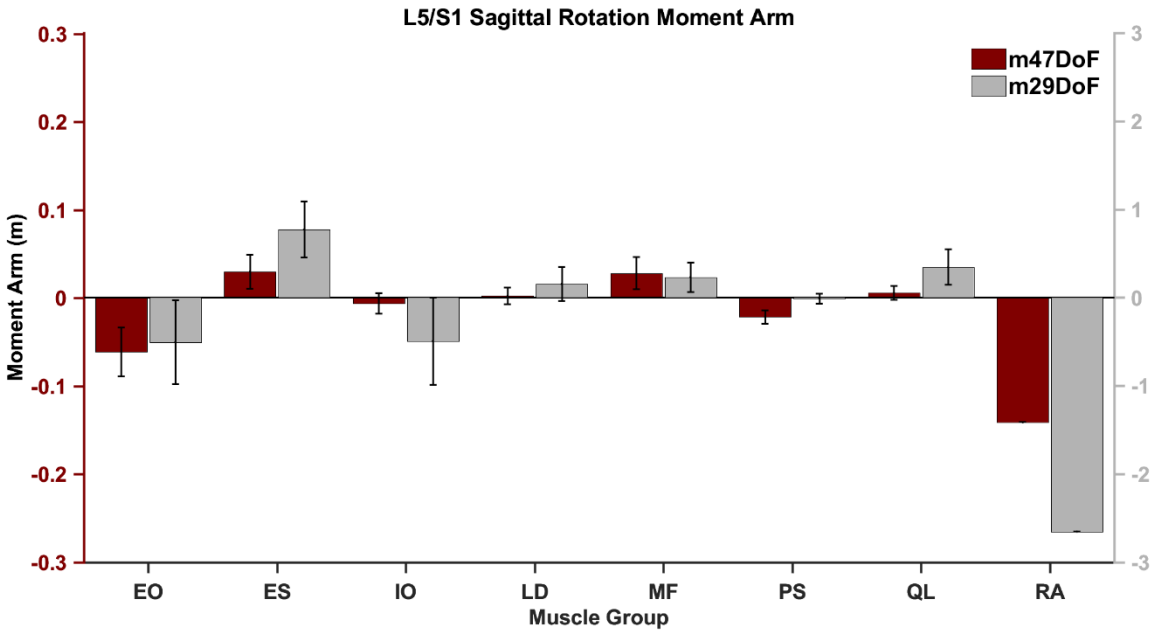

Figure C.2. Average muscle group sagittal plane moment arms about the L5/S1 joint for the *m29DoF* and *m47DoF* models during a neutral standing posture. Positive moment arms denote the potential to generate an internal extension moment. Data whiskers indicate ±1 standard deviation. Note the left (pertaining to the *m47DoF* model and the *maroon bars*) versus right (pertaining to the *m29DoF* model and the *grey bars*) ordinate scaling differences and the unnatural magnitude for the m29DoF model. Abbreviations: external obliques (EO), erector spinae (ES), internal obliques (IO), latissimus dorsi (LD), multifidus (MF), quadratus lumborum (QL), and rectus abdominis (RA).

Table C.1. Individual musculotendon actuator characteristics. Musculotendon actuators (MTAs) were characterized by a muscle grouping, "*.osim*" force set name, default maximal isometric force (F_{max}), optimal fiber length (OFL), tendon slack length (T_{sl}), pennation angle, electromyography (EMG) electrode assigned for EMG optimization (EMGopt), and EMGopt lower optimization limit. Default F_{max} values are based on physiological cross-sectional areas and an assumed maximal muscle stress of 100N/cm^2 (Bruno et al., 2015). OFL and T_{sl} were calculated from the model in a neutral standing posture (Bruno et al., 2015). Pennation angles were taken from Christophy et al. (2012). Assignment of EMG electrodes and lower "*g*" limits were based on previous studies (Cholewicki and McGill, 1994; Gagnon et al., 2011; McGill et al., 1996; Stokes and Gardner-Morse, 1999). Generic parameters for all MTAs include maximum tendon strain (0.033), active force-length (FL) factor (0.45), passive FL shape factor (5.0), force-velocity shape factor (0.25), maximum normalized lengthening force (1.8 of F_{max}), and activation (0.01 seconds) and a deactivation (0.04 seconds) time constants (Millard et al., 2013; Thelen, 2003; Zajac, 1989). All 119 MTA are modeled bilaterally (total 238). Abbreviations: external obliques (EO), iliocostalis lumborum pars thoracis (IL), internal obliques (IO), latissimus dorsi (LD), longissimus thoracis pars thoracis (LT), and rectus abdominis (RA).

Muscle Group	Force Set	F_{max} (N)	OFL (m)	T_{sl} (m)	Pennation Angle (rad)	EMG Electrode Site	EMGopt "*g*" Lower Limit
EO	*EO1*	81.0	0.1108	0.0123	0.0000	EO	0.50
	EO2	159.0	0.1562	0.0174	0.0000		
	EO3	215.0	0.1813	0.0201	0.0000		
	EO4	246.0	0.2136	0.0237	0.0000		

	EO5	175.0	0.0905	0.0101	0.0000		
	EO6	175.0	0.0673	0.0075	0.0000		
Erector Spinae	*IL_L1*	147.0	0.0533	0.1209	0.2409	IL	0.50
	IL_L2	183.0	0.0377	0.0856	0.2409		
	IL_L3	217.0	0.0261	0.0591	0.2409		
	IL_L4	415.0	0.0185	0.0420	0.2409		
	IL_R5	57.0	0.1672	0.2341	0.2409		
	IL_R6	73.0	0.1632	0.1971	0.2409		
	IL_R7	88.0	0.1608	0.1689	0.2409		
	IL_R8	78.0	0.1451	0.1466	0.2409		
	IL_R9	96.0	0.1608	0.0947	0.2409		
	IL_R10	192.0	0.1327	0.0781	0.2409		
	IL_R11	235.0	0.1152	0.0576	0.2409		
	IL_R12	206.0	0.0853	0.0427	0.2409		
	LTpT_T1	326.0	0.1080	0.2557	0.2199	LT	
	LTpT_T2	241.0	0.1107	0.2662	0.2199		
	LTpT_T3	173.0	0.1121	0.2697	0.2199		
	LTpT_T4	61.0	0.1093	0.2629	0.2199		
	LTpT_T5	57.0	0.1035	0.2489	0.2199		
	LTpT_T6	81.0	0.1059	0.2420	0.2199		
	LTpT_T7	80.0	0.1221	0.2309	0.2199		
	LTpT_T8	120.0	0.1314	0.2076	0.2199		
	LTpT_T9	139.0	0.1287	0.2181	0.2199		
	LTpT_T10	121.0	0.1169	0.1981	0.2199		
	LTpT_T11	115.0	0.1006	0.1704	0.2199		
	LTpT_T12	94.0	0.0803	0.1361	0.2199		
	LTpT_R4	60.0	0.1416	0.2399	0.2199		
	LTpT_R5	57.0	0.1322	0.2241	0.2199		
	LTpT_R6	81.0	0.1387	0.2125	0.2199		
	LTpT_R7	80.0	0.1350	0.2257	0.2199		
	LTpT_R8	130.0	0.1106	0.2255	0.2199		
	LTpT_R9	111.0	0.0946	0.2311	0.2199		
	LTpT_R10	120.0	0.1113	0.1913	0.2199		
	LTpT_R11	115.0	0.1081	0.1540	0.2199		
	LTpT_R12	94.0	0.0683	0.1328	0.2199		
	LTpL_L5	158.0	0.0263	0.0306	0.2199		
	LTpL_L4	152.0	0.0434	0.0478	0.2199		
	LTpL_L3	121.0	0.0588	0.0639	0.2199		
	LTpL_L2	108.0	0.0740	0.0798	0.2199		
	LTpL_L1	106.0	0.2083	0.0041	0.2199		
IO	*IO1*	196.0	0.0436	0.0662	0.0000	IO	0.50
	IO2	202.0	0.0433	0.0656	0.0000		
	IO3	192.0	0.0459	0.0695	0.0000		
	IO4	233.0	0.0746	0.0503	0.0000		
	IO5	204.0	0.0621	0.0418	0.0000		
	IO6	180.0	0.0590	0.0398	0.0000		
LD	*LD_L1*	90.0	0.3459	0.0755	0.0000	LD	0.50
	LD_L2	85.0	0.3695	0.0807	0.0000		
	LD_L3	105.0	0.3874	0.0846	0.0000		
	LD_L4	101.0	0.4022	0.0878	0.0000		
	LD_L5	102.0	0.4195	0.0861	0.0000		
	LD_T12	54.0	0.3295	0.0677	0.0000		
	LD_T11	63.0	0.3075	0.0631	0.0000		
	LD_T10	64.0	0.3025	0.0473	0.0000		

	LD_T9	41.0	0.2761	0.0432	0.0000		
	LD_T8	41.0	0.2500	0.0513	0.0000		
	LD_T7	37.0	0.2379	0.0489	0.0000		
	LD_R12	43.0	0.2720	0.0558	0.0000		
	LD_R11	63.0	0.2617	0.0537	0.0000		
	LD_Il	65.0	0.4673	0.0202	0.0000		
Multifidus	*MF_m1s*	81.0	0.0474	0.0197	0.0000	$\frac{(LT+IC)}{2}$	0.01
	MF_m1t_1	72.0	0.0762	0.0229	0.0000		
	MF_m1t_2	60.0	0.0953	0.0286	0.0000		
	MF_m1t_3	100.0	0.1099	0.0330	0.0000		
	MF_m2s	54.0	0.0443	0.0171	0.0000		
	MF_m2t_1	57.0	0.0653	0.0199	0.0000		
	MF_m2t_2	146.0	0.0872	0.0266	0.0000		
	MF_m2t_3	161.0	0.0970	0.0295	0.0000		
	MF_m3s	84.0	0.0403	0.0168	0.0000		
	MF_m3t_1	91.0	0.0974	0.0324	0.0000		
	MF_m3t_2	91.0	0.0809	0.0269	0.0000		
	MF_m3t_3	91.0	0.0809	0.0269	0.0000		
	MF_m4s	101.0	0.0375	0.0237	0.0000		
	MF_m4t_1	90.0	0.0538	0.0218	0.0000		
	MF_m4t_2	90.0	0.0692	0.0280	0.0000		
	MF_m4t_3	90.0	0.0807	0.0327	0.0000		
	MF_m5s	35.0	0.0161	0.0102	0.0000		
	MF_m5t_1	35.0	0.0760	0.0307	0.0000		
	MF_m5t_2	35.0	0.0568	0.0230	0.0000		
	MF_m5t_3	35.0	0.0407	0.0165	0.0000		
	MF_m1_laminar	39.0	0.0310	0.0118	0.0000		
	MF_m2_laminar	31.0	0.0267	0.0101	0.0000		
	MF_m3_laminar	36.0	0.0251	0.0095	0.0000		
	MF_m4_laminar	26.0	0.0283	0.0107	0.0000		
	MF_m5_laminar	56.0	0.0293	0.0111	0.0000		
Psoas Major	*Ps_L1_VB*	267.0	0.2049	0.0609	0.1868	$\frac{(EO+IO)}{2}$	0.01
	Ps_L1_TP	77.0	0.2018	0.0599	0.1868		
	Ps_L1_L2_IVD	147.0	0.1894	0.0562	0.1868		
	Ps_L2_TP	259.0	0.1793	0.0532	0.1868		
	Ps_L2_L3_IVD	151.0	0.1667	0.0495	0.1868		
	Ps_L3_TP	128.0	0.1582	0.0470	0.1868		
	Ps_L3_L4_IVD	45.0	0.1438	0.0427	0.1868		
	Ps_L4_TP	203.0	0.1374	0.0408	0.1868		
	Ps_L4_L5_IVD	85.0	0.1197	0.0355	0.1868		
	Ps_L5_TP	186.0	0.1195	0.0355	0.1868		
	Ps_L5_VB	233.0	0.1063	0.0316	0.1868		
Quadratus Lumborum	*QL_post_I_1_L3*	75.0	0.0396	0.0333	0.1292	IC	0.01
	QL_post_I_2_L4	156.0	0.0272	0.0229	0.1292		
	QL_post_I_2_L3	59.0	0.0400	0.0336	0.1292		
	QL_post_I_2_L2	37.0	0.0547	0.0460	0.1292		
	QL_post_I_3_L1	77.0	0.0704	0.0592	0.1292		
	QL_post_I_3_L2	56.0	0.0521	0.0437	0.1292		
	QL_post_I_3_L3	96.0	0.0371	0.0312	0.1292		
	QL_mid_L3_12_3	42.0	0.0557	0.0289	0.1292		
	QL_mid_L3_12_2	48.0	0.0591	0.0307	0.1292		
	QL_mid_L3_12_1	80.0	0.0643	0.0334	0.1292		
	QL_mid_L2_12_1	156.0	0.0418	0.0217	0.1292		
	QL_mid_L4_12_3	42.0	0.0741	0.0385	0.1292		

	QL_ant_I_2_T12	45.0	0.1121	0.0582	0.1292		
	QL_ant_I_3_T12	85.0	0.1073	0.0557	0.1292		
	QL_ant_I_2_12_1	28.0	0.1012	0.0526	0.1292		
	QL_ant_I_3_12_1	53.0	0.1022	0.0531	0.1292		
	QL_ant_I_3_12_2	35.0	0.0967	0.0502	0.1292		
	QL_ant_I_3_12_3	41.0	0.0906	0.0471	0.1292		
RA	*rect_abd*	662.0	0.3137	0.0853	0.0000	RA	0.50

Table C.2. Lumbar and abdomen coordinate coupler constraints applied to the *m29DoF* model. Coordinate coupler constraints (CCC) distribute the total trunk rotation between the vertebral joints. Numbers indicate orthogonal CCC coefficients expressed as a multiple of the L5/S1 angle. Coefficients are based off from Bruno et al. (2015). * Includes thoracic contributions from T3/T4 to T12/L1. The T3/T4 cutoff was estimated from the location of the superior markers of the trunk cluster. **Abdomen CCC were estimated as half the total lumbar rotation.

Joint Set	Axial	Lateral	Sagittal
T12/L1*	20.028	16.730	11.065
L1/L2	0.806	1.378	3.950
L2/L3	0.861	1.838	3.276
L3/L4	1.056	1.784	2.818
L4/L5	1.056	1.324	2.005
L5/S1	1.000	1.000	1.000
Abdomen**	2.389	3.662	6.525

D. Experimental Muscle Fatigue Test

Muscle fatigue can impact task and muscle performance (Enoka and Duchateau, 2008; Kamen and Caldwell, 1996). Various physiological and psychological fatigue effects lead to muscle fiber conduction velocity decreases and compensatory increases in motor-unit recruitment. These phenomena are apparent in surface electromyography (EMG) recordings and characterized by increasing amplitudes and decreasing median frequencies as fatigue worsens (Kallenberg et al., 2007; Kamen and Caldwell, 1996). To ensure that our primary experimental protocol did not cause overt fatigue levels which could complicate the interpretation of our results, we administered an objective test to determine if muscle fatigue had occurred.

Bilateral iliocostalis lumborum and longissimus thoracis muscle fatigue was assessed from surface EMG (see Study 1 for hardware specifics) recorded while participants performed a modified Biering-Sorensen (1984) test prior to (pre) and following (post) experimental conditions In the Biering-Sorensen test, participants were instructed to lie prone on the edge of the exam table with their lower limbs secured while maintaining their upper body in an unsupported horizontal position for 30 seconds (Fig. D.1). The recorded data were band-pass filtered (20 - 500 Hz) and full-wave rectified prior to analysis. Median frequencies were calculated from the filtered data for twenty-five 1-second windows extracted from the final 25 seconds of each test. Similarly, twenty-five average amplitudes levels were calculated from the rectified data. Slopes of median frequency and amplitude across the 25 seconds were determined with best fit lines for each of muscle. Paired t-tests ($\alpha < .05$) compared pre and post-test slopes across all participants to elucidate if muscle fatigue was evident in the experimental protocol.

Figure D.1. Horizontal position used for the 30-second fatigue test against body weight. The position was modeled from Biering-Sorensen's (1984) lower back muscular endurance test.

As expected, the EMG median frequency slope decreased, and EMG amplitude increased throughout the fatigue tests (Fig. D.2). However, neither muscle fatigue phenomena were different pre versus post-test (Fig. D.2; *p*-values for all muscles > .06), indicating that participants were not fatigued by the primary experimental protocol.

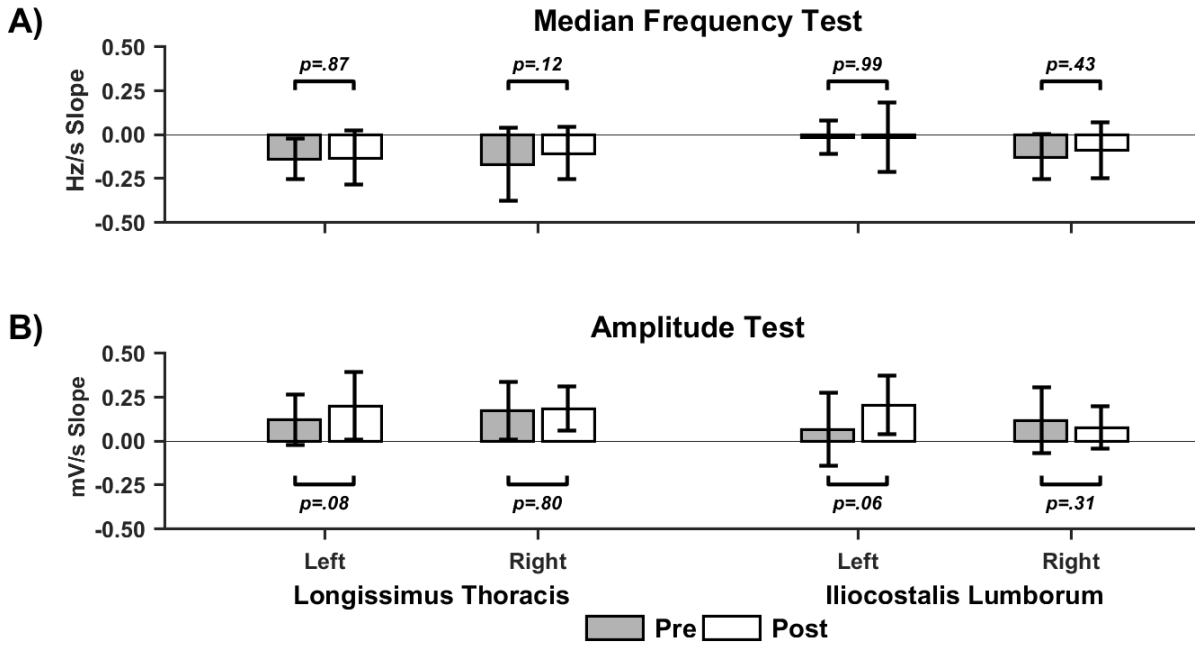

Figure D.2. Muscle fatigue test results. Figures depict comparisons between pre-test (*grey bars*) and post-test (*white bars*) muscle fatigue test average slope values for A) median frequency (Hz / s) and B) amplitude (mV/s). Data whiskers indicate ±1 standard deviation and *p*-values are the result from paired t-tests ($\alpha < .05$) of like pre and post-test measures.

BIBLIOGRAPHY

Acasio, J.C., Shojaei, I., Banerjee, R., Dearth, C.L., Bazrgari, B., Hendershot, B.D., 2019. Trunk-Pelvis motions and spinal loads during upslope and downslope walking among persons with transfemoral amputation. J. Biomech. 95, 109316.

Actis, J.A., Honegger, J.D., Gates, D.H., Petrella, A.J., Nolasco, L.A., Silverman, A.K., 2018a. Validation of lumbar spine loading from a musculoskeletal model including the lower limbs and lumbar spine. J. Biomech. 68, 107–114.

Actis, J.A., Nolasco, L.A., Gates, D.H., Silverman, A.K., 2018b. Lumbar loads and trunk kinematics in people with a transtibial amputation during sit-to-stand. J. Biomech. 69, 1–9.

Ada, L., Dean, C.M., Hall, J.M., Bampton, J., Crompton, S., 2003. A Treadmill and Overground Walking Program Improves Walking in Persons Residing in the Community After Stroke : Arch. Phys. Med. Rehabil. 84, 1486–1491.

Adams, M.A., 2004. The Biomechanics of Back Pain. Acupunct. Med. 22, 178–188.

Adams, M.A., Dolan, P., 2005. Spine biomechanics. J. Biomech. 38, 1972–1983.

Ahern, D.K., Follick, M.J., Council, J.R., Laser-Wolston, N., 1986. Reliability of Lumbar Paravertebral EMG Assessment in Chronic Low Back Pain. Arch. Phys. Med. Rehabil. 67, 762–765.

Alam, U., Riley, D.R., Jugdey, R.S., Azmi, S., Rajbhandari, S., D'Aout, K., Malik, R.A., 2017. Diabetic Neuropathy and Gait : A Review. Diabetes Ther. 8, 1253–1264.

Allegri, M., Montella, S., Salici, F., Valente, A., Marchesini, M., Compagnone, C., Baciarello, M., Manferdini, M.E., Fanelli, G., 2016. Mechanisms of low back pain: a guide for diagnosis and therapy. F1000Research 5, 1–11.

Alton, F., Baldey, L., Caplan, S., Morrissey, M.C., 1998. A kinematic comparison of overground and treadmill walking. Clin. Biomech. 13, 434–440.

An, D.-H., Yoon, J.-Y., Yoo, W.-G., Kim, K.-M., 2010. Comparisons of the gait parameters of young Korean women carrying a single-strap bag. Nurs. Heal. Sci. 12, 87–93.

Anders, C., Wagner, H., Puta, C., Grassme, R., Petrovitch, A., Scholle, H.-C., 2007. Trunk muscle activation patterns during walking at different speeds. J. Electromyogr. Kinesiol. 17, 245–252.

Anderson, A.E., Ellis, B.J., Weiss, J.A., 2007. Verification, Validation and Sensitivity Studies in Computational Biomechanics. Comput. Methods Biomech. Biomed. Engin. 10, 171–184.

Anderson, F.C., Pandy, M.G., 1999. A Dynamic Optimization Solution for Vertical Jumping in Three Dimensions. Comput. Methods Biomech. Biomed. Engin. 2, 201–231.

Andersson, G.B.J., 1999. Epidemiological features of chronic low-back pain. Lancet 354, 581–585.

Andersson, G.B.J., 1997. The Epidemiology of Spinal Disorders, in: Frymoyer, J. (Ed.), The Adult Spine: Principles and Practice. Lippincott-Raven, Philadelphia, pp. 93–141.

Angelini, L., Damm, P., Zander, T., Arshad, R., Di Puccio, F., Schmidt, H., 2018. Effect of arm swinging on lumbar spine and hip joint forces. J. Biomech. 70, 185–195.

Arjmand, N., Gagnon, D., Plamondon, A., Shirazi-Adl, A., Larivière, C., 2009. Comparison of trunk muscle forces and spinal loads estimated by two biomechanical models. Clin. Biomech. 24, 533–541.

Arjmand, N., Shirazi-Adl, A., 2006a. Role of intra-abdominal pressure in the unloading and stabilization of the human spine during static lifting tasks. Eur. Spine J. 15, 1265–1275.

Arjmand, N., Shirazi-Adl, A., 2006b. Sensitivity of kinematics-based model predictions to optimization criteria in static lifting tasks. Med. Eng. Phys. 28, 504–514.

Arjmand, N., Shirazi-Adl, A., 2006c. Model and in vivo studies on human trunk load partitioning and stability in isometric forward flexions. J. Biomech. 39, 510–521.

Arjmand, N., Shirazi-Adl, A., Bazrgari, B., 2006. Wrapping of trunk thoracic extensor muscles influences muscle forces and spinal loads in lifting tasks. Clin. Biomech. 21, 668–675.

Arnold, E.M., Ward, S.R., Lieber, R.L., Delp, S.L., 2010. A model of the lower limb for analysis of human movement. Ann. Biomed. Eng. 38, 269–279.

Arshad, R., Angelini, L., Zander, T., Di Puccio, F., El-Rich, M., Schmidt, H., 2018. Spinal loads and trunk muscles forces during level walking – A combined in vivo and in silico study on six subjects. J. Biomech. 70, 113–123.

Assogba, T.F., Boulet, S., Detrembleur, C., Mahaudens, P., 2018. The effects of real and artificial Leg Length Discrepancy on mechanical work and energy cost during the gait. Gait Posture 59, 147–151.

Axler, C.T., McGill, S.M., 1997. Low back loads over a variety of abdominal exercises: searching for the safest abdominal challenge. Med. Sci. Sport. Exerc. 29, 804–811.

Ayoub, M.M., El-Bassoussi, M.M., 1976. Dynamic Biomechanical Model for Sagittal Lifting Activities. Hum. Factors 20, 355–361.

Azari, F., Arjmand, N., Shirazi-Adl, A., Rahimi-Moghaddam, T., 2018. A combined passive and active musculoskeletal model study to estimate L4-L5 load sharing. J. Biomech. 70, 157–165.

Azizan, N.A., Basaruddin, K.S., Salleh, A.F., 2018. The Effects of Leg Length Discrepancy on Stability and Kinematics-Kinetics Deviations: A Systematic Review. Appl. Bionics Biomech. 2018, 1–22.

Badawy, M., Schall Jr., M.C., Sesek, R.F., Gallagher, S., Davis, G.A., Capanoglu, M.F., 2018. One-handed carrying among elderly and obese individuals : A systematic review to identify research gaps. Ergonomics Apr 30, 1–24.

Bae, T.S., Choi, K., Hong, D., Mun, M., 2007. Dynamic analysis of above-knee amputee gait. Clin. Biomech. 22, 557–566.

Baker, R., 2001. Pelvic angles: A mathematically rigorous definition which is consistent with a conventional clinical understanding of the terms. Gait Posture 13, 1–6.

Balague, F., Mannion, A.F., Pellise, F., Cedraschi, C., 2012. Non-specific low back pain. Lancet 379, 482–491.

Banks, J.J., Umberger, B.R., Caldwell, G.E., 2019. Development of an EMG Optimization Framework for use in a Complex OpenSim Lower Back Musculoskeletal Model, in: XII International Symposium on Computer Simulation in Biomechanics: July 28th - 30th. Alberta, Canada.

Bartelink, D.L., 1957. The Role of Abdominal Pressure in Relieving the Pressure on the Lumbar Intervertebral Discs. J. Bone Jt. Surg. 39B, 718–725.

Beal, M.C., 1977. The Short Leg Problem. J. Am. Osteopath. Assoc. 76, 745–751.

Bean, J.C., Chaffin, D.B., 1988. Biomechanical Model Calcuation of Muscle Contraction Forces: A Double Linear Programming Method. J. Biomech. 21, 59–66.

Beaucage-Gauvreau, E., Robertson, W.S.P., Brandon, S.C.E., Fraser, R., Freeman, B.J.C., Graham, R.B., Thewlis, D., Jones, C.F., 2019. Validation of an OpenSim full-body model with detailed lumbar spine for estimating lower lumbar spine loads during symmetric and asymmetric lifting tasks. Comput. Methods Biomech. Biomed. Engin. epub, 1–14.

Bergmann, G., Graichen, F., Rohlmann, A., Linke, H., 1997. Hip Joint Forces During Load Carrying. Clin. Orthop. Relat. Res. 335, 190–201.

Bergmark, A., 1989. Stability of the lumbar spine: A study in mechanical engineering. Acta Orthop. Scand. 60, 1–54.

Bernard, B.P., 1997. A Critical Review of Epidemiologic Evidence for Work-Related Musculoskeletal Disorders of the Neck, Upper Extremity, and Low Back, Musculoskeletal Disorders and Workplace Factors.

Biering-Sorensen, F., 1984. Physical Measurements as Risk Indicators for Low-Back Trouble Over a One-Year Period. Spine (Phila. Pa. 1976). 9, 106–119.

Bigos, S., Bowyer, O., Braen, G., et al., 1994. Acute low back problems in adults: Assessment and Treatment, AHCPR Clinical practice guideline, quick reference guide number 14. Rockville, MD.

Bobet, J., Norman, R.W., 1984. Effects of Load Placement on Back Muscle Activity in Load Carriage. Eur. J. Appl. Physiol. 53, 71–75.

Bogduk, N., 1983. The Innervation of the Lumbar Spine. Spine (Phila. Pa. 1976). 8, 286–293.

Bogduk, N., Macintosh, J.E., Pearcy, M.J., 1992a. A Universal Model of the Lumbar Back Muscles in the Upright Position. Spine (Phila. Pa. 1976). 17, 897–913.

Bogduk, N., Pearcy, M.J., Hadfield, G., 1992b. Anatomy and Biomechanics of Psoas Major. Clin. Biomech. 7, 109–119.

Boyer, K.A., Johnson, R.T., Banks, J.J., Jewell, C.M., Hafer, J.F., 2017. Systematic review and meta-analysis of gait mechanics in young and older adults. Exp. Gerontol. 95, 63–70.

Brand, R.A., Pedersen, D.R., Friederich, J.A., 1986. The Sensitivity of Muscle Force Predictions to Changes in Physiological Cross-Sectional Area. J. Biomech. 19, 589–596.

Braun, J., Baraliakos, X., Regel, A., Kiltz, U., 2014. Assessment of spinal pain. Best Pract. Res. Clin. Rheumatol. 28, 875–887.

Brereton, L.C., McGill, S.M., 1998. Frequency response of spine extensors during rapid isometric contractions: Effects of muscle length and tension. J. Electromyogr. Kinesiol. 8, 227–232.

Brinckmann, P., 1986. Injury of the Annulus Fibrosus and Disc Protrusions. Spine (Phila. Pa. 1976). 11, 149–153.

Brinckmann, P., Biggemann, M., Hilweg, D., 1988. Fatigue fracture of human lumbar vertebrae. Clin. Biomech. 3, S1–S23.

Brown, O.H., Barnett, C.T., Sale, C., 2018. Investigating the effects of joint restriction to simulate prosthetic gait on loading and movement asymmetries in able-bodied individuals, in: 8th World Congress of Biomechanics. Dublin, Ireland, p. P3604.

Brown, S.H.M., Potvin, J.R., 2005. Constraining spine stability levels in an optimization model leads to the prediction of trunk muscle cocontraction and improved spine compression force estimates. J. Biomech. 38, 745–754.

Bruno, A.G., Bouxsein, M.L., Anderson, D.E., 2015. Development and Validation of a Musculoskeletal Model of the Fully Articulated Thoracolumbar Spine and Rib Cage. J. Biomech. Eng. 137, 081003.

Bruno, A.G., Mokhtarzadeh, H., Allaire, B.T., Velie, K.R., De Paolis Kaluza, M.C., Anderson, D.E., Bouxsein, M.L., 2017. Incorporation of CT-based measurements of trunk anatomy into subject-specific musculoskeletal models of the spine influences vertebral loading predictions. J. Orthop. Res. 35, 2164–2173.

Buchanan, T.S., 1995. Evidence that maximum muscle stress is not a constant: differences in specific tension in elbow flexors and extensors. Med. Eng. Phys. 17, 529–536.

Buchbinder, R., Blyth, F.M., March, L.M., Brooks, P., Woolf, A.D., Hoy, D., 2013. Placing the global burden of low back pain in context. Best Pract. Res. Clin. Rheumatol. 27, 575–589.

Burkhart, K.A., Bruno, A.G., Bouxsein, M.L., Bean, J.F., Anderson, D.E., 2018. Estimating Apparent Maximum Muscle Stress of Trunk Extensor Muscles in Older Adults using Subject-Specific Musculoskeletal Models. J. Orthop. Res. 36, 498–505.

Butowicz, C.M., Acasio, J.C., Dearth, C.L., Hendershot, B.D., 2018. Trunk muscle activation patterns during walking among persons with lower limb loss: Influences of walking speed. J. Electromyogr. Kinesiol. 40, 48–55.

Butowicz, C.M., Silfies, S.P., Vendemia, J., Farrokhi, S., Hendershot, B.D., 2020. Characterizing and Understanding the Low Back Pain Experience Among Persons with Lower Limb Loss. Pain Med. 21, 1068–1077.

Caldwell, G.E., 2014. Muscle Modeling, in: Robertson, D.G.E., Caldwell, G.E., Hamill, J., Kamen, G., Whittlesey, S.N. (Eds.), Research Methods in Biomechanics. Human Kinetics, Champaign, IL, pp. 203–231.

Callaghan, J.P., McGill, S.M., 2001. Low back joint loading and kinematics during standing and unsupported sitting. Ergonomics 44, 280–294.

Callaghan, J.P., Patla, A.E., McGill, S.M., 1999. Low back three-dimensional joint forces, kinematics, and kinetics during walking. Clin. Biomech. 14, 203–216.

Cappozzo, A., 1984. Compressive Loads in the Lumbar Vertebral Column During Normal Level Walking. J. Orthop. Res. 1, 292–301.

Cappozzo, A., 1983. The Forces and Couples in the Human Trunk During Level Walking. J. Biomech. 16, 265–277.

Cappozzo, A., 1981. Forces and Couples in the Lumbar Vertebral Column During Level Walking at Different Speeds, in: Stokes, I.A.F. (Ed.), Mechanical Factors and the Skeleton. John Libbey, London, pp. 15–22.

Cappozzo, A., Figura, F., Gazzani, F., Marchetti, M., 1982. Angular Displacement in the Upper Body of AK Amputees During Level Walking. Prosthet. Orthot. Int. 6, 131–138.

Cappozzo, A., Gazzani, F., 1982. Spinal Loading During Abnormal Walking, in: Huiskes, R; van Campen, D; De Wijn, J. (Ed.), Biomechanics: Principles and Applications. Martinus Nijhoff Publishers, pp. 141–148.

Carlson, H., Thorstensson, A., Nilsson, J., 1988. Lumbar Back Muscle Activity During Locomotion: Effects of Voluntary Modifications of Normal Trunk Movements. Acta Physiol. Scand. 133, 343–353.

Ceccato, J.C., de Sèze, M., Azevedo, C., Cazalets, J.R., 2009. Comparison of trunk activity during gait initiation and walking in humans. PLoS One 4, 1–15.

Chaffin, D.B., 2006. Occupational Biomechanical Models, in: Chaffin, D.B., Andersson, G.B.J., Martin, B. (Eds.), Occupational Biomechanics. John Wiley & Sons Inc., pp. 109–160.

Chaffin, D.B., 1969. A Computerized Biomechanical Model - Development of and Use in Studying Gross Body Actions. J. Biomech. 2, 429–441.

Chaffin, D.B., Andersson, G.B.J., Martin, B.J., 2006. Occupational Biomechanics, 4th ed. John Wiley & Sons Inc., New York, NY.

Chapman, A.E., 1985. The Mechanical Properties of Human Muscle. Exerc. Sport Sci. Rev. 13, 443–501.

Cheng, C.-K., Chen, H.-H., Chen, C.-S., Lee, S.-J., 1998a. Influences of walking speed change on the lumbosacral joint force distribution. Biomed. Mater. Eng. 8, 155–65.

Cheng, C.-K., Chen, H.-H., Kuo, H.-H., Lee, C.-L., Chen, W.-J., Liu, C.-L., 1998b. A three-dimensional mathematical model for predicting spinal joint force distribution during manual liftings. Clin. Biomech. 13, S59–S64.

Choi, H., Vanderby, R.J., 1999. Comparison of Biomechanical Human Neck Models: Muscle Forces and Spinal Loads at C4/5 Level. J. Appl. Biomech. 15, 120–138.

Choi, J.T., Bastian, A.J., 2007. Adaptation reveals independent control networks for human walking. Nat. Neurosci. 10, 1055–1062.

Cholewicki, J., McGill, S.M., 1996. Mechanical stability of the in vivo lumbar spine: Implications for injury and chronic low back pain. Clin. Biomech. 11, 1–15.

Cholewicki, J., McGill, S.M., 1994. EMG Assisted Optimization: A Hybrid Approach for Estimating Muscle Forces in an Indeterminate Biomechanical Model. J. Biomech. 27, 1287–1289.

Cholewicki, J., McGill, S.M., Norman, R.W., 1995. Comparison of muscle forces and joint load from an optimization and EMG assisted lumbar spine model: Towards development of a hybrid approach. J. Biomech. 28.

Cholewicki, J., McGill, S.M., Norman, R.W., 1991. Lumbar spine loads during the lifting of extremely heavy weights. Med. Sci. Sport. Exerc. 23, 1179–1186.

Chow, D.H.K., Holmes, A.D., Lee, C.K.L., Sin, S.W., 2006. The effect of prosthesis alignment on the symmetry of gait in subjects with unilateral transtibial amputation. Prosthet. Orthot. Int. 30, 114–128.

Chow, D.H.K., Kwok, M.L.Y., Au-yang, A.C.K., Holmes, A.D., Cheng, J.C.Y., Yao, F.Y.D., Wong, M.S., 2005. The effect of backpack load on the gait of normal adolescent girls The effect of backpack load on the gait of normal adolescent girls. Ergonomics 48, 642–656.

Christophy, M., Senan, N.A.F., Lotz, J.C., O'Reilly, O.M., 2012. A Musculoskeletal model for the lumbar spine. Biomech. Model. Mechanobiol. 11, 19–34.

Constantinou, M., Barrett, R.S., Brown, M., Mills, P., 2014. Spatial-Temporal Gait Characteristics in Individuals With Hip Osteoarthritis: A Systematic Literature Review and Meta-analysis. J. Orthop. Sport. Phys. Ther. 44, 291–303.

Cook, T.M., Neumann, D.A., 1987. The effects of load placement on the EMG activity of the low back muscles during load carrying by men and women. Ergonomics 30, 1413–1423.

Corcos, D.M., Gottlieb, G.L., Latash, M.L., Almeida, G.L., Agarwal, G.C., 1992. Electromechanical Delay: An Experimental Artifact. J. Electromyogr. Kinesiol. 2, 59–68.

Crisco, J.J., Panjabi, M.M., 1991. The Intersegmental and Multisegmental Muscles of the Lumbar Spine: A Biomechanical Mmodel Comparing Lateral Stabilizing Potential. Spine (Phila. Pa. 1976). 16, 793–799.

Cromwell, R., Schultz, A.B., Beck, R., Warwick, D., 1989. Loads on the Lumbar Trunk During Level Walking. J. Orthop. Res. 7, 371–377.

Crosbie, J., Flynn, W., Rutter, L., 1994. Effect of side load carriage on the kinematics of gait. Gait Posture 2, 103–108.

Crosbie, J., Vachalathiti, R., Smith, R., 1997. Patterns of spinal motion during walking. Gait Posture 5, 6–12.

Crowe, A., Samson, M.M., 1997. 3-D analysis of gait: The effects upon symmetry of carrying a load in one hand. Hum. Mov. Sci. 16, 357–365.

Crownshield, R.D., Brand, R.A., 1981. A Physiologically Based Criterion of Muscle Force Prediction in Locomotion. J. Biomech. 14, 793–801.

da Costa, B.R., Vieira, E.R., 2010. Risk factors for work-related musculoskeletal disorders : A systematic review of recent longitudinal studies. Am. J. Ind. Med. 53, 285–323.

Daggfeldt, K., Thorstensson, A., 2003. The mechanics of back-extensor torque production about the lumbar spine. J. Biomech. 36, 815–825.

Daggfeldt, K., Thorstensson, A., 1997. The role of intra-abdominal pressure in spinal unloading. J. Biomech. 30, 1149–1155.

Dananberg, H.J., 1993. Gait Style as an Etiology to Chronic Postural Pain: Part II. Postural Compensatory Process. J. Am. Podiatr. Med. Assoc. 83, 615–624.

Dananberg, H.J., Guiliano, M., 1999. Chronic Low-Back Pain and Its Response to Custom-Made Foot Orthoses. J. Am. Podiatr. Med. Assoc. 89, 109–117.

Datta, S.R., Ramanathan, N.L., 1971. Ergonomic Comparision of Seven Modes of Carrying Loads on the Horizontal Plane. Ergonomics 14, 269–278.

Davis, K.G., Jorgensen, M.J., 2005. Biomechanical modeling for understanding of low back injuries : A systematic review. Occup. Ergon. 5, 57–76.

Davis, K.G., Marras, W.S., 2005. Load spatial pathway and spine loading: How does lift origin and destination influence low back response? Ergonomics 48, 1031–1046.

Davis, K.G., Marras, W.S., Waters, T.R., 1998. Evaluation of Spinal Loading During Lowering and Lifting. Clin. Biomech. 13, 141–153.

Davis, P.R., 1981. The Use of Intra-Abdominal Pressure in Evaluating Stresses on the Lumbar Spine. Spine (Phila. Pa. 1976). 6, 90–92.

de Looze, M.P., Kingma, I., Bussmann, J.B., Toussaint, H.M., 1992. Validation of a dynamic linked segment model to calculate joint moments in lifting. Clin. Biomech. 7, 161–169.

de Zee, M., Hansen, L., Wong, C., Rasmussen, J., Simonsen, E.B., 2007. A generic detailed rigid-body lumbar spine model. J. Biomech. 40, 1219–1227.

Della Croce, U., Leardini, A., Chiari, L., Cappozzo, A., 2005. Human movement analysis using stereophotogrammetry Part 4: Assessment of anatomical landmark misplacement and its effects on joint kinematics. Gait Posture 21, 226–237.

Delp, S.L., Anderson, F.C., Arnold, A.S., Loan, J.P., Habib, A., John, C.T., Guendelman, E., Thelen, D.G., 2007. OpenSim: Open source to create and analyze dynamic simulations of movement. IEEE Trans. Biomed. Eng. 54, 1940–1950.

Delp, S.L., Loan, J.P., Hoy, M.G., Zajac, F.E., Topp, E.L., Rosen, J.M., 1990. An Interactive Graphics-Based Model of the Lower Extremity to Study Orthopaedic Surgical Procedures. IEEE Trans. Biomed. Eng. 37, 757–767.

Devan, H., Carman, A.B., Hendrick, P.A., Ribeiro, D.C., Hale, L.A., 2015. Perceptions of low back pain in people with lower limb amputation: a focus group study. Disabil. Rehabil. 37, 873–883.

Devan, H., Hendrick, P.A., Hale, L.A., Carman, A.B., Dillon, M.P., Ribeiro, D.C., 2017. Exploring Factors Influencing Low Back Pain in People With Nondysvascular Lower Limb Amputation: A National Survey. Phys. Med. Rehabil. 9, 949–959.

Devan, H., Hendrick, P.A., Ribeiro, D.C., Hale, L.A., Carman, A.B., 2014. Asymmetrical movements of the lumbopelvic region: Is this a potential mechanism for low back pain in people with lower limb amputation? Med. Hypotheses 82, 77–85.

Devan, H., Tumilty, S., Smith, C., 2012. Physical activity and lower-back pain in persons with traumatic transfemoral amputation: A national cross-sectional survey. J. Rehabil. Res. Dev. 49, 1457.

DeVita, P., Hong, D., Hamill, J., 1991. Effects of Asymmetric Load Carrying on the Biomechanics of Walking. J. Biomech. 24, 1119–1129.

Deyo, R.A., Weinstein, J.N., 2001. Low Back Pain. N. Engl. J. Med. 344, 363–370.

Dick, R.B., Hudock, S.D., Lu, M.-L., Waters, T.R., Putz-Anderson, V., 2017. Manual Materials Handling, in: Stave, G.M., Wald, P.H. (Eds.), Physical and Biological Hazards of the Workplace. John Wiley & Sons Inc., pp. 33–52.

Dietz, V., Zijlstra, W., Duysens, J., 1994. Human Neuronal Interlimb Coordination during Split-Belt Locomotion. Exp. Brain Res. 101, 513–520.

Dingwell, J.B., Davis, B.L., Frazier, D.M., 1996. Use of an instrumented treadmill for real-time gait symmetry evaluation and feedback in normal and trans-tibial amputee subjects. Prosthet. Orthot. Int. 20, 101–110.

Dolan, P., Adams, M.A., 1993. The Relationship Between EMG Activity and Extensor Moment Generation in the Erector Spinae Muscles During Bending and Lifting Activities. J. Biomech. 26, 513–522.

Dreischarf, M., Shirazi-Adl, A., Arjmand, N., Rohlmann, A., Schmidt, H., 2016. Estimation of loads on human lumbar spine: A review of in vivo and computational model studies. J. Biomech. 49, 833–845.

Ehde, D.M., Smith, D.G., Czerniecki, J.M., Campbell, K.M., Malchow, D.M., Robinson, L.R., 2001. Back pain as a secondary disability in persons with lower limb amputations. Arch. Phys. Med. Rehabil. 82, 731–734.

Eklund, J.A.E., Corlett, E.N., 1984. Shrinkage as a Measure of the Effect of Load on the Spine. Spine (Phila. Pa. 1976). 9, 189–194.

El-Rich, M., Shirazi-Adl, A., Arjmand, N., 2004. Muscle Activity, Internal Loads, and Stability of the Human Spine in Standing Postures: Combined Model and In Vivo Studies. Spine (Phila. Pa. 1976). 29, 2633–2642.

Enoka, R.M., Duchateau, J., 2008. Muscle fatigue: What, why and how it influences muscle function. J. Physiol. 586, 11–23.

Ephraim, P.L., Wegener, S.T., MacKenzie, E.J., Dillingham, T.R., Pezzin, L.E., 2005. Phantom pain, residual limb pain, and back pain in amputees: Results of a national survey. Arch. Phys. Med. Rehabil. 86, 1910–1919.

Faber, G.S., Kingma, I., Bakker, A.J.M., van Dieën, J.H., 2009. Low-back loading in lifting two loads beside the body compared to lifting one load in front of the body. J. Biomech. 42, 35–41.

Farrokhi, S., Mazzone, B., Schneider, M., Gombatto, S.P., Mayer, J., Highsmith, M.J., Hendershot, B.D., 2017. Biopsychosocial risk factors associated with chronic low back pain after lower limb amputation. Med. Hypotheses 108, 1–9.

Fathallah, F.A., Marras, W.S., Parnianpour, M., 1998. An Assessment of Complex Spinal Loads During Dynamic Lifting Tasks. Spine (Phila. Pa. 1976). 23, 706–716.

Feipel, V., De Mesmaeker, T., Klein, P., Rooze, M., 2001. Three-dimensional kinematics of the lumbar spine during treadmill walking at different speeds. Eur. Spine J. 10, 16–22.

Finley, J.M., Bastian, A.J., Gottschall, J.S., 2013. Learning to be economical: The energy cost of walking tracks motor adaptation. J. Physiol. 591, 1081–1095.

Finley, J.M., Long, A., Bastian, A.J., Torres-Oviedo, G., 2015. Spatial and Temporal Control Contribute to Step Length Asymmetry During Split-Belt Adaptation and Hemiparetic Gait. Neurorehabil. Neural Repair 29, 786–795.

Fisher, B.O., 1967. Analysis of Spinal Stresses During Lifting a Biomechanical Model. University of Michigan.

Floyd, W.F., Silver, P.H.S., 1955. The function of the erectores spinae muscles in certain movements and postures in man. J. Physiol. 129, 184–203.

Fowler, N.E., Rodacki, A.L.F., Rodacki, C.D., 2006. Changes in stature and spine kinematics during a loaded walking task. Gait Posture 23, 133–141.

Freburger, J.K., Holmes, G.M., Agans, R.P., Jackman, A.M., Darter, J.D., Wallace, A.S., Castel, L.D., Kalsbeek, W.D., Carey, T.S., 2009. The Rising Prevalence of Chronic Low Back Pain. Arch. Intern. Med. 169, 251–258.

Freivalds, A., Chaffin, D.B., Garg, A., Lee, K.S., 1984. A dynamic biomechanical evaluation of lifting maximum acceptable loads. J. Biomech. 17, 251–262.

Friberg, O., 1984. Biomechanical significance of the correct length of lower limb prostheses: a clinical and radiological study. Prosthet. Orthot. Int. 8, 124–129.

Friberg, O., 1983. Clinical Symptoms and Biomechanics of Lumbar and Hip Joint in Leg Length Inequality. Spine (Phila. Pa. 1976). 8, 643–651.

Friel, K., Domholdt, E., Smith, D.G., 2005. Physical and functional measures related to low back pain in individuals with lower-limb amputation: An exploratory pilot study. J. Rehabil. Res. Dev. 42, 155.

Froud, R., Patterson, S., Eldridge, S., Seale, C., Pincus, T., Rajendran, D., Fossum, C., Underwood, M., 2014. A systematic review and meta-synthesis of the impact of low back pain on people's lives. BMC Musculoskelet Disord. 15, 1–14.

Fujii, R., Sakaura, H., Mukai, Y., Hosono, N., Ishii, T., Iwasaki, M., Yoshikawa, H., Sugamoto, K., 2007. Kinematics of the lumbar spine in trunk rotation: In vivo three-dimensional analysis using magnetic resonance imaging. Eur. Spine J. 16, 1867–1874.

Gage, J.R., 1990. An Overview of Normal Walking. Instr. Course Lect. 39, 291–303.

Gagnon, D., Arjmand, N., Plamondon, A., Shirazi-Adl, A., Larivière, C., 2011. An improved multi-joint EMG-assisted optimization approach to estimate joint and muscle forces in a musculoskeletal model of the lumbar spine. J. Biomech. 44, 1521–1529.

Gagnon, D., Larivière, C., Loisel, P., 2001. Comparative ability of EMG, optimization, and hybrid modelling approaches to predict trunk muscle forces and lumbar spine loading during dynamic sagittal plane lifting. Clin. Biomech. 16, 359–372.

Gagnon, D., Plamondon, A., Larivière, C., 2018. A comparison of lumbar spine and muscle loading between male and female workers during box transfers. J. Biomech. 81, 76–85.

Gagnon, D., Plamondon, A., Larivière, C., 2016. A biomechanical comparison between expert and novice manual materials handlers using a multi-joint EMG-assisted optimization musculoskeletal model of the lumbar spine. J. Biomech. 49, 2938–2945.

Gallagher, S., Marras, W.S., 2012. Tolerance of the lumbar spine to shear: A review and recommended exposure limits. Clin. Biomech. 27, 973–978.

Gallagher, S., Marras, W.S., Litsky, A.S., Burr, D., 2005. Torso flexion loads and the fatigue failure of human lumbosacral motion segments. Spine (Phila. Pa. 1976). 30, 2265–2273.

Ganguli, S., Datta, S.R., 1977. Studies in Load Carrying in BK amutees with a PTB Prosthesis System. J. Med. Eng. Technol. 1, 151–154.

Ghezelbash, F., Arjmand, N., Shirazi-Adl, A., 2015. Effect of intervertebral translational flexibilities on estimations of trunk muscle forces, kinematics, loads, and stability. Comput. Methods Biomech. Biomed. Engin. 18, 1760–1767.

Giles, L.G.F., Taylor, J.R., 1981. Low-Back Pain Associated with Leg Length Inequality. Spine (Phila. Pa. 1976). 6, 510–521.

Godfrey, C.M., Brett, R., Jousse, A.T., 1977. Foot Mass Effect on Gait in the Prosthetic Limb. Arch. Phys. Med. Rehabil. 58, 268–269.

Gofton, J.P., 1971. Studies in osteoarthritis of the hip: Part IV. Biomechanics and Clinical Considerations. Can. Med. Assoc. J. 104, 1007–1011.

Goh, J.C.H., Thanbyah, A., Bose, K., 1998. Effects of varying backpack loads on peak forces in the lumbosacral spine during walking. Clin. Biomech. 13, S26–S31.

Goldman, R.F., 1962. Energy cost of load carriage. J. Appl. Physiol. 17, 675–676.

Golob, A.L., Wipf, J.E., 2014. Low Back Pain. Med. Clin. North Am. 98, 405–428.

Goujon-Pillet, H., Sapin, E., Fodé, P., Lavaste, F., 2008. Three-Dimensional Motions of Trunk and Pelvis During Transfemoral Amputee Gait. Arch. Phys. Med. Rehabil. 89, 87–94.

Gracovetsky, S., 1990. Musculoskeletal Function of the Spine, in: Winters, J.M., Woo, S.L.-Y. (Eds.), Multiple Muscle Systems: Biomechanics and Movement Organization. Springer-Verlag, New York, pp. 410–437.

Gracovetsky, S., 1985. An hypothesis for the role of the spine in human locomotion: A challenge to current thinking. J. Biomed. Eng. 7, 205–216.

Gracovetsky, S., Farfan, H.F., Lamy, C., 1981. The Mechanism of the Lumbar Spine. Spine (Phila. Pa. 1976). 6, 249–262.

Gracovetsky, S., Farfan, H.F., Lamy, C., 1977. A Mathematical Model of the Lumbar Spine Using an Optimized System to Control Muscles and Ligaments. Orthop. Clin. North Am. 8, 135–153.

Granata, K.P., Marras, W.S., 1995a. An EMG-assisted Model of Trunk Loading During Free-dynamic Lifting. J. Biomech. 28, 1309–1317.

Granata, K.P., Marras, W.S., 1995b. The Influence of Trunk Muscle Coactivity on Dynamic Spinal Loads. Spine (Phila. Pa. 1976). 20, 913–919.

Granata, K.P., Marras, W.S., 1993. An EMG-assisted model of loads on the lumbar spine during asymmetric trunk extensions. J. Biomech. 26, 1429–1438.

Granata, K.P., Marras, W.S., Davis, K.G., 1999. Variation in spinal load and trunk dynamics during repeated lifting exertions. Clin. Biomech. 14, 367–375.

Granata, K.P., Orishimo, K.F., 2001. Response of trunk muscle coactivation to changes in spinal stability. J. Biomech. 34, 1117–1123.

Granhed, H., Jonson, R., Hansson, T.H., 1987. The Loads on the Lumbar Spine During Extreme Weight Lifting. Spine (Phila. Pa. 1976). 12, 146–149.

Graves, J.E., Pollock, M.L., Carpenter, D.M., Leggett, S.H., Jones, A., MacMillan, M., Fulton, M., 1990. Quantitative Assessment of Full Range-of-Motion Isometric Lumbar Extension Strength. Spine (Phila. Pa. 1976). 15, 289–294.

Grillner, S., Nilsson, J., Thorstensson, A., 1978. Intra-abdominal Pressure Changes During Natural Movements in Man. Acta Physiol. Scand. 103, 275–283.

Gross, R.H., 1978. Leg Length Discrepancy: How Much is Too much? Orthopedics 1, 307–310.

Gulgin, H., Hall, K., Luzadre, A., Kayfish, E., 2018. 3D gait analysis with and without an orthopedic walking boot. Gait Posture 59, 76–82.

Gundersen, L.A., Valle, D.R., Barr, A.E., Danoff, J. V., Stanhope, S.J., Snyder-Mackler, L., 1989. Bilateral Analysis of the Knee and Ankle During Gait: An Examination of the Relationship Between Lateral Dominance and Symmetry. Phys. Ther. 69, 640–650.

Hafner, B.J., Sanders, J.E., Czerniecki, J.M., Fergason, J., 2002. Energy storage and return prostheses: Does patient perception correlate with biomechanical analysis? Clin. Biomech. 17, 325–344.

Hamner, S.R., Seth, A., Delp, S.L., 2010. Muscle contributions to propulsion and support during running. J. Biomech. 43, 2709–2716.

Han, K.S., Zander, T., Taylor, W.R., Rohlmann, A., 2012. An enhanced and validated generic thoraco-lumbar spine model for prediction of muscle forces. Med. Eng. Phys. 34, 709–716.

Hannah, R.E., Morrison, J.B., Chapman, A.E., 1984. Kinematic Symmetry of the Lower Limbs. Arch. Phys. Med. Rehabil. 65, 155–158.

Hansen, L., de Zee, M., Rasmussen, J., Andersen, T.B., Wong, C., Simonsen, E.B., 2006. Anatomy and Biomechanics of the Back Muscles in the Lumbar Spine with Reference to Biomechanical Modeling. Spine (Phila. Pa. 1976). 21, 1888–1899.

Hart, L.G., Deyo, R.A., Cherkin, D.C., 1995. Physcian Office Visits for Low Back Pain. Spine (Phila. Pa. 1976). 20, 11–19.

Hendershot, B.D., Bazrgari, B., 2020. Evolution of Fatigue Damage in the L5-S1 Intervertebral Disc Resulting from Walking Exposures Among Persons with Lower Limb Loss. Ann. Biomed. Eng. 48, 1678–1682.

Hendershot, B.D., Shojaei, I., Acasio, J.C., Dearth, C.L., Bazrgari, B., 2018. Walking speed differentially alters spinal loads in persons with traumatic lower limb amputation. J. Biomech. 70, 249–254.

Hendershot, B.D., Wolf, E.J., 2014. Three-dimensional joint reaction forces and moments at the low back during over-ground walking in persons with unilateral lower-extremity amputation. Clin. Biomech. 29, 235–242.

Herzog, W., Nigg, B.M., Read, L.J., Olsson, E., 1989. Asymmetries in Ground Reaction Force Patterns in Normal Human Gait. Med. Sci. Sport. Exerc. 21, 110–114.

Hicks, J.L., Uchida, T.K., Seth, A., Rajagopal, A., Delp, S.L., 2015. Is My Model Good Enough? Best Practices for Verification and Validation of Musculoskeletal Models and Simulations of Movement. J. Biomech. Eng. 137, 020905.

Highsmith, M.J., Goff, L.M., Lewandowski, A.L., Farrokhi, S., Hendershot, B.D., Hill, O.T., Rábago, C.A., Russell-Esposito, E., Orriola, J.J., Mayer, J.M., 2019. Low back pain in persons with lower extremity amputation: a systematic review of the literature. Spine J. 19, 552–563.

Hill, A.V., 1938. The Heat of Shortening and the Dynamic Constants of Muscle. Proc. R. Soc. B Biol. Sci. 126, 136–195.

Hinkle, D., Wiersma, W., Jurs, S.G., 2003. Applied Statistics for Behavioral Sciences, 5th ed. Houghton Mifflin Harcourt.

Holzbaur, K.R.S., Murray, W.M., Delp, S.L., 2005. A model of the upper extremity for simulating musculoskeletal surgery and analyzing neuromuscular control. Ann. Biomed. Eng. 33, 829–840.

Honegger, J.D., Actis, J.A., Gates, D.H., Silverman, A.K., Munson, A.H., Pertrella, A.J., 2020. Development of a multiscale model of the human lumbar spine for investigation of tissue loads in people with and without a transtibial amputation during sit-to-stand. Biomech. Model. Mechanobiol.

Hoogendoorn, W.E., van Poppel, M.N.M., Bongers, P.M., Koes, B.W., Bouter, L.M., 1999. Physical Load During Work and Leisure Time as Risk Factors for Back Pain. Scand. J. Work. Enviroment Heal. 25, 387–403.

Hoy, D., Bain, C., Williams, G., March, L.M., Brooks, P., Blyth, F.M., Woolf, A.D., Vos, T., Buchbinder, R., 2012. A systematic review of the global prevalence of low back pain. Arthritis Rheum. 64, 2028–2037.

Hoy, D., Brooks, P., Blyth, F.M., Buchbinder, R., 2010a. The Epidemiology of low back pain. Best Pract. Res. Clin. Rheumatol. 24, 769–781.

Hoy, D., March, L.M., Brooks, P., Blyth, F.M., Woolf, A.D., Bain, C., Williams, G., Smith, E., Vos, T., Barendregt, J., Murray, C., Burstein, R., Buchbinder, R., 2014. The global burden of low back pain: Estimates from the Global Burden of Disease 2010 study. Ann. Rheum. Dis. 73, 968–974.

Hoy, D., March, L.M., Brooks, P., Woolf, A.D., Blyth, F.M., Vos, T., Buchbinder, R., 2010b. Measuring the global burden of low back pain. Best Pract. Res. Clin. Rheumatol. 24, 155–165.

Hsiang, S.M., Brogmus, G.E., Courtney, T.K., 1997. Low back pain (LBP) and lifting technique - A review. Int. J. Ind. Ergon. 19, 59–74.

Huang, T.P., Kuo, A.D., 2014. Mechanics and energetics of load carriage during human walking. J. Exp. Biol. 217, 605–613.

Hwang, J., Knapik, G.G., Dufour, J.S., Aurand, A., Best, T.M., Khan, S.N., Mendel, E., Marras, W.S., 2016. A biologically-assisted curved muscle model of the lumbar spine: Model structure. Clin. Biomech. 37, 53–59.

Hwang, J., Knapik, G.G., Dufour, J.S., Marras, W.S., 2017. Curved muscles in biomechanical models of the spine: a systematic literature review. Ergonomics 60, 577–588.

Ignasiak, D., Ferguson, S.J., Arjmand, N., 2016. A rigid thorax assumption affects model loading predictions at the upper but not lower lumbar levels. J. Biomech. 49, 3074–3078.

Jaegers, S.M.H.J., Arendzen, J.H., de Jongh, H.J., 1996. An Electromyographic Study of Hip Muscles of Transfemoral Amputees in Walking. Clin. Orthop. Relat. Res. 328, 119–128.

Jäger, M., Luttmann, A., 1989. Biomechanical analysis and assessment of lumbar stress during load lifting using a dynamic 19-segment human model. Ergonomics 32, 93–112.

Jensen, R.C., 1987. Disabling Back Injuries Among Nursing Personnel: Research Needs and Justification. Res. Nurs. Health 10, 29–38.

Jia, B., Kim, S., Nussbaum, M.A., 2011. An EMG-based model to estimate lumbar muscle forces and spinal loads during complex, high-effort tasks: Development and application to residential construction using prefabricated walls. Int. J. Ind. Ergon. 41, 437–446.

Jordan, C., Luttmann, A., Theilmeier, A., Kuhn, S., Wortmann, N., Jäger, M., 2011. Characteristic values of the lumbar load of manual patient handling for the application in workers' compensation procedures. J. Occup. Med. Toxicol. 6, 1–13.

Kakushima, M., Miyamoto, K., Shimizu, K., 2003. The Effect of Leg Length Discrepency on Spinal Motion During Gait. Spine (Phila. Pa. 1976). 28, 2472–2476.

Kallenberg, L.A.C., Schulte, E., Disselhorst-Klug, C., Hermens, H.J., 2007. Myoelectric manifestations of fatigue at low contraction levels in subjects with and without chronic pain. J. Electromyogr. Kinesiol. 17, 264–274.

Kamen, G., Caldwell, G.E., 1996. Physiology and Interpretation of the Electromyogram. Clin. Neurophysiol. 13, 366–384.

Katz, J.N., 2006. Lumbar disc disorders and low-back pain: socioeconomic factors and consequences. J. Bone Jt. Surg. 88, 21–24.

Kaufman, K.R., Miller, L.S., Sutherland, D.H., 1996. Gait Asymmetry in Patients with Limb-Length Inequality. J. Pediatr. Orthop. 16, 144–150.

Kelsey, J.L., Githens, P.B., White, A.A., Holford, T.R., Walter, S.D., O'Connor, T., Ostefeld, A.M., Weil, U., Southwick, W.O., Calogero, J.A., 1984. An Epidemiologic Study of Lifting and Twisting on the Job and Risk for Acute Prolapsed Lumbar Intervertebral Disc. J. Orthop. Res. 2, 61–66.

Khamis, S., Carmeli, E., 2017. Relationship and significance of gait deviations associated with limb length discrepancy: A systematic review. Gait Posture 57, 115–123.

Khoo, B.C.C., Goh, J.C.H., Bose, K., 1995. A biomechanical model to determine lumbrosacral loads during single stance phase in normal gait. Med. Eng. Phys. 17, 27–35.

Khoo, B.C.C., Goh, J.C.H., Lee, S.M., Bose, K., 1994. A Comparision of Lumbosacral Loads During Static and Dynamic Activities. Australas. Phys. Eng. 17, 55–63.

Kienbacher, T., Paul, B., Habenicht, R., Starek, C., Wolf, M., Kollmitzer, J., Ebenbichler, G., 2014. Reliability of isometric trunk moment measurements in healthy persons over 50 years of age. J. Rehabil. Med. 46, 241–249.

Kim, H.K., Zhang, Y., 2017. Estimation of lumbar spinal loading and trunk muscle forces during asymmetric lifting tasks: application of whole-body musculoskeletal modelling in OpenSim. Ergonomics 60, 563–576.

Kim, Y.-W., Jo, S.-Y., Byeon, Y.-I., Kwon, J.-H., Im, S.-H., Cheon, S.-H., Kim, E.-J., 2019. Effects of Artificial Leg Length Discrepancies on the Dynamic Joint Angles of the Hip, Knee, and Ankle During Gait. J. Korean Soc. Phys. Med. 14, 53–61.

Kingma, I., Baten, C.T.M., Dolan, P., Toussaint, H.M., van Dieën, J.H., De Looze, M.P., Adams, M.A., 2001. Lumbar loading during lifting: A comparative study of three measurement techniques. J. Electromyogr. Kinesiol. 11, 337–345.

Kingma, I., De Looze, M.P., Toussaint, H.M., Klijnsma, H.G., Bruijnen, T.B.M., 1996. Validation of a full body 3-D dynamic linked segment model. Hum. Mov. Sci. 15, 833–860.

Kingma, I., Faber, G.S., van Dieën, J.H., 2016. Supporting the upper body with the hand on the thigh reduces back loading during lifting. J. Biomech. 49, 881–889.

Knapik, G.G., Marras, W.S., 2009. Spine loading at different lumbar levels during pushing and pulling. Ergonomics 52, 60–70.

Knapik, J., Harman, E., Reynolds, K., 1996. Load carriage using packs : A review of physiological , biomechanical and medical aspects. Appl. Ergon. 27, 207–216.

Knutson, G.A., 2005a. Anatomic and functional leg-length inequality : A review and recommendation for clinical decision-making . Part I , anatomic leg-length inequality: prevelance, magnitude, effects and clinical significance. Chiropr. Osteopat. 13, 1–10.

Knutson, G.A., 2005b. Anatomic and functional leg-length inequality : A review and recommendation for clinical decision-making . Part II , the functional or unloaded leg-length asymmetry. Chiropr. Osteopat. 13, 1–6.

Kubo, M., Holt, K.G., Saltzman, E., Wagenaar, R.C., 2006. Changes in axial stiffness of the trunk as a function of walking speed. J. Biomech. 39, 750–757.

Kuslich, S.D., Ulstrom, C.L., Michael, C.J., 1991. The Tissue Origin of Low Back Pain and Sciatica: A Report of Pain Response to Tissue Stimulation During Operations on the Lumbar Spine Using Local Anesthesia. Orthop. Clin. North Am. 22, 181–187.

Lauzière, S., Betschart, M., Aissaoui, R., Nadeau, S., 2014. International Journal of Physical Medicine & Rehabilitation Understanding Spatial and Temporal Gait Asymmetries in Individuals Post Stroke. Int. J. Phys. Med. Rehabil. 2, 1–11.

Le, P., Best, T.M., Khan, S.N., Mendel, E., Marras, W.S., 2017. A review of methods to assess coactivation in the spine. J. Electromyogr. Kinesiol. 32, 51–60.

Lee, L.-F., Umberger, B.R., 2016. Generating optimal control simulations of musculoskeletal movement using OpenSim and MATLAB. PeerJ 4, 1–18.

Lee, S.J., Hidler, J., 2008. Biomechanics of overground vs. treadmill walking in healthy individuals. J. Appl. Physiol. 104, 747–755.

Legg, S.J., 1985. Comparison of Different Methods of Load Carriage. Ergonomics 28, 197–212.

Lehman, G.J., 2002. Clinical Considerations in the Use of Surface Electromyography: Three Experimental Studies. J. Manipulative Physiol. Ther. 25, 293–299.

Lemaire, E.D., Nielen, D., Paquin, M.A., 2000. Gait evaluation of a transfemoral prosthetic simulator. Arch. Phys. Med. Rehabil. 81, 840–843.

Lewandowski, A., 1982. Issues in model validation. Angew. Syst. 3, 2–11.

Li, S.S.W., Chow, D.H.K., 2019. Comparison of Predictions Between an EMG- Assisted Approach and Two Optimization-Driven Approaches for Lumbar Spine Loading During Walking With Backpack Loads. Hum. Factors epub.

Li, S.S.W., Chow, D.H.K., 2018. Effects of backpack load on critical changes of trunk muscle activation and lumbar spine loading during walking. Ergonomics 61, 553–565.

Liberty Mutual Research Institute for Safety, 2018. 2018 Liberty Mutual Workplace Safety Index Risk Control from Liberty Mutual Insurance, From Research to Reality.

Lind, A.R., McNicol, G.W., 1968. Cardiovascular responses to holding and carrying weights by hand and by shoulder harness. J. Appl. Physiol. 25, 261–267.

Liu, X.-C., Fabry, G., Molenaers, G., Lammens, J., Moens, P., 1998. Kinematic and Kinetic Asymmetry in Patients with Leg-Length Disrepancy. J. Pediatr. Orthop. 18, 187–189.

Lloyd, D.G., Besier, T.F., 2003. An EMG-driven musculoskeletal model to estimate muscle forces and knee joint moments in vivo. J. Biomech. 36, 765–776.

Lovejoy, C.O., 2005. The natural history of human gait and posture Part 1. Spine and pelvis. Gait Posture 21, 95–112.

Majumdar, Deepti, Pul, M.S., Majumdar, Dhurjati, 2010. Effects of military load carriage on kinematics of gait. Ergonomics 53, 782–791.

Malakoutian, M., Street, J., Wilke, H.-J., Stavness, I., Fels, S., Oxland, T., 2018. A musculoskeletal model of the lumbar spine using ArtiSynth–development and validation. Comput. Methods Biomech. Biomed. Eng. Imaging Vis. 6, 483–490.

Malone, L.A., Bastian, A.J., Torres-Oviedo, G., 2012. How does the motor system correct for errors in time and space during locomotor adaptation? J. Neurophysiol. 108, 672–683.

Mansouri, M., Reinbolt, J.A., 2012. A platform for dynamic simulation and control of movement based on OpenSim and MATLAB. J. Biomech. 45, 1517–1521.

Marras, W.S., 2008. The Working Back: A Systems View. John Wiley & Sons, Inc., Hoboen, NJ.

Marras, W.S., 2000. Occupational Low Back Disorders Causation and Control. Ergonomics 43, 880–902.

Marras, W.S., 1988. Predictions of Force Acting Upon the Lumbar Spine Under Isometric and Isokinetic Conditions: A Model - Experimental Comparison. Int. J. Ind. Ergon. 3, 19–27.

Marras, W.S., Davis, K.G., 1998. Spine loading during asymmetric lifting using one versus two hands. Ergonomics 41, 817–834.

Marras, W.S., Davis, K.G., Kirking, B.C., Bertsche, P.K., 1999a. A comprehensive analysis of low-back disorder risk and spinal loading during the transferring and repositioning of patients using different techniques. Ergonomics 42, 904–926.

Marras, W.S., Granata, K.P., 1997a. The development of an EMG-assisted model to assess spine loading during whole-body free-dynamic lifting. J. Electromyogr. Kinesiol. 7, 259–268.

Marras, W.S., Granata, K.P., 1997b. Spine Loading During Trunk Lateral Bending Motions. J. Biomech. 30, 697–703.

Marras, W.S., Granata, K.P., 1995. A Biomechanical Assessment and Model of Axial Twisting in the Thoracolumbar Spine. Spine (Phila. Pa. 1976). 20, 1440–1451.

Marras, W.S., Granata, K.P., Davis, K.G., 1999b. Variability in spine loading model performance. Clin. Biomech. 14, 505–514.

Marras, W.S., Lavender, S.A., Leurgans, S.E., Fathallah, F.A., Ferguson, S.A., Allread, W.G., Rajulu, S.L., 1995. Biomechanical Risk Factors for Occupationally Related Low Back Disorders. Ergonomics 38, 377–410.

Marras, W.S., Lavender, S.A., Leurgans, S.E., Rajulu, S.L., Allread, W.G., Fathallah, F.A., Ferguson, S.A., 1993. The Role of Dynamic Three-Dimensional Trunk Motion in Occupationally-Related Low Back Disorders: The Effects of Workplace Factors, Trunk Position, and Trunk Motion Characteristics on Risk of Injury. Spine (Phila. Pa. 1976). 18, 617–628.

Marras, W.S., Mirka, G.A., 1992. A Comprehensive Evaluation of Trunk Response to Asymmetric Trunk Motion. Spine (Phila. Pa. 1976). 17, 318–326.

Marras, W.S., Parakkat, J., Chany, A.M., Yang, G., Burr, D., Lavender, S.A., 2006. Spine loading as a function of lift frequency, exposure duration, and work experience. Clin. Biomech. 21, 345–352.

Marras, W.S., Sommerich, C.M., 1991a. A Three-Dimensional Motion Model of Loads on the Lumbar Spine: II. Model Validation. Hum. Factors 33, 139–149.

Marras, W.S., Sommerich, C.M., 1991b. A Three-Dimensional Motion Model of Loads on the Lumbar Spine: I. Model Structure. Hum. Factors 33, 123–137.

Marras, W.S., Walter, B.A., Purmessur, D., Mageswaran, P., Wiet, M.G., 2016. The contribution of biomechanical-biological interactions of the spine to low back pain. Hum. Factors 58, 965–975.

Martin, P.E., Nelson, R.C., 1986. The Effect of Carried Loads on the Walking Patterns of Men and Women. Ergonomics 29, 1191–1202.

Matsas, A., Taylor, N.F., McBurney, H., 2000. Knee joint kinematics from familiarised treadmill walking can be generalised to overground walking in young unimpaired subjects. Gait Posture 11, 46–53.

Mazaheri, R., Sanjari, M.A., Radmehr, G., Halabchi, F., Angoorani, H., 2016. The activation pattern of trunk and lower limb muscles in an electromyographic assessment; comparison between ground and treadmillwalking. Asian J. Sports Med. 7, 1–6.

McGill, S.M., 2007. Low Back Disorders: Evidence-Based Prevention and Rehabilitation, 2nd ed. Human Kinetics.

McGill, S.M., 1992. A Myoelectrically Based Dynamic Three-Dimensional Model to Predict Loads on Lumbar Spine Tissues During Lateral Bending. J. Biomech. 25, 395–414.

McGill, S.M., 1991. Electromyographic Activity of the Abdominal and Low Back Musculature During the Generation of Isometric and Dynamic Axial Trunk Torque: Implications for Lumbar Mechanics. J. Orthop. Res. 9, 91–103.

McGill, S.M., Juker, D., Kropf, P., 1996. Appropriately placed surface EMG electrodes reflect deep muscle activity (psoas, quadratus lumborum, abdominal wall) in the lumbar spine. J. Biomech. 29, 1503–1507.

McGill, S.M., Marshall, L.W., 2012. Kettlebell Swing, Snatch, and Bottoms-Up Carry: Back and Hip Muscle Activation, Motion, and Low Back Loads. J. Strength Cond. Res. 26, 16–27.

McGill, S.M., Marshall, L.W., Andersen, J., 2013. Low back loads while walking and carrying: comparing the load carried in one hand or in both hands. Ergonomics 56, 293–302.

McGill, S.M., McDermott, A., Fenwick, C.M.J., 2009. Comparison of Different Strongman Events: Trunk Muscle Activation and Lumbar Spine Motion, Load, and Stiffness. J. Strength Cond. Res. 23, 1148–1161.

McGill, S.M., Norman, R.W., 1987. Effects of an Anatomically Detailed Erector Spinae Model on L4/L5 Disc Compression and Shear. J. Biomech. 20, 591–600.

McGill, S.M., Norman, R.W., 1986. Partitioning of the L4-L5 Dynamic Moment into Disc, Ligamentous, and Muscular Components During Lifting. Spine (Phila. Pa. 1976). 11, 666–678.

McGill, S.M., Norman, R.W., 1985. Dynamically and statically determined low back moments during lifting. J. Biomech. 18.

Meng, X., Bruno, A.G., Cheng, B., Wang, W., Bouxsein, M.L., Anderson, D.E., 2015. Incorporating Six Degree-of-Freedom Intervertebral Joint Stiffness in a Lumbar Spine Musculoskeletal Model—Method and Performance in Flexed Postures. J. Biomech. Eng. 137, 1–9.

Merskey, H., Bogduk, N., 1994. Classification of Chronic Pain, 2nd ed. IASP Press, Seattle, WA.

Micklewright, D., St Clair Gibson, A., Gladwell, V., Al Salman, A., 2017. Development and Validity of the Rating-of-Fatigue Scale. Sport. Med. 47, 2375–2393.

Millard, M., Uchida, T.K., Seth, A., Delp, S.L., 2013. Flexing Computational Muscle: Modeling and Simulation of Musculotendon Dynamics. J. Biomech. Eng. 135, 1–11.

Mirka, G.A., 1991. The Quantification of EMG Normalization Error. Ergonomics 34, 343–352.

Mital, A., Kromodihardjo, S., 1986. Kinetic analysis of manual lifting activities: Part II-Biomechanical analysis of task variables. Int. J. Ind. Ergon. 1, 91–101.

Molinaro, D.D., King, A.S., Young, A.J., 2020. Biomechanical Analysis of Common Solid Waste Collection Throwing Techniques Using OpenSim and an EMG-Assisted Solver. J. Biomech.

Morgenroth, D.C., Orendurff, M.S., Shakir, A., Segal, A., Shofer, J., Czerniecki, J.M., 2010. The relationship between lumbar spine kinematics during gait and low-back pain in transfemoral amputees. Am. J. Phys. Med. Rehabil. 89, 635–643.

Morris, J.M., Lucas, D.B., Bresler, B., 1961. Role of the Trunk in Stability of the Spine. J. Bone Jt. Surg. 43-A, 327–351.

Müller, R., Strässle, K., Wirth, B., 2010. Isometric back muscle endurance: An EMG study on the criterion validity of the Ito test. J. Electromyogr. Kinesiol. 20, 845–850.

Mündermann, A., Dyrby, C.O., Andriacchi, T.P., 2005. Secondary gait changes in patients with medial compartment knee osteoarthritis: Increased load at the ankle, knee, and hip during walking. Arthritis Rheum. 52, 2835–2844.

Murray, K.J., Azari, M.F., 2015. Leg length discrepancy and osteoarthritis in the knee, hip and lumbar spine. J. Can. Chiropr. Assoc. 59, 226–37.

Nachemson, A., 1976. The Lumbar Spine An Orthopaedic Challenge. Spine (Phila. Pa. 1976). 1, 59–71.

Nachemson, A., 1966. The load on lumbar disks in different positions of the body. Clin. Orthop. Relat. Res. 45, 107–122.

Nachemson, A., 1965. The Effect of Forward Leaning on Lumbar Intradiscal Pressure. Acta Orthop. Scand. 35, 314–328.

Nachemson, A., 1960. Lumbar intradiscal pressure. Experimental studies on post-mortem material. Acta Orthop. Scand. Suppl. 43, 1–104.

Nachemson, A., Andersson, G.B.J., Schultz, A.B., 1986. Valsalva Maneuver Biomechanics: Effects on Lumbar Trunk Loads of Eleveated Intraabdominal Pressures. Spine (Phila. Pa. 1976). 11, 476–479.

Nachemson, A., Elfstrom, G., 1970. Intravital Dynamic Pressure Measurements in Lumbar Discs. Scand. J. Work. Enviroment Heal. 1, 1–40.

Narici, M., 1999. Human skeletal muscle architecture studied in vivo by non-invasive imaging techniques: Functional significance and applications. J. Electromyogr. Kinesiol. 9, 97–103.

National Research Council, 2001. Musculoskeletal Disorders and the Workplace: Low Back and Upper Extremities. The National Academies Press, Washington, D.C.

Neptune, R.R., 2000. Neptune_2000_PMRCNA.pdf. Sci. Princ. Sport. Rehabil. 11, 417–434.

Neumann, D.A., 1996. Hip Abductor Muscle Activity in Persons With a Hip Prosthesis While Carrying Loads in One Hand. Phys. Ther. 76, 1320–1330.

Neumann, D.A., Cook, T.M., 1985. Effect of Load and Carrying Position on the Electromyographic Activity of the Gluteus Medius Muscle During Walking. Phys. Ther. 65, 305–311.

Neumann, D.A., Cook, T.M., Sholty, R.L., Sobush, D.C., 1992. An electromyographic analysis of hip abductor muscle activity when subjects are carrying loads in one or both hands. Phys. Ther. 72, 207–217.

NIOSH, 1981. Work Practices Guide for Manual Lifting: NIOSH Technical Report No. 81-122. Cincinnati, OH.

Noble, J.W., Prentice, S.D., 2006. Adaptation to unilateral change in lower limb mechanical properties during human walking. Exp. Brain Res. 169, 482–495.

Nolan, L., Wit, A., Dudzinski, K., Lees, A., Lake, M., Wychowanski, M., 2003. Adjustments in gait symmetry with walking speed in trans-femoral and trans-tibial amputee. Gait Posture 17, 142–151.

Norman, R.W., Wells, R.P., Neumann, P., Frank, J.S., Shannon, H., Kerr, M., Onterio Universities Back Pain Study (OUBPS) Group, 1998. A comparison of peak vs cumulative physical work exposure risk factors for the reporting of low back pain in the automotive industry. Clin. Biomech. 13, 561–573.

Nottrodt, J.W., Manley, P., 1989. Acceptable Loads and Locomotor Patterns Selected in Different Carriage Methods. Ergonomics 32, 945–957.

Novacheck, T.F., 1998. The Biomechanics of Running. Gait Posture 7, 77–95.

Nussbaum, M.A., Chaffin, D.B., Martin, B.J., 1995a. A back-propagation neural network model of lumbar muscle recruitment during moderate static exertions. J. Biomech. 28, 1015–1024.

Nussbaum, M.A., Chaffin, D.B., Rechtien, C.J., 1995b. Muscle lines-of-action affect predicted forces in optimization-based spine muscle modeling. J. Biomech. 28, 401–409.

Nutter, P., 1988. Aerobic Exercise in the Treatment and Prevention of Low Back Pain. Occup. Med. (Chic. Ill). 3, 137–145.

Oreskes, N., Shrader-Frechette, K., Belitz, K., 1994. Verification,validation, and confirmation of numerical models in the earth sciences. Science (80-.). 263, 641–647.

Ornetti, P., Maillefert, J., Laroche, D., Morisset, C., Dougados, M., Gossec, L., 2010. Gait analysis as a quantifiable outcome measure in hip or knee osteoarthritis : A systematic review. Jt. Bone Spine 77, 421–425.

Owings, T.M., Grabiner, M.D., 2004. Step width variability , but not step length variability or step time variability , discriminates gait of healthy young and older adults during treadmill locomotion. J. Biomech. 37, 935–938.

Owings, T.M., Grabiner, M.D., 2003. Measuring step kinematic variability on an instrumented treadmill : how many steps are enough ? J. Biomech. 36, 1215–1218.

Panjabi, M.M., 1992. The Stabilizing System of the Spine. Part II. Neutral Zone and Instability Hypothesis. J. Spinal Disord. 5, 390–397.

Parvizi, J., Pour, A.E., Hillibrand, A., Goldberg, G., Sharkey, P.F., Rothman, R.H., 2010. Back pain and total hip arthroplasty: A prospective natural history study. Clin. Orthop. Relat. Res. 468, 1325–1330.

Pearcy, M.J., 1986. Measurement of back and spinal mobility. Clin. Biomech. 1, 44–51.

Perttunen, J.R., Anttila, E., Sodergard, J., Merikanto, J., Komi, P.V., 2004. Gait Asymmetry in Patients with Limb Length Discrepancy. Scand. J. Med. Sci. Sports 14, 49–56.

Plamondon, A., Gagnon, M., Gagnon, D., 1995. Moments at the L5/S1 joint during asymmetrical llifting: effects of different load trajectories and initial load positions. Clin. Biomech. 10, 128–136.

Pollo, F.E., Gowling, T.L., Jackson, R.W., 1999. Walking Boot Design: A Gait Analysis Study. Orthopedics 22, 503–507.

Powell, D., Clowers, K.G., Keefer, M., Zhang, S., 2012. Alterations in neuromuscular activation patterns associated with walking in short-leg walking boots. J. Sport Heal. Sci. 1, 43–48.

Punnett, L., Fine, L.J., Keyserling, W.M., Herrin, G.D., Chaffin, D.B., 1991. Back disorders and nonneutral trunk postures of automobile assembly worker. Scand. J. Work. Environ. Heal. 17, 337–346.

Raabe, M.E., Chaudhari, A.M.W., 2018. Biomechanical consequences of running with deep core muscle weakness. J. Biomech. 67, 98–105.

Raabe, M.E., Chaudhari, A.M.W., 2016. An investigation of jogging biomechanics using the full-body lumbar spine model: Model development and validation. J. Biomech. 49, 1238–1243.

Rab, G.T., Chao, E.Y.S., Stauffer, R.N., 1997. Muscle Force Analysis of the Lumbar Spine. Orthop. Clin. North Am. 8, 193–199.

Rabuffetti, M., Recalcati, M., Ferrarin, M., 2005. Trans-femoral amputee gait: Socket-pelvis constraints and compensation strategies. Prosthet. Orthot. Int. 29, 183–192.

Ramakrishnan, T., 2014. Asymmetric Unilateral Transfemoral Prosthetic Simulator. University of South Florida.

Ready, L. V., Fisk, E.G., Ciurylo, W., Chiodo, C.P., Bluman, E.M., Smith, J.T., 2018. Associated Joint Pain With Controlled Ankle Movement Walker Boot Wear. JAAOS Glob. Res. Rev. 2, e044.

Reid, M.J., Prentice, S.D., 2001. Strategies Associated with Altered Segment Parameters during Voluntary Gait Modifications. Neurosci. Res. Commun. 29, 79–87.

Reilly, T., Tyrrell, A., Troup, J.D.G., 1984. Circadian Variation in Human Stature. Chronobiol. Int. 1, 121–126.

Reisman, D.S., Block, H.J., Bastian, A.J., 2005. Interlimb Coordination During Locomtion: What can be Adapted and Stored? J. Neurophysiol. 94, 2403–2415.

Resende, R.A., Kirkwood, R.N., Deluzio, K.J., Morton, A.M., Fronseca, S.T., 2016. Mild leg length discrepancy affects lower limbs, pelvis and trunk biomechanics of individuals with knee osteoarthritis during gait. Clin. Biomech. Biomech. 38, 1–7.

Rice, J., Kaliszer, M., Walsh, M., Jenkinson, A., O'Brien, T., 2004. Movements at the low back during normal walking. Clin. Anat. 17, 662–666.

Riley, P.O., Paolini, G., Della Croce, U., Paylo, K.W., Kerrigan, D.C., 2007. A kinematic and kinetic comparison of overground and treadmill walking in healthy subjects. Gait Posture 26, 17–24.

Roberts, S., Evans, H., Trivedi, J., Menage, J., 2006. Histology and pathology of the human intervertebral disc. J. Bone Jt. Surg. 88, 10–14.

Robertson, L.S., 2018. Injury Epidemiology : Fourth Edition, 4th ed. Lulu.

Robinson, R.O., Herzog, W., Nigg, B.M., 1987. Use of Force Platform Variables to Quantify the Effects of Chiropractic Manipulation on Gait Symmetry. J. Manipulative Physiol. Ther. 10, 172–176.

Roemmich, R.T., Stegemöller, E.L., Hass, C.J., 2012. Lower extremity sagittal joint moment production during split-belt treadmill walking. J. Biomech. 45, 2817–2821.

Rohlmann, A., Bergmann, G., Graichen, F., 1997. Loads on an Internal Spinal Fixation Device During Walking. J. Biomech. 30, 41–47.

Rohlmann, A., Dreischarf, M., Zander, T., Graichen, F., Bergmann, G., 2014a. Loads on a vertebral body replacement during locomotion measured in vivo. Gait Posture 39, 750–755.

Rohlmann, A., Dreischarf, M., Zander, T., Graichen, F., Strube, P., Schmidt, H., Bergmann, G., 2013. Monitoring the load on a telemeterised vertebral body replacement for a period of up to 65 months. Eur. Spine J. 22, 2575–2581.

Rohlmann, A., Graichen, F., Kayser, R., Bender, A., Nat, R., Bergmann, G., 2008. Loads on a Telemeterized Vertebral Body Replacement Measured in Two Patients. Spine (Phila. Pa. 1976). 11, 1170–1179.

Rohlmann, A., Pohl, D., Bender, A., Graichen, F., Dymke, J., Schmidt, H., Bergmann, G., 2014b. Activities of everyday life with high spinal loads. PLoS One 9, 1–10.

Rohlmann, A., Zander, T., Graichen, F., Schmidt, H., Bergmann, G., 2014c. How does the way a weight is carried affect spinal loads? Ergonomics 57, 262–270.

Roper, J.A., Roemmich, R.T., Tillman, M.D., Terza, M.J., Hass, C.J., 2017. Split-belt treadmill walking alters lower extremity frontal plane mechanics. J. Appl. Biomech. 33, 256–260.

Rose, J.D., Mendel, E., Marras, W.S., 2013. Carrying and spine loading. Ergonomics 56, 1722–1732.

Rowe, P.J., White, M., 1996. Three dimensional, lumbar spinal kinematics during gait, following mild musculo-skeletal low back pain in nurses. Gait Posture.

Roy, S.H., De Luca, C.J., Casavant, D.A., 1989. Lumbar Muscle Fatigue and Chronic Lower Back Pain. Spine (Phila. Pa. 1976). 14, 992–1001.

Royer, T.D., Martin, P.E., 2005. Manipulations of Leg Mass and Moment of Inertia : Effects on Energy Cost of Walking. Med. Sci. Sport. Exerc. 37, 649–656.

Rozumalski, A., Schwartz, M.H., Wervey, R., Swanson, A., Dykes, D.C., Novacheck, T.F., 2008. The in vivo three-dimensional motion of the human lumbar spine during gait. Gait Posture 28, 378–384.

Rueda, F.M., Diego, I.M.A., Sánchez, A.M., Tejada, M.C., Montero, F.M.R., Page, J.C.M., 2013. Knee and hip internal moments and upper-body kinematics in the frontal plane in unilateral transtibial amputees. Gait Posture 37, 436–439.

Sadeghi, H., Allard, P., Prince, F., Labelle, H., 2000. Symmetry and limb dominance in able-bodied gait: A review. Gait Posture 12, 34–45.

Sagawa, Y., Turcot, K., Armand, S., Thevenon, A., Vuillerme, N., Watelain, E., 2011. Biomechanics and physiological parameters during gait in lower-limb amputees: A systematic review. Gait Posture 33, 511–526.

Samaei, S.E., Mostafaee, M., Jafarpoor, H., Hosseinabadi, M.B., 2017. Effects of patient-handling and individual factors on the prevalence of low back pain among nursing personnel. Work 56, 551–561.

Sanderson, D.J., Martin, P.E., 1997. Lower extremity kinematic and kinetic adaptations in unilateral below-knee amputees during walking. Gait Posture 6, 126–136.

Sato, K., Kikuchi, S., Yonezawa, T., 1999. In Vivo Intradiscal Pressure Measurement in Healthy Individuals and in Patients With Ongoing Back Problems In Vivo Intradiscal Pressure Measurement in Healthy Individuals and in Patients With Ongoing Back Problems. Spine (Phila. Pa. 1976). 24, 2468–2474.

Saunders, J.B., Inman, V.T., Eberhart, H.D., 1953. The Major Determinants in Normal and Pathological Gait. J. Bone Jt. Surg. 35-A, 543–558.

Schultz, A.B., 1990. Models for analysis of lumbar spine loads. Appl. Mech. Rev. 43, S119–S125.

Schultz, A.B., Andersson, G.B.J., 1981. Analysis of Loads on the Lumbar Spine. Spine (Phila. Pa. 1976). 6, 76–82.

Schultz, A.B., Andersson, G.B.J., Ortengren, R., Haderspeck, K., Nachemson, A., 1982. Loads on the Lumbar Spine: Validation of a Biomechanical Analysis by Measurement of Intradiscal Pressures and Myoelectric Signals. J. Bone Jt. Surg. 64A, 713–720.

Seay, J.F., 2015. Biomechancis of Load Carriage - Historical Perspectives and Recent Insights. J. Strength Cond. Res. 29, 129–133.

Seay, J.F., Selbie, W.S., Hamill, J., 2008. In vivo lumbo-sacral forces and moments during constant speed running at different stride lengths. J. Sports Sci. 26, 1519–1529.

Selbie, W.S., Hamill, J., Kepple, T.M., 2014. Three-Dimensional Kinetics, in: Robertson, D.G.E., Caldwell, G.E., Hamill, J., Kamen, G., Whittlesey, S.N. (Eds.), Research Methods in Biomechanics. Human Kinetics, Champaign, IL, pp. 151–176.

Selles, R.W., Bussmann, J.B., Wagenaar, R.C., Stam, H.J., 1999. Effects of Prosthetic Mass and Mass Distribution on Kinematics and Energetics of Prosthetic Gait: A Systematic Review. Arch. Phys. Med. Rehabil. 80, 1593–1599.

Selles, R.W., Wagenaar, R.C., Smit, T.H., Wuisman, P.I.J.M., 2001. Disorders in trunk rotation during walking in patients with low back pain : a dynamical systems approach. Clin. Biomech. 16, 175–181.

Senteler, M., Weisse, B., Rothenfluh, D.A., Snedeker, J.G., 2016. Intervertebral reaction force prediction using an enhanced assembly of OpenSim models. Comput. Methods Biomech. Biomed. Engin. 19, 538–548.

Seroussi, R.E., Gitter, A., Czerniecki, J.M., Weaver, K., 1996. Mechanical Work Adaptations of Above-Knee Amputee Ambulation. Arch. Phys. Med. Rehabil. 77, 1209–1214.

Seth, A., Sherman, M., Reinbolt, J.A., Delp, S.L., 2011. OpenSim: A musculoskeletal modeling and simulation framework for in silico investigations and exchange. Procedia IUTAM 2, 212–232.

Shaw, J.M., Hamad, N.M., Coleman, T.J., Egger, M.J., Hsu, Y., Hitchcock, R., Nygaard, I.E., 2014. Intra-abdominal pressures during activity in women using an intra-vaginal pressure transducer. J. Sports Sci. 32, 1176–1185.

Shirazi-Adl, A., 2006. Analysis of large compression loads on lumbar spine in flexion and in torsion using a novel wrapping element. J. Biomech. 39, 267–275.

Shojaei, I., Hendershot, B.D., Acasio, J.C., Dearth, C.L., Ballard, M., Bazrgari, B., 2019. Trunk muscle forces and spinal loads in persons with unilateral transfemoral amputation during sit-to-stand and stand-to-sit activities. Clin. Biomech. 63, 95–103.

Shojaei, I., Hendershot, B.D., Wolf, E.J., Bazrgari, B., 2016. Persons with unilateral transfemoral amputation experience larger spinal loads during level-ground walking compared to able-bodied individuals. Clin. Biomech. 32, 157–163.

Skinner, H.B., Barrack, R.L., 1990. Ankle Weighting Effect on Gait in Able-bodied Adults. Arch. Phys. Med. Rehabil. 71, 112–115.

Skotte, J.H., Essendrop, M., Hansen, A.F., Schibye, B., 2002. A dynamic 3D biomechanical evaluation of the load on the low back during different patient-handling tasks. J. Biomech. 35, 1357–1366.

Smidt, G.L., Herring, T., Amundsen, L., Rogers, M., Russell, A., Lehmann, T., 1983. Assessment of Abdominal and Back Extensor Function: A Quantitative Approach and Results for Chronic Low-Back Patients. Spine (Phila. Pa. 1976). 8, 211–219.

Smith, D.G., Ehde, D.M., Legro, M.W., Reiber, G.E., del Aguila, M., Boon, D.A., 1999. Phantom Limb, Residual Limb, and Back Pain After Lower Extremity Amputations. Clin. Orthop. Relat. Res. 3961, 29–38.

Smith, J.D., Martin, P.E., 2007. Walking patterns change rapidly following asymmetrical lower extremity loading. Hum. Mov. Sci. 26, 412–425.

Solomonow, M., 2004. Ligaments: A source of work-related musculoskeletal disorders. J. Electromyogr. Kinesiol. 14, 49–60.

Sparto, P.J., Parnianpour, M., Marras, W.S., Granata, K.P., Reinsel, T.E., Simon, S.R., 1998. Effect of Eltromyogram-Force Relationships and Method of Gain Estimation on the Predictions of an Electromyogram-Driven Model of Spinal Loading. Spine (Phila. Pa. 1976). 23, 423–429.

Stokes, I.A.F., Gardner-Morse, M.G., 2001. Lumbar spinal muscle activation synergies predicted by multi-criteria cost function. J. Biomech. 34, 733–740.

Stokes, I.A.F., Gardner-Morse, M.G., 1999. Quantitative anatomy of the lumbar musculature. J. Biomech. 32, 311–316.

Stokes, I.A.F., Gardner-Morse, M.G., 1995. Lumbar spine maximum efforts and muscle recruitment patterns predicted by a model with multijoint muscles and joints with stiffness. J. Biomech. 28, 173–186.

Stokes, I.A.F., Gardner-Morse, M.G., Henry, S.M., 2011. Abdominal muscle activation increases lumbar spinal stability: Analysis of contributions of different muscle groups. Clin. Biomech. 26, 797–803.

Stokes, I.A.F., Gardner-Morse, M.G., Henry, S.M., 2010. Intra-abdominal pressure and abdominal wall muscular function: Spinal unloading mechanism. Clin. Biomech. 25, 859–866.

Stokes, I.A.F., Henry, S.M., Single, R.M., 2003. Surface EMG electrodes do not accurately record from lumbar multifidus muscles. Clin. Biomech. 18, 9–13.

Stokes, I.A.F., Moffroid, M., Rush, S., Haugh, L.D., 1988. Comparison of acoustic and electrical signals from erectores spinae muscles. Muscle Nerve 11, 331–336.

Su, P.-F., Gard, S.A., Lipschutz, R.D., Kuiken, T.A., 2007. Gait characteristics of persons with bilateral transtibial amputations. J. Rehabil. Res. Dev. 44, 491.

Takahashi, I., Kikuchi, S.I., Sato, K., Sato, N., 2006. Mechanical load of the lumbar spine during forward bending motion of the trunk-A biomechanical study. Spine (Phila. Pa. 1976). 31, 18–23.

Tanaka, S., Matsumoto, S., Fujii, K., Tamari, K., Mitani, S., Tsubahara, A., 2015. Factors related to low back pain in patients with hip osteoarthritis. J. Back Musculoskelet. Rehabil. 28, 409–414.

Tankisi, H., Burke, D., Cui, L., de Carvalho, M., Kuwabara, S., Nandedkar, S.D., Rutkove, S., Stålberg, E., van Putten, M.J.A.M., Fuglsang-Frederiksen, A., 2020. Standards of instrumentation of EMG. Clin. Neurophysiol. 131, 243–258.

Taylor, N.F., Evans, O.M., Goldie, P.A., 1996. Angular movements of the lumbar spine and pelvis can be reliably measured after 4 minutes of treadmill walking. Clin. Biomech. 11, 484–486.

Tazawa, E., 1997. Analysis of torso movement of trans-femoral amputees during level walking. Prosthetics Orthot. Int. 21, 129–140.

Tesio, L., Rota, V., 2019. The Motion of Body Center of Mass During Walking: A Review Oriented to Clinical Applications. Front. Neurol. 10, 1–22.

Thacker, B.H., 2001. ASME Standards Committee on Verification and Validation in Computational Solid Mechanics.

Thelen, D.G., 2003. Adjustment of Muscle Mechanics Model Parameters to Simulate Dynamic Contractions in Older Adults. J. Biomech. Eng. 125, 70.

Thelen, D.G., Anderson, F.C., 2006. Using computed muscle control to generate forward dynamic simulations of human walking from experimental data. J. Biomech. 39, 1107–1115.

Thelen, D.G., Anderson, F.C., Delp, S.L., 2003. Generating dynamic simulations of movement using computed muscle control. J. Biomech. 36, 321–328.

Thorstensson, A., Carlson, H., Zomlefer, M.R., Nilsson, J., 1982. Lumbar back muscle activity in relation to trunk movements during locomotion in man. Acta Physiol. Scand. 116, 13–20.

Thorstensson, A., Nilsson, J., Carlson, H., Zomlefer, M.R., 1984. Trunk movements in human locomotion. Acta Physiol. Scand. 121, 9–22.

Tilbury-Davis, D.C., Hooper, R.H., 1999. The kinetic and kinematic effects of increasing load carriage upon the lower limb. Hum. Mov. Sci. 18, 693–700.

Troup, J.D.G., 1965. Relation of Lumbar Spine Disorders to Heavy Manual Work and Lifting. Lancet 285, 857–861.

Troup, J.D.G., Chapman, A.E., 1969. The Strength of the Flexor and Extensor Muscles of the Trunk. J. Biomech. 2, 49–62.

Tudor-Locke, C., Craig, C.L., Aoyagi, Y., Bell, R.C., Croteau, K.A., De Bourdeaudhuij, I., Ewald, B., Gardner, A.W., Hatano, Y., Lutes, L.D., Matsudo, S.M., Ramirez-Marrero, F.A., Rogers, L.Q., Rowe, D.A., Schmidt, M.D., Tully, M.A., Blair, S.N., 2011. How many steps/day are enough? For older adults and special populations. Int. J. Behav. Nutr. Phys. Act. 8, 1–19.

Umberger, B.R., Caldwell, G.E., 2014. Musculoskeletal Modeling, in: Robertson, D.G.E., Caldwell, G.E., Hamill, J., Kamen, G., Whittlesey, S.N. (Eds.), Research Methods in Biomechanics. Human Kinetics, Champaign, IL, pp. 247–276.

University of Michigan, 2017. 3D Static Strength Prediction Program User's Manual.

van den Bogert, A.J., Nigg, B.M., 2006. Simulation, in: Nigg, B.M., Herzog, W. (Eds.), Biomechanics of the Musculo-Skeletal System. John Wiley & Sons Inc., pp. 622–657.

van der Hulst, M., Vollenbroek-Hutten, M.M., Rietman, J.S., Hermens, H.J., 2010. Lumbar and abdominal muscle activity during walking in subjects with chronic low back pain: Support of the "guarding" hypothesis? J. Electromyogr. Kinesiol. 20, 31–38.

van der Linden, M.L., Solomonidis, S.E., Spence, W.D., Li, N., Paul, J.P., 1999. A methodology for studying the effects of various types of prosthetic feet on the biomechanics of trans-femoral amputee gait. J. Biomech. 32, 877–889.

van Dieën, J.H., 2005. Effects of antagonistic co-contraction on differences between electromyography based and optimization based estimates of spinal forces. Ergonomics 48, 411–426.

van Dieën, J.H., 1997. Are recruitment patterns of the trunk musculature compatible with a synergy based on the maximization of endurance? J. Biomech. 30, 1095–1100.

van Dieën, J.H., Heijblom, P., 1996. Reproducibility of Isometric Trunk Extension Torque , Trunk Extensor Endurance , and Related Electromyographic Parameters in the Context of Their Clinical Applicability. J. Orthop. Res. 14, 139–143.

van Dieën, J.H., Heijblom, P., Bunkens, H., 1998a. Extrapolation of time series of EMG power spectrum parameters in isometric endurance tests of trunk extensor muscles. J. Electromyogr. Kinesiol. 8, 35–44.

van Dieën, J.H., Kingma, I., 1999. Total trunk muscle force and spinal compression are lower in asymmetric moments as compared to pure extension moments. J. Biomech. 32, 681–687.

van Dieën, J.H., van der Burg, P., Raaijmakers, T.A.J., Toussaint, H.M., 1998b. Effects of repetitive lifting on kinematics: Inadequate anticipatory control or adaptive changes? J. Mot. Behav. 30, 20–32.

van Dieën, J.H., Visser, B., 1999. Estimating net lumbar sagittal plane moments from EMG data. The validity of calibration procedures. J. Electromyogr. Kinesiol. 9, 309–315.

van Melick, N., Meddeler, B.M., Hoogeboom, T.J., Nijhuis-van der Sanden, M.W.G., Cingel, R.E.H., 2017. How to determine leg dominance: The agreement between self-reported and observed performance in healthy adults. PLoS One 12, e0189876.

Vanicek, N., Sanderson, D.J., Chua, R., Kenyon, D., Inglis, J.T., 2007. Kinematic adaptations to a novel walking task with a prosthetic simulator. J. Prosthetics Orthot. 19, 29–35.

Vasavada, A.N., Li, S., Delp, S.L., 1998. Influence of Muscle Morphometry and Moment Arms on the Moment-Generating Capacity of Human Neck Muscles. Spine (Phila. Pa. 1976). 23, 412–422.

Vaughan, C.L., Davis, B.L., O'Connor, J.C., 1999. Dynamics of Human Gait, 2nd ed. Kiboho, Cape Town, South Africa.

Vink, P., Huson, A., 1988. Lumbar Back Muscle Activity during Walking with a Leg Inequality. Acta Morphol. Neerl. Scand. 25, 261–271.

Walker, B.F., 2000. The prevalence of low back pain: a systematic review of the literature from 1966 to 1998. J. Spinal Disord. 13, 205–217.

Walsh, M., Connolly, P., Jenkinson, A., Brien, T.O., 2000. Leg length discrepancy — an experimental study of compensatory changes in three dimensions using gait analysis. Gait Posture 12, 156–161.

Wang, H., Frame, J., Ozimek, E., Leib, D., Dugan, E.L., 2013. Research Quarterly for Exercise and Sport The Effects of Load Carriage and Muscle Fatigue on Lower-Extremity Joint Mechanics. Res. Q. Exerc. Sport 84, 305–312.

Wang, J., Gillette, J.C., 2018. Carrying asymmetric loads while walking on an uneven surface. Gait Posture 65, 39–44.

Wang, J., Gillette, J.C., 2017. Carrying asymmetric loads during stair negotiation. Gait Posture 53, 67–72.

Wasser, J.G., Vincent, K.R., Herman, D.C., Vincent, H.K., 2019. Potential lower extremity amputation-induced mechanisms of chronic low back pain: role for focused resistance exercise. Disabil. Rehabil. 8288.

Waters, R.L., Morris, J.M., 1972. Electrical activity of muscles of the trunk during walking. J. Anat. 111, 191–199.

Waters, T.R., Putz-Anderson, V., Garg, A., Fine, L.J., 1993. Revised NIOSH equation for the design and evaluation of manual lifting tasks. Ergonomics 36, 749–776.

Webb, D., Bratsch, S., 2017. Experience and practice in carrying a heavy, unilateral load: footprint evidence. J. Mech. Med. Biol. 17, 1–11.

White, R., Schuren, J., Wardlaw, D., Diamandopoulos, Z., Anderson, R., 1999. Biomechanical assessment of gait in below-knee walking casts. Prosthetics Orthot. Int. 23, 142–151.

Whittle, M.W., Levine, D., 1995. Sagittal Plane Motion of the Lumbar Spine During Normal Gait. Gait Posture 3, 82.

Wilke, H.-J., Neef, P., Caimi, M., Hoogland, T., Claes, L.E., 1999. New In Vivo measurements of pressures in the invertebral disc in daily life. Spine (Phila. Pa. 1976). 24, 755--762.

Wilke, H.-J., Neef, P., Hinz, B., Seidel, H., Claes, L.E., 2001. Intradiscal pressure together with anthropometric data – a data set for the validation of models. Clin. Biomech. 16, S111–S126.

Windrich, M., Grimmer, M., Christ, O., Rinderknecht, S., Beckerle, P., 2016. Active lower limb prosthetics: A systematic review of design issues and solutions. Biomed. Eng. Online 15, 5–19.

Winter, D.A., 2009. Biomechanics and Motor Control of Human Movement, 4th ed. John Wiley & Sons, Inc., Hoboken, NJ.

Winter, D.A., 1987. The Biomechanics and Motor Control of Human Gait. University of Waterloo Press, Waterloo, Ontario, Canada.

Wolfe, F., Hawley, D.J., Peloso, P.M., Wilson, K., Anderson, J., 1996. Back Pain in Osteoarthritis of the Knee. Arthritis Care Res. 9, 376–383.

Wong, K.W.N., Luk, K.D.K., Leong, J.C.Y., Wong, S.F., Wong, K.K.Y., 2006. Continuous Dynamic Spinal Motion Analysis. Spine (Phila. Pa. 1976). 31, 414–419.

Wu, A., March, L., Zheng, X., Huang, J., Wang, X., Zhao, J., Blyth, F.M., Smith, E., Buchbinder, R., Hoy, D., 2020. Global low back pain prevalence and years lived with disability from 1990 to 2017: estimates from the Global Burden of Disease Study 2017. Ann. Transl. Med. 8, 1–14.

Wu, G., Siegler, S., Allard, P., Kirtley, C., Leardini, A., Rosenbaum, D., Whittle, M.W., D'Lima, D.D., Cristofolini, L., Witte, H., Schmid, O., Stokes, I.A.F., 2002. ISB recommendation on definitions of joint coordinate system of various joints for the reporting of human joint motion—part I: ankle, hip, and spine. J. Biomech. 35, 543–548.

Yang, F., King, G.A., 2016. Dynamic gait stability of treadmill versus overground walking in young adults. J. Electromyogr. Kinesiol. 31, 81–87.

Yang, H., Haldeman, S., Lu, M.-L., Baker, D., 2016. Low Back Pain Prevalence and Related Workplace Psychosocial Risk Factors: A Study Using Data From the 2010 National Health Interview Survey. J. Manipulative Physiol. Ther. 39, 459–472.

Yang, J.F., Winter, D.A., 1983. Electromyography Reliability in Maximal and Submaximal Isometric Contractions. Arch. Phys. Med. Rehabil. 64, 417–420.

Yoder, A.J., Petrella, A.J., Silverman, A.K., 2015. Trunk-pelvis motion, joint loads, and muscle forces during walking with a transtibial amputation. Gait Posture 41, 757–762.

Yu, C., Hung, Y.-C., Lin, Y.-H., Chen, G.-X., Wei, S.-H., Huang, C.-H., Chen, C.-S., 2014. A 3D mathematical model to predict spinal joint and hip joint force for trans-tibial amputees with different SACH foot pylon adjustments. Gait Posture 40, 545–548.

Zajac, F.E., 1989. Muscle and tendon: properties, models, scaling, and application to biomechanics and motor control. Crit. Rev. Biomed. Eng.

Zatsiorky, V.M., Werner, S.L., Kaimin, M.A., 1994. Basic Kinematics of Walking. J. Sports Med. Phys. Fitness 34, 109–134.

Zeni, J.A., Richards, J.G., Higginson, J., 2008. Two simple methods for determining gait events during treadmill and overground walking using kinematic data. Gait Posture 27, 710–714.

Zetterberg, C., Andersson, G.B.J., Schultz, A.B., 1987. The Activity of Individual Trunk Muscles During Heavy Physical Loading. Spine (Phila. Pa. 1976). 12, 1035–1040.

Zhang, S., Clowers, K.G., Powell, D., 2006. Ground reaction force and 3D biomechanical characteristics of walking in short-leg walkers. Gait Posture 24, 487–492.

Zhang, Y., Jordan, J.M., 2010. Epidemiology of Osteoarthritis. Clin. Geriatr. Med. 26, 355–369.

Zhu, X.Y., Kim, H.K., Zhang, Y., 2017. Development of an Enhanced Musculoskeletal Model for Simulating Lumbar Spine Loading During Manual Lifting Tasks. Lect. Notes Comput. Sci. July, 229–237.

Ziegler-Graham, K., MacKenzie, E.J., Ephraim, P.L., Travison, T.G., Brookmeyer, R., 2008. Estimating the Prevalence of Limb Loss in the United States: 2005 to 2050. Arch. Phys. Med. Rehabil. 89, 422–429.